HOLOCENE VARIABILITY OF SURFACE AND DEEP WATER ADVECTION TO THE ARCTIC OCEAN – A MULTIPROXY PERSPECTIVE FROM THE EASTERN FRAM STRAIT

Dissertation

Zur Erlangung des Doktorgrades der Mathematisch-Naturwissenschaftlichen Fakultät der Christian-Albrechts-Universität zu Kiel

vorgelegt von

Kirstin Werner

Kiel, 2011

Referent	Prof. Dr. Martin Frank
Korreferent	Prof. Dr. Ralph Schneider
Tag der Disputation	28. November 2011
Zum Druck genehmigt	28. November 2011

gez. Prof. Dr. Lutz Kipp, Dekan

SUMMARY

Micropaleontological, geochemical, and sedimentological parameters of two sediment cores from the eastern Fram Strait have been studied to reconstruct the variability of surface and deep water advection and related fluctuations of the marginal ice zone during the past ca ~9,000 years with multidecadal resolution. The Fram Strait between Greenland and Svalbard is the only deep connection between the Arctic and adjacent subpolar oceans and is often referred to as the 'Arctic Gateway'. Fram Strait thus plays a crucial role for the energy budget and density pattern of the Arctic Ocean. Large amounts of warm and saline Atlantic Water derived from the North Atlantic Drift transport most of the heat through eastern Fram Strait to the Arctic basin, resulting in year-round ice-free conditions. Arctic sea ice and cold and fresh waters exit the western part of the strait southward along the Greenland shelf. Compared to the ice-covered Arctic Ocean, the strong east-west temperature gradient results in higher bioproductivity and sedimentation rates in the eastern Fram Strait which allows for suitably tracking Holocene variations of the heat flux to the Arctic Ocean in continuous high-resolution sediment sequences.

The multiproxy results presented in this thesis suggest that the Holocene climate and oceanographic development in the Fram Strait and possibly the Arctic Ocean was much more variable than previously assumed. The variation and interaction between warm and saline advection of Atlantic Water at the surface to subsurface into the Arctic Ocean and a correspondingly fluctuating sea ice margin characterise the eastern Fram Strait throughout the Holocene. The data imply that the transition from deglacial/Early Holocene to modern-like conditions occurred stepwise. Inferred from the high relative abundance of the subpolar planktic foraminifer species *Turborotalia quinqueloba*, intense advection of warm Atlantic Water to the Arctic Ocean marks the Early and Mid-Holocene interval (~9,000 to 5,000 years before present), concurrent with high insolation at that time. Superimposed on optimum climate conditions, repeated cold events such as the well-known '8,200 year cold event' are observed. These cold events are likely related to repeated advances of the sea ice margin and the Arctic freshwater layer. A roughly 550-year cyclicity of bottom water inflow, indicated by benthic carbon isotope data, coincide with North Atlantic bottom sediment proxy records and may suggest that deepwater variations in the Fram Strait were linked to changes in thermohaline convection processes in the Nordic Seas.

Modern (pre-industrial) climate conditions evolved after 5,000 years before present, simultaneous to the decreasing insolation and postglacial sea level highstand which likely resulted in the onset of modern-like sea ice production on the shallow Siberian shelves. Dominance of the coldwater-indicating planktic foraminifer *Neogloboquadrina pachyderma* and a significantly increasing amount of ice rafted material point to a weaker and/or cool subsurface Atlantic Water inflow and

advances of the Arctic Front during the Late Holocene Neoglacial phase. Strong southeastward advances of Arctic sea ice and polar water likely prevailed and caused heavy winter sea ice conditions and relatively short ice-free summer seasons in the eastern Fram Strait during this period.

Distinct changes linked to the variable Atlantic Water inflow and fluctuations of the sea ice margin occurred during the past ~2,000 years. More stable conditions and reduced influence of the sea ice margin characterise the well-known Medieval Climate Anomaly. Subsequently, colder conditions mark the onset of the Little Ice Age period which occurred in two phases in the eastern Fram Strait. A first phase from ~1350 to 1750 AD was characterised by frequent shifts of the marginal ice zone, indicated by high amounts of ice rafted material and highly fluctuating planktic foraminifer fluxes. After ~1750 AD a second, very cold phase with heavy sea ice conditions established, concomitant with an increased abundance of icebergs from advancing Svalbard glaciers. Changes in all studied proxies in the uppermost sediment layer confirm a strong climate shift during the past few decades. Highest relative abundance of subpolar planktic foraminifer species in the uppermost sediment layer and the application of two independent temperature reconstruction methods reveal a temperature increase of ~2°C within the past ~120 years.

Seawater-derived neodymium and lead isotope compositions stored in ferromanganese oxyhydroxide coatings of sediment particles were investigated to reconstruct Holocene variations of deep water exchanges between the Nordic Seas and the Arctic Ocean through Fram Strait. Inflow of deep waters from the Nordic Seas into the Arctic Ocean can clearly be deduced for the period between 9,000 and 3,000 years before present. Thereafter, coeval with the Neoglacial cooling trend in the northern North Atlantic region and the onset of modern Arctic sea ice production, significantly more radiogenic neodymium isotope compositions may be related to the enhanced release of ice rafted material in the eastern Fram Strait during the Late Holocene.

ZUSAMMENFASSUNG

Im Rahmen dieser Arbeit wurden zwei Sedimentkerne vom westlichen Kontinentalhang Spitzbergens (östliche Framstraße) auf Veränderungen des Oberflächen- und Tiefenwassereinstroms in die Arktis sowie die damit in Verbindung stehenden Verschiebungen der Eisgrenze während der vergangenen 9000 Jahre untersucht. Die Untersuchungen wurden anhand von mikropaläontologischen, geochemischen und sedimentologischen Methoden in multidekadischer Auflösung durchgeführt. Die Framstraße liegt zwischen Grönland und Spitzbergen und ist die einzige tiefe Verbindung zwischen dem Arktischen Ozean und den anliegenden subpolaren Meeren. Für den Energiehaushalt und die Dichteverteilung im Arktischen Ozean spielt sie daher eine entscheidende Rolle. Warmes, salines Atlantikwasser wird aus dem Süden durch die östliche Framstraße in die Arktis transportiert. Das warme Atlantikwasser führt zu ganzjährig eisfreien Verhältnissen in der östlichen Framstraße. Im Gegensatz dazu bleibt die westliche Framstraße ganzjährig von Eis bedeckt, da hier kaltes, geringer salines Oberflächenwasser aus der Arktis entlang des Grönlandschelfs nach Süden ins Europäische Nordmeer transportiert wird. Im Vergleich zum Arktischen Ozean, wo aufgrund der permanenten Eisbedeckung nur geringe Sedimentationsraten vorherrschen, führt der Temperaturgradient zwischen östlicher und westlicher Framstraße zu höheren Sedimentationsraten und vermehrter Produktion von biogenem Material. Die in der Framstraße verfügbaren, kontinuierlichen Sedimentablagerungen mit hoher zeitlicher Auflösung bieten sich somit insbesondere für die Untersuchung der Holozänen Veränderungen des Wärmeeinstroms in die Arktis an.

Die verschiedenen in dieser Arbeit verwendeten Indikatoren zeigen, dass die klimatischen und ozeanographischen Entwicklungen im Holozän vielfältiger waren, als bisher angenommen. Der veränderliche Einstrom von warmem, salinem Atlantikwasser und die Verschiebungen der Meereisgrenze standen während des gesamten Holozäns in der östlichen Framstraße deutlich miteinander in Wechselbeziehung. Die Untersuchungen legen nahe, dass der Übergang von den Umweltbedingungen im Frühholozän (etwa 11700 bis 8000 Jahre vor heute, J. v. h.) zu modernen (vorindustriellen) Bedingungen schrittweise erfolgte. Hohe relative Häufigkeiten der subpolaren planktischen Foraminiferenart *Turborotalia quinqueloba* während des Früh- und Mittelholozäns (bis etwa 5000 J. v. h.) verdeutlichen einen starken Einstrom von warmem Atlantischen Wasser in die Arktis und sind zeitgleich mit der damaligen, relativ hohen Sonneneinstrahlung. Diesem warmen Trend überlagert waren zwischen 9000 und 5000 J. v. h. wiederholte vorübergehende Kälteereignisse, beispielsweise das weithin bekannte Abkühlungsereignis vor etwa 8200 Jahren. Diese temporären Abkühlungen sind sehr wahrscheinlich auf wiederholte südostwärts gerichtete Vorstöße des polaren, gering salinen Oberflächenwassers aus der Arktis zurückzuführen.

Benthische Kohlenstoffisotopendaten deuten eine Zyklizität von etwa 550 Jahren im Tiefenwasser an, und lassen, in Übereinstimmung mit Ergebnissen von Sedimentanalysen im Nordatlantik, auf einen möglichen Zusammenhang zwischen Veränderungen im Tiefenwasser der östlichen Framstraße und Prozessen der Thermohalinen Konvektion im Europäischen Nordmeer schließen.

Moderne (vorindustrielle) Verhältnisse entwickelten sich nach 5000 J. v. H., zeitgleich mit einer verringerten Sonneneinstrahlung und dem postglazialen Meersspiegelhöchststand, der vermutlich die moderne Meereisproduktion auf den flachen Schelfen Sibiriens einleitete. Im Spätholozän, das wegen der wieder einsetzenden Vergletscherungen in der nördlichen Hemisphäre oftmals auch als Neoglazialphase bezeichnet wird, verursachten starke südostwärts gerichtete Vorstöße der Meereisgrenze sowie ein abgeschwächter Einstrom von Atlantikwasser strenge winterliche Meereisbedingungen und relativ kurze eisfreie Sommer, wie aus der Dominanz der polaren planktischen Foraminiferenart *Neogloboquadrina pachyderma* und dem deutlichen Anstieg von eistransportiertem Material abzuleiten ist.

Die klimatischen und ozeanographischen Veränderungen während der letzen 2000 Jahre sind ebenfalls durch die Wechselwirkung der Intensität des Atlantikwassereinstroms mit Verschiebungen der Meereisgrenze gekennzeichnet. Die planktischen Foraminiferendaten weisen auf stabile Verhältnisse und geringen Einfluss der Meereisgrenze während der Mittelalterlichen Warmzeit im Untersuchungsgebiet hin. Die darauf folgende Abkühlung markiert den Beginn der Kleinen Eiszeit, die in der östlichen Framstraße in zwei Phasen verlief. Der hohe Anteil von eistransportiertem Material und deutliche Schwankungen der planktischen Foraminifenhäufigkeiten in der ersten Phase (zwischen 1350 und 1750 AD, AD = anno domini) deuten auf starke Schwankungen der Eisrandlage hin. Nach etwa 1750 AD setzte eine zweite, sehr kalte Phase mit strengen winterlichen Eisbedingungen ein, an denen verstärkt auch in den Fjorden Spitzbergens gebildete Eisberge beteiligt waren. Die in den obersten Sedimentschichten beobachteten signifikanten Veränderungen in allen untersuchten Indikatoren markieren einen deutlichen Wandel der klimatischen und ozeanographischen Verhältnisse in den vergangenen Jahrzehnten. Sehr hohe relative Häufigkeiten von subpolaren planktischen Foraminiferenarten und die Anwendung von zwei voneinander unabhängigen Temperaturrekonstruktionen belegen einen Temperaturanstieg des in die östliche Framstraße einströmenden Atlantikwassers von etwa 2°C innerhalb der vergangenen etwa 120 Jahre.

Um weitere Hinweise auf Holozäne Veränderungen des Tiefenwasseraustauschs zwischen dem Europäischem Nordmeer und dem Arktischen Ozean zu erhalten, wurden an beiden Sedimentkernen zusätzlich die Isotopenverhältnisse von Neodym und Blei in Eisenmanganüberzügen an Sedimentpartikeln untersucht. Die Neodym- und Bleiüberzüge

werden durch Meerwasser erzeugt und geben daher Auskunft über die Signaturen der Quellgebiete. Für den Zeitabschnitt vor 3000 J. v. h. konnte der Einstrom von Tiefenwasser aus dem Europäischen Nordmeer in die Arktis nachgewiesen werden. Signifikant höher radiogene Neodym-Isotopenverhältnisse wurden für die Zeit nach 3000 J. v. h. ermittelt. Sie stehen möglicherweise mit der verstärkten Ablagerung von eistransportiertem Material in der Framstraße während des Spätholozäns in Verbindung.

DANKSAGUNG

In erster Linie bedanke ich mich bei Dr. Robert Spielhagen und Prof. Dr. Martin Frank für die Vergabe und Betreuung dieser Arbeit. Prof. Dr. Ralph Schneider gilt mein ausdrücklicher Dank für die Übernahme des Korreferats.

Ein ganz großes Dankeschön geht an Robert Spielhagen für die Einführung in die Welt der Framstraße und für die vielfältige Unterstützung, Beratung und Rückendeckung sowie die Einbindung in internationale Kooperationen. Bei Martin Frank bedanke ich mich ganz herzlich für die immer offene Tür und für die Beratung vor allem in Neodym-Fragen. Ein Riesendank gilt Nicolas Van Nieuwenhove für das sorgfältige Korrekturlesen der Manuskripte, vor allem aber für über drei Jahre währendes, ausdauerndes Zuhören und so manch geteiltes Mittagessen. Juliane Müller danke ich für regen wissenschaftlichen Austausch und wichtige Anhaltspunkte aus der ‚Meereis-Perspektive' sowie für die gute Zeit im Projekt überhaupt. Für konstruktive Diskussionen und unzählige fachliche und außerfachliche Gespräche, Ideen und Ratschläge geht mein besonderer Dank an Dorothea Bauch. Henning Bauch danke ich insbesondere für kritische Anregungen und Erläuterungen. Für die Einweisung in die Foraminiferen-Taxonomie bin ich Evgeniya Kandiano zu großem Dank verpflichtet. Carolyn Wegner danke ich ganz ungemein für die unentwegte Motivierung und für die regelmäßige halbe Stunde Zeit. Torben Klagge sei ausdrücklich für den ‚Rund-um-die-Uhr-Beistand" bei jeglichem technischen Hilferuf (Fleecejackenreißverschluss!) gedankt. Der gesamten ‚Kaffeerunde' danke ich für humorvolle Stunden und tausendmal erzählte Anekdoten, für die gute Gemeinschaft und Unterstützung bei jeglichen Problemen. Ein großer Dank geht an Lulzim Haxhiaj, der mich gründlichst in die Welt des zuweilen recht widerborstigen Massenspektrometers einwies und unzählige Foraminiferenschalen ‚in den Ofen schob'. Des Weiteren danke ich Claudia Teschner für die Einführung in die Welt des Reinraumlabors und der Säulenchemie sowie der ganzen Clean Lab-Mannschaft für den Beistand bei so manchen Fragen und leeren Säurebehältern. Bei Roland Stumpf bedanke ich mich insbesondere für das Inspizieren meiner Bleidaten. Weiterhin möchte ich mich vor allem bei Jan Oesterwalbesloh, Torben Struve, Marieke Göser und David Poggemann sowie weiteren studentischen Hilfskräften bedanken, ohne sie wäre diese Arbeit nicht möglich gewesen. Ein herzlicher Dank geht auch an Warner Brückmann für das Core-Logging. Katrine Husum, Katarzyna Zamelczyk und Steffen Aagaard-Sørensen danke ich für die Ermöglichung und angenehme Arbeitsatmosphäre während meines Aufenthalts in Tromsø und der Ausfahrt mit RV Jan Mayen. Ermöglicht wurde diese Arbeit durch die finanzielle Unterstützung der Deutschen Forschungsgemeinschaft (DFG) im Rahmen des Schwerpunktprogramms 1266 INTERDYNAMIK (Projekt HOVAG).

Meinen Eltern, meiner Tante und meinem Onkel sowie meinen Freunden, insbesondere Janin, Jacob und Anja, danke ich für die vielseitige Motivierung, Unterstützung und Zuversicht.

Erklärung

Hiermit versichere ich an Eides statt, dass ich diese Dissertation selbständig und nur mit Hilfe der angegebenen Quellen und Hilfsmittel und der Beratung durch meine Betreuer unter Einhaltung der Regeln guter wissenschaftlicher Praxis der Deutschen Forschungsgemeinschaft angefertigt habe. Ferner versichere ich, dass der Inhalt dieser Arbeit weder in dieser, noch in veränderter Form einer weiteren Prüfungsbehörde vorliegt.

Kiel, den 6. Oktober 2011

TABLE OF CONTENTS

1 INTRODUCTION

1.1. The Arctic Ocean – Backbone of global climate, yet highly sensitive

Currently, the Arctic Ocean is rapidly responding to global warming (e.g., Moritz et al., 2002; Polyakov et al., 2004, 2005, 2011; Polyak et al., 2009). It has been identified as one of the most sensitive areas with respect to ongoing climate changes. Consequences of the well-documented modern rise in greenhouse gases and its associated warming of the atmosphere are especially pronounced over the Arctic Ocean, a phenomenon known as 'Arctic Amplification' (Manabe and Stouffer, 1980; Serreze et al., 2007, 2009). Here, the loss of sea ice and the resulting reduction of the ice albedo generate stronger heat absorption of the ocean which again increases sea ice melt (e.g., Serreze et al., 2009). The Arctic sea ice extent is continuously declining since ~1970 (Vinje, 2001) and peaked in September 2007 (Giles et al., 2008; Stroeve et al., 2011, in press; Fig. 1.1a), most likely in response to the increase in surface air temperatures (Moritz et al., 2002; Fig. 1.1b) and the observed increased influx of warm Atlantic Water from the North Atlantic Ocean through Fram Strait during the 1990s and early 2000s (e.g., Polyakov et al., 2004; 2011; Dmitrenko et al., 2010; Fig. 1.1c). Continuing the trend of rapidly decreasing summer sea ice, this year's minimum of sea ice extent has just been reported to appear as the second lowest in the satellite record, after the year 2007 (NSDIC 2011, Fig. 1.1a).

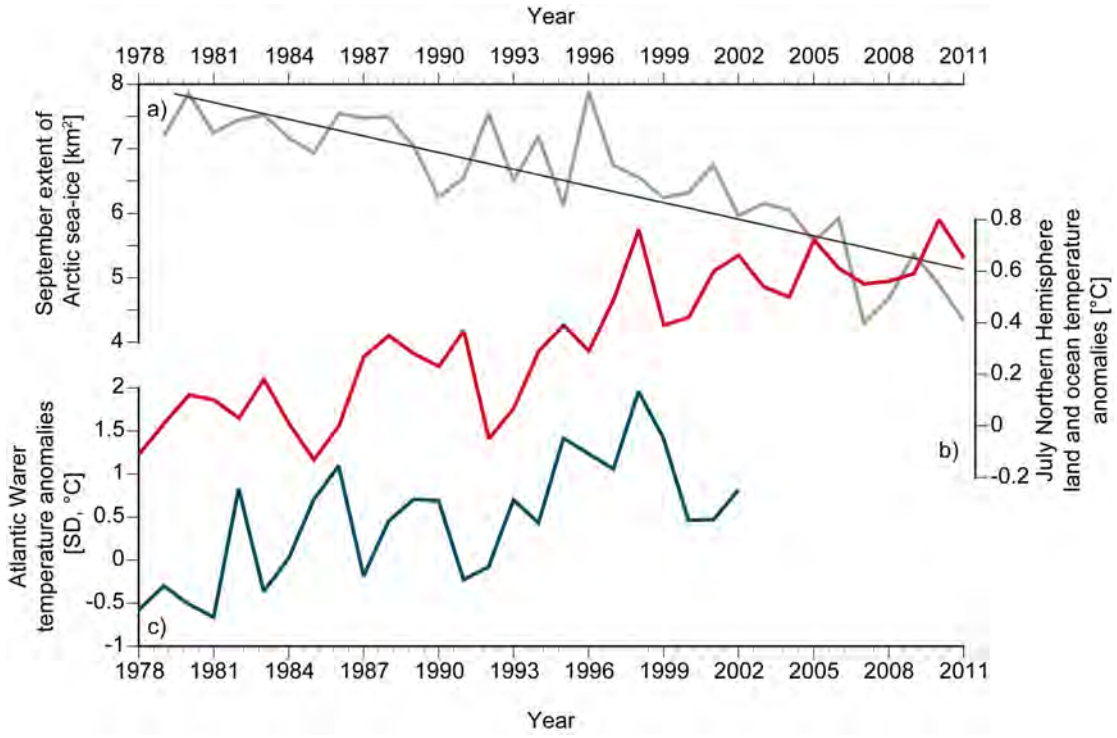

Fig. 1.1: a) Extent of Arctic sea ice in September, 1978-2011 (data from National Snow and Ice Data Center, Boulder, Colorado; Fetterer et al., 2002, updated 2009; NSDIC, 2011) **b)** July Northern Hemisphere land and ocean temperature anomalies on a 1901-2000 base period (data from National Oceanic and Atmospheric Administration (NOAA), Global Historical Climatology Network-Monthly version 3 dataset) c) Normalised 6-year running mean of Atlantic Water temperature anomalies after Polyakov et al. (2004).

Arctic sea ice coverage not only controls atmospheric and ocean surface temperatures through its albedo and insulating effects but also provides freshwater to the regions of deepwater formation in the Nordic Seas. The modern regime (hereby referring to the period prior to the 1990s' Arctic warming) of thermohaline circulation (THC) processes maintaining relatively mild winters in Northern Europe is sensitively balanced by the export of Arctic sea ice and freshwater. Only small amounts of excess freshwater added to the surface in the regions of deepwater formation are sufficient to prevent convection (Aagaard and Carmack, 1989; Lohmann and Gerdes, 1998).

During the last deglaciation, large amounts of meltwater from retreating ice sheets caused a shallower THC cell in the northern North Atlantic, and areas of deepwater formation and the sea ice margin were shifted to a southern position compared to today (Lehmann and Keigwin, 1992; Lohmann and Gerdes, 1998). Changes in North Atlantic overturning processes are also known from the near past, though compared to the last deglacial they were of modest extent (Häkkinen, 1999). During the 'Great Salinity Anomaly' in the 1960s export of enormous amounts of Arctic ice and freshwater caused a widespread freshening in the northern North Atlantic (Häkkinen, 1993, 1999). The freshening noted in the upper 500 to 800 m water depth propagated around the subpolar gyre during the following 14 years (Dickson et al., 1988; Aagaard and Carmack, 1989) and resulted in a reduction of deepwater formation in the Labrador Sea (Lazier, 1988).

Future consequences of a seasonally ice-free Arctic Ocean and a transition to a new Arctic state may include shifts not only in the Arctic's freshwater and surface energy budgets but also of atmospheric circulation and precipitation affecting the mid-latitudes (Serreze et al., 2007). Predictions of a weakened thermohaline circulation in the North Atlantic as the Arctic and sub-Arctic oceans become warmer and fresher in response to increasing atmospheric greenhouse-gas concentration were corroborated by the observation that recent changes already have lead to a sustained and widespread freshening of the deep ocean (Dickson et al., 2002). Consequences of shifts in thermohaline convection processes for future climate scenarios are much debated (e.g., Bjerknes, 1964; Delworth et al., 1993, 1997; Rahmstorf, 1995; Levermann et al., 2007; Polyak et al., 2009) but there is general consensus about a warming of the Arctic Ocean to impact climate on a global scale through a variety of climate feedback mechanisms (e.g., Moritz et al., 2002).

Knowledge about past climate variability is mandatory for understanding and modelling recent and future climate trends (Jones et al., 2001). Proxy data provide information about the mechanisms, forcing factors, and spatial and temporal ranges of past climatic variations prior to the era of instrumental measurements (Houghton et al., 1996; Jones et al., 2001). Climate variations during the Holocene period (since ca 11.7 cal ka BP) are preferably used as analogues for present-day and potential future climate scenarios since - compared to glacial periods - they

occurred under roughly the same boundary conditions and were of much smaller scale, possibly similar to variations expected in the near future.

During the past few decades a considerable amount of studies has increased our knowledge about past climatic variations of the Arctic realm (e.g., Svendsen et al., 2004b; Darby et al., 2006; Polyak et al., 2009; Miller et al., 2010). However, continuous high-resolution reconstructions of the past variability in particular of the Arctic Ocean's heat budget and sea ice extent are still lacking. Not only logistic difficulties to access the regions covered by sea ice but also low sedimentation rates and fluxes of biogenic materials (Darby et al., 2006) providing widely used paleoceanographic tools, have complicated detailed investigations of continuous high-resolution paleodata sets in the Arctic Ocean. Here, materials from the Fram Strait as the only deep connection between the North Atlantic and the Arctic Ocean may fill a gap. Through eastern Fram Strait the major fraction of heat and salt is supplied to the Arctic Ocean by warm and saline Atlantic Water inflow. In the western part of the strait, Arctic sea ice and polar surface water as well as cooled and saline Arctic intermediate and deep waters exit the Arctic Ocean towards the Nordic Seas where they play a major role for deepwater renewal processes. Strong east-west temperature gradients and a highly fluctuating sea ice margin result in higher sedimentation rates and bioproductivity in the Fram Strait. Studies of the past behaviour of its twofold current system can therefore provide substantial insight on the Arctic Ocean's variability and the interaction between the Arctic and the Nordic Seas.

1.2. Modern surface circulation and sea ice pattern in the Fram Strait

The Fram Strait between Greenland and Svalbard, often referred to as the 'Arctic Gateway', is the only deep connection between the Arctic and adjacent subpolar oceans. Serving as the major conduit for heat and salt, Fram Strait plays a crucial role for the energy budget and density pattern of the Arctic Ocean (Karcher et al., 2003; Schauer et al., 2004). Two major surface current systems characterise the hydrographic situation in the Fram Strait (Fig. 1.2). Relatively warm (2 to 6°C; Spielhagen et al., 2011) and saline (34.9 to 35.2) Atlantic Water (AW) deriving from North Atlantic Drift waters is transported by the West Spitsbergen Current (WSC) through the eastern Fram Strait into the Arctic Ocean. The WSC is topographically constrained to the Barents Sea and Spitsbergen continental slopes (Hopkins, 1991). It submerges north of 78°N beneath a cool and fresh upper mixed layer of Arctic origin and continues as a subsurface current into the Arctic Ocean (Johannessen, 1986). Part of AW propagates north and west of the Yermak Plateau as the Yermak Branch, whereas the Svalbard Branch transports AW masses northeastwards into the Arctic Ocean (Fig. 1.2; Manley, 1995; Rudels et al., 2000; Saloranta and Haugan, 2001). Atlantic Water additionally enters the Arctic via Barents Sea but the bulk heat

flux of the Arctic Ocean is carried by the WSC through Fram Strait (Schauer et al., 2004). The East Spitsbergen Current (ESC) carries cold water and sea ice from the Arctic Ocean southward along the east coast of Svalbard to the south and west around Spitsbergen (Hopkins, 1991; Loeng, 1991). Part of it, eventually mixing with brine-enriched shelf water from Storfjorden (Quadfasel et al., 1988; Schauer, 1995), joins the WSC to the west, thereby cooling and freshening the north-flowing Atlantic Water masses (Hopkins, 1991, and references therein).

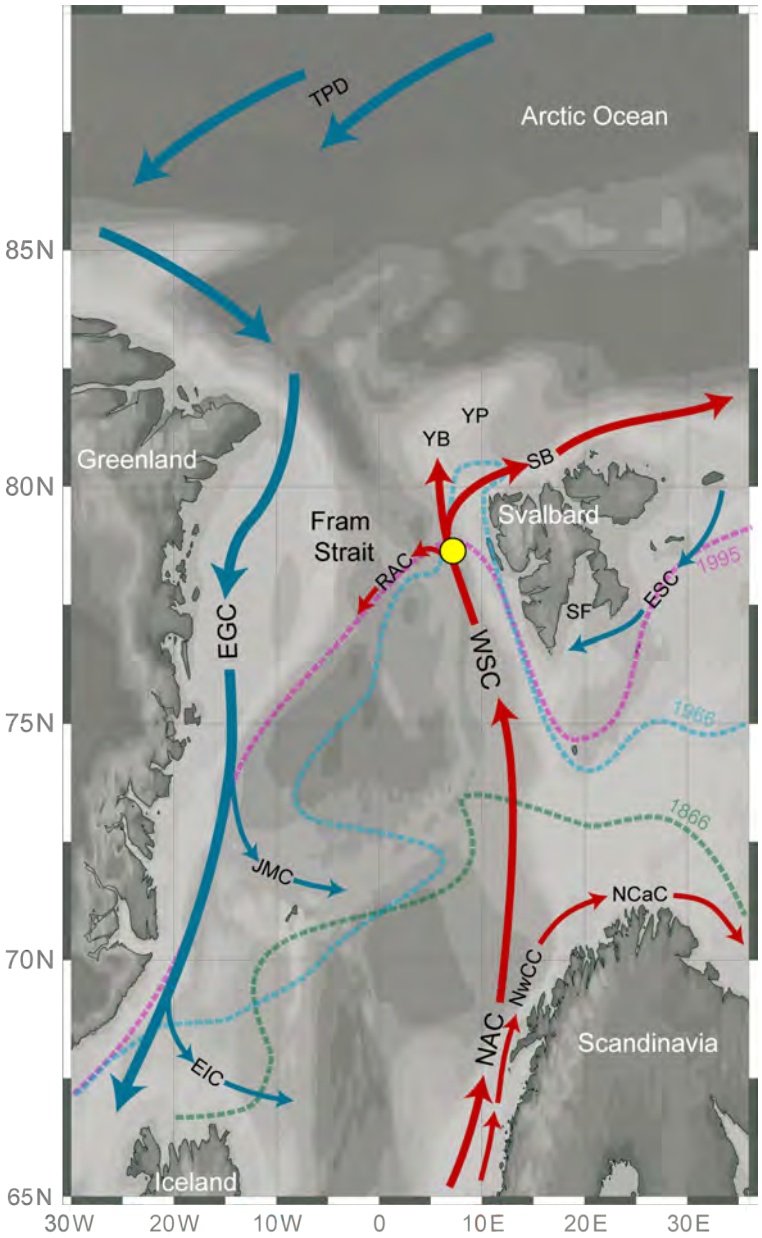

Fig. 1.2: Map of the Fram Strait with modern surface circulation and varying positions of the sea ice margin (dashed lines with year specification) during the past ca 150 years after Vinje (2001). Red arrows indicate warm and saline Atlantic Water, blue arrows mark cold and fresh outflow of polar surface waters. Yellow dot marks study site discussed in this thesis. AW=Atlantic Water, EGC=East Greenland Current, EIC=East Icelandic Current, ESC=East Spitsbergen Current, JMC=Jan Mayen Current, NAC=North Atlantic Current, NCaC=North Cape Current, NwCC=Norwegian Coastal Current, RAC=Return Atlantic Current, SB=Svalbard Branch, WSC=West Spitsbergen Current, YB=Yermak Branch, YP=Yermak Plateau.

In the western Fram Strait, the East Greenland Current (EGC) transports Arctic sea ice and polar waters with temperatures close to freezing point and salinities below 34.4 in the upper 400 m water depth (Schlichtholz and Houssais, 1999; Rabe et al., 2009) southward along the Greenland continental slope into the Nordic Seas where minor currents such as the Jan Mayen Current and the East Icelandic Current branch off eastward (Fig. 1.2; Hopkins, 1991).

Strong recirculation of Atlantic Water to the south takes place in the northern part of Fram Strait. At the western edge of the WSC meso-scale eddies are generated which carry Atlantic Water westward across the Fram Strait (Johannessen et al., 1987). This part of cooled, dense AW submerges in the central and western Fram Strait beneath the cold, ice-covered EGC waters and flows as the subsurface Return Atlantic Current southward where it contributes to deepwater formation processes in the Nordic Seas (Gascard et al., 1988; Carstens et al., 1997; Marnela et al., 2008).

The complex hydrographic regime of two strongly contrasting surface/subsurface ocean currents results in a distinct seasonal sea ice distribution pattern and significant fluctuations of the sea ice margin in the Fram Strait (Fig. 1.2). Melting effects of the Atlantic layer advected into the Arctic Ocean through eastern Fram Strait control the sea ice extent in the eastern Fram Strait; at present large areas in the west and north of Svalbard remain ice-free all year (Steele and Boyd, 1998; Saloranta and Haugan, 2004). In contrast, the western part of Fram Strait is perennially covered by sea ice due to steady export of polar surface waters and sea ice by the EGC. During the past ca 150 years the position of the sea ice margin in the eastern Fram Strait has varied significantly (Vinje, 2001; Fig. 1.2), most likely in response to the intensity of the inflowing warm Atlantic Water.

1.3. State of the art: Climate variability in the (sub-)Arctic during the deglacial and Holocene intervals

The onset of the Holocene is usually defined by the end of the Younger Dryas cold episode about 11.7 ka ago (Rasmussen et al., 2006). The transition from the Last Glacial Maximum (LGM) at about 20 ka to modern conditions was caused by orbitally driven variations of insolation. Maximum summer insolation occurred at about 10 ka and has been declining since then (Berger and Loutre, 1991). Accordingly, warmest conditions during the Early Holocene led to intense melting of large parts of the Arctic ice sheets surrounding the Arctic Ocean (Koerner and Fisher, 1990, 2002; Svendsen et al., 2004b). Holocene thermal maximum (HTM) conditions have been reported from many (sub-)Arctic sites for the Early Holocene interval (Eurasian Arctic: e.g., Polyak and Mikhailov, 1996; Pisaric et al., 2001; Andreev et al., 2009; Nordic Seas

and Fram Strait: e.g., Birks and Koç, 2002; Moros et al., 2004, 2006; Hald et al., 2007, Ślubowska-Woldengen et al., 2008; for the Arctic Ocean: e.g., Cronin et al., 2010a; for northern North America: e.g., Koerner and Fisher, 1990; Kerwin et al., 2004), though with spatial and temporal differences (Kaufman et al., 2004; Williams et al., 2011). Early Holocene temperatures exceeded those of the 20th century average by 1.3 to 3.5°C (Koerner and Fisher, 2002; Kaufman et al., 2004).

As the LGM sea level was about 120 m lower than present (Fairbanks, 1989; Lambeck et al., 2002) increasing atmospheric temperatures and the widespread ice melt caused a progressive sea level rise throughout the deglacial and the Early and Mid-Holocene which had a substantial impact on the formation of the modern current system and climate, including the inflow of relatively warm Pacific Water to the Arctic Ocean resulting from the re-opening of the shallow Bering Strait due to the sea level increase at 13.4 to 13.2 cal ka BP (England and Furze, 2008).

Large parts of the Arctic shelves were covered by ice sheets during the LGM but the Eurasian continental margins east of Taymyr Peninsula were exposed subaerially due to the lowered sea level (Bauch et al., 2001b; Svendsen et al., 2004b). During the Early Holocene, the Laptev Sea shelf became gradually flooded in response to increasing temperatures and the postglacial sea level rise (Bauch et al., 1999, 2001b; Spielhagen et al., 2005). Until ca 10 ka increased deposition of plant debris and terrestrial organic matter unveiled river discharge and coastal erosion as the dominant sediment sources the Laptev Sea continental margin (Bauch et al., 1999; Stein et al., 2001). The onset of postglacial marine transgression was marked by the first appearance of marine bivalves at ca 10 ka (Bauch et al., 1999). Shelf flooding lasted until ca 6 ka, indicated by gradually increasing TOC content and $\delta^{13}C_{org}$. After 6 to 5 cal ka BP low sedimentation rates reflected full marine conditions associated with maximum Holocene sea level (Bauch et al., 1999; 2001b) and probably increased Atlantic Water inflow onto the Laptev Sea shelf (Stein et al., 2001).

Atlantic Water advection through Fram Strait to the Arctic basin continuously increased during the Early Holocene, driven by maximum insolation and wind force and/or thermohaline circulation (Ślubowska et al., 2005). This is in contrast to the strongly reduced heat flux to the sea ice covered Arctic Ocean during the LGM when Atlantic Water entered only as a narrow coastal current along the Eurasian coast reaching not farther than 84 to 85°N (Nørgaard-Pedersen et al., 2003). Marine studies from the north, west and south of Svalbard agree on warmest sea surface temperatures during the Early Holocene commencing ~10 cal ka BP (e.g., Bauch et al., 2001a; Hald et al., 2004, 2007; Ślubowska et al., 2005; Ebbesen et al., 2007; Rasmussen et al., 2007; Ślubowska-Woldengen et al., 2007, 2008) in accordance with findings of thermophilous molluscs

on Svalbard after 10 cal ka BP (Salvigsen et al., 1992; Salvigsen, 2002). Most studies also indicate a cooling trend after ~8 cal ka BP (Hald et al., 2004; Ślubowska-Woldengen et al., 2007). However, a significantly warmer Mid-Holocene and thus probably an increased heat flux to the Arctic Ocean had been detected by some studies from the Barents Sea/Svalbard area, suggesting temperatures higher than for the remainder of the Holocene, though not approximating those of the Early Holocene (e.g., Sarnthein et al., 2003; Hald et al., 2007; Rasmussen et al., 2007).

Except for local ice caps over Svalbard, Franz Josef Land and possibly Novaya Zemlya the marine-based Barents-Kara ice sheet had probably disappeared after the Younger Dryas cooling (Svendsen et al., 2004a). Early deglaciation of northwestern Spitsbergen commenced at about 13 ka whereas the Svalbard-Barents Sea Ice Sheet retreated not before 10.5 to 10 ka from eastern Svalbard (Forman et al., 2004; Landvik et al., 2005). Maximum paleosalinities recorded between 7.5 and 6 cal ka BP were probably associated with enhanced influx of Atlantic Water to the Kara Sea (Polyakova and Stein, 2004). In accordance to findings from the Laptev Sea shelf, on the southern Kara Sea the sea level highstand has been also determined to about 6 to 5 cal ka BP (Stein et al., 2002, 2004; Simstich et al., 2004).

The Arctic regions of North America were strongly influenced by the collapse of the Laurentide Ice Sheet (LIS) during the deglacial and Holocene periods which started about 14 ^{14}C ka BP (17.0 to 16.5 cal ka BP; Dyke et al., 2002). While earliest indications of Holocene thermal maximum conditions have been reported from Beringia prior to the onset of the Holocene between 14 and 13 ka, the onset of the HTM was delayed in central and eastern Canada probably due to the cooling effect of the adjacent LIS (Kaufman et al., 2004).

The Nordic Seas were largely influenced by the deglacial and Holocene development of both, the retreating Laurentide Ice Sheet to the west and the Fennoscandian Ice Sheet to the east. Northward flow of Atlantic Water through an ice-free corridor persisted probably since ca 14.5 cal ka BP throughout the Holocene with variable strength and geographic distribution (Ślubowska-Woldengen et al., 2008; Koç et al., 1993). A prominent cold event at about 8.2 cal ka BP was noted in Greenland ice core and in many records from the northern North Atlantic (Alley et al., 1997; Risebrobakken et al., 2003; Hall et al., 2004; Moros et al, 2004; Hald et al., 2007; Kleiven et al., 2008). It has been linked to a major outburst drainage from the glacial lakes Agassiz/Ojibway during the final collapse of the LIS and a subsequent discharge of large amounts of meltwater into the Labrador Sea and the North Atlantic (Stuiver et al., 1995; Barber et al., 1999; Rohling and Pälike, 2005).

During Holocene maximum conditions in the Nordic Seas the sea ice cover and oceanic fronts probably retreated to a northwestern position hereby opening the major pathway for surface Atlantic Water advection along the Norwegian coasts and the Barents Sea shelf towards

Svalbard and the Arctic Ocean (Koç et al., 1993; Ślubowska-Woldengen et al., 2008). A recent review of foraminifer-based studies of Holocene trends in the northern North Atlantic showed that reconstructions of maximum summer sea surface temperatures do not indicate a consistent pattern of early to Mid-Holocene warm conditions (Andersson et al., 2010). In the Nordic Seas, indications of optimum sea surface temperatures vary between 11 and 5 cal ka BP (e.g., Koç et al., 1993; Andersen et al., 2004; Hald et al., 2007; Ślubowska-Woldengen et al., 2008), a confusion which may have been caused by the application of various proxies reflecting conditions of different habitat depths in surface and subsurface water layers (Andersson et al., 2010). In addition, the oceanic circulation in the Nordic Seas has been influenced by the 'seesaw effect' (van Loon and Rogers, 1978) during most of the Holocene (e.g., Seidenkrantz et al., 2007, 2008) which may have caused further inconsistencies in paleoceanographic reconstructions.

Bond et al. (1997, 2001) suggested that southward advances of polar waters indicated by an increased discharge of ice-rafted debris into the Nordic Seas correlates with times of diminished solar output (as seen from proxies of solar irradiance such as ^{10}Be and ^{14}C) at intervals of about 1,500 years. However, later studies do not reveal a clear correlation of millennial-scale cyclicity in solar output and drift ice signals and possibly impacts on the North Atlantic Deep Water formation (e.g., Risebrobakken et al., 2003; Andrews et al., 2006, Polyak et al., 2009). No consistent evidence of significant Holocene climate cyclicity has been found so far in the northern North Atlantic (e.g., Schulz et al., 2004; Wanner et al., 2011). In a statistical analysis of worldwide distributed proxy time series, Wanner et al. (2011) found indications for several cold relapses which interrupted periods of relatively stable and warmer climate during the Holocene at ca 8.2, 6.5 to 5.9, and 4.8 to 4.5 ka BP. The cold relapses were, however, not of strictly regular or cyclic appearance but may be caused by a combination of decreasing solar insolation, possibly a slow-down of the thermohaline circulation, regional effects and possibly feedbacks (Wanner et al., 2011).

At about 6 ka, sea level and ice volume were close to modern ones (e.g., Miller et al., 2010), and the modern-type sea ice stream trajectories of the Transpolar Drift (TPD) and the Beaufort Gyre (BG) were established, as concluded from driftwood pathways across the Arctic (Dyke et al., 1997). Consistent with the decreasing summer insolation during the Late Holocene, conditions cooler and more stable prevailed, compared to the preceding Early and Mid-Holocene intervals, and were accompanied by re-advances of glaciers and increased abundance of sea ice (e.g. Koç and Jansen, 1994; Bauch et al., 2001a; Jennings et al., 2002; Andersson et al., 2003; Miller et al., 2005; Seidenkrantz et al., 2007; Sicre et al., 2008; Vinther et al., 2008). The Late Holocene, also referred to as the 'Neoglacial', peaked in the Little Ice Age cooling with coldest conditions between ~1400 and 1900 AD (Bradley et al., 2003, Klitgaard Kristensen et al., 2004;

Moberg et al, 2005; Mann et al., 2009). Studies of Svalbard glaciers have elucidated the LIA glaciation as the most extensive Late Holocene glacier advance recognised on Spitsbergen while during the Early and Mid-Holocene the glacier coverage had been strongly reduced (Tarussov, 1992; Werner, 1993; Svendsen and Mangerud, 1997; Isaksson et al., 2005). Northern hemisphere temperatures of the LIA (1600 AD) were about 0.7 K below the average of 1961-90 (Moberg et al., 2005).

Beside the general cooling trend during the Late Holocene, there have been also warmer periods during the Late Holocene, such as the Medieval Climate Anomaly (MCA) between ca 950 and 1250 AD (e.g., Lamb, 1965; Dahl-Jensen et al., 1998; Eiriksson et al., 2006; IPCC, 2007; Sicre et al., 2008; Bjune et al., 2009, Cronin et al., 2010b). The MCA is of particular interest for climate researchers and many studies have focussed on the question if northern hemisphere temperatures of the MCA were as high as those of the Modern Warming (Hughes and Diaz, 1994; Broecker, 2001; Moberg et al., 2005; IPCC, 2007; Mann et al., 2009). Recent results, however, suggest that Medieval warmth was heterogeneous in terms of its precise timing and regional expressions (IPCC, 2007), and it probably did not exceed temperatures of the post-1990 period in the northern hemisphere (Moberg et al., 2005).

The distinct temperature increase in the 20th century not only in (sub-)Arctic regions but also on a global scale was the strongest of the past two millennia and reversed an overall cooling trend which was caused by continuously decreasing insolation (Overpeck et al., 1997; Moberg et al., 2005, Kaufman et al., 2009). Modelling studies show that a continuous ongoing greenhouse-gas induced temperature rise may lead to an ice-free Arctic Ocean during summer in the 21th century and possibly already in the next few decades (Holland et al., 2006; Stroeve et al., 2007, in press; Comiso et al., 2008).

1.4. Research questions and outline of the thesis

The purpose of this study was to derive high-resolution information on the Holocene climate and oceanographic variability in the eastern Fram Strait as the main pathway of Atlantic Water to enter the Arctic Ocean. Two AMS radiocarbon dated sediment cores (box core MSM5/5-712-1 and kastenlot core MSM5/5-712-2) obtained from the western Svalbard continental margin (78°54.94'N, 6°46.04'E, 1490.5 m water depth) during cruise leg MSM5/5 with RV „Maria S. Merian" in summer 2007 were studied by means of surface and deepwater proxies such as planktic foraminifer assemblages, planktic and benthic stable isotope signatures, lithological parameters, and radiogenic isotope tracers.

The presented thesis addresses the following research questions:

- How was the Holocene climate and oceanographic variability expressed in the eastern Fram Strait with regard to the intensity of Atlantic Water advection and related fluctuations of oceanic heat flux to the Arctic Ocean?
- How did the sea ice margin and associated changes of marine productivity during the Holocene respond to variable Atlantic Water inflow?
- How did surface, subsurface and bottom water mass intensity, stratification and temperature vary during the past ca 9,000 years?
- Were the changes consistent to global climate variations during the Holocene or did special "Arctic" features appear to be superimposed on general trends?
- Are the ongoing climate changes and the amplified warming of the Arctic Ocean exceptional with respect to the climate variability during the past two millennia and before?
- Did the variability follow distinct cycles in the frequency range of decades to millennia?
- Can radiogenic isotope tracers (Nd, Pb) help to determine past variability of deepwater exchanges between the Nordic Seas and the Arctic Ocean through Fram Strait?

This thesis is divided into two introduction chapters (**Chapter 1 and 2**) and four chapters presented in the form of manuscripts that either have been published or are in general state for submission (**Chapter 3 to 6**). **Chapter 1** includes a short description of a changing Arctic Ocean as the motivation for research work presented here (1.1), a brief overview of the hydrographic pattern in the Fram Strait (1.2), a summary of the Holocene climate and oceanographic variability in the northern high latitudes compiled from the literature (1.3.), the outline of the thesis (this section), and a synthesis where the main results of this study are summarized (1.5). In **Chapter 2** a detailed description of the methods applied within this study is presented.

Chapter 3 encompasses a high-resolution study on a sediment sequence from the Western Svalbard margin covering the last two millennia (published in *Palaeogeography, Palaeoclimatology, Palaeoecology*). Several co-authors contributed to this chapter. My contribution comprised the preparation of the samples (sieving procedures etc.), counting of planktic foraminifer fauna in size fraction 100-250 μm and IRD contents, collecting planktic foraminifer tests in preparation of AMS radiocarbon datings and for stable isotope measurements, and interpreting the data and writing the manuscript. Individual inputs by the co-authors to this chapter were as follows: D. Bauch provided fundamental assistance on the calculation of sea surface salinities and modern equilibrium calcite $\delta^{18}O$ ad $\delta^{13}C$ values. H.C. Hass provided sortable silt mean grain size data. E. Kandiano carried out the estimation of sea surface temperatures by the SIMMAX transfer function based on countings of planktic foraminifers in size fraction 150-250 μm performed by

K. Zamelczyk. All co-authors were included in the process of writing and contributed by many discussions, corrections, and suggestions to improve the manuscript.

The unprecedented warming in the eastern Fram Strait in the last ca 150 years in contrast to the climate and oceanographic development within last 2,000 years is discussed in **Chapter 4** (published in *Science*). To this study I contributed as a co-author by preparing the samples (sieving procedures etc.), providing percentage and flux data of planktic foraminifer fauna in size fraction 100-250 μm as well as with discussions and suggestions to improve the manuscript.

Focus of **Chapter 5** is the variability of Atlantic Water advection during the past 9,000 years studied on a high-resolution sediment sequence from the West Spitsbergen continental margin. To this chapter I contributed as follows: sampling of the sediment core, counting planktic foraminifers in size fraction 100-250 μm, measuring the main part of stable isotopes at a Finnigan MAT 253 mass spectrometer system (IFM-GEOMAR), conducting the time series analyses, interpreting the data and writing the manuscript. R. F. Spielhagen contributed with many valuable discussions and profound suggestions to improve the manuscript. H.C. Hass provided the sortable silt mean size data and valuable comments on the manuscript, and T. Struve conducted part of the planktic foraminiferal census data. In addition, several student assistants helped in the laboratory and preparation work.

Chapter 6 consists of a first investigation of seawater-derived radiogenic isotope compositions stored in coatings of sediment particles in the eastern Fram Strait. My contribution to the manuscript included sampling of the sediment core, preparing the samples for radiogenic isotope measurements, interpreting the data and writing the manuscript. C. Teschner carried out the measurements of the radiogenic isotope signatures and greatly contributed by providing major assistance and detailed instruction on the sample preparation. M. Frank and R. F. Spielhagen contributed with many valuable discussions and profound suggestions to improve the manuscript. Proxy data used in this manuscript for comparison with radiogenic isotope data are the same as in Chapter 3 and 5.

1.5. Synthesis/Major results of this study

The results obtained by the research presented here contribute to an improved understanding of the climate variability in the eastern Fram Strait and the Arctic Ocean during the past ca 9,000 years. Holocene climate and oceanographic development in the eastern Fram Strait was much more variable than previously concluded from proxy records and the characteristics of the Greenland ice core records. The data presented in this thesis suggest the variation and interaction between warm and saline advection of Atlantic Water at the surface to subsurface into the Arctic Ocean and a correspondingly fluctuating sea ice margin characterise

the eastern Fram Strait throughout the Holocene. Continuous abundance of the subpolar planktic foraminifer species *Turborotalia quinqueloba*, indicative of Atlantic Water inflow in the eastern Fram Strait (Volkmann, 2000), document the uninterrupted inflow of Atlantic Water to the Arctic Ocean via Fram Strait during the past 9 ka.

According to the results presented in chapter 5, the transition from the Early Holocene thermal optimum conditions to the modern oceanographic situation in the Fram Strait occurred stepwise, most probably in response to the postglacial sea level rise and the related onset of modern sea ice production on the shallow Siberian shelves. A first phase comprised the relatively warm late Early and Mid-Holocene intervals (9 to 5 ka) and was characterized by rather unstable conditions. Prior to 5 ka, remarkably high presence of the subpolar planktic foraminifer *T. quinqueloba* suggests high heat flux to the Arctic basin by strong inflow of warm and saline Atlantic Water and/or high temperatures of the inflowing AW, in response to maximum insolation during the Early Holocene (Berger and Loutre, 1991). Light oxygen isotope values derived from the planktic foraminifer species *Neogloboquadrina pachyderma* (sinistral coiling) were probably linked to warmer sea surface temperatures of the inflowing AW but may also indicate increased addition of cold and fresh water to surface waters due to postglacial retreat of ice sheets.

Superimposed on the optimum conditions, planktic foraminifer data infer repeated short-lived cold events such as the well-known '8.2 ka cold event'. While the cooling at ~8.2 ka was caused by the final break-up of the Laurentide Ice Sheet and extensive release of meltwater into the North Atlantic (Stuiver et al., 1995; Barber et al., 1999; Rohling and Pälike, 2005), other cooling pulses at 6.9, 6.1, and 5.2 cal ka BP which were partly of '8.2 ka'-character were probably associated with a southeast advance of the polar front and the sea ice margin. Consistent with the decreasing insolation, a slightly lowered presence of *T. quinqueloba* after ~8 ka implies a modest temperature reduction and/or weakening of the inflowing AW. Relatively strong Atlantic Water advection and/or high AW temperatures, however, prevailed until ca 5.2 cal ka BP.

After the cooling event at 5.2 cal ka BP, modern (pre-industrial) conditions established, simultaneous to the complete postglacial flooding of Arctic shallow shelves and the initiation of modern sea ice production. Related to the onset of Neoglacial conditions, after ~5 cal ka BP more stable but significantly cooler conditions with increased abundances of sea ice/icebergs and strong stratification of the water column prevailed in the eastern Fram Strait indicated by the uninterrupted dominance of the polar planktic foraminifer species *N. pachyderma* (sin.), increased ice-rafted debris (IRD) contents, and increasing differences of planktic and benthic stable isotope values. During that time, strong advances of Arctic sea ice and polar water transported southeastward by the ice-covered East Greenland Current probably caused heavy winter sea ice

conditions and relatively short ice-free summer seasons in the eastern Fram Strait, most likely in combination with a weaker/subsiding subsurface Atlantic Water inflow and/or inflow of cool Atlantic Water. A slight strengthening of AW inflow after ~3 cal ka BP seen in planktic foraminifer assemblages coincides with the establishment of a low-density upper surface layer and an associated density-driven migration of planktic foraminifers to lesser ventilated subsurface water masses, as concluded from lower planktic carbon isotope values. The drop in planktic $\delta^{13}C$ values is in accordance with other records from the northern North Atlantic (e.g., Bauch and Weinelt, 1997; Bauch et al., 2001a; Sarnthein et al., 2003) and may imply a wider distribution of an upper low-salinity layer in the Nordic Seas and the Fram Strait, potentially associated with reduced evaporation due to cooler atmospheric temperatures during the Late Holocene.

A second study (chapters 3 and 4) focussed on a closer inspection of the climate and oceanographic variability during the past 2,000 years on the Western Svalbard margin. Compared to the Early and Mid-Holocene interval, climate variability within the past two millennia has been of much lower amplitude. However, the obtained proxy datasets imply that distinct changes occurred which were linked to the interaction between a variable intensity of Atlantic Water inflow and fluctuations of the sea ice margin. In parts, detected variations of eastern Fram Strait climate and oceanographic conditions could be correlated to climate intervals in Europe and the North Atlantic. Stepwise increasing IRD contents point to increasing iceberg/sea ice abundance over the study site, confirming a Neoglaciation trend which has been documented also by other studies from the North Atlantic area (e.g., Seppä and Birks, 2001; Jennings et al., 2002; Moros et al., 2004; Seidenkrantz et al., 2008, Andrews et al., 2009, 2010). High and strongly variable planktic foraminifer fluxes and increased IRD fluxes indicate that the study site was probably located in the area of a fluctuating ice margin from ~1 to 700 AD and from ~1350 to 1730 AD.

The well-known Medieval Warm Period (also referred to as the Medieval Climate Anomaly, MCA) was characterized in general by more stable conditions concluded from lower and less variable planktic foraminifer fluxes. Planktic foraminifer assemblages, however, showed that conditions during the MCA varied between warmer (1000-1200 AD, after 1300 AD) and cooler (1200-1300 AD) periods.

The Little Ice Age period apparently occurred in two phases in the eastern Fram Strait. A first phase lasting from ~1350 to 1750 AD was characterized by high IRD contents and high planktic foraminifer fluxes pointing to cold conditions and a fluctuating sea ice margin at the site. After ~1750 AD a second, very cold phase established, as seen from very low planktic foraminifer fluxes and high IRD contents. Heavy sea ice conditions which have been also reported from historical observations and instrumental records (e.g., Vinje, 2001) prevailed over the study site probably in combination with increased iceberg abundance generated by advancing

Svalbard glaciers. Low fluxes and planktic foraminifer percentages of the 100-250 μm size fraction suggest that cool surface water conditions of the LIA prevailed well into the 20th century.

Highest relative abundance of subpolar planktic foraminifer species in the uppermost sediment layer of box core 712-1 point to unprecedented strong oceanic heat advection during the past ~150 years associated with the polar amplification of global warming (Chapters 3 and 4). In Chapter 4 the modern warming related to strengthened Atlantic Water inflow and/or warmest temperatures of advected AW to the Arctic Ocean is discussed. Two independent temperature reconstruction methods, the SIMMAX modern analogue technique (Pflaumann et al. 1996) applied on planktic foraminifer assemblages, and Mg/Ca measurements on the planktic foraminifer species *N. pachyderma* (sinistral) reveal a temperature increase of ~2°C within the past ~120 years. Changes in all studied proxies presented in Chapters 3 and 4 confirm a strong climate shift during the past few decades, most likely associated with increased heat flux to the Arctic Ocean, and coincide with positive Atlantic Water temperature anomalies and a retreating sea ice margin for the ca last 100 years (Divine and Dick, 2006; Polyakov et al., 2004, 2005).

The proxy datasets presented in Chapters 3 and 4 indicate that the strong modern heat flux to the Arctic Ocean by far exceeds the variability of MCA climate conditions between ~1000 and 1200 AD, consistent with the authors of the IPCC (2007) who presume that the warmest period prior to the 20th century likely occurred between 950 and 1100 AD. Comparison of the modern rise of subpolar planktic foraminifers with the observed high percentages of *T. quinqueloba* during the Early and Mid-Holocene intervals is critical because of strongly different climate regimes. During the Early Holocene intervals maximum insolation probably caused extraordinary high surface air and ocean temperatures. Also, the thermohaline circulation regime was in a transitional state since areas if deepwater formation were located further south during the last deglaciation (Jones and Keigwin, 1988; Lehmann and Keigwin, 1992; Lohmann and Gerdes, 1998). The modern sea level was only attained between ca 6 and 5 cal ka BP (Bauch et al., 1999; Stein et al., 2004) which had implications for a restricted sea ice production in the Arctic Ocean during the Early Holocene phase. In contrast, modern oceanic and climate conditions since ca 5 ka are characterised by reduced summer insolation (Berger and Loutre, 1991; Kaufman et al., 2004) in combination with intensive thermohaline-controlled overturning processes in the Nordic Seas as a major driver of the global climate (Broecker, 1991). The recent changes in the Arctic appear especially anomalous since orbital changes have made ice melting less likely at present than during past millennia since the deglacial (Polyak et al., 2009). Early to Mid-Holocene conditions were thus strongly different from present-day oceanic and climate

conditions and cannot serve as an appropriate analogue for the modern amplified warming in the Arctic Ocean.

In addition to the multiproxy investigations discussed above, the sediment cores 712-1 and 712-2 were studied for seawater-derived neodymium and lead isotope compositions stored in ferromanganese oxyhydroxide coatings of the sediment particles in order to test if this method can further the reconstruction of Holocene variations of exchanges between the Nordic Seas and the Arctic Ocean through Fram Strait (chapter 6). The radiogenic isotope data were combined with a multitude of proxy indicators for the climatic and oceanographic development of the eastern Fram Strait during the past 8,500 years revealed from chapters 3, 4, and 5 to extend the proxy dataset by a relatively new method that has been already applied successfully to pre-Quaternary and Quaternary sediments from the Arctic Ocean and North Atlantic (Winter et al., 1997; Haley et al., 2007; Crocket et al., 2011). In order to obtain a calibration of the Nd and Pb isotope compositions extracted from the sediments to modern bottom water mass signatures in the area, a set of core top samples from different water depths in the eastern Fram Strait was additionally investigated for present-day Nd and Pb isotope signatures. Core top samples revealed relatively high (radiogenic) neodymium isotope compositions between -9.7 and -9.1 which correspond well to radiogenic downcore isotope signatures between -9.1 and -8.8 of the uppermost ca 40 cm (ca the past 2,000 years). In contrast, downcore data prior to 2 cal ka BP display lower (less radiogenic) neodymium isotope ratios between -10.6 to -10.1, similar to present-day seawater in the Nordic Seas. A significantly higher inflow of deepwater produced in the Nordic Seas to the core site is thus inferred for the earlier periods of the Holocene. Three hypotheses are discussed in chapter 6 for the radiogenic neodymium isotope compositions after 2.8 cal ka BP. Increased boundary exchange of seawater with basaltic formations at the margins of the Nordic Seas (hypothesis 1) or increased inflow of Canadian Basin Deep Water which carries a Pacific component (hypothesis 2) are potential reasons but can neither be proved nor disproved in the framework of the study presented in chapter 6. A third and favoured explanation considers the Fram Strait as a major ablation area for ice-rafted material entrained by Arctic sea ice and later delivered by the Transpolar Drift ice stream to the Fram Strait. As indicated by other proxies, the marked shift to more radiogenic neodymium isotope compositions occurs coeval with the well-known Late Holocene Neoglacial trend in the northern North Atlantic region and the onset of modern Arctic sea ice production. Enhanced contribution of sea ice-rafted fine (IRF) material to bottom sediments at the investigated site during the Late Holocene is consistent with the general increase in sea ice abundance in the eastern Fram Strait (Chapters 3, 4 and 5) and in the northern North Atlantic (Seppä and Birks, 2001; Jennings et al., 2002; Moros et al., 2004; Seidenkrantz et al., 2008). Possible source areas for highly radiogenic

IRF are the shallow Siberian shelves where at present the main production of sea ice occurs. In particular, the Kara Sea shelf which today has seawater neodymium isotope compositions of -6 to -5 (Porcelli et al., 2009) may serve as a potential source area for the radiogenic neodymium isotope values of the IRF material. Low $^{206}Pb/^{204}Pb$ values (~18.4) in the investigated core top samples and within the uppermost ca 15 cm of the sediment core document an overprint of anthropogenic lead, as seen also in other studies from the North Atlantic and the Arctic Ocean (e.g., Hamelin et al., 1990; Alleman et al., 1999; Gobeil et al., 2001), and indicate bioturbation mixing in the uppermost sediment layer. Higher $^{206}Pb/^{204}Pb$ values (>19.0) during the warm Early and Mid-Holocene periods may be related to enhanced chemical weathering on Svalbard and increased glacial and riverine input of young granitic (more radiogenic) material to the West Spitsbergen margin.

References

Aagaard, K. and Carmack, E.C. (1989) The Role of Sea ice and Other Fresh Water in the Arctic Circulation. *Journal of Geophysical Research* 94/C10, 14485-14498.

Alleman, L.Y., Véron, A.J., Church, T.M., Flegal, A.R. and Hamelin, B. (1999) Invasion of the abyssal North Atlantic by modern anthropogenic lead. *Geophysical Research Letters* 26, 1477-1480.

Alley, R.B., Mayewski, P.A., Sowers, T., Stuiver, M., Taylor, K.C. and Clark, P.U. (1997) Holocene climatic instability: A prominent, widespread event 8200 years ago. *Geology* 25/6, 483-486.

Andersen, C., Koç, N. and Moros M. (2004) A highly unstable Holocene climate in the subpolar North Atlantic: evidence from diatoms, *Quaternary Science Reviews* 23, 2155-2166.

Andersson, C., Risebrobakken, B., Jansen, E. and Dahl, S.O. (2003) Late Holocene surface ocean conditions of the Norwegian Sea (Vøring Plateeau). *Paleoceanography* 18/2, 1044.

Andersson, C., Pausata, F.S.R., Jansen, E., Risebrobakken, B. and Telford, R.J. (2010) Holocene trends in the foraminifer record from the Norwegian Sea and the North Atlantic Ocean. *Climate of the Past* 6, 179-193.

Andreev, A.A., Grosse, G., Schirrmeister, L., Kuznetsova, T.V., Kuzmina, S.A., Bobrov, A.A., Tarasov, P.E., Novenko, E.Y., Meyer, H., Derevyagin, A.Y., Kienast, F., Bryantseva, A. and Kunitsky, V.V. (2009) Weichselian and Holocene palaeoenvironmental history of the Bol'shoy Lyakhovsky Island, New Siberian Archipelago, Arctic Siberia. *Boreas* 38, 72-110.

Andrews, J.T., Jennings, A.E., Moros, M., Hillaire-Marcel, C. and Eberl, D. (2006) Is there a pervasive Holocene ice-rafted debris (IRD) signal in the northern North Atlantic? The answer appears to be either no, or it depends on the proxy! *PAGES Newsletter* 14, 7-9.

Andrews, J.T., Belt, S.T., Olafsdottir, S., Massé, G. and Vare, L.L. (2009) Sea ice and marine climate variability for NW Iceland/Denmark Strait over the last 2000 cal. yr BP. *The Holocene* 19, 775-784.

Andrews, J.T., Jennings, A.E., Coleman, G.C. and Eberl, D.D. (2010) Holocene variations in mineral and grain size composition along the East Greenland glaciated margin (ca 67°-

70°N): local versus long-distance sediment transport. *Quaternary Science Reviews* 29, 2619-2632.

Barber, D.C., Dyke, A., Hillaire-Marcel, C., Jennings, A.E., Andrews, J.T., Kerwin, M.W., Bilodeau, G., McNeely, R., Southon, J., Morehead, M.D. and Gagnoni, J.-M. (1999) Forcing of the cold event of 8,200 years ago by catastrophic drainage of Laurentide lakes. *Nature* 400*,* 344-348.

Bauch, H.A., Kassens, H., Erlenkeuser, H., Grootes, P.M. and Thiede, J. (1999) Depositional environment of the Laptev Sea (Arctic Siberia) during the Holocene. *Boreas* 28*,* 194-204.

Bauch, H.A., Erlenkeuser, H., Spielhagen, R.F., Struck, U., Matthiessen, J., Thiede, J. and Heinemeier, J. (2001a) A multiproxy reconstruction of the evolution of deep and surface waters in the subarctic Nordic seas over the last 30,000 yr. *Quaternary Science Reviews* 20, 659-678.

Bauch, H.A., Mueller-Lupp, T., Taldenkova, E., Spielhagen, R.F., Kassens, H., Grootes, P.M., Thiede, J., Heinemeier, J. and Petryashov, V.V. (2001b) Chronology of the Holocene trangression at the North Siberian margin, *Global and Planetary Change* 31, 125-139.

Bauch, H.A. and Weinelt, M.S. (1997) Surface Water Changes in the Norwegian Sea during last Deglacial and Holocene Times. *Quaternary Science Reviews* 16, 1115-1124.

Berger, A. and Loutre, M.F. (1991) Insolation values for the Climate of the last 10 Million Years. *Quaternary Science Reviews* 10, 297-317.

Birks, C.J.A. and Koç, N. (2002) A high-resolution diatom record of late-Quaternary sea-surface temperatures and oceanographic conditions from the eastern Norwegian Sea. *Boreas* 31, 323-344.

Bjerknes, J. (1964) Atlantic air-sea interaction. *Advances in Geophysics* 10, 1-82.

Bjune, A.E., Seppä, H. and Birks, H.J.B. (2009) Quantitative summer-temperature reconstructions for the last 2000 years based on pollen-stratigraphical data from northern Fennoscandia. *Journal of Paleolimnology* 41, 43-56.

Bond, G., Showers, W., Cheseby, M., Lotti, R., Almasi, P., deMenocal, P., Priore, P., Cullen, H., Hajdas, I. and Bonani, G. (1997) A Pervasive Millennial-Scale Cycle in North Atlantic Holocene and Glacial Climates. *Science* 278*,* 1257-1266.

Bond, G., Kromer, B., Beer, J., Muscheler, R., Evans, M.N., Showers, W., Hoffmann, S., Lotti-Bond, R., Hajdas, I. and Bonani, G. (2001) Persistent Solar Influence on North Atlantic Climate During the Holocene. *Science 294,* 2130-2136.

Bradley, R.S., Hughes, M.K. and Diaz, H.F. (2003) Climate in Medieval Time. *Science* 302, 404-405.

Broecker, W.S. (1991) The Great Ocean Conveyor. *Oceanography* 4, 79-89.

Broecker, W.S. (2001) Was the Medieval Warm Period global? *Science* 291, 1497-1499.

Carstens, J., Hebbeln, D. and Wefer, G. (1997) Distribution of planktic foraminifera at the ice margin in the Arctic (Fram Strait). *Marine Micropaleontology* 29, 257-269.

Comiso, J.C., Parkinson, C.L., Gersten, R. and Stock, L. (2008) Accelerated decline in the Arctic sea ice cover. *Geophysical Research Letters* 35, L01703.

Crocket, K.C., Vance, D., Gutjahr, M., Foster, G.L. and Richards, D.A. (2011) Persistent Nordic deep-water overflow to the glacial North Atlantic. *Geology* 39, 515-518.

Cronin, T.M., Gemery, L., Briggs Jr., W.M., Jakobsson, M., Polyak, L. and Brouwers, E.M. (2010a) Quaternary Sea-ice history in the Arctic Ocean based on a new Ostracode sea-ice proxy. *Quaternary Science Reviews* 10*,* 3415-3429.

Cronin, T.M., Hayo, K., Thunell, R.C., Dwyer, G.S., Saenger, C. and Willard, D.A. (2010b) The Medieval Climate Anomaly and Little Ice Age in Chesapeake Bay and the North Atlantic Ocean. *Palaeogeography, Palaeoclimatology, Palaeoecology* 297*,* 299-310.

Dahl-Jensen, D., Mosegaard, K., Gundestrup, N., Clow, G.D., Jonsen, S.J., Hansen, A.W. and Balling, N. (1998) Past Temperatures Directly from the Greenland Ice Sheet. *Science* 282, 268-271.

Darby, D.A., Polyak, L. and Bauch, H.A. (2006) Past glacial and interglacial conditions in the Arctic Ocean and marginal seas – a review. *Progress in Oceanography* 71, 129-144.

Delworth, T., Manabe, S. and Stouffer, R.J. (1993) Interdecadal Variations of the Thermohaline Circulation in a Coupled Ocean-Atmosphere Model. *Journal of Climate* 6, 1993-2011.

Delworth, T., Manabe, S. and Stouffer, R.J. (1997) Multidecadal climate variability in the Greenland Sea and surrounding regions: a coupled model simulation. *Geophysical Research Letters* 24/3, 257-260.

Dickson, B., Yashayaev, I., Meincke, J., Turrell, B., Dye, S. and Holfort, J. (2002) Rapid freshening of the deep North Atlantic Ocean over the past four decades. *Nature* 416, 832-837.

Divine, D.V. and Dick, C. (2006) Historical variability of sea ice edge position in the Nordic Seas. *Journal of Geophysical Research* 111, C01001.

Dmitrenko, I., Kirillov, S.A., Tremblay, L.B., Bauch, D., Hölemann, J.A., Krumpen, T., Kassens, H., Wegner, C., Heinemann, G. and Schröder, D. (2010) Impact of the Arctic Ocean Atlantic water layer on Siberian shelf hydrography. *Journal of Geophysical Research 115,* C08010.

Dyke, A.S., England, J., Reimnitz, E. and Jetté, H. (1997) Changes in driftwood delivery to the Canadian Arctic Archipelago – The hypothesis of postglacial oscillations of the Transpolar Drift. *Arctic* 50*,* 1-16.

Dyke, A.S., England, J.H., Miller, G.H., Shaw, J., Veillette, J.J., Andrews, J.T. and Clark, P.U. (2002) The Laurentide and Innuitian ice sheets during the Last Glacial Maximum. *Quaternary Science Reviews* 21*,* 9-31.

Ebbesen, H., Hald, M. and Eplet, T.H. (2007) Lateglacial and early Holocene climatic oscillations on the Svalbard margin, European Arctic. *Quaternary Science Reviews* 26*,* 1999-2011.

Eiríksson, J., Bartels-Jónsdóttir, H.B., Cage, A.G., Gudmundsdóttir, E.R., Klitgaard Kristensen, D., Marret, F., Rodrigues, T., Abrantes, F., Austin, W.E.N., Jiang, H., Knudsen, K.-L. and Sejrup, H.-P. (2006) Variability of the North Atlantic Current during the last 2000 years based on shelf bottom water and sea surface temperatures along an open ocean/shallow marine transect in western Europe. *The Holocene* 16(7), 1017-1029.

England, J.H. and Furze, M.F.A. (2008) New evidence from the western Canadian Arctic Archipelago for the resubmergence of Bering Strait. *Quaternary Research* 70*,* 60-67.

Fairbanks, R.G. (1989) A 17,000-year glacio-eustatic sea level record: influence of glacial melting rates on the Younger Dryas event and deep-ocean circulation. *Nature* 342, 637-642.

Fetterer, F., Knowles, K., Meier, W. and Savoie, M. (2002, updated 2009) *Sea Ice Index*. National Snow and Ice Data Center, Boulder, CO, USA. Digital media.

Forman, S.L. Lubinski, D.J., Ingólfsson, O., Zeeberg, J.J., Snyder, J.A., Siegert, M.J., and Matishov, G.G. (2004) A review of postglacial emergence on Svalbard, Franz Josef Land and Novaya Zemlya, northern Eurasia. *Quaternary Science Reviews* 23, 1391-1434.

Gascard, J.-C., Kergomard, C., Jeannin, P.-F. and Fily, M. (1988) Diagnostic Study of the Fram Strait Marginal Ice Zone During Summer from 1983 and 1984 Marginal Ice Zone Experiment Lagrangian Observations. *Journal of Geophysical Research* 93/C4, 3613-3641.

Giles, K.A., Laxon, S.W. and Ridout, A.L. (2008) Circumpolar thinning of Arctic sea ice following the 2007 record ice extent minimum. *Geophysical Research Letters* 35, L22502.

Gobeil, C., Macdonald, R.W., Smith, J.N. and Beaudin, L. (2001) Atlantic Water Flow Pathways Revealed by Lead Contamination in Arctic Basin Sediments. *Science* 293, 1301-1304.

Häkkinen, S. (1993) An Arctic source for the Great Salinity Anomaly: Simulation of the Arctic ice ocean system for 1955-1975. *Journal of Geophysical Research* 98, 16397-16410.

Häkkinen, S. (1999) A Simulation of Thermohaline Effects of a Great Salinity Anomaly. *Journal of Climate* 12, 1781-1795.

Haley, B., Frank, M., Spielhagen, R.F. and Eisenhauer, A. (2007) Influence of brine formation on Arctic Ocean circulation over the past 15 million years. *Nature Geoscience* 1, 68-72.

Hald, M., Ebbesen, H., Forwick, M., Godtliebsen, F., Khomenko, L., Korsun, S., Ringstad Olsen, L. and Vorren, T.O. (2004) Holocene paleoceanography and glacial history of the West Spitsbergen area, Euro-Arctic margin. *Quaternary Science Reviews* 23, 2075-2088.

Hald, M., Andersson, C., Ebbesen, H., Jansen, E., Klitgaard-Kristensen, D., Risebrobakken, B., Salomonsen, G.R., Sarnthein, M., Sejrup, H.P. and Telford, R.J. (2007) Variations in temperature and extent of Atlantic Water in the northern North Atlantic during the Holocene. *Quaternary Science Reviews* 26, 3423-3440.

Hamelin, B., Grousset, F. and Sholkovitz, E.R. (1990) Pb isotopes in surficial pelagic sediments from the North Atlantic. *Geochimica et Cosmochimica Acta* 54, 37-47.

Holland, M.M., Bitz, C.M. and Tremblay, B. (2006) Future abrupt reductions in the summer Arctic sea ice. *Geophysical Research Letters* 33, L23503.

Hopkins, T.S. (1991) The GIN Sea – a synthesis of its physical oceanography and literature review 1972-1985. *Earth Science Reviews* 30, 175-318.

Houghton, J.T., Meira Filho, L.G., Callander, B.A., Harris, N., Kattenberg, A. and Maskell, K. (Eds.) (1996) Climate Change 1995. The science of climate change. Contribution of Working Group 1 to the Second Assessment Report of the Intergovernmental Panel on Climate Change. Cambridge University Press, Cambridge, 572 pp.

Hughes, M.K., Diaz, H.F. (1994) Was there a 'Medieval Warm Period', and if so, where and when? *Climatic Change* 26, 109-142.

IPCC (2007) IPCC Fourth Assessment Report: Climate Change 2007. In: Solomon, S., Qin, D., Manning, M., Chen, M., Marquis, M., Averyt, K.B., Tignor, M. and Miller, H.L. (Eds.), Contribution of Working Group I to the Fourth Assessment Report of the

Intergovernmental Panel on Climate Change. Cambridge University Press, Cambridge, United Kingdom and New York, USA.

Isaksson, E., Kohler, J., Pohjola, V., Moore, J., Igarashi, M., Karlöf, L., Martma, T., Meijer, H., Motoyama, H., Vaikmäe, R. and van de Wal, R.S.W. (2005) Two ice-core $\delta^{18}O$ records from Svalbard illustrating climate and sea ice variability over the last 400 years. *The Holocene* 15, 501-509.

Jennings, A.E., Knudsen, K.L., Hald, M., Vigen Hansen, C. and Andrews, J.T. (2002) A mid-Holocene shift in Arctic sea-ice variability on the East Greenland Shelf. *The Holocene* 12/1, 49-58.

Johannessen, O.M. (1986) Brief overview of the physical oceanography. In: Hurdle, B.G. (Ed.), The Nordic Seas. Springer, New York, pp. 103-127.

Johannessen, O.M. (1987) Introduction: Summer Marginal Ice Zone Experiments During 1983 and 1984 in Fram Strait and the Greenland Sea. *Journal of Geophysical Research* 92/C7, 6716-6718.

Jones, P.D., Osborn, T.J. and Briffa, K.R. (2001) The evolution of climate over the last millennium. *Science* 292, 662-667.

Jones, G.A. and Keigwin, L.D. (1988) Evidence from Fram Strait (78°N) for early deglaciation. *Nature* 336, 56-59.

Karcher, M.J., Gerdes, R., Kauker, F. and Köberle, C. (2003) Arctic warming: Evolution and spreading of the 1990s warm event in the Nordic seas and the Arctic Ocean. *Journal of Geophysical Research* 108, 3034.

Kaufmann, D.S., Ager, T.A., Anderson, N.J., Anderson, P.M., Andrews, J.T., Bartlein, P.J., Brubaker, L.B., Coats, L.L., Cwynar,, L.C., Duvall, M.L., Dyke, A.S., Edwards, M.E., Eisner, W.R., Gajewski, K., Geirsdóttir, A., Hu, F.S., Jennings, A.E., Kaplan, M.R., Kerwin, M.W., Lozhkin, A.V., MacDonald, G.M., Miller, G.H., Mock, C.J., Oswald, W.W., Otto-Bliesner, B.L., Porinchu, D.F., Rühland, K., Smol, J.P., Steig, E.J. and Wolfe, B.B. (2004) Holocene thermal maximum in the western Arctic (0-180° W). *Quaternary Science Reviews* 23, 529-560.

Kerwin, M.W., Overpeck, J.T., Webb, R.S. and Anderson, K.H. (2004) Pollen-based summer temperature reconstruction for the eastern Canadian boreal forest, subarctic, and Arctic. *Quaternary Science Reviews* 23, 1901-1924.

Kleiven, H.F., Kissel, C., Laj, C., Ninnemann, U.S., Richter, T.O. and Cortijo, E. (2008) Reduced North Atlantic Deep Water Coeval with the Glacial Lake Agassiz Freshwater Outburst. *Science* 319, 60-64.

Klitgaard Kristensen, D., Sejrup, H.P., Haflidason, H., Berstad, I.M., Mikalsen, G. (2004) Eight-hundred-year temperature variability from the Norwegian continental margin and the North Atlantic thermohaline circulation. *Paleoceanography* 19, 2007.

Koç, N., Jansen, E. and Haflidason, H. (1993) Paleoceanographic reconstructions of surface ocean conditions in the Greenland, Iceland and Norwegian Seas through the last 14 ka based on diatoms. *Quaternary Science Reviews* 12, 115-140.

Koç, N. and Jansen, E. (1994) Response of the high-latitude Northern Hemisphere to orbital climate forcing: Evidence from the Nordic Seas. *Geology* 22, 523-526.

Koerner, R.M. and Fisher, D.A. (1990) A record of Holocene summer climate from a Canadian high-Arctic ice core. *Nature* 343, 630-631.

Koerner, R.M. and Fisher, D.A. (2002) Ice-core evidence for widespread Arctic glacier retreat in the Last Interglacial and the early Holocene. *Annals of Glaciology* 35, 19-24.

Lamb, H.H. (1965) The early Medieval Warm Epoch and its sequel. *Palaeogeography, Palaeoclimatology, Palaeoecology* 1, 13-37.

Lambeck, K., Yokohama, Y. and Purcell, T. (2002) Into and out of the Last Glacial Maximum – Sea-level change during oxygen isotope stages 3 and 2. *Quaternary Science Reviews* 21, 343-360.

Landvik, J.Y., Bondevik, S., Elverhøi, A., Fjeldskaar, W., Mangerud, J., Siegert, M.J., Salvigsen, O., Svendsen, J. and Vorren, T.O. (1998) The Last Glacial Maximum of Svalbard and the Barents Sea area: ice sheet extent and configuration. *Quaternary Science Reviews* 17, 43-75.

Landvik, J.Y., Ingolfsson, O., Mienert, J., Lehmann, S.J., Solheim, A., Elverhøi, A. and Ottesen, D. (2005) Rethinking Late Weichselian ice-sheet dynamics in coastal NW Svalbard. *Boreas* 34, 7-24.

Lazier, J.R.N. (1988) Temperature and salinity changes in the deep Labrador Sea, 1962-1986. *Deep-Sea Research* 35, 1247-1253.

Lehmann, S.J. and Keigwin, L.D. (1992) Sudden changes in North Atlantic circulation during the last deglaciation. *Nature* 356, 757-762.

Levermann, A., Mignot, J., Nawrath, S. and Rahmstorf, S. (2007) The role of Northern sea ice cover for the weakening of the thermohaline circulation under global warming. *Journal of Climate* 20, 4160-4171.

Loeng, H. (1991) Features of the physical oceanographic conditions of the Barents Sea. In Sakshaug, E., Hopkins, C.C.E. and Øritsland, N.A. (Eds.), Proceedings of the Pro Mare Symposium on Polar Marine Ecology, Trondheim, 12-16 May 1990. *Polar Research* 10, 5-18.

Lohmann, G. and Gerdes, R. (1998) Sea Ice Effects on the Sensitivity of the Thermohaline Circulation. *Journal of Climate* 11, 2789-2803.

Manabe, S. and Stouffer, R.J. (1980) Sensitivity of a Global Climate Model to an Increase of CO_2 Concentration in the Atmosphere. *Journal of Geophysical Research* 85/C10, 5529-5554.

Manley, T.O. (1995) Branching of Atlantic Water within the Greenland-Spitsbergen passage: an estimate of recirculation. *Journal of Geophysical Research* 100/C10, 20627-20634.

Mann, M.E., Zhang, Zh., Rutherford, S., Bradley, R.S., Hughes, M.K., Shindell, D., Ammann, C., Faluvegi, G. and Ni, F. (2009) Global Signatures and Dynamical Origins of the Little Ice Age and Medieval Climate Anomaly. *Science* 326, 1256-1260.

Marnela, M., Rudels, B., Olsson, K.A., Anderson, L.G., Jeansson, E., Torres, D.J., Messias, M.-J., Swift, J.H. and Watson, A.J. (2008) Transports of Nordic Seas water masses and excess SF_6 through Fram Strait to the Arctic Ocean. *Progress in Oceanography* 78, 1-11.

Miller, G.H., Wolfe, A.P., Briner, J.P., Sauer, P.E. and Nesje, A. (2005) Holocene glaciation and climate evolution of Baffin Island, Arctic Canada. *Quaternary Science Reviews* 24, 1703-1721.

Miller, G.H., Brigham-Grette, J., Alley, R.B., Anderson, L., Bauch, H.A., Douglas, M.S.V., Edwards, M.E., Elias, S.A., Finney, B.P., Fitzpatrick, J.J., Funder, S.V., Herbert, T.D., Hinzman, L.D., Kaufman, D.S., MacDonald, G.M., Polyak, L., Robock, A., Serreze, M.C.,

Smol, J.P., Spielhagen, R.F., White, J.W.C., Wolfe, A.P. and Wolff, E.W. (2010) Temperature and precipitation history of the Arctic. *Quaternary Science Reviews* 29, 1679-1715.

Moberg, A., Sonechkin, D.M., Holmgren, K., Datsenko, N.M., Karlén, W., (2005) Highly variable Northern Hemisphere temperatures reconstructed from low- and high-resolution proxy data. *Nature* 433, 613-617.

Moritz, R.E., Bitz, C.M. and Steig, E.J. (2002) Dynamics of Recent Climate Change in the Arctic. *Science* 297, 1497-1502.

Moros, M., Emeis, K., Risebrobakken, B., Snowball, I., Kuijpers, A., McManus, J. and Jansen, E. (2004) Sea surface temperatures and ice rafting in the Holocene North Atlantic; climate influences on northern Europe and Greenland. *Quaternary Science Reviews* 23, 2113-2126.

Moros, M., Jensen, K.G. and Kuijpers, A. (2006) Mid- to late-Holocene hydrological and climatic variability in Disko Bugt, central West Greenland. *The Holocene* 16, 357-367.

Nørgaard-Pedersen, N., Spielhagen, R.F., Erlenkeuser, H., Grootes, P.M., Heinemeier, J. and Knies, J. (2003) Arctic Ocean during the Last Glacial Maximum: Atlantic and polar domains of surface water mass distribution and ice cover. *Paleoceanography* 18, 1063.

NSDIC (2011) Media Advisory: Arctic sea ice reaches lowest extent for 2011. http://nsidc.org/arcticseaicenews/2011/091511.html, 15 September 2011.

Overpeck, J., Hughen, K., Hardy, D., Bradley, R., Case, R., Douglas, M., Finney, B., Gajewski, K., Jacoby, G., Jennings, A., Lamoureux, S., Lasca, A., MacDonald, G., Moore, J., Retelle, M., Smith, S., Wolfe, A. and Zielinski, G. (1997) Arctic Environmental Change of the Last Four Centuries. *Science* 278, 1251-1256.

Pisaric, M.F.J., MacDonald, G.M., Velichko, A.A. and Cwynar, L.C. (2001) The Lateglacial and Postglacial vegetation history of the northwestern limits of Beringia, based on pollen, stomata and tree stump evidence. *Quaternary Science Reviews* 20, 235-245.

Polyak, L., Andrews, J.T., Brigham-Grette, J., Darby, D., Funder, S., Holland, M., Jennings, A., Savelle, J., Serreze, M. and Wolff, E. (2009) History of Arctic sea ice. In: Past Climate Variability and Change in the Arctic and at High Latitudes. A report by the U.S. Climate Change Science Program and Subcommittee on Global Change Research. U.S. Geological Survey, Reston, VA, pp. 159-184.

Polyak, L. and Mikhailov, V. (1996) Post-glacial environments of the southeastern Barents Sea: foraminiferal evidence. In: Andrews, J.T. (Ed.), Late Quaternary Paleoceanography of the North Atlantic Margins. Geological Society Special Publication, Vol. 111, pp. 323-337.

Polyakov, I.V., Alekseev, G.V., Timokhov, L.A., Bhatt, U.S., Colony, R.L., Simmons, H.L., Walsh, D., Walsh, J.E. and Zahkharov, V.F. (2004) Variability of the intermediate Atlantic Water of the Arctic Ocean over the last 100 years. *Journal of Climate* 17, 4485-4497.

Polyakov, I.V., Beszczynka, A., Carmack, E.C., Dmitrenko, I., Fahrbach, E., Frolov, I.E., Gerdes, R., Hansen, E., Holfort, J., Ivanov, V.V., Johnson, M.A., Karcher, M., Kauker, F., Morison, J., Orvik, K.A., Schauer, U., Simmons, H.L., Skagseth, Ø., Solokov, V.T., Steele, M., Timokhov, L.A., Walsh, D. and Walsh, J.E. (2005) One more step toward a warmer Arctic. *Geophysical Research Letters* 32, L17605.

Polyakov, I.V., Alekseev, G.V., Ashik, I.M., Bacon, S., Beszczynka-Möller, A., Carmack, E.C., Dmitrenko, I., Fourtier, L., Gascard, J.-C., Hansen, E., Hölemann, J., Ivanov, V.V., Kikuchi, T., Kirillov, S., Lenn, Y.-D., McLaughlin, F.A., Piechura, J., Repina, I., Timokhov, L.A., Walczowski, W. and Woodgate, R. (2011) Fate of Early 2000s Arctic Warm Water Pulse. *Bulletin of the American Meteorological Society* 92/5, 561-566.

Polyakova, Ye.I. and Stein, R. (2004) Holocene environmental implications of diatom and organic carbon records from the southeastern Kara Sea (Siberian Margin). *Quaternary Research* 62, 256-266.

Porcelli, D., Andersson, P.S., Baskaran, M., Frank, M., Björk, G. and Semiletov, I. (2009) The distribution of neodymium isotopes in Arctic Ocean basins. *Geochimica et Cosmochimica Acta* 73, 2645-2659.

Quadfasel, D., Rudels, B. and Kurz, K. (1988) Outflow of dense water from a Svalbard fjord into the Fram Strait. *Deep Sea Research* 35, 1153-1150.

Rabe, B., Schauer, U., Mackensen, A., Karcher, M., Hansen, E. and Beszczynska-Möller, A. (2009) Freshwater components and transports in the Fram Strait – recent observations and changes since the late 1990s. *Ocean Science* 5*,* 219-233.

Rahmstorf, S. (1995) Bifurcations of the Atlantic thermohaline circulation in response to changes in the hydrological cycle. *Nature* 378*,* 145-149.

Rasmussen, S.O., Andersen, K.K., Svensson, A.M., Steffensen, J.P., Vinther, B.M., Clausen, H.B., Siggaard-Andersen, M.-L., Johnsen, S.J., Larsen, L.B., Dahl-Jensen, D., Bigler, M., Röthlisberger, R., Fischer, H., Goto-Azuma, K., Hansson, M.E. and Ruth, U. (2006) A new Greenland ice core chronology for the last glacial termination. *Journal of Geophysical Research* 111*,* D06102.

Rasmussen, T.L., Thomsen, E., Ślubowska, M.A., Jessen, S., Solheim, A. and Koç, N. (2007) Paleoceanographic evolution of the SW Svalbard margin (76°N) since 20,000 ^{14}C yr BP. *Quaternary Research* 67*,* 100-114.

Risebrobakken, B., Jansen, E., Andersson, C., Mjelde, E. and Hevrøy, K. (2003) A high-resolution study of Holocene paleoclimatic and paleoceanographic changes in the Nordic Seas. *Paleoceanography* 18/1, 1017.

Rohling, E.J. and Pälike, H. (2005) Centennial-scale climate cooling with a sudden cold event around 8,200 years ago. *Nature* 434, 975-979.

Rudels, B., Meyer, R., Fahrbach, E., Ivanov, V.V., Østerhus, S. and Quadfasel, D. (2000) Water mass distribution in Fram Strait and over the Yermak Plateau in summer 1997. *Annales Geophysicae* 18, 687-705.

Saloranta, T.M. and Haugan, P.M. (2001) Interannual variability in the hydrography of Atlantic water northwest of Svalbard. *Journal of Geophysical Research* 106(C7), 13931-13943.

Saloranta, T.M. and Haugan, P.M. (2004) Northward cooling and freshening of the warm core of the West Spitsbergen Current. *Polar Research* 23(1), 447-461.

Salvigsen, O., Forman, S.L. and Miller, G.H. (1992) Thermophilous molluscs on Svalbard during the Holocene and their Paleoclimatic implications. *Polar Research* 11(1), 1-10.

Salvigsen, O. (2002) Radiocarbon-dated *Mytilus edulis* and *Modiolus modiolus* from northern Svalbard: climatic implications. *Norwegian Journal of Geography* 56, 56-61.

Sarnthein, M., van Kreveld, S., Erlenkeuser, H., Grootes, P.M., Kucera, M., Pflaumann, U. and Schulz, M. (2003) Centennial-to-millennial-scale periodicities of Holocene climate and sediment injections off the western Barents shelf, 75°N. *Boreas* 32, 447-461.

Schauer, U. (1995) The release of brine-enriched shelf water from Storfjord into the Norwegian Sea. *Journal of Geophysical Research* 100, 16,015-16,028.

Schauer, U., Fahrbach, E., Østerhus, S. and Rohardt, G. (2004) Arctic warming through the Fram Strait: oceanic heat transport from 3 years of measurements. *Journal of Geophysical Research* 109, C06026.

Schlichtholz, P. and Houssais, M.-N. (1999) An inverse modelling study in Fram Strait. Part II: water mass distribution and transports. *Deep-Sea Research* 46*,* 1137-1168.

Schulz, M., Paul, A. and Timmermann, A. (2004) Glacial-interglacial contrast in climate variability at centennial-to-millennial timescales: observations and conceptual model. *Quaternary Science Reviews* 23*,* 2219-2230.

Seidenkrantz, M.-S., Aagaard-Sørensen, S., Sulsbrück H., Kuijpers, A., Jensen, K.G. and Kunzendorf, H. (2007) Hydrography and climate of the last 4400 years in a SW Greenland fjord: implications for Labrador Sea paleoceanography. *The Holocene* 17/3, 387-401.

Seidenkrantz, M.-S., Roncaglia, L., Fischel A., Heilmann-Clausen, C., Kuijpers, A. and Moros, M. (2008) Variable North Atlantic climate seesaw patterns documented by a late Holocene marine record from Disko Bugt, West Greenland. *Marine Micropaleontology* 68, 66-83.

Seppä, H. and Birks, H.J.B. (2001) July mean temperature and annual precipitation trends during the Holocene in the Fennoscandian tree-line area: pollen-based climate reconstructions. *The Holocene* 11*,* 527-539.

Serreze, M.C., Holland, M.M. and Stroeve, J. (2007) Perspectives on the Arctic's Shrinking Sea-Ice Cover. *Science* 315*,* 1533-1536.

Serreze, M.C., Barrett, A., Stroeve, J., Kindig, D. and Holland, M.M. (2009) The emergence of surface-based Arctic amplification. *The Cryosphere* 3*,* 11-19.

Sicre, M.-A., Jacob, J., Ezat, U., Rousse, S., Kissel, C., Yiou, P., Eiríksson, J., Knudsen, K.-L., Jansen, E. and Turon, J.-L. (2008) Decadal variability of sea surface temperatures off North Iceland over the last 2000 years. *Earth and Planetary Science Letters* 268, 137-142.

Simstich, J., Stanovoy, V., Bauch, D., Erlenkeuser, H. and Spielhagen, R.F. (2004) Holocene variability of bottom water hydrography on the Kara Sea shelf (Siberia) depicted in multiple single-valve analyses of stable isotopes in ostracods. *Marine Geology* 206, 147-164.

Ślubowska, M.A., Koç, N., Rasmussen, T.L. and Klitgaard-Kristensen, D. (2005) Changes in the flow of Atlantic water into the Arctic Ocean since the last deglaciation: Evidence from the northern Svalbard continental margin, 80°N. *Paleoceanography* 20, PA4014.

Ślubowska-Woldengen, M., Rasmussen, T.L., Koç, N., Klitgaard-Kristensen, D., Nilsen, F. and Solheim, A. (2007) Advection of Atlantic Water to the western and northern Svalbard shelf since 17,500 cal yr BP. *Quaternary Science Reviews* 26, 463-478.

Ślubowska-Woldengen, M.A., Koç, N., Rasmussen T.L., Klitgaard-Kristensen, D., Hald, M. and Jennings, A.E. (2008) Time-slice reconstructions of ocean circulation changes on the

continental shelf in the Nordic and Barents Sea during the last 16,000 cal yr B.P. *Quaternary Science Reviews* 27, 1476-1492.

Spielhagen, R.F., Erlenkeuser, H. and Siegert, C. (2005) History of freshwater runoff across the Laptev Sea (Arctic) during the last deglaciation. *Global and Planetary Change* 48, 187-207.

Spielhagen, R.F., Werner, K., Aagaard Sørensen, S., Zamelczyk, K., Kandiano, E., Budéus, G., Husum, K., Marchitto, T.M. and Hald, M. (2011) Enhanced Modern Heat Transfer to the Arctic by Warm Atlantic Water. *Science* 331, 450-453.

Steele, M. and Boyd, T. (1998) Retreat of the cold halocline layer in the Arctic Ocean. *Journal of Geophysical Research* 103/C5, 10419-10435.

Stein, R., Boucsein, B., Fahl, K., Garcia de Oteyza, T., Knies, J. and Niessen, F. (2001) Accumulation of particulate organic carbon at the Eurasian continental margin during late Quaternary times: controlling mechanisms and paleoenvironmental significance. *Global and Planetary Change* 31, 87-104.

Stein, R., Niessen, F., Dittmers, K., Levitan, M., Schoster, F., Simstich, J., Steinke, T. and Stepanets, O.V. (2002) Siberian river run-off and Late Quaternary glaciation in the southern Kara Sea, Arctic Ocean: preliminary results. *Polar Research* 21, 315-322.

Stein, R., Dittmers, K., Fahl, K., Kraus, M., Matthiessen, J., Niessen, F., Pirrung, M., Polyakova, Ye., Schoster, F., Steinke, T. and Fütterer, D.K. (2004) Arctic (paleo) river discharge and environmental chage: evidence from the Holocene Kara Sea sedimentary record. *Quaternary Science Reviews* 23, 1485-1511.

Stroeve, J.C., Holland, M.M., Meier, W., Scambos, T. and Serreze, M. (2007) Arctic sea ice decline: Faster than forecast. *Geophysical Research Letters* 34, L09501.

Stroeve, J.C., Maslanik, J., Serreze, M.C., Rigor, I., Meier, W. and Fowler, C. (2011) Sea ice response to an extreme negative phase of the Arctic Oscillation during winter 2009/2010. *Geophysical Research Letters* 38, L02502.

Stroeve, J.C., Serreze, M.C., Holland, M.M., Kay, J.E., Malanik, J. and Barrett, A.P. (in press) The Arctic's rapidly shrinking sea ice cover: a research synthesis. *Climatic Change*.

Stuiver, M., Grootes, P.M. and Bara-ziunas, T.F. (1995) The GISP2 $\delta^{18}O$ Climate Record of the Past 16,500 Years and the Role of the Sun, Ocean, and Volcanoes. *Quaternary Research* 44, 341-354.

Svendsen, J.I., Gataullin, V., Mangerud, J. and Polyak, L. (2004a) The glacial History of the Barents and Kara Sea Region. *Developments in Quaternary Science* 2/1, 369-378.

Svendsen, J.I., Alexanderson, H., Astakhov, V.I., Demidov, I., Dowdeswell, J.A., Funder, S., Gataullin, V., Henriksen, M., Hjort, C., Houmark-Nielsen, M., Hubberten, H.W., Ingólfsson, O., Jakobsson, M., Kjær, K., Larsen, E., Lokrantz, H., Lunkka, J.P., Lysså, A., Mangerud, J., Matiouchkov, A., Murray, A., Möller, P., Niessen, F., Nikolskaya, O., Polyak, L., Saarnisto, M., Siegert, C., Siegert, M.J., Spielhagen, R.F. and Stein, R. (2004b) Late Quaternary ice sheet history of northern Eurasia. *Quaternary Science Reviews* 23, 1229-1271.

Svendsen, J.I. and Mangerud, J. (1997) Holocene glacial and climatic variations on Spitsbergen, Svalbard. *The Holocene* 7/1, 45-57.

Tarussov, A. (1992) The Arctic from Svalbard to Severnaya Zemlya: climatic reconstructions from ice cores, in: Bradley, R.S. and Jones, P.D. (Eds.), Climate since A.D. 1500. Routledge, London, New York, pp. 505-516.

Van Loon, H. and Rogers, J.C. (1978) The Seesaw in Winter Temperatures between Greenland and Northern Europe. Part I: General Description. *Monthly Weather Review* 106, 296-310.

Vinje, T. (2001) Anomalies and Trends of Sea ice Extent and Atmospheric Circulation in the Nordic Seas during the Period 1864-1998. *Journal of Climate* 14, 255-267.

Vinther, B.M., Clausen, H.B., Johnsen, S.J., Rasmussen, S.O., Andersen, K.K., Buchardt, S.L., Dahl-Jensen, D., Seierstad, I.K., Siggaard-Andersen, M.-L., Steffensen, J.P., Svensson, A., Olsen, J. and Heinemeier, J. (2006) A synchronized dating of three Greenland ice cores throughout the Holocene. *Journal of Geophysical Research* 111, D13102.

Volkmann, R. (2000) Planktic foraminifer ecology and stable isotope geochemistry in the Arctic Ocean: implications from water column and sediment surface studies for quantitative reconstructions of oceanic parameters. *Berichte zur Polarforschung* 361, 1-128.

Wanner, H., Solomina, O., Grosjean, M., Ritz, S.P. and Jetel, M. (2011) Structure and origin of Holocene cold events. *Quaternary Science Reviews* 30, 3109-3123.

Werner, A. (1993) Holocene moraine chronology, Spitsbergen, Svalbard: lichenometric evidence for multiple Neoglacial advances in the Arctic. *The Holocene* 3, 128-137.

Williams, J.W., Tarasov, P., Brewer, S. and Notaro, M. (2011) Late Quaternary variations in tree cover at the northern forest-tundra ecotone. *Journal of Geophysical Research* 116, G01017.

Winter, B.L., Johnson, C.M. and Clark, D.L. (1997) Strontium, neodymium, and lead isotope variations of authigenic and silicate sediment components from the Late Cenozoic Arctic Ocean: Implications for sediment provenance and the source of trace metals in seawater. *Geochimica et Cosmochimica Acta* 61, 4181-4200.

2 MATERIAL AND METHODS

Two sediment cores (box core MSM5/5-712-1 and kastenlot core MSM5/5-712-2) were retrieved from the western Svalbard continental margin (78°54.94' N, 6°46.04' E, 1490.5 m water depth, Fig. 1.2) during cruise leg MSM5/5 with RV „Maria S. Merian" in summer 2007.

2.1. Sample preparation

The sediment cores were sampled in 0.5 and 1 cm thick slices. The samples were freeze-dried and weighed to obtain the dry bulk weight of the samples. All samples were wet-sieved in deionized water through a 63 μm-sized mesh to remove clay and silt material. Dry sieving into size fractions 63-125 μm, 125-250 μm, 250-500 μm, 500-1000 μm, and >1000 μm was carried out on a Gilson Autosiever (Model GA-1). Fractions were weighed to obtain percentages of each size fraction. To obtain dry bulk density (DBD) values every 5 to 10 cm ca 10 cm^3 of wet material was sampled by means of plastic syringes with 10 ml content.

2.2. AMS radiocarbon dating

Age control of the studied sediment cores is based on accelerator mass spectrometry (AMS) radiocarbon dates. Analyses were conducted at the Leibniz Laboratory of Kiel University, Germany, the University Bordeaux (EPOC), France, and the Poznan Radiocarbon Laboratory, Poland. In order to obtain the required amount of about 1 mg carbon (or 10 mg calcium carbonate), calcareous tests of planktic foraminifers were handpicked. Except for the surface sample of MSM5/5-712-1 all measurements were carried out monospecifically, using about 10 mg of calcareous tests of the planktic foraminifer species *Neogloboquadrina pachyderma* (sin.). Due to an insufficient amount of *N. pachyderma* (sin.), additional planktic foraminifer species including *N. pachyderma* (dextral coiling), *Turborotalia quinqueloba*, and *Globigerina bulloides* were used for age determination of the surface sample in core MSM5/5-712-1.

The radiocarbon dates were converted to calendar years BP (present = AD 1950) applying the calibration software Calib version 6.0 (Stuiver and Reimer 1993) with the use of the Marine09 calibration data set (Reimer et al., 2009), including a standard reservoir correction of 402 years. Chronology is established between the calibrated calendar ages by linear interpolation, assuming uniform sedimentation rates between the dates. We refrained from applying a regional average correction ΔR value since all values provided by the Marine Reservoir Correction Database in CALIB (http://calib.qub.ac.uk/marine/) were obtained from the shallow Svalbard coast area and seem not appropriate as a suitable ΔR value for our site at ca 1500 m water depth. Nevertheless we are aware of a possible shift to younger ages due to the ΔR effect when applying our age-depth models.

2.3. Stable oxygen and carbon isotope analysis

About 25 calcareous tests of the planktic foraminifer species *N. pachyderma* (sin.) and *T. quinqueloba* were picked from size fraction 100-250 μm for stable oxygen and carbon isotopes analyses. In order to prevent possible ecological biases of different morphotypes (Healy-Williams, 1992) only "square-shaped" (four-chambered) specimens of *N. pachyderma* (sin.) were used. About 15 specimens of the benthic foraminifer species *Cibicidoides wuellerstorfi* were picked from the 250-500 μm size class and, if not sufficient, from the 100-250 μm size fraction. The tests were crunched and mingled in order to obtain well-mixed aliquots for measurements.

Analysis was performed at the IFM-GEOMAR Stable Isotope Lab using a Finnigan MAT 253 mass spectrometer system and a Kiel IV Carbonate Preparation Device. The carbonate was treated with orthophosphoric acid at 70°C. The analytical accuracy of the system was <0.06‰ for $\delta^{18}O$ and <0.03‰ for $\delta^{13}C$. All measurements were calibrated to Pee Dee Belemnite (PDB) standard (international standard NBS 19). Oxygen isotope data of *C. wuellerstorfi* were corrected for their disequilibrium effect by +0.64‰ (Duplessy et al., 2002; Shackleton and Opdyke, 1973). For stable oxygen and carbon isotope data of *T. quinqueloba* a vital effect correction of +1.3‰ and +2.6‰ was applied, respectively (Volkmann, 2000).

For comparison, oxygen isotope data of *N. pachyderma* (sin.) and *C. wuellerstorfi* were corrected for the ice volume effect following Meland et al. (2008). An ice volume component of 1.05‰ (Duplessy et al., 2002) and the sea level curve by Lighty et al. (1982) were applied, assuming a sea level 120 m lower than today during the Last Glacial Maximum (Fairbanks et al., 1989).

2.4. Planktic foraminiferal assemblages

Census of the planktic foraminiferal assemblages was carried out on the size fractions 150-250 μm and 100–250 μm in order to capture also smaller sized species. The fraction >250 μm was neglected due to an almost complete absence of planktic foraminifers. Prior to the counting procedure the samples were split by means of a microsplitter to obtain a numerable fraction of the sample containing at least 300 planktic foraminiferal tests. For counting the sample fraction was evenly distributed on the picking tray and the representative split of ca 300 planktic foraminiferal tests was counted and identified to species level under the light microscope. The number of counted specimens was multiplied by the corresponding split factor in order to estimate the number of planktic foraminifer tests of the entire sample. If a sample, for instance, had been split four times, the split fraction contains 1/16 of the sample. Thus, the number of counted tests in the sample fraction has to be multiplied by 16 to estimate the number of tests in

the entire sample. Planktic foraminifer fluxes were calculated on dry bulk density values and linear sedimentation rates.

2.5. Reconstruction of sea surface temperatures and salinity

For calculation of the sea surface temperatures of the past 2000 years, the SIMMAX procedure by Pflaumann et al. (1996) was applied. Summer SST variations at 50 m water depth were estimated from counts of planktic foraminiferal assemblages in the 150-250 μm size fraction using the SIMMAX transfer function (Pflaumann et al., 1996). The fraction >250 μm was neglected due to an almost complete absence of planktic foraminifers. Temperature estimates were calculated as an average of modern SST corresponding to the best analogous samples weighed by similarity measure.

In order to reconstruct salinity variations, we used the paleotemperature equation (O'Neil et al., 1969):

$$T = 16.9\text{-}4.38(\delta_c\text{-}\delta_w)+0.1(\delta_c\text{-}\delta_w)^2.$$

to derive $\delta^{18}O$ of the ocean water (δ_w in V-SMOW) from SST used from the SIMMAX reconstruction (T) and the measured $\delta^{18}O$ values of *N. pachyderma* (sin.) (δ_c). In order to derive salinities from δ_w we applied a modern salinity/$\delta^{18}O$ correlation of the water column on the Western Svalbard margin from 100 to 500 m water depth, which covers the depth of the Atlantic Water within the West Spitsbergen Current. Data from Frank (1996) and Meredith et al. (2001) were retrieved from the Global Seawater Oxygen-18 Database (Schmidt et al., 1999):

$$\delta^{18}O = 0.471*S\text{-}16.195.$$

Since the calculated salinity value of about 35.5 for the core top sample was slightly higher than a salinity of 35.1 seen in present-day Atlantic Water at this position, we corrected our salinity calculations by a shift of -0.2‰ in foraminiferal $\delta^{18}O$ in order to fit present-day Atlantic Water salinity of 35.1.

2.6. Ice-rafted debris and sortable silt mean size

Investigation of ice-rafted debris (IRD) was carried out on a representative split (>100 grains) of the 150-250 μm size fraction. Lithic fragments were counted following the same procedure as described in section 2.4. IRD fluxes were calculated based on dry bulk density values and linear sedimentation rates.

Sortable silt size analysis was carried out every 1 cm using an aliquot of the freeze-dried samples. To remove carbonate and organic matter samples were treated with acetic acid and hydrogen peroxide, respectively. After adding sodium polyphosphate for better dispersion the samples were put on a shaker for at least 24 hours. Measurements were performed with a CILAS 1180L laser-diffraction particle analyser. The sortable silt size mean grain size 10-63 μm (Robinson and McCave, 1994) was calculated using the entire granulometric data sets based on vol.%.

2.7. Sediment colour measurements

Colour scanning was carried out every 1 cm, using a handheld Minolta CM-2002 Spectrophotometer. The spherical L*a*b* colour space was used with lightness L*, red-green chromaticity a* and blue-yellow chromaticity b*.

2.8. Time series analysis

In order to test the existence of possible periodic or quasiperiodic behaviour (Risebrobakken et al., 2003) proxy data sets were spectrally analyzed by the Blackman-Tukey method (Blackman and Tukey, 1958) using the AnalySeries 2.0 software (Paillard et al., 1996). In order to remove linear trends we followed the presetting of the software in resampling at 32- to 100-year intervals. The confidence level was set to 90%.

2.9. Radiogenic isotopes

2.9.1. Sample preparation

Extraction of seawater neodymium and lead isotope signatures from early diagenetic ferromanganese oxyhydroxide coatings of bulk sediments was carried out following a slightly modified version of the methods suggested by Gutjahr et al. (2007) and Stumpf et al. (2010). The sample preparation procedure is summarized in Fig. 2.1. About 2 g of freeze-dried and coarsely ground bulk sediment material was transferred into acid-cleaned polypropylene 50 ml centrifuge tubes. Samples were rinsed twice with 20 ml of deionised water (Milli-Q system, MQ). A 44%-acetic acid/1M-Na acetate buffer was used to remove carbonate. In those cases where the carbonate was not completely dissolved the samples were put on a shaker overnight in a solution of 10 ml MQ water and 10 ml acetic acid to remove the remaining carbonate and were thoroughly rinsed with MQ water thereafter. For the leaching process to dissolve the ferromanganese oxyhydroxide coatings about 20 ml of the leaching solution (0.05 M-hydroxylamine hydrochloride/15%-acetic acid solution buffered to pH 3.6. with NaOH) was

added to the samples and was left to react in an ultrasonic bath for about 1 h followed by reaction in a shaker for 2 h. After centrifugation, the supernatant (ca 20 ml) containing the dissolved seawater fraction of Nd and Pb within the coatings was pipetted into Teflon vials (30 ml) for further chemical treatment. Solid residuals of the bulk sediments were rinsed three times in MQ water and stored in 20 ml of MQ water.

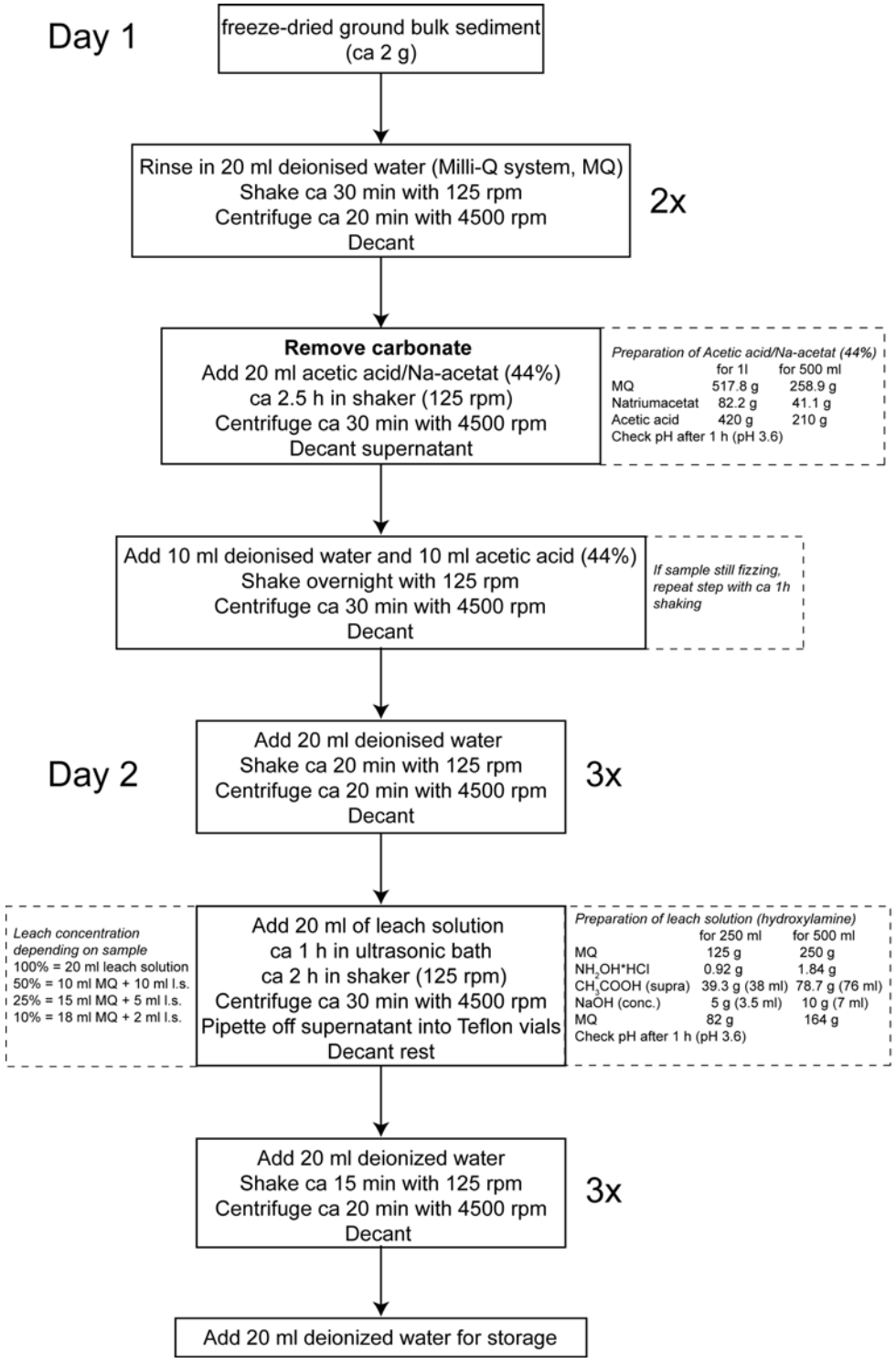

Fig. 2.1: Analytical preparation scheme for the extraction of ferromanganese oxyhydroxide coatings from marine sediments.

2.9.1.1. Purification and separation of individual elements

Ion chromatographic separation and purification of the elements was conducted following standard procedures of Galer and O'Nions (1989), Lugmair and Galer (1992) for lead; Horwitz et al. (1992), Bayon et al. (2002) for strontium; Cohen et al. (1988), Barrat et al. (1996), Le Fèvre and Pin (2005) for neodymium. Purification of Pb was carried out on anion exchange columns (50 µl AG1-X8 resin, mesh 100-200 µm). Alkaline elements were separated from rare earth elements (REEs) on cation exchange columns (0.8 ml AG50W-X12 resin, mesh 200-400 µm). Separation of Nd from other REEs was performed on columns with 2 ml Ln Spec resin (mesh 50-100 µm). Purification of Sr was achieved on columns with 50 µl Sr Spec resin (mesh 50-100 µm).

Prior to the procedure, the samples were heated overnight (100-105°C) and evaporated to dryness. Thereafter 2x1 ml conc. HNO_3 was added and evaporated each time. 1 ml conc. HNO_3 was then added to the sample for reflux (ca 100°C, 20-30 min). After cooling down, samples were transferred from Teflon vials into 1.5 ml labelled safe-lock tubes and centrifuged (14000 rpm, 5 min). Thereafter, the samples (without residual crystals) were separated and transferred into Teflon vials (7 ml) and were evaporated to dryness. Detailed procedures of the column separation are presented in the analytical schemes (Figs. 2.2 to 2.5). All laboratory work was carried out in the clean laboratory facilities of IFM-GEOMAR, Kiel, Germany.

Pb separation

Prior to the Pb column procedure the samples (ca 0.9 ml) were twice taken up and dried down with 300 µl 2 M HBr. For purification of Pb, anion exchange columns (50 µl AG1-X8 resin, mesh size 100-200 µm) were used. The samples were loaded in solution A (Fig. 2.2). Eluents that were later used for further purification of strontium and rare earth elements (REE) were collected separately in Teflon vials. The Pb samples were eluted in solution B and collected separately in Teflon vials (Fig. 2.2). Thereafter the samples containing Pb were evaporated to dryness. 100 µl concentrated HNO_3 were added and Pb samples were then dried down again. Thereafter, 100 µl concentrated H_2O_2 were added to the samples for destruction of organic matter. After evaporation, the samples were stored in 2% HNO_3 until measurement.

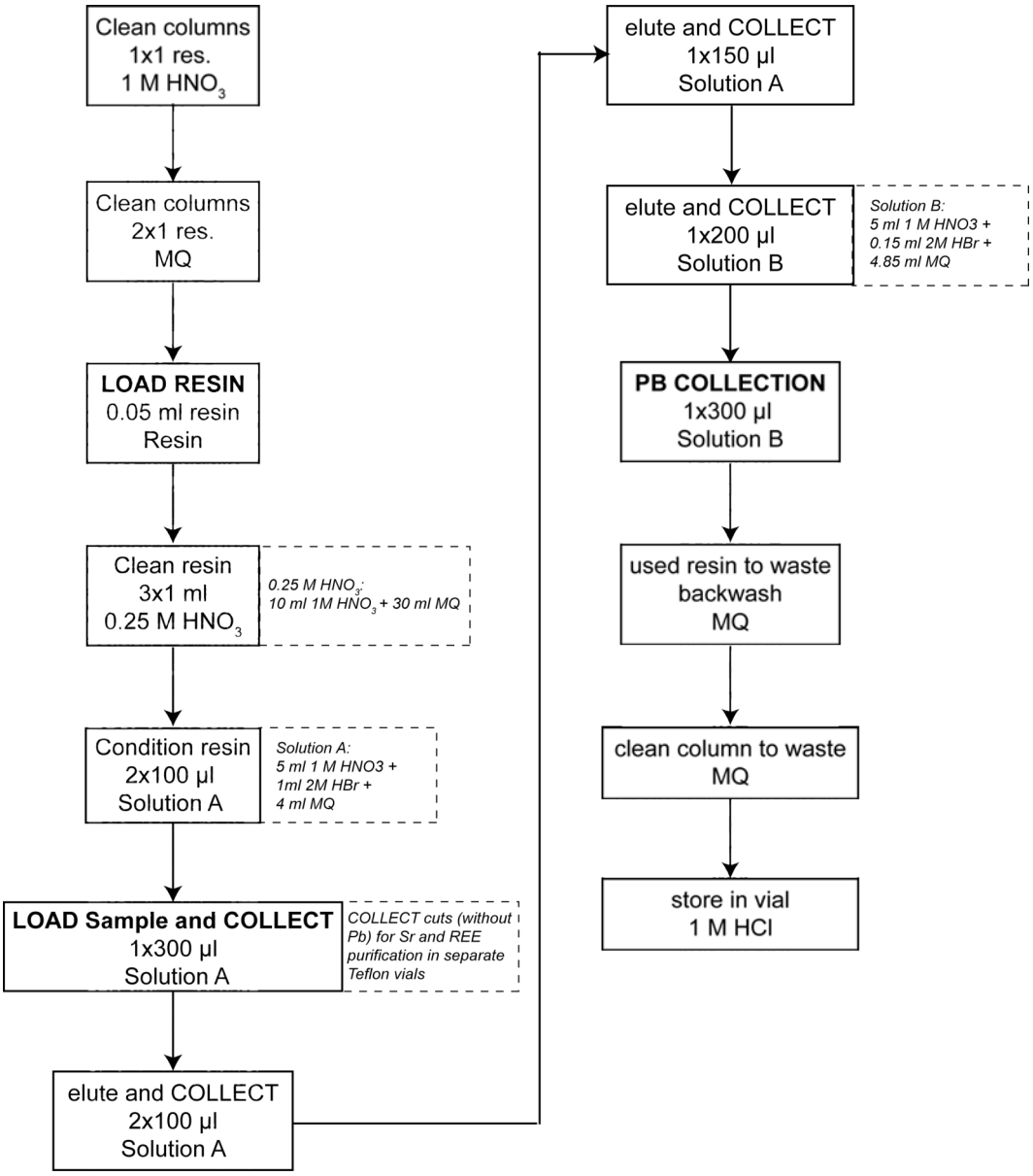

Fig. 2.2: Analytical procedure for separation of Pb.

Sr-REE separation

The eluent containing the REE and Sr which was collected at the Pb column procedure was used for the following cation exchange column procedures (0.8 ml AG50W-X12 resin, mesh size 200-400 μm). To convert the samples into the HCl form, 2x1 ml 6M HCl was added and dried down every time. To load the sample, 0.5 ml 1M HCl was added, in which the samples were completely dissolved. After loading the samples and collection of Sr in HCl form, the acid was changed to HNO_3 and REE samples were collected separately (Fig. 2.3).

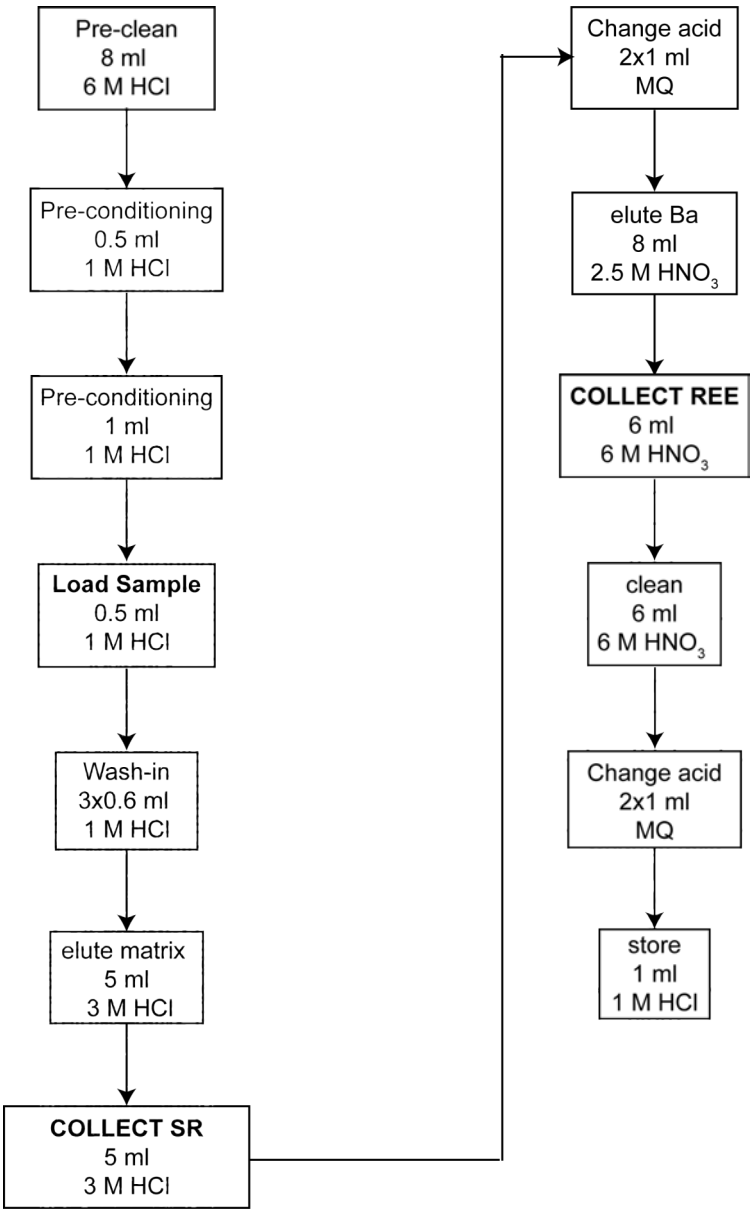

Fig. 2.3: Analytical procedure for separation of REE from Sr.

Nd separation

For separation of Nd from the other REEs (Fig. 2.4) the REE cut from of the previous column procedure was evaporated to dryness. To convert the samples into HCl form, 2x1 ml 6M HCl was added to the samples which were then evaporated to dryness twice. To load the samples in the appropriate solution, 0.5 ml 0.1 HCl were added, in which the samples were completely dissolved. Separation of Nd was carried out on cation exchange columns with 2 ml Ln Spec resin (50-100 μm). After the samples were loaded in 0.1 M HCl, Nd samples were collected in 0.25 M HCl. After the samples with Nd were evaporated to dryness and oxidized with 100 μl concentrated HNO_3 and 100 μl concentrated H_2O_2, they were stored in 2% HNO_3 until measurement.

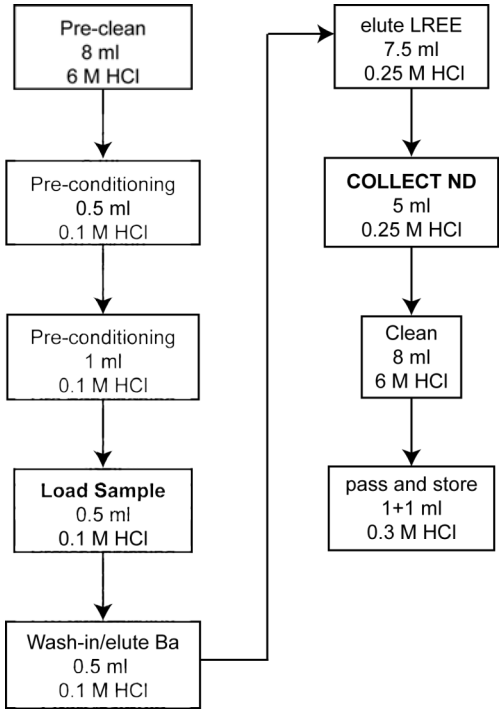

Fig. 2.4: Analytical procedure for separation of Nd.

Sr separation

The Sr cut collected in HCl during the REE column procedure was converted into HNO_3 form with 300 µl 3M HNO_3 and dried down. For Sr purification (Fig. 2.5) cation exchange columns were loaded with 50 µl Sr-Spec resin (mesh size 50-100 µm). To load the sample in HNO_3, 50 µl 3M HNO_3 were added, in which the samples were completely dissolved. After loading of the samples in 3M HNO_3, Sr samples were collected in MQ water. After the samples had been evaporated to dryness and oxidized with 100 µl concentrated HNO_3 and 100 µl concentrated H_2O_2, samples were stored in 2% HNO_3 until measurement.

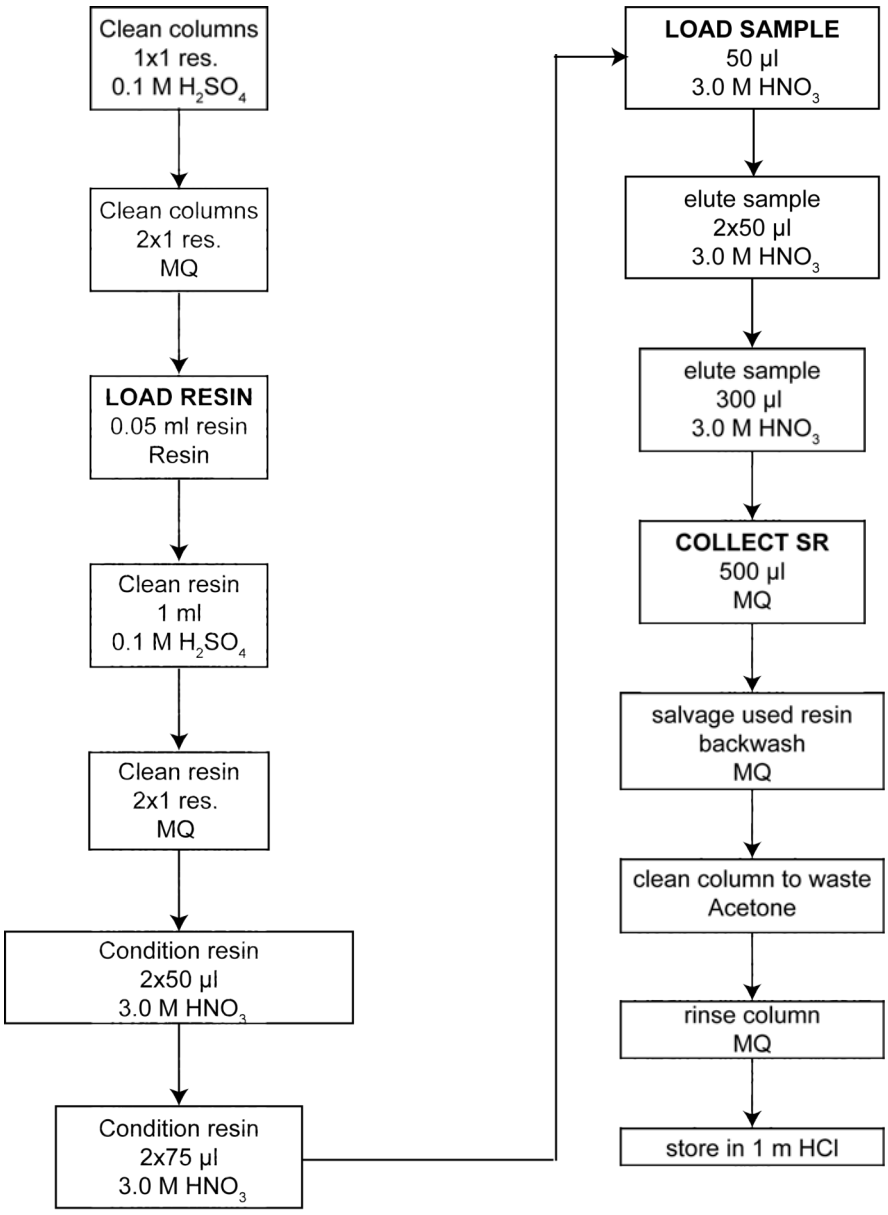

Fig. 2.5: Analytical procedure for separation of Sr.

2.9.2. Isotope measurements

Nd, Pb and Sr isotope analyses were performed on the Nu Plasma MC-ICPMS at IFM-GEOMAR, Kiel. All Nd isotope ratios presented ($^{143}Nd/^{144}Nd$) were mass bias corrected following an exponential law using $^{146}Nd/^{144}Nd = 0.7219$ and normalized to the accepted value of the JNdi-1 standard of 0.512115 (Tanaka et al., 2000). Repeated measurements of the JNdi-1 standard during the two measurement sessions revealed an average reproducibility of ± 0.28 ε_{Nd} units (2σ) or 0.44 and 0.00023 ε_{Nd} units (2σ) for the separate sessions.

A standard bracketing method following Albarède et al. (2004) was applied to determine lead isotope ratios. All presented Pb isotope values were normalized to the accepted values for the NBS981 standard (Abouchami et al., 1999). The reproducibility for NBS981 was 0.0075 for $^{206}Pb/^{204}Pb$, 0.0101 for $^{207}Pb/^{204}Pb$, 0.0326 for $^{208}Pb/^{204}Pb$, 0.0009 for $^{208}Pb/^{206}Pb$, and 0.0002 for $^{207}Pb/^{206}Pb$.

The $^{87}Sr/^{86}Sr$ signature was measured on aliquots of the same samples to support the seawater origin of the extracted Nd and Pb isotope signals from the ferromanganese coatings (Rutberg et al., 2000; Piotrowski et al., 2005; Gutjahr et al., 2007). $^{87}Sr/^{86}Sr$ ratios were corrected for isobaric interference (^{86}Kr, ^{87}Rb) and mass bias (using $^{86}Sr/^{88}Sr = 0.1194$; Steiger and Jäger, 1977). All presented Sr isotope data were normalized to the accepted value of standard NBS987 ($^{87}Sr/^{86}Sr = 0.710245$). The 2σ reproducibility during the measurements was $\pm$ 0.00002.

References

Abouchami, W., Galer, S.J.G. and Koschinsky, A. (1999) Pb and Nd isotopes in NE Atlantic Fe-Mn crust: proxies for trace metal paleosources and paleocean circulation. *Geochimica et Cosmochimica Acta* 63, 1489-1505.

Albarède, F., Telouk, P., Blichert-Toft, J., Boyet, M., Agranier, A. and Nelson, B. (2004) Precise and accurate isotopic measurements using multiple-collector ICPMS. *Geochimica et Cosmochimica Acta* 68, 2725-2744.

Barrat, J.A., Keller, F. and Amossé, J. (1996) Determination of rare earth elements in sixteen silicate reference samples by ICP-MS after Tm addition and ion exchange separation. *Geostandard Newsletter* 20, 133-139.

Bayon, G., German, C.R., Boella, R.M., Milton, J.A., Taylor, R.N. and Nesbitt, R.W. (2002) An improved method for extracting marine sediment fractions and its application to Sr and Nd isotopic analysis. *Chemical Geology* 187, 179-199.

Cohen, A.S., O'Nions, R.K., Siegenthaler, R. and Griffin, W.L. (1988) Chronology of the pressure-temperature history recorded by a granulite terrain. *Contributions to Mineralogy and Petrology* 98, 303-311.

Duplessy, J.-C., Labeyrie, L. and Waelbroeck, C. (2002) Constraints on the ocean oxygen isotope enrichment between the Last Glacial Maximum and the Holocene: paleoceanographic implications. *Quaternary Science Reviews* 21, 315-330.

Frank, M. (1996) Spurenstoffuntersuchungen zur Zirkulation im Eurasischen Becken des Nordpolarmeeres. PhD thesis Ruprecht-Karls-Universität Heidelberg.

Galer, S.J.G. and O'Nions, R.K. (1989) Chemical and isotopic studies of ultramafic inclusions from the San Carlos volcanic field, Arizona: a bearing on their petrogenesis. *Journal of Petrology* 30, 1033-1064.

Gutjahr, M., Frank, M., Stirling, C.H., Klemm, V., van de Flierdt, T. and Halliday, A.N. (2007) Reliable extraction of a deepwater trace metal isotope signal from Fe-Mn oxyhydroxide coatings of marine sediments. *Chemical Geology* 242, 351-370.

Healy-Williams, N. (1992) Stable isotope difference among morphotypes of *Neogloboquadrina pachyderma* (Ehrenberg): implications for high-latitude palaeoceanographic studies. *Terra Nova* 4, 693-700.

Horwitz, E.P., Chiarizia, R. and Dietz, M.L. (1992) A novel strontium-selective extraction chromatographic resin. *Solvent Extraction and Ion Exchange* 10, 313-336.

Le Fèvre, B. and Pin, C. (2005) A straightforward separation scheme for concomitant Lu-Hf and Sm-Nd isotope ratio and isotope dilution analysis. *Analytica Chimica Acta* 543, 209-221.

Lugmair, G.W. and Galer, S.J.G. (1992) Age and isotopic relationships among the angrites Lewis Cliff 86010 and Angra dos Reis. *Geochimica et Cosmochimica Acta* 56, 1673-1694.

Meredith, M., Heywood, K., Dennis, P., Goldson, L., White, R., Fahrbach, E., Schauer, U. and Østerhus, S. (2001) Freshwater fluxes through the Western Fram Strait. *Geophysical Research Letters* 28, 1615-1618.

O'Neil, J.R., Clayton, R.N. and Mayeda, T.K. (1969) Oxygen isotope fractionation in divalent metal carbonates. *Journal of Chemical Physics* 51, 5547-5558.

Pflaumann, U., Duprat, J., Pujol, C. and Labeyrie, L.D. (1996) SIMMAX: A modern analog technique to deduce Atlantic sea surface temperatures from planktonic foraminifera in seep-sea sediments. *Paleoceanography* 1*,* 15-35.

Piotrowski, A.M., Goldstein, S.L., Hemming, S.R. and Fairbanks, R.G. (2005) Temporal relationships of carbon cycle and ocean circulation at glacial boundaries. *Science* 307, 1933-1938.

Reimer, P.J., Baillie, M.G.L., Bard, E., Bayliss, A., Beck, J.W., Blackwell, P.G., Bronk Ramsey, C., Buck, C.E., Burr, G.S., Edwards, R.L., Friedrich, M., Grootes, P.M., Guilderson, T.P., Hajdas, I., Heaton, T.J., Hogg, A.G., Hughen, K.A., Kaiser, K.F., Kromer, B., McCormac, F.G., Manning, S.W., Reimer, R.W., Richards, D.A., Southon, J.R., Talamo, S., Turney, C.S.M., van der Plicht, J. and Weyhenmeyer, C.E. (2009) INTCAL09 and MARINE09 Radiocarbon Age Calibration Curves, 0-50,000 years Cal BP. *Radiocarbon* 51, 1111-1150.

Robinson, S.G. and McCave, I.N. (1994) Orbital forcing of bottom-current enhanced sedimentation of Feni Drift, NE Atlantic, during the mid-Pleistocene. *Paleoceanography* 9/6, 943-972.

Rutberg, R.L., Hemming, S.R. and Goldstein, S.L. (2000) Reduced North Atlantic Deep Water flux to the glacial Southern Ocean inferred from neodymium isotope ratios. *Nature* 405, 935-938.

Schmidt, G.A., Bigg, G.R., Rohling, E.J.(1999) Global Seawater Oxygen-18 Database. http://data.giss.nasa.gov/o18data/.

Shackleton, N.J. and Opdyke, N.D. (1973) Oxygen isotope and paleomagnetic stratigraphy of equatorial Pacific core V28-238: oxygen isotope temperature and ice volumes on a 10^5 and 10^6 year scale. *Quaternary Research* 3, 39-55.

Steiger, R.H. and Jäger, E. (1977) Subcommission on geochronology: convention on the use of decay constants in geo- and cosmochronology. *Earth and Planetary Science Letters* 36, 359-362.

Stuiver, M. and Reimer, P.J. (1993) Extended ^{14}C Data Base and Revised Calib 3.0 ^{14}C Calibration Program. *Radiocarbon* 35, 215-230.

Stumpf, R., Frank, M., Schönfeld, J. and Haley, B.A. (2010) Late Quaternary variability of Mediterranean Outflow Water from radiogenic Nd and Pb isotopes. *Quaternary Science Reviews* 29, 2462-2472.

Tanaka, T., Togashi, S., Kamioka, H., Amakawa, H., Kagami, H., Hamamoto, T., Yuhara, M., Orihashi, Y., Yoneda, S., Shimizu, H., Kunimaru, T., Takahashi, K., Yanagi, T., Nakano, T., Fujimaki, H., Shinjo, R., Asahara, Y., Tamimizu, M. and Dragusanu, C. (2000) JNdi-1: a neodymium isotopic reference in consistency with LaJolla neodymium. *Chemical Geology* 168, 279-281.

Volkmann, R. (2000) Planktic foraminifer ecology and stable isotope geochemistry in the Arctic Ocean: implications from water column and sediment surface studies for quantitative reconstructions of oceanic parameters. *Berichte zur Polarforschung* 361, 1-128.

CHAPTER 3

ATLANTIC WATER ADVECTION TO THE EASTERN FRAM STRAIT – MULTIPROXY EVIDENCE FOR LATE HOLOCENE VARIABILITY

From [Werner, K., Spielhagen, R.F., Bauch, D., Hass, H.C., Kandiano, E. and Zamelczyk, K. (2011), Atlantic Water advection to the eastern Fram Strait – Multiproxy evidence for late Holocene variability, *Palaeogeography, Palaeoclimatology, Palaeoecology, 308*, 264-276.]. Reprinted with permission from Elsevier.

Original paper available online at
http://www.sciencedirect.com/science/article/pii/S0031018211002756
Data available online at http://doi.pangaea.de/10.1594/PANGAEA.761540

3 ATLANTIC WATER ADVECTION TO THE EASTERN FRAM STRAIT – MULTIPROXY EVIDENCE FOR LATE HOLOCENE VARIABILITY

Kirstin Werner[a]*, Robert F. Spielhagen[a,b], Dorothea Bauch[a,b], H. Christian Hass[c], Evgeniya Kandiano[a], Katarzyna Zamelczyk[d]

[a]Leibniz Institute of Marine Sciences IFM-GEOMAR, Wischhofstraße 1-3, 24148 Kiel, Germany
[b]Academy of Sciences, Humanities, and Literature Mainz, Geschwister-Scholl-Straße 2, 55131 Mainz, Germany
[c]Alfred Wegener Institute for Polar and Marine Research, Wadden Sea Station Sylt, Hafenstraße 43, 25992 List/Sylt, Germany
[d]University of Tromsø, Department of Geology, Dramsveien 201, NO-9037 Tromsø, Norway

*Corresponding author. Tel.: +49 600 2888; fax: +49 600 2961
E-mail addresses: kwerner@ifm-geomar.de (K. Werner), rspielhagen@ifm-geomar.de (R. Spielhagen), dbauch@ifm-geomar.de (D. Bauch), christian.hass@awi.de (H.C. Hass), ekandiano@ifm-geomar.de (E. Kandiano), katarzyna.zamelczyk@uit.no (K. Zamelczyk)

Abstract

A multiproxy data set of an AMS radiocarbon dated 46 cm long sediment core from the continental margin off western Svalbard reveals multidecadal climatic variability during the past two millennia. Investigation of planktic and benthic stable isotopes, planktic foraminiferal fauna, and lithogenic parameters aims to unveil the Atlantic Water advection to the eastern Fram Strait by intensity, temperatures, and salinities. Atlantic Water has been continuously present at the site over the last 2,000 years. Superimposed on the increase in sea ice/icebergs, a strengthened intensity of Atlantic Water inflow and seasonal ice-free conditions were detected at ~1000 to 1200 AD, during the well-known Medieval Climate Anomaly (MCA). However, temperatures of the MCA never exceeded those of the 20th century. Since ~1400 AD significantly higher portions of ice rafted debris and high planktic foraminifer fluxes suggest that the site was located in the region of a seasonal highly fluctuating sea ice margin. A sharp reduction in planktic foraminifer fluxes around 800 AD and after 1730 AD indicates cool summer conditions with major influence of sea ice/icebergs. High amounts of the subpolar planktic foraminifer species *Turborotalia quinqueloba* in size fraction 150-250 μm indicate strengthened Atlantic Water inflow to the eastern Fram Strait already after ~1860 AD. Nevertheless surface conditions stayed cold well into the 20th century indicated by low planktic foraminiferal fluxes. Most likely at the beginning

of the 20th century, cold conditions of the terminating Little Ice Age period persisted at the surface whereas warm and saline Atlantic Water already strengthened, hereby subsiding below the cold upper mixed layer. Surface sediments with high abundances of subpolar planktic foraminifers indicate a strong inflow of Atlantic Water providing seasonal ice-free conditions in the eastern Fram Strait during the last few decades.

Keywords

Late Holocene, Fram Strait, Atlantic Water, multiproxy, stable oxygen and carbon isotopes, planktic foraminifers

3.1. Introduction

In the recent climate discussion the Arctic Ocean has been identified as one of the most sensitive areas with respect to ongoing global warming processes. In particular, the term "Arctic amplification" has become popular when explaining the enforced warming in the Arctic. In high latitudes, greenhouse gas-induced rises in atmospheric temperatures generate a lowering of the albedo due to sea ice loss. As a consequence, compared to the Northern Hemisphere as a whole, more heat is transported from the Arctic Ocean to the atmosphere, especially during winter (e.g., Manabe and Stouffer, 1980; Serreze et al., 2009). The Fram Strait is the only deepwater passage for relatively warm and saline Atlantic Water (AW) masses to enter the Arctic Ocean. While its western part is perennially ice-covered, Atlantic Water enters the Arctic Ocean through the eastern part of Fram Strait, keeping it ice-free all year (Fig. 3.1). Today, Fram Strait plays a crucial role for the heat budget and the sea ice extent of the Arctic. During the past few decades it has shown major variabilities in the flow strength of Atlantic Water (e.g., Karcher et al., 2003; Schauer et al., 2004). As a consequence, enhanced heat influx by Atlantic Water led to almost completely absence of ice in Kongsfjorden (Svalbard) during winter/spring 2006 (Hop et al., 2006) and subsequently to a delayed and reduced spring bloom (Hegseth and Tverberg, 2008). During the following two winters a reduced ice cover persisted which may be an indication for a warming of the entire fjord system that may have passed a tipping point (Hop et al., 2010) with most likely major impacts on the biological system.

Proxy data provide knowledge of past climate variability that is essential for understanding and modelling of current and future climate trends (Jones et al., 2001). In extending the record of climate variability beyond the era of instrumental measurements, proxy records provide information about the mechanisms, forcing factors, and spatial and temporal ranges of climatic variations (Houghton et al., 1996; Jones et al., 2001).

Terrestrial proxy studies and marine low-resolution proxy data reveal a pervasive cooling during the past two millennia in the Arctic realm that is mainly attributed to the orbitally driven reduction in summer insolation (Kaufman et al., 2009; Moberg et al., 2005). Beside the general cooling trend, climate fluctuations, in particular the Medieval Climate Anomaly (MCA) and the Little Ice Age (LIA), have been noticed in the North Atlantic region (e.g., Bjune et al., 2009; Eiríksson et al., 2006). Notably, it has been debated whether temperatures during the MCA exceeded those of the warming in the past few decades and if there was a warming during the medieval at all (Broecker, 2001; Hughes and Diaz, 1994; IPCC, 2007; Moberg et al., 2005). In the Fram Strait area such climate variability is expressed in the glacier history on Svalbard. Studies on Svalbard glaciers have unveiled the Little Ice Age glaciation as the most extensive late-Holocene glacier advance recognised on Spitsbergen (Isaksson et al., 2005; Svendsen and Mangerud, 1997; Tarussov, 1992; Werner, 1993).

In this paper, we present high-resolution, multidecadal proxy records off West Spitsbergen where surface waters primarily are influenced by the relatively warm and saline Atlantic-derived water masses of the West Spitsbergen Current (WSC). While high-resolution marine proxy reconstructions are still lacking for the latest Holocene in the Arctic Ocean, a few studies are available from the Nordic Seas (e.g., Eiríksson et al., 2006; Klitgaard Kristensen et al., 2004; Sicre et al., 2008) and the Fram Strait (Bonnet et al., 2010). In reconstructing sea-surface temperatures (SST) by alkenones at the North Icelandic shelf, Sicre et al. (2008) found an abrupt increase of SST at ca 1000 AD, related to the onset of the MCA. A sharp cooling after ca 1350 AD is attributed to the beginning of the LIA (Sicre et al., 2008). Indicated by planktic foraminifer assemblages and planktic stable isotopes, Eiríksson et al. (2006) reported an overall cooling trend throughout the last ca 1000 years north of Iceland and at the Norwegian margin. Klitgaard Kristensen et al. (2004) indicate lower-than-present temperatures from 1225 to 1450 and 1650 to 1905 AD in the eastern Norwegian Sea, the latter interval attributed to the Little Ice Age. The past 80 years have been described as warmest within the last 800 years period at the Norwegian margin (Klitgaard Kristensen et al., 2004).

A marine record from the West Spitsbergen continental margin with similar time resolution was obtained from station JM06-WP-04 MC (78°54'N, 6°46'E) in the very vicinity to our study site (Bonnet et al., 2010). Interrupted by short cooling pulses, conditions warmer than present were reconstructed for near-surface waters before ~1650 AD by studies on dinocyst assemblages (Bonnet et al., 2010). Warmest sea surface temperatures with ice-free conditions were detected in this study around ~1320 cal years BP (ca 630 AD). During the last ~300 cal years BP Bonnet et al. (2010) indicated a cooling trend of surface waters with significantly increasing sea ice coverage.

In the eastern Fram Strait Atlantic Water submerges beneath a less saline and cooler upper mixed water layer (e.g., Ślubowska et al., 2005) keeping a large part of eastern Fram Strait ice-free throughout the year. Dinocyst assemblages mainly reflect surface ocean conditions (e.g., Serjeant, 1974; Taylor, 1987). Reconstructing the past behaviour of the complex ocean current system in the eastern Fram Strait is essential to understand ongoing changes in the Arctic Ocean. It requires reliable indicators of both, surface and subsurface water layers. Planktic foraminifers are a useful tool to detect conditions in different water depths. While the polar species *Neogloboquadrina pachyderma* calcifies its tests at the base of the surface water layer in 50 to 200 m water depth the subpolar species *Turborotalia quinqueloba* is known as a symbiont-bearing surface dweller (Simstich et al., 2003) bound to seasonally open conditions (Kucera et al., 2005). By using the isotopic composition of planktic and benthic foraminifers, planktic foraminiferal assemblages and lithogenic parameters, our study tracks variations in the intensity of Atlantic Water inflow and changes in the sea ice extent in the eastern Fram Strait, and hence, variations of the heat transfer to the Arctic Ocean during the last two millennia.

3.2. Regional Setting

In the eastern Fram Strait, relatively warm and saline water masses deriving from the North Atlantic Current are carried poleward with the WSC into the Arctic basin (Quadfasel et al., 1987; Fig. 3.1). Part of the inflowing Atlantic Water continues north and west of the Yermak Plateau as the Yermak Branch, whereas the Svalbard Branch transports these water masses eastwards into the Arctic Ocean (Manley, 1995; Rudels et al., 2000; Saloranta and Haugan, 2001). The East Spitsbergen Current (ESC) carries cold water and sea ice from the Arctic Ocean southward along the east coast of Svalbard to the south and west around Spitsbergen (Hopkins, 1991; Loeng, 1991). Part of it, eventually mixing with brine-enriched shelf water from Storfjorden (Quadfasel et al., 1988; Schauer, 1995), joins the WSC to the west (Hopkins, 1991, and references therein), thereby cooling and freshening the north-flowing Atlantic Water masses. The western part of the Fram Strait is controlled by the southward directed East Greenland Current (EGC), which transports cold fresh water and sea ice along the Greenland continental slope into the Nordic Seas where minor currents such as the Jan Mayen Current and the East Icelandic Current branch off eastward (Fig. 3.1; Hopkins, 1991).

The hydrography of the Fram Strait controls the persistence of a specific seasonal sea ice distribution pattern (Fig. 3.1). The western part in the vicinity of the Greenland coast is perennially covered by sea ice, whereas the eastern Fram Strait has seasonally varying ice conditions. Large areas in the west and north of Svalbard stay ice-free all year, affected by the warmer, higher saline Atlantic Water inflow (Aagaard et al., 1987; Rudels et al., 2000).

Norwegian Sea Deep Water (NSDW), that originates from thermohaline processes in the Greenland Sea, flows northwards underneath the WSC in the eastern Fram Strait (Swift and Koltermann, 1988; Schlichtholz and Houssais, 1999).

During the past ~150 years, the investigated site experienced alternating positions of the winter sea ice margin (Vinje, 2001). Thus, similar sea ice variability can be anticipated also for the last two millennia. Today, the study site is situated under seasonal ice-free conditions, impacted by the Atlantic Water-bearing WSC (Fig. 3.1).

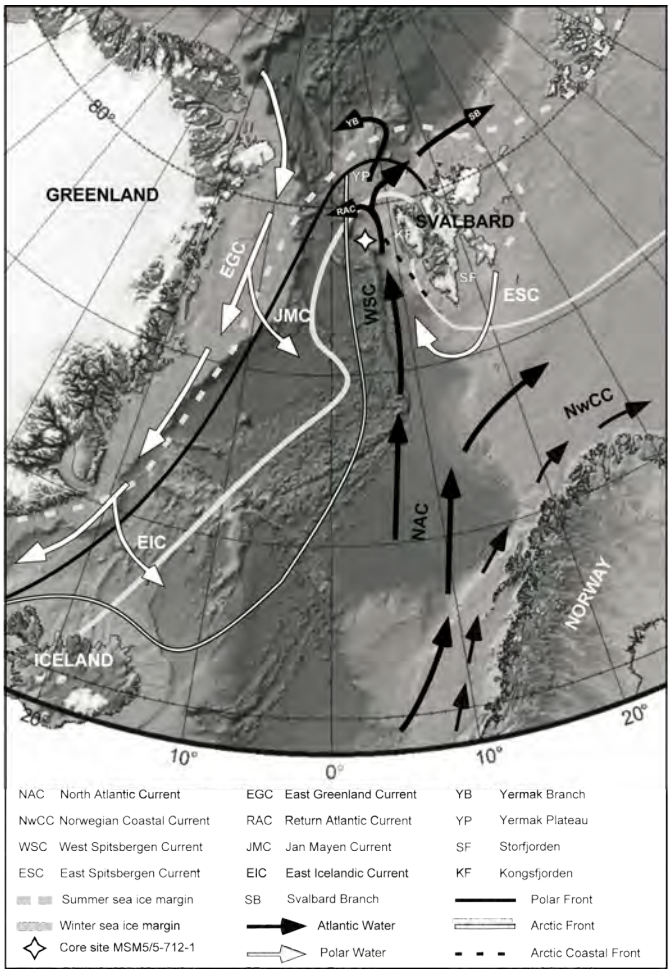

Fig. 3.1: Map of the Norwegian-Greenland Sea with respect to the major currents and the hydrography of the Fram Strait (modified after Slubowska-Woldengen et al., 2007 and references therein). Also indicated is the core site MSM5/5-712-1.

3.3. Material and methods

The 46 cm long sediment core (box core) MSM5/5-712-1 was retrieved from the western Svalbard continental margin (78°54.94' N, 6°46.04' E, 1490.5 m water depth, Fig. 3.1) during cruise leg MSM5/5 with RV „Maria S. Merian" in summer 2007.

Sampling was carried out every 0.5 cm throughout the core section for the analysis of planktic and benthic isotopes, for ice rafted debris (IRD) and grain size studies, and for the investigation of planktic foraminiferal assemblages in the 100-250 μm size fraction. Studies on planktic foraminifer assemblages in size fraction 150-250 μm and the reconstruction of sea surface temperatures and salinities were carried out in 0.5 cm steps in the upper 5 cm and every 1 cm in the remainder of the record. Planktic foraminifer species involve *Neogloboquadrina pachyderma*, *Turborotalia quinqueloba*, *Neogloboquadrina incompta*, *Globigerinita* sp., and *Globigerina bulloides*. We refer to the term *N. incompta* following Darling et al. (2006) who identified *N. pachyderma* (sinistral coiling) (now redefined to *N. pachyderma*) and *N. pachyderma* (dextral coiling) (redefined to *N. incompta*) as different species. The samples were freeze-dried and wet-sieved in deionised water through a 63 μm-sized mesh to remove clay and silt material. Dry bulk density was determined every 5 cm from defined 10 cm^3 samples.

Age control is based on five accelerator mass spectrometry (AMS) radiocarbon dates published in Spielhagen et al. (2011) (Table 1). Analyses were conducted at the Leibniz Laboratory of Kiel University using ca 10 mg of $CaCO_3$. Except for the surface sample all measurements were carried out on a single species *N. pachyderma*. Due to an insufficient amount of *N. pachyderma* additional planktic foraminifer species including *T. quinqueloba*, *G. bulloides*, and *N. incompta* were used for age determination of the surface sample. Furthermore the amount of Rosa Bengal stained benthic foraminifers was counted in the surface sample to estimate the quantity of living species immediately after core recovery and thus to confirm a possible modern age of the surface sample.

The radiocarbon dates were converted to calendar years BP (present = 1950 AD) applying the calibration software Calib version 6.0 (Stuiver and Reimer, 1993) with the use of the Marine09 calibration data set (Reimer et al., 2009), including a reservoir correction of ~400 years. Chronology is established using the calibrated calendar ages and assuming uniform sedimentation rates between them by linear interpolation. If not marked specifically all ages discussed here are given in calendar years AD. Since the age-depth model reveals bidecadal time-resolution we rounded all ages accordingly. We refrained from applying a regional average correction ΔR value since all values provided by the Marine Reservoir Correction Database in CALIB (http://calib.qub.ac.uk/marine/) were obtained from the shallow Svalbard coast area and therefore seem not appropriate as a suitable ΔR value for our site at ca 1500 m water depth. Nevertheless we are aware of a possible shift to younger ages due to the ΔR effect when applying our age-depth model.

For investigation of ice rafted debris lithic fragments were counted on a representative split (> 100 grains) of the 150-250 μm size fraction. No significant changes in lithology were noted

throughout the core and thus we present undifferentiated IRD data only. IRD fluxes were calculated based on dry bulk density values and linear sedimentation rates.

Sortable silt mean grain size analysis was carried out every 1 cm using an aliquot of the freeze-dried samples. To remove carbonate and organic matter, samples were treated with acetic acid and hydrogen peroxide, respectively. After adding sodium polyphosphate for better dispersion the freeze-dried samples were put on a shaker for at least 24 hours. Measurements were performed with a CILAS 1180 laser-diffraction particle analyser. The sortable silt mean grain size 10-63 μm (Robinson and McCave, 1994) was calculated using the entire granulometric data sets based on vol.%. When considering a certain contamination of the current-transported sortable silt with sea ice-transported silt, it is likely that a fine sortable silt content results from less coarser silt material due to less sea ice melting (Hass, 2002).

The planktic foraminifer *N. pachyderma* and the benthic foraminifer *Cibicidoides wuellerstorfi* were chosen for stable oxygen and carbon isotope analyses because of their continuous presence in the sediment core. In order to prevent possible ecological biases of different morphotypes (Healy-Williams, 1992) only "square-shaped" (four-chambered) specimens of *N. pachyderma* were used. Analysis was performed at the IFM-GEOMAR Stable Isotope Lab using a Finnigan MAT 253 mass spectrometer system and a Kiel IV Carbonate Preparation Device. The carbonate was treated with orthophosphoric acid at 70°C. The analytical accuracy is 0.06‰ for $\delta^{18}O$ and 0.03‰ for $\delta^{13}C$ or smaller. All measurements were calibrated to Pee Dee Belemnite (PDB) standard (international standard NBS 19). Oxygen isotope data of *C. wuellerstorfi* were corrected for their disequilibrium effect by +0.64‰ (Duplessy et al., 2002; Shackleton and Opdyke, 1973).

Planktic foraminiferal assemblages were studied on the size fractions 100–250 μm and 150-250 μm (see Spielhagen et al., 2011). A representative split of at least 300 planktic foraminiferal tests was counted and identified to species level. The fraction >250 μm was neglected due to an almost complete absence of planktic foraminifers. Planktic foraminifer fluxes were calculated on dry bulk density values and linear sedimentation rates (Spielhagen et al., 2011).

For calculation of sea surface temperatures (SST) we used the planktic foraminifer census data of size fraction 150-250 μm following the SIMMAX procedure of Pflaumann et al. (1996) (for details see Spielhagen et al., 2011). In order to reconstruct salinity variations we used the paleotemperature equation (O'Neil et al., 1969)

$$T = 16.9\text{-}4.38(\delta_c\text{-}\delta_w)+0.1(\delta_c\text{-}\delta_w)^2$$

to derive $\delta^{18}O$ of the ocean water (δ_w in V-SMOW) from SST used from our SIMMAX reconstruction (T) and our measured $\delta^{18}O$ values of *N. pachyderma* (δ_c). In order to derive

salinities from δ_w we applied a modern salinity/$d^{18}O$ correlation of the water column on the Western Svalbard margin from 100 to 500 m water depth, which covers the depth of the AW core within the WSC. Data from Frank (1996) and Meredith et al. (2001) were retrieved from the Global Seawater Oxygen-18 Database (Schmidt et al., 1999; Fig. 3.2):

$$\delta^{18}O = 0.471 * S - 16.195.$$

Overall, the applied data show a relative small range of variations. The observed correlation is very similar to a mixing line between Atlantic Water ($\delta^{18}O$ of 0.3‰ vs. SMOW; salinity 35.1) and measurements made for fjord waters at the Svalbard coast (100-500 m water depth in the nearby Kongsfjorden; MacLachlan et al., 2007). Here, freshwater mainly consists of glacial melt water and the mixing line with Atlantic Water reveals a relationship of $\delta^{18}O = 0.43 * S - 14.69$ (MacLachlan et al., 2007).

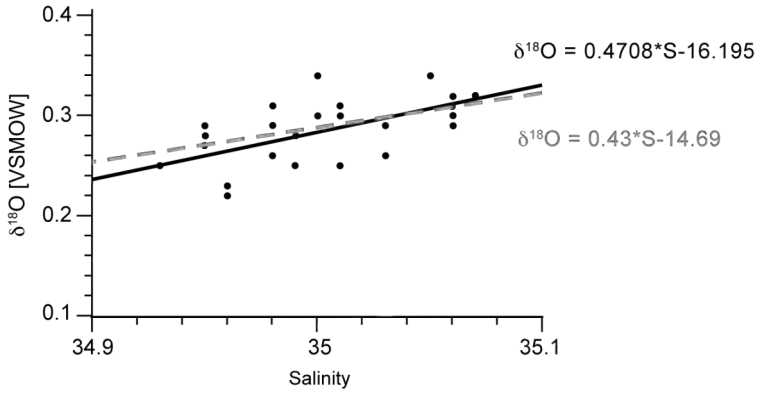

Fig. 3.2: The salinity/$d^{18}O$ relationship of the water column in the eastern Fram Strait (100-500 m water depth; Frank, 1996; Meredith et al., 2001; black dots and black correlation line). Also shown is the mixing line from the nearby Kongsfjorden, Svalbard based on MacLachlan et al. (2007) (grey dashed line).

Due to the similarity between mixing lines of water in the WSC and fjord waters (Fig. 3.2), we expect the glacier melt influence to cause variations seen in the modern inflow of AW in the eastern Fram Strait and suppose that glacial melt water also had some influence on the water masses at our investigated site.

The calculated salinity value of about 35.5 for the core top sample is slightly higher than a salinity of 35.1 seen in present-day Atlantic Water at this position (Fig. 3.4g). We correct our salinity calculations by a shift of -0.2‰ in foraminiferal $\delta^{18}O$ in order to fit present-day Atlantic Water salinity of 35.1. A $\delta^{18}O$ vital effect for *N. pachyderma* cannot explain the calculated high salinity values as estimates vary between 0.8 and 1.3‰ for the Arctic (Bauch et al., 1997; Kohfeld et al., 1996; Volkmann and Mensch, 2001) and 0.4‰ for the eastern Fram Strait (Spielhagen and Erlenkeuser; 1994). Instead a shift of -0.2‰ in foraminiferal $\delta^{18}O$ may be generated by a

temperature shift of roughly 1°C in reconstructed relative to actual temperatures. A temperature shift at the core position may easily occur as temperatures within the West Spitsbergen Current are rapidly decreasing northward (Saloranta and Haugan, 2004) and SIMMAX SST may still partly represent higher temperatures found upstream. Corrected foraminiferal $\delta^{18}O$ (-0.2‰ shift) are used for salinity reconstructions only, and for the interpretation of reconstructed salinities only salinity trends are used. We like to note that the calculated SSS values are not an independent proxy but rather a translation of measured planktic $\delta^{18}O$ values and calculated SIMMAX SST.

Based on the paleotemperature equation (O'Neil et al., 1969) present-day oxygen equilibrium calcite values were calculated for subsurface (50 to 200 m) and bottom (1000 to 1600 m) water depths, respectively (Frank, 1996; Meredith et al., 2001; Schmidt et al., 1999). Oxygen isotope values of seawater (in V-SMOW) were transferred into $d^{18}O$ (PDB) (Bemis et al., 1998).

3.4. Results and interpretation

3.4.1. Sedimentation rates and lithological variations

The stratigraphic record of box core MSM5/5-712-1 extends ca 2,000 years (Table 1, Fig. 3.3a, for details see Spielhagen et al., 2011). Linear sedimentation rates vary between 18 and 20 cm/kyr in the lower core section and are 28.3 cm/kyr after 1500 AD (Fig. 3.3b). The time span of each 0.5 cm thick sample slice ranges between 25.1 and 27.7 years until 1500 AD, and is 17.7 years/0.5 cm sample for the past ca 500 years. Time resolution of planktic foraminiferal investigation of size fraction 150-250 μm, of the SST and SSS calculations, and of the sortable silt varies between 50.3 and 55.4 years/1 cm sample in the lower core section. During the past 500 years sortable silt samples cover a time span of 35.3 years/1 cm sample whereas samples of planktic foraminiferal study of size fraction 150-250 μm and the SST and SSS calculations range between 35.3 (1500-1850 AD) and 17.7 (since 1850 AD) years/0.5 cm sample. Dry bulk density values and linear sedimentation rates were used to calculate accumulation rates, which vary between 11.1 and 17.7 $g/cm^{2}*kyr$.

On a sediment core from the same site (JM06-WP-04-MC, 78°54'N, 6°46' E) mean sedimentation rates of ~18 cm/kyr contrast high sedimentation rates for the uppermost 11.5 cm (between 30 an 50 cm/kyr) based on AMS-^{14}C and ^{137}Cs measurements (Bonnet et al., 2010; Carignan et al., 2008). The high uppermost sedimentation rates have been attributed to an increased proportion of the coarse material that might possibly result from increased ice rafting (Bonnet et al., 2010). The same applies to our record where high sedimentation rates in the uppermost ~15 cm correspond to higher input of IRD and coarse-grained material as well as higher planktic foraminifer fluxes (Fig. 3.4a, c). Carignan et al. (2008) measured the

anthropogenic lead distribution of the upper 20 cm of the JM06-WP-04-MC sediment core. A systematic decrease of high ^{210}Pb and anthropogenically-induced, less radiogenic input within the uppermost sediment layers and constant concentrations below confirmed mixing effects caused by bioturbation in the uppermost 8 cm of the sediment core (Carignan et al., 2008). Thus, the obtained ^{210}Pb data could not be used to document sedimentation rates (Bonnet et al., 2010).

Table 3.1: AMS radiocarbon dates and calibrated dates for box core MSM5/5-712-1 (see also Spielhagen et al., 2011).

Depth, cm	Dated material	^{14}C age, yr	Cal. age, yr BP (1σ)	Cal. age, yr AD	Lab. no
0	planktic foraminifers		0	>1954 (103.47 0.32 pMC corrected)	KIA 39656
14.5-15.0	*N. pachyderma*	820 ± 25	464 ± 23	1486 ± 23	KIA 39262
21.0-22.0	*N. pachyderma*	1290 ± 30	838 ± 45	1112 ± 45	KIA 39041
30.5-31.0	*N. pachyderma*	1760 ± 25	1303 ± 26	647 ± 26	KIA 39263
41.5-42.5	*N. pachyderma*	2270 ± 25	1878 ± 39	72 ± 39	KIA 38079

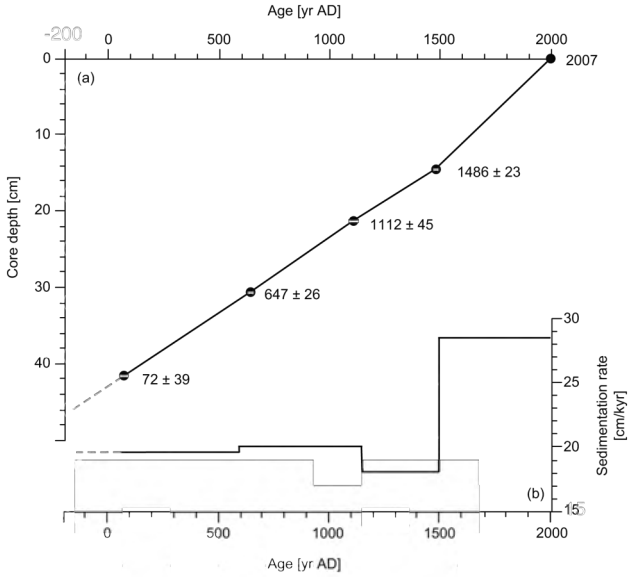

Fig. 3.3: (a) Age-depth model. Calendar years vs. core depth for box core MSM5/5-712-1 (Table 1, Spielhagen et al., 2011). Radiocarbon dates were converted into calendar ages using the Calib version 6.0 software (Stuiver and Reimer, 1993). Dots indicate calibrated ages with a 1s uncertainty (white bars within black dots). (b) The sedimentation rates are indicated to the corresponding linear interpolation curves, respectively.

IRD flux is relatively low until ~1300 AD with average values of ca 1,500 grains/cm^2*kyr (Fig. 3.4c). After 1350 AD it increases significantly. Lowest fluxes occur between 100 and 400 AD while a maximum of more than 5,400 grains/cm^2*kyr is observed ~1890 AD.

The sortable silt mean grain size is comparably small (around 25 μm) during almost the whole core section (Fig. 3.4d). After 1920 AD it increases significantly with a maximum of 33 μm around 1950 AD. The modern value falls back to 28 μm (Fig. 3.4d). Since various influences on the sortable silt grain size e.g., by bottom currents, their sediment loads and by possible IRD contamination are not fully understood at the moment, we refrain from a detailed interpretation but draw our conclusions on the main trends seen in the sortable silt record.

The sand content (63-1000 μm) varies between 1.7 and 9.0% (Fig. 3.4e). Lowest portions not exceeding 2% coincide with those observed in the IRD flux at 100-400 AD. Since 1700 AD the sand content parallels the trend in IRD flux and increases with average values of more than 4.5%. It reveals its maximum of more than 9% in the surface sample.

Fig. 3.4 (next page): Multiproxy data set of box core MSM5/5-712-1. Approximate time frames for North Atlantic climate events are given above. Grey and white bars mark time intervals referred to in the text (RWP: Roman Warm Period, DACP: Dark Ages Cold Period, MCA: Medieval Climate Anomaly; LIA: Little Ice Age). Black dots indicate AMS datings with 1s uncertainty (white bars). Ranges of present-day conditions (temperature, salinity, equilibrium calcite $d^{18}O$) are indicated by grey dashed lines.

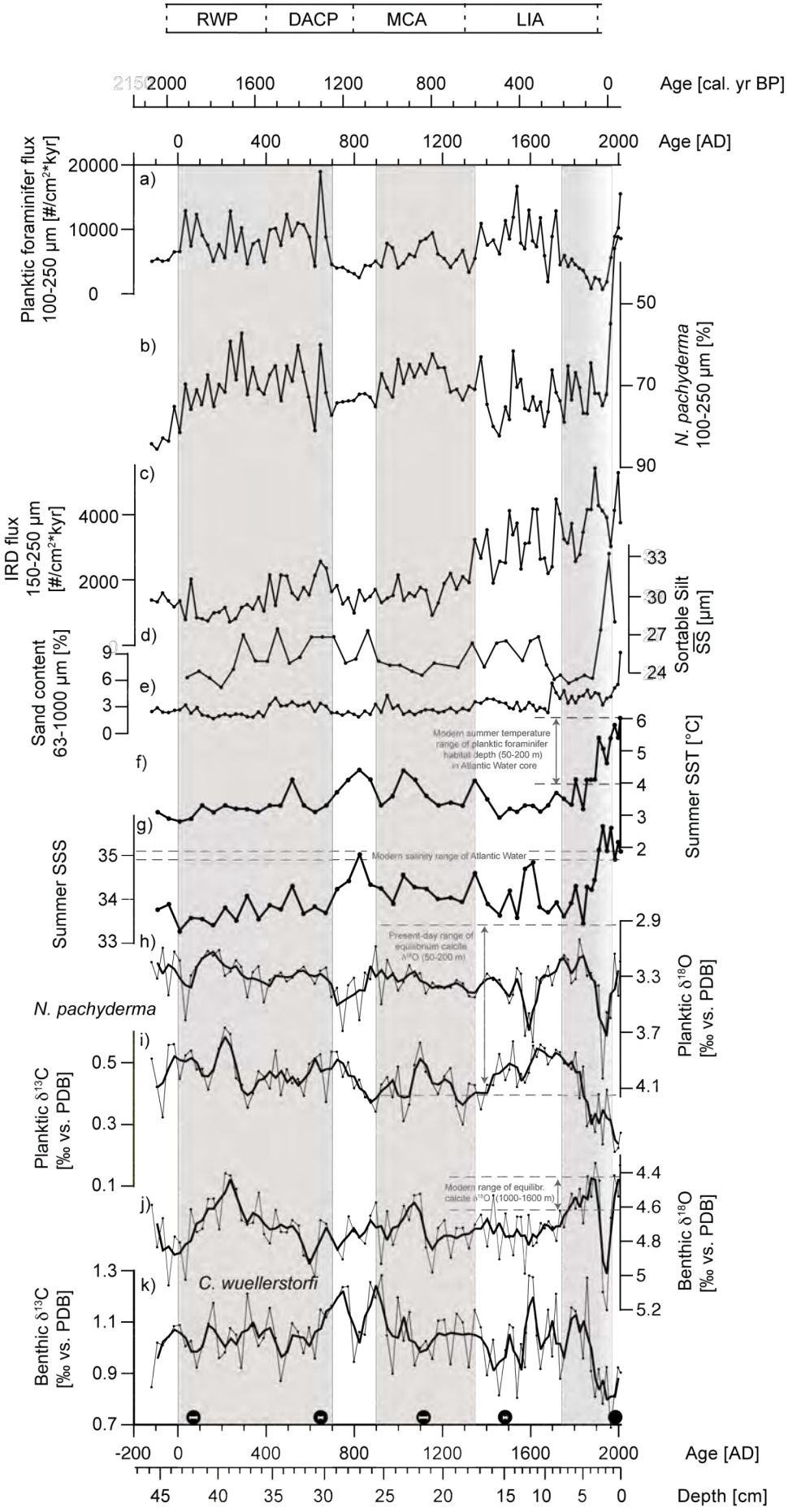
RWP
DACP
MCA
LIA
Age [cal. yr BP]
Age [AD]
Planktic foraminifer flux 100-250 µm [#/cm²*kyr]
a)
b)
N. pachyderma 100-250 µm [%]
IRD flux 150-250 µm [#/cm²*kyr]
c)
Sortable Silt SS [µm]
Sand content 63-1000 µm [%]
d)
e)
Modern summer temperature range of planktic foraminifer habitat depth (50-200 m) in Atlantic Water core
f)
Summer SST [°C]
g)
Summer SSS
Modern salinity range of Atlantic Water
h)
Present-day range of equilibrium calcite Δ18O (50-200 m)
Planktic δ18O [‰ vs. PDB]
N. pachyderma
i)
Planktic δ13C [‰ vs. PDB]
j)
Modern range of equilibr. calcite δ18O (1000-1600 m)
Benthic δ18O [‰ vs. PDB]
k)
C. wuellerstorfi
Benthic δ13C [‰ vs. PDB]
Depth [cm]

3.4.2. Stable oxygen and carbon isotopes

Variations of planktic $d^{18}O$ values range between 3.0 and 4.0‰ (Fig. 3.4h). Episodes of outstanding heavy values of more than 3.6‰ occur at ~30, 750-820, 1570-1610, and 1930-1960 AD. Light intervals are observed at ~100-200 and 1730-1840 AD. Benthic $d^{18}O$ values range from 4.4 to 5.2‰ (Fig. 3.4j). Light values (<4.6‰) appear around 250 AD, before 1100 AD, and between 1850 and 1910 AD. The interval between 1930 and 1960 AD is characterized by a sharp increase to maximum values of up to >5.0‰. Thereafter, benthic $d^{18}O$ values shift to light values of up to 4.4‰.

Modern $\delta^{18}O$ equilibrium values of the 50 to 200 m water depth range between 2.93 and 4.16‰ covering not only the planktic $\delta^{18}O$ value measured on the surface sample but the entire planktic $\delta^{18}O$ range of the past 2000 years (Fig. 3.4h). The range of modern $\delta^{18}O$ equilibrium values from 1000 to 1600 m water depth is relatively narrow (4.41 to 4.61‰) and cannot explain a large part of the recorded benthic $\delta^{18}O$ values (Fig. 3.4j). However, the values of the uppermost samples are in good accordance to the present-day oxygen equilibrium range.

Planktic $d^{13}C$ values vary from 0.2 to 0.6‰ (Fig. 3.4i). Lightest values (<0.3‰) occur in the upper 4.5 cm, in agreement with Spielhagen and Erlenkeuser (1994) who reported modern planktic $d^{13}C$ of <0.4‰ in the eastern Fram Strait. Heavier values are noticed around 200 and between 1500 and 1800 AD. The benthic $d^{13}C$ record ranges between 0.7 and 1.3‰ (Fig. 3.4k). Values are higher at ~750-920 and ~1600-1850 AD. Considerably lighter values occur in the uppermost core section comprising the past ca 100 years.

3.4.3. Planktic foraminifer diversity and flux

Planktic foraminiferal data and corresponding SIMMAX temperature reconstructions from core MSM5/5-712-1 were reported by Spielhagen et al. (2011) and are presented here to support conclusions from other proxies. On the western Svalbard margin the planktic foraminifer fluxes and percentages in the 100-250 μm size fraction are highly variable during the last 2,000 years (Fig. 3.4a, b). At ~1-700 and ~1350–1750 AD planktic foraminifer fluxes were high (mean values around 9,000 ind./cm^2*kyr) and fluctuated strongly (Fig. 3.4a). Lower and less fluctuating fluxes appeared at ~700-1350 AD (5,300 ind./cm^2*kyr on average) and ~1730-1950 AD (1,700 ind./cm^2*kyr on average).

Except for the core top section, percentages of *N. pachyderma* vary between 55 and 86% throughout the past two millennia (Fig. 3.4b). In the uppermost core section, subpolar planktic foraminifers up to 66% (Fig. 3.5b, c, 3.6c) characterize high planktic foraminifer fluxes (up to 15,500 ind./cm^2*kyr, Fig. 3.4a, 3.6b). Subpolar species include *T. quinqueloba*, *N. incompta*, *Globigerinita* sp., and *G. bulloides*. The main species are shown in Fig. 3.5b, c. *Globigerinita* sp.

combines findings of *Globigerinita uvula* and *Globigerinita glutinata* which cannot always be differentiated when smaller than 150 µm. Subpolar planktic foraminifers are present throughout the whole core section (Fig. 3.6c). After ~1950 AD a drastic increase of *T. quinqueloba* up to 38% is observed in size fraction 100-250 µm, paralleled by increasing portions of *Globigerinita* sp., which reach up to values of 27% (Fig. 3.5c; Spielhagen et al., 2011).

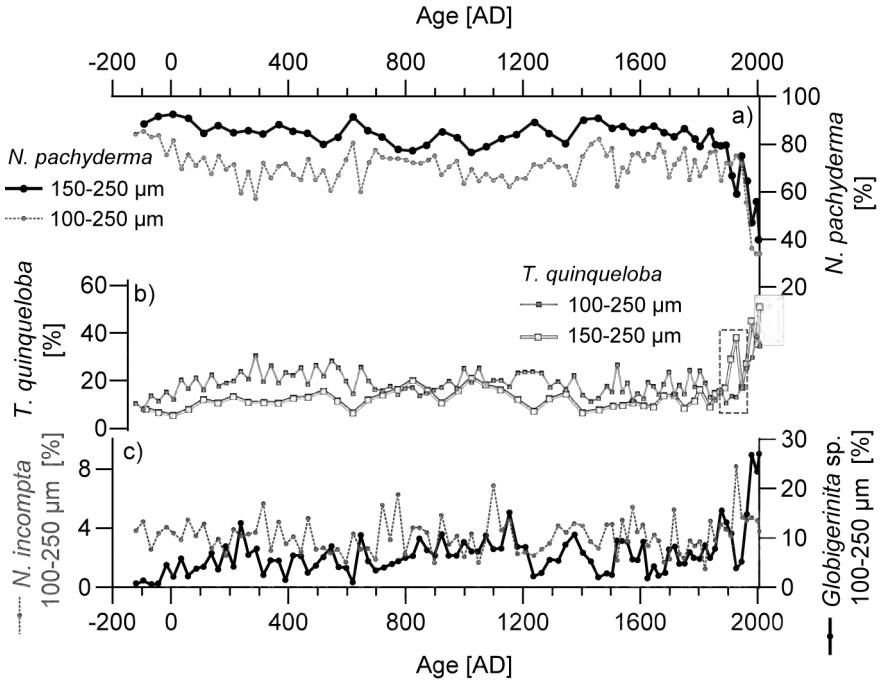

Fig. 3.5: Planktic foraminifer percentages of (a) *N. pachyderma* and (b) *T. quinqueloba* shown for different size fractions. Dashed square indicates interval with percentages of *T. quinqueloba* in size fraction 150-250 µm exceeding those in size fraction 100-250 µm. (c) Percentages of *Globigerinita* sp. (black) and *N. incompta* (grey) in size fraction 100-250 µm.

Previous investigations have demonstrated the advantage of employing small-sized fractions for paleoceanographic reconstructions (Kandiano and Bauch, 2002). Often, small specimens and juvenile forms of the planktic foraminifers *G. glutinata, G. uvula*, and *T. quinqueloba* are not included in the analysis when using a coarser size fraction (e.g., Bauch, 1994; Carstens et al., 1997; Kandiano and Bauch, 2002). In size fraction 150-250 µm, average portions of 80% and 15% are noticed for *N. pachyderma* and *T. quinqueloba*, respectively (Fig. 3.5a, b). A significant increase in percentages of *T. quinqueloba* is reflected in both size fraction during the last few decades. The increased content of *T. quinqueloba* in size fraction 150-250 µm ~1930 AD is not seen in the 100-250 µm fraction due to higher percentages of small-sized *N. pachyderma* specimens.

3.4.4. Sea surface temperature and salinity reconstruction

SIMMAX results based on the planktic foraminifer assemblages in the 150-250 µm size fraction reveal higher summer SST between 650 and 1400 AD with maximum temperatures of

4.4°C (Fig. 3.4f). Highest SST are noticed from ~1800 AD to present time, with maximum temperatures (6°C) reconstructed from the sediment surface sample. They correspond well to instrumental measurements of summer temperatures in the planktic foraminifer habitat depth (50-200 m) of the Atlantic Water core (4 to 6°C) in the eastern Fram Strait (Fig. 3.4f; Spielhagen et al., 2011).

A peak in sea surface salinity of 35.0 similar to the modern one is recorded after 800 AD (Fig. 3.4g). Higher-than-modern-salinities are reconstructed after 1910 AD with a maximum salinity of 35.7 after ~1960 AD. Since salinities of more than 35.2 are not realistic for this area today, we refrain from a detailed interpretation of the reconstructed sea surface salinities. However, trends in the surface salinity record will be used for further interpretation.

3.5. Discussion

3.5.1. Neoglaciation and Atlantic Water inflow

Covering the last ca 2,000 years, our proxy data set suggests variable oceanographic and climatic conditions in the eastern Fram Strait, which we attribute to the variable strength of Atlantic Water inflow and the position of the sea ice margin. Stepwise increasing IRD contents (Fig. 3.4c, 3.6a) unveil a background trend of increasing iceberg/sea ice abundance on the western Svalbard margin during the last two millennia. In high latitude areas, such an increase may reflect either warmer or cooler conditions. Glaciers can grow and discharge more icebergs both in warmer climates with more precipitation on the mountains (Nesje, 2009) and in cooler climates for which less snow melt in summer can be assumed. Coarse lithic particles may also be picked up by seasonal sea ice in littoral zones and released at the sea ice margin upon melting. During the late Holocene, decreasing solar insolation (e.g., Berger and Loutre, 1991) and increasing snow precipitation during generally milder winters in the high northern latitudes (Moros et al., 2004; Nesje et al., 2008) are attributed to a neoglaciation trend. It is pronounced in many terrestrial archives in northern Europe and Greenland (e.g., Bjune et al., 2009; Dahl and Nesje, 1996; Matthews et al., 2000; Nesje et al., 1991, 2000) and seems to have also affected marine sediments from the North Atlantic (e.g., Andrews, et al., 2009, 2010; Koç and Jansen, 2002; Jennings et al., 2002; Moros et al., 2004; Seidenkrantz et al., 2008). A stepwise IRD increase in our record confirms the neoglaciation trend (Fig. 3.6a) which, however, does not necessarily reflect a continuous cooling during the past two millennia. Although coldest conditions of our reconstruction are linked to the Little Ice Age period, we also observe cold conditions at the site between 700 and 900 AD indicated by low and less fluctuating planktic foraminifer fluxes and a dominance of polar planktic species (>70%, Fig. 3.6b, c).

Continuous abundance of the subpolar planktic foraminifer species *T. quinqueloba* indicates that Atlantic Water has been permanently present during the past two millennia at the West Spitsbergen continental margin. *T. quinqueloba*, today dominating the Atlantic-derived water masses of the WSC with >80% (Volkmann, 2000), never falls below 8% in the 100-250 μm size fraction (Fig. 3.5b). Further south, Andersson et al. (2003) reported the uninterrupted abundance of *T. quinqueloba* for the past 3,000 years from the Vøring Plateau. Ślubowska-Woldengen et al. (2007) found evidence for a continuous presence of Atlantic Water at the sea floor on the western and northern Svalbard margins since approximately 15,000 cal year BP.

Fig. 3.6 (next page): A clear neoglaciation trend is marked by IRD increase (a) during the last two millennia. Planktic foraminifer flux (b) is used to indicate whether sea ice coverage (white box and arrow), ice-free (grey box and arrow) or sea ice marginal conditions (dashed box and arrow) prevailed at the site. Strong Atlantic Water inflow is correlated to percentages of subpolar vs. polar planktic foraminifers in size fraction 100-250 μm (c), and to percentages of *T. quinqueloba* in size fraction 150-250 μm (d). Heavy $d^{18}O$ values of *N. pachyderma* (planktic) and *C. wuellerstorfi* (epibenthic) (e) may be attributed to strengthened Atlantic Water (AW) inflow and to temperature (T) or salinity (S) changes (black arrows). Planktic and epibenthic $d^{13}C$ records are used to reconstruct conditions of the living habitat of planktic and benthic foraminifers (ventilation, stratification, bioproduction) in subsurface and bottom water (f). Black arrows in the SST (g) and SSS (h) records highlight certain trends of AW inflow. Summer SST and summer SSS reconstructions derived from dinocyst assemblages by Bonnet et al. (2010) are also shown (MAT: grey dashed line, ANN (based on MAT sites): grey solid line). (i) Normalized 6-year running mean of Atlantic Water temperature anomalies since 1895 (i; Polyakov et al., 2004) confirm increasing temperatures and salinities of our reconstruction (SD = standard deviation) during the past ca 100 years. Black dots indicate AMS datings with 1s uncertainty (white bars).

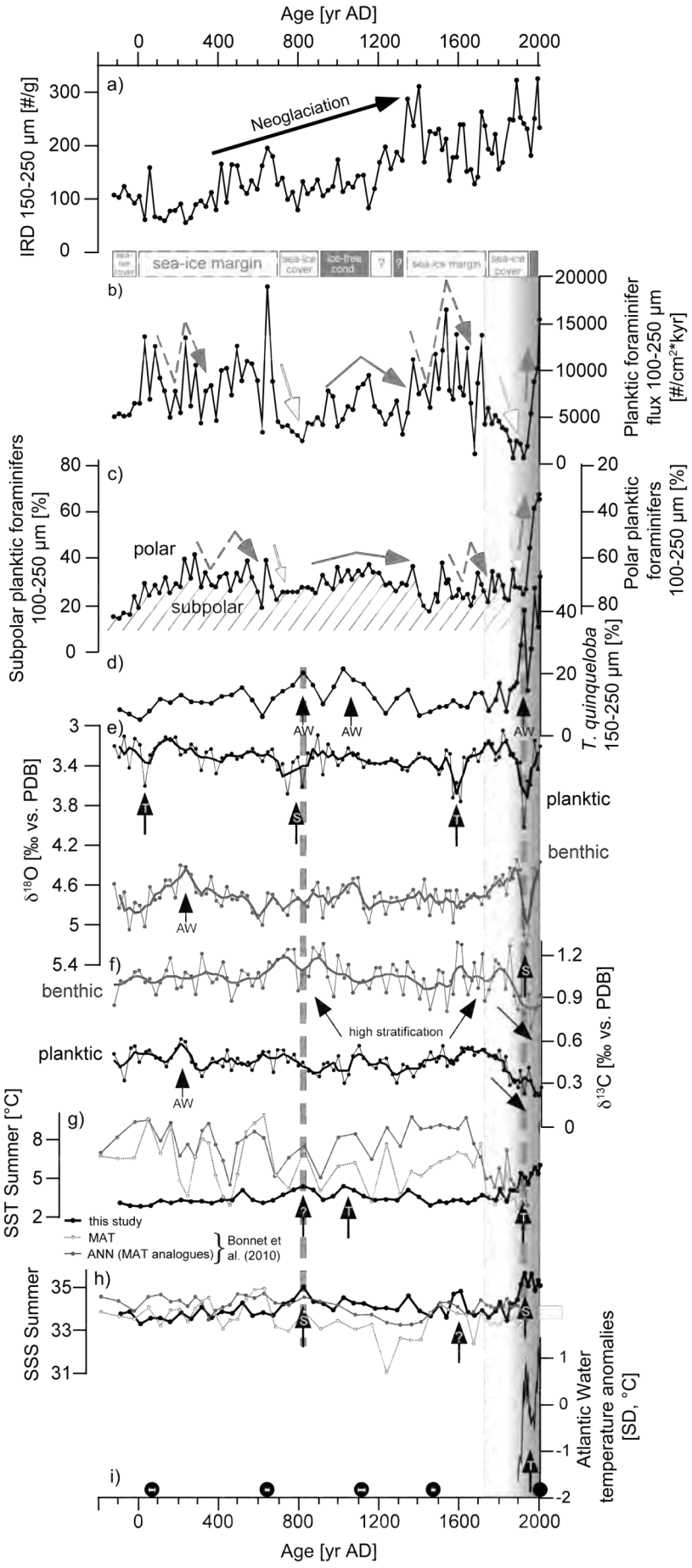
Age [yr AD]
0
400
800
1200
1600
2000
a)
IRD 150-250 µm [#/g]
300
200
100
0
Neoglaciation
sea-ice margin
sea-ice cover
ice-free cond.
?
?
sea-ice margin
sea-ice cover
b)
20000
15000
10000
5000
0
Planktic foraminifer flux 100-250 µm [#/cm²*kyr]
c)
Subpolar planktic foraminifers 100-250 µm [%]
80
60
40
20
0
polar
subpolar
20
40
60
80
Polar planktic foraminifers 100-250 µm [%]
d)
T. quinqueloba 150-250 µm [%]
20
0
e)
AW
AW
AW
3
3.4
3.8
4.2
4.6
5
5.4
δ18O [‰ vs. PDB]
planktic
benthic
AW
f)
benthic
high stratification
planktic
AW
1.2
0.9
0.6
0.3
0
δ13C [‰ vs. PDB]
g)
SST Summer [°C]
8
5
2
this study
MAT
ANN (MAT analogues)
Bonnet et al. (2010)
h)
SSS Summer
35
33
31
1
0
-1
-2
Atlantic Water temperature anomalies [SD, °C]
i)
0
400
800
1200
1600
2000
Age [yr AD]

3.5.2. Paleoceanographic reconstruction and climatic implications

On a transect across the Fram Strait, Hebbeln and Wefer (1991) found highest particle flux rates at the sea ice margin, characterized by maximum and strongly fluctuating planktic foraminifer fluxes (Carstens et al., 1997). Accordingly, we use variations in the planktic foraminifer flux record to subdivide our record into seven time intervals (Fig. 3.4). High and strongly variable fluxes at 1 - 700 AD and 1350 - 1730 AD are interpreted as indicative of a fluctuating ice margin located close to the study site (for detailed discussion see Zamelczyk et al., in prep.). A proximity to the ice margin is also inferred from increased IRD fluxes at 400-700 AD and after 1350 AD which indicate periods of prolonged sea ice melt. Lower and less variable planktic foraminifers flux rates characterize three intervals, the first two also displaying low IRD fluxes. For these periods ~120 BC to 1 AD, 700 to 1350 AD, and ~1730 to 1900 AD we propose more stable conditions. The interval after ~1900 AD has several special characteristics and is treated separately.

3.5.2.1. Time interval ~120 BC and ~1 AD

From ~120 BC to 1 AD the studied sediments are characterized by low subpolar planktic foraminifer percentages and low planktic foraminifer fluxes, medium high IRD fluxes, and slightly increasing planktic and benthic $d^{18}O$ and $d^{13}C$ values (Fig. 3.4, 3.6). The microfossil and IRD proxies point to rather cool conditions with possibly extended seasonal ice coverage. Increasing planktic $d^{18}O$ and $d^{13}C$ values may result from a progressively cooling and moderately well-ventilated environment in the upper water column, consistent with a south-easterly extension of Polar Water in the Fram Strait. Intermediate water conditions at the Western Svalbard margin may have been influenced by enhanced sea ice formation from cool, salty surface waters in the Barents Sea, leading to an admixture of high-density brines with high $d^{18}O$ and $d^{13}C$ values to the intermediate and deeper waters, as proposed by Rasmussen and Thomsen (2009) for earlier parts of the Holocene.

3.5.2.2. Time interval ~1 AD to ~700 AD

Between 1 and 700 AD, strong fluctuations in the percentages and total fluxes of planktic foraminifers indicate a varying intensity of AW inflow (Fig. 3.6b, c). Highest particle fluxes with significant fluctuations at the sea ice margin in the Fram Strait are evidence of a summer sea ice margin prevailing over the investigated site. This is indicated particularly after 400 AD by high IRD contents (Fig. 3.4c, 3.6a). *N. pachyderma* dominated the planktic foraminifer fauna, but a greater influence of the subpolar planktic foraminifer species (up to 42%) suggests temporarily a

stronger impact of Atlantic Water to the site (Fig. 3.6c). Reconstructed summer SST are slightly increasing until ~700 AD with a peak of 4.1°C around 520 AD (Fig. 3.6g).

Between 100 and 300 AD low planktic and benthic $d^{18}O$ may indicate increased temperatures and a strengthened AW advection that may also have affected the bottom water layer. As was shown by Karcher et al. (2003) and Schauer et al. (2004) Atlantic Water warming during the past decades has been caused not only by increased heat transport but also by stronger flow and increased volume transport. Recent vertical variability of the AW layer has been demonstrated in south-eastern Fram Strait (Schlichtholz and Goszczko, 2006). For the past we consider a similar increase in AW volume to likely result in a downward expansion of AW possibly also affecting the bottom water layers at our site.

Intensified AW inflow is furthermore supported by increased portions of subpolar planktic foraminifers (up to 40%) and high planktic $d^{13}C$ values around 200 AD which may suggest *N. pachyderma* migrating to cooler surface waters with a more suitable, better-ventilated near-surface habitat (Carstens and Wefer, 1992, Volkmann, 2000). Raised planktic foraminifer fluxes (>12,500 individuals/cm^2*kyr) indicate that the ice margin probably had prevailed close to the site. In the eastern Fram Strait, Bonnet et al. (2010) reported surface water conditions between 500 and 650 AD as warm as during the modern interval (Fig. 3.6g). Although we find a peak in subsurface water temperatures around 520 AD, portions of *N. pachyderma* at ~550 and ~650 AD vary between 60 to 80%, (Fig. 3.4b, 3.5a, b) indicating strong climate fluctuations most likely associated with a position close to the summer sea ice margin (Hebbeln and Wefer, 1991; Carstens et al., 1997).

3.5.2.3. Time interval ~700 AD to ~900 AD

Between 700 and 900 AD percentages of *N. pachyderma* (72-80%) in both size fractions (Fig. 3.5a) and low planktic foraminifer fluxes (<5,000 ind./cm^2*kyr) (Fig. 3.6b) indicate rather cool conditions. Consistently, Bonnet et al. (2010) reported a cooling pulse in surface waters ~750 AD indicated by dinocyst assemblages (Fig. 3.6g). Cold surface conditions are supported by high planktic $d^{18}O$ values. However, considering a certain salinity effect, high planktic $d^{18}O$ and decreasing planktic $d^{13}C$ are likely to mirror the subsurface Atlantic Water signature reported by Spielhagen and Erlenkeuser (1994) and may thus likely be attributed to increased AW advection and stronger stratification. Strengthened AW inflow is furthermore supported by a local maximum (20%) of *T. quinqueloba* (subpolar) content in size fraction 150-250 μm ~800 AD (Fig. 3.6d) and its associated higher SST and SSS (Fig. 3.6g, h). The 100-250 μm fraction is represented by a high *N. pachyderma* content of conspicuously low variability (75 ± 2%) and a subpolar foraminifer content of about 28% (Fig. 3.6c). It seems therefore likely that the subsurface

advection of Atlantic Water carried allochthonous subpolar species to the site, while the dominance of *N. pachyderma* might be associated with growth of autochthonous *N. pachyderma* within locally cold surface conditions. Nørgaard-Pedersen et al. (2003) reported an overestimation of SIMMAX-derived sea surface temperatures for the western Fram Strait where relatively warm, high-density surface water with 'warm' planktic foraminifers submerges below colder, low salinity and low-density surface water. A similar situation may have been present in the eastern Fram Strait between 700 and 900 AD. Such strong surface-to-subsurface water differences have both past and present analogues. From low biological productivity but significant presence of AW, indicated by benthic foraminifera, Ślubowska et al. (2005) concluded that strongest subsurface influx of Atlantic-derived water took place below a sea ice-covered surface at the northern Svalbard margin during the Bølling-Allerød interstadial. Bauch et al. (1997) described a similar situation for the modern northern Nansen Basin with a core of Atlantic Water overlain by a thick halocline and summer sea ice coverage of about 80-90%.

3.5.2.4. Time interval ~900 AD to ~1350 AD

Between ~900 and 1350 AD slightly lower and significantly less variable planktic foraminifer fluxes point to more stable conditions than during the preceding interval ~1 to 700 AD, coinciding with higher sea surface temperatures and salinities at around ~1000 AD and ~1300-1350 AD (Fig. 3.6b, g, h). Reconstructed warmer SST concur with increased percentages of subpolar species (37%) in both size fractions (Fig. 3.6d, g). Lower IRD fluxes suggest ice-free conditions during most of the year, possibly linked to a strengthened AW inflow. Planktic $d^{13}C$ values fluctuate between 0.3 and 0.57‰ and may be associated with a migration of *N. pachyderma* to variable water depths with optimal living conditions (Carstens and Wefer, 1992). Increased percentages of *T. quinqueloba* at ~1000 to 1200 AD and ~1300 to 1350 AD especially noted in the 150-250 μm size fraction (Fig. 3.6d) may point to strengthened inflow of Atlantic-derived water.

Warmer conditions since ~1000 AD are consistent with many studies from the North Atlantic that have documented the Medieval Climate Anomaly (MCA) (e.g., Lamb, 1965; Dahl-Jensen et al., 1998; Moberg et al., 2005). According to the IPCC and references therein (2007) the medieval warmth was heterogeneous in terms of its precise timing and regional expressions. Although there is not enough evidence available, the authors of the IPCC (2007) acknowledge that the warmest period prior to the 20th century likely occurred between 950 and 1100 AD. This is consistent with our reconstruction of warm conditions lasting from ~1000 to 1200 AD.

Warmer conditions ceased after ~1200 AD when planktic foraminifer fluxes decreased and portions of *N. pachyderma* increased to >70%. An associated cooling pulse was also detected by Bonnet et al. (2010) at ~1150 AD in the surface water layer (Fig. 3.6g). Consistently, in our

record decreasing SST and SSS after ~1150 AD (Fig. 3.6g, h) infer an influence of the mixed water layer which could be linked to decreasing planktic $d^{13}C$ values after 1250 AD pointing to a migration of *N. pachyderma* to greater water depth (Carstens et al., 1997). A drastic decrease in sea surface salinity between 1200 and 1400 AD is also supported by Bonnet et al. (2010) (Fig. 3.6h). After 1300 AD increased subpolar planktic foraminifers and planktic foraminifer fluxes suggest warmer conditions returning to the site but may also be attributed to more sea ice marking the transition to colder conditions of the subsequent Little Ice Age period.

Reconstructed warm conditions and strong AW impact in the North Atlantic domain during the MCA exhibit dating discrepancies which however could be induced by regionalism, uncertainties in age models, or different sensitivities of the applied proxies (Bonnet et al., 2010). On the Vøring Plateau, Andersson et al. (2003) indicated a warmer period around 1200-1400 AD while on the Norwegian margin Berstad et al. (2003) reported the MCA before 1400 AD. From benthic stable isotopes Eiríksson et al. (2006) determined the MCA at the Norwegian margin to the interval 900-1400 AD. North of Iceland Sicre et al. (2008) assigned a warming between 1000 and 1350 AD to stronger heat transport across Denmark Strait by the North Icelandic Irminger Current. In essence, the relatively warm period in our Fram Strait record is thus in good correlation to other reconstruction from the Nordic Seas area.

3.5.2.5. Little Ice Age Period I (~1350 AD to ~1730 AD)

Representing the early phase of the LIA, the period between ~1350 and 1730 AD is characterized by highly variable planktic foraminifer fluxes and high variations of *N. pachyderma* abundance (Fig. 3.6b, c). Records from the North Atlantic reveal the LIA commencing mainly between 1300 and 1400 AD (Andersson et al., 2003; Berstad et al., 2003; Eiríksson et al., 2006). Svalbard ice cores displayed a significant cooling not before 1500 AD (Isaksson et al., 2005).

Increasing IRD contents indicate a major importance of sea ice/icebergs at the investigated site. Increasing planktic $d^{13}C$ values (up to 0.56‰) approach the high $d^{13}C$ signal known from Arctic waters (>0.4‰, Spielhagen & Erlenkeuser, 1994) and indicate that under a permanent ice cover *N. pachyderma* may have migrated to better-ventilated near-surface waters for reasons of food availability (Volkmann, 2000). Planktic foraminifer assemblages in both size fractions and the SST based on the size fraction 150-250 µm (3.3°C) suggest varying but prevalently cool conditions (Fig. 3.6c, d, g). The heavy planktic $d^{18}O$ signal at ~1600 AD (Fig. 3.6e) is likely associated with a strong cooling pulse. Bonnet et al. (2010) observed a freshwater peak in surface waters during that time (Fig. 3.6h). In contrast, summer sea surface salinities calculated on the basis of planktic $d^{18}O$ and SIMMAX-derived temperatures (see 3.) reveal high values and suggest strengthened AW inflow at ~1600 AD. Intensified AW inflow, however,

would be linked to warmer temperatures. Instead, all other proxies reveal cool conditions. Thus, we render our calculated high SSS values erroneous for this time interval and question that the modern salinity/$d^{18}O$ relation on which our SSS estimation is based is applicable around 1600 AD. A cold upper mixed water layer and entrained sea ice may have produced the heavy $d^{18}O$ values of *N. pachyderma*. In contrast, SIMMAX SST calculations are based on planktic foraminiferal assemblages which are to a certain part transported with the warm Atlantic subsurface water from the south, therefore likely suggesting warmer temperatures than those which actually occurred at the site.

We rely on the calculated SSS trends further on since for all other intervals discussed here the obtained salinity values correspond well to our proxy interpretation. The invalidity of the obtained modern salinity/$d^{18}O$ relationship around 1600 AD seems to be an exception which is furthermore supported by a coinciding peak in benthic $d^{13}C$ values. It remains speculative what caused the modification of inflowing water masses. It may have been induced by cold lateral advections, possibly originating from brine formation in the Storfjorden area (Rasmussen and Thomsen, 2009).

From dinocyst assemblages Bonnet et al. (2010) detected a major transition to colder conditions within the surface water layer and increased sea ice cover around 1650 AD (Fig. 3.6g). The apparent offset in the timing of this drastic cold spell between the record of Bonnet et al. (2010) and our data set is most probably a problem of the different core chronologies. Both proxies confirm a shift to colder conditions in the surface and subsurface water layer which point to a major cold event affecting a large part of the entire water column. We note that from a combination of northern hemispheric low-resolution proxies and treering-data Moberg et al. (2005) concluded on minimum temperatures for the Little Ice Age period around 1600 AD.

3.5.2.6. Little Ice Age Period II (after ~1730 AD)

Similar to our findings, Andersson et al. (2003) found a two-phase LIA with cooling events centred around 1600 and 1900 AD. A second phase of the Little Ice Age is inferred from gradually decreasing planktic foraminifer fluxes and high percentages of *N. pachyderma* (64 to 78%) after 1730 AD (Fig. 3.6b, c). IRD contents slightly decrease between ~1750 and 1820 AD (Fig. 3.6a) and point to sea ice coverage due to restricted dispersion of ice-transported material into the water (Hebbeln and Wefer, 1991). Low sortable silt mean size values are potentially linked to a weakened intermediate and deepwater circulation in the Norwegian-Greenland-Sea where the silt-transporting deepwater is produced. Low sortable silt mean size values from ~1700 to 1900 AD (Fig. 3.4d) thus possibly indicate a weakened meridional overturning circulation (MOC) during the Little Ice Age caused by massive intrusion of freshwater and sea ice from the

Arctic (after Sicre et al., 2008). Alternatively, assuming a certain contamination of current-transported sortable silt with sea ice-transported silt, it is likely that the low sortable silt mean size values recorded from ~1700 to 1900 AD (Fig. 3.4d) result from less coarser silt material due to less sea ice melting.

After ~1830 AD the IRD flux continuously increased. Concurrently, planktic foraminifer fluxes reveal lowest values between ~1850 and 1950 AD (750 to 2500 ind./cm^2*kyr). All these findings are best explained by cool conditions with extensive sea ice cover and an increased number of icebergs resulting from glacier growth on Svalbard. Indeed, historical observations from the archipelago corroborate a sea ice-dominated regime in the Fram Strait during the late LIA (e.g., Divine and Dick, 2006). For the period before 1920 AD sea ice reconstructions by Vinje (1999, 2001) showed intervals of heavy sea ice interrupted by periods of modest sea ice conditions. A possible impact of glacial melt water is supported by the comparison between mixing lines of modern water in the WSC (see 3.) and fjord waters at the Svalbard coast (MacLachlan et al., 2007), the latter mainly consisting of freshwater originating from glacial melt water (Fig. 3.2). Despite of the distance to the fjords, we suppose that glacial melt had some influence also on the water masses at our core site. Svalbard ice core studies revealed coldest conditions of the Little Ice Age for the period ~1760 to 1900 AD (Isaksson et al., 2005). Little Ice Age moraines on Svalbard have been widely described to represent the Holocene glacial maximum (Svendsen and Mangerud, 1997). Glacier advances during the Little Ice Age were reported for the Svalbard region (e.g., Humlum et al., 2005; Isaksson et al., 2005; Svendsen and Mangerud, 1997; Werner, 1993) and must have released icebergs into Svalbard fjords. Thus, it seems likely that IRD transported with icebergs also reached the study site.

3.5.2.7. Modern warming

There are discrepancies in our records concerning the end of the LIA. The gradual increase of *T. quinqueloba* in size fraction 150-250 μm (38%) and the associated temperature and salinity reconstructions (Fig. 3.5b, 3.6d, g, h) suggest a strong intensity of Atlantic Water since ~1850 AD (see also Spielhagen et al., 2011). In contrast, planktic foraminifer fluxes of size fraction 100-250 μm increase only after ~1950 AD (Fig. 3.6b). Before 1930 AD light planktic $d^{18}O$ values are most likely attributed to a cold and fresh upper mixed water layer (Fig. 3.6e). A sudden change is observed around 1930 AD when both, planktic and benthic foraminifer tests display a short-lived but very strong increase in $d^{18}O$ (4.03 and 4.56‰, respectively, Fig. 3.6e), pointing to an event that obviously affected the entire water column. An abrupt warming around the 1930s followed a temperature minimum in 1917 AD initiating the early 20th century warming in the Arctic (Isaksson et al., 2005 and references therein, Polyakov et al., 2004; Fig. 3.6i). A

significant warming in the 1930s is also known from instrumental data from Svalbard (e.g., Førland et al., 2009). In contrast, Klitgaard Kristensen et al. (2004) attributed $d^{18}O$ increases of ~0.3-0.6‰ around 1925 AD in two cores from the Norwegian Sea and adjacent fjords to a cold period at 1905-1925 AD in the Southern Norwegian Sea. Our $d^{18}O$ changes of >0.47‰ (planktic) and >0.5‰ (benthic) (Fig. 3.6e) may accordingly be interpreted as a cold spell. The maximum in $d^{18}O$, however, corresponds to high reconstructed SST and a peak in *T. quinqueloba* in size fraction 150-250 μm at ~1930 AD. We therefore rather suggest a significantly Atlantic Water pulse to have caused the high planktic and benthic $d^{18}O$ values, hereby affecting also bottom water layers. Simultaneously, a salinity effect on $d^{18}O$ is supported by high summer SSS pointing to strengthened AW inflow. Low fluxes and relatively high percentages of *N. pachyderma* in size fraction 100-250 μm do, however, not support warmer conditions. We therefore assume high abundances of small-sized *N. pachyderma* most likely indicating locally limited foraminifer growth due to cold conditions at the surface. Most likely at the beginning of the 20th century, the surface layer may have been still impacted by a thick cold and fresh mixed water layer as a retarding effect of the terminating Little Ice Age while warm and saline Atlantic Water already strengthened, hereby subsiding below the cold upper mixed layer.

Variations in planktic foraminifer fluxes and percentages as well as two independent temperature reconstructions during the last 2,000 years have already been discussed with respect to the unprecedented warming after 1860 AD (Spielhagen et al., 2011). The drastic increase in subpolar planktic foraminifers is particularly attributed to significant increases in *T. quinqueloba* and *Globigerinita sp.* (Spielhagen et al., 2011; Fig. 3.5b, c). Svalbard ice core studies have elucidated the 20th century as the warmest century within at least the past 600 years (Isaksson et al., 2005). Changes occur in all studied proxies since 1950 AD (Fig. 3.6) and coincide with positive Atlantic Water temperature anomalies for the ca last 100 years in the Arctic Ocean (Polyakov et al., 2004; Fig. 3.6i) and a retreating sea ice margin in the Nordic Seas (Divine and Dick, 2006). High sea surface salinities and light planktic $d^{18}O$ values likely reflect warmer sea surface temperatures and strengthened AW inflow (Fig. 3.6e, h).

Stable high IRD fluxes indicate a high abundance of sea ice/icebergs after 1860 AD. A significant increase in sortable silt mean size (Fig. 3.4d) was likely caused by silt-sized IRD indicating a high impact of sea ice at the site. It may also point to a continuous strengthening of the MOC intensity (Sicre et al., 2008) linked to increased deepwater production in the Norwegian-Greenland Sea.

Planktic and benthic $d^{13}C$ values decreased during the last 100 years (Fig. 3.6f). Bauch et al. (2000) found *N. pachyderma* in the water column depleted in $d^{13}C$ compared to core top sediments in the Arctic Ocean. Considering the multidecadal resolution of our data set, low $d^{13}C$

values could be reflected in planktic foraminifers of the uppermost sediment layer studied here, while they were not observed in surface sediments from the Arctic Ocean characterized by extremely low sedimentation rates. Olsen and Ninnemann (2010) discussed the global distribution of light $d^{13}C$ values in modern water masses which are strongly departing from preindustrial values due to the Suess effect which involves the anthropogenically induced addition of isotopically light fossil carbon to the carbon system. Our recorded low $d^{13}C$ values may therefore be attributed to the Suess effect.

It has been debated whether temperatures of the Medieval Climate Anomaly have been similar to those of the past 100 years (Broecker, 2001; Hughes and Diaz, 1994; IPCC, 2007). Regarding percentages of subpolar planktic foraminifers of the two periods (up to 37% during MCA, up to 66% during past 100 years; Fig. 3.5b, c) we conclude that temperatures of the MCA in the eastern Fram Strait were considerably lower than those of the 20th century. This is also shown by two independent temperature reconstructions of core MSM5/5-712-1 indicating that modern summer temperatures of the uppermost AW layer are >1.5°C higher than multidecadal mean temperature maxima during the MCA (Spielhagen et al., 2011).

3.5.3. Analogies and disparities to dinocyst-based reconstruction – apparent conflicts between surface and subsurface water indicators

Our proxy reconstruction based on planktic foraminifer assemblages, stable isotopes of planktic and benthic foraminifera, and lithic characteristics partly contradicts results of Bonnet et al. (2010) derived from dinocyst assemblages. Figure 3.6g and h show summer SST and SSS reconstructions obtained by Bonnet et al. (2010) along with those of the present study. SST by Bonnet et al. (2010) are significantly higher during the ~1650 AD so that differences to SST of this study can easily reveal up to 6°C. Also, fluctuations of SST revealed by Bonnet et al. (2010) are considerably higher. A major temperature drop initiating the Little Ice Age period after a relatively warm interval has been detected by Bonnet et al. (2010) ~1650 AD, which we find in our record at least 300 years earlier. High fluctuations in SST (Bonnet et al., 2010) may indicate a fluctuating sea ice margin at the site, as it has been indicated by the present study ~1-700 AD and after ~1350 AD. There is agreement to data of Bonnet et al. (2010) about a cooling pulse around 750 AD, which may correspond to an observed cold spell in our record around 800 AD. As pointed out by Krawczyk et al. (2010), inconsistencies in proxy data comparison may arise from different living depths of the applied microfossil proxies. Due to their (direct or indirect) dependence on photosynthesis, most cyst-producing dinoflagellate species live in the upper mixed water layer (e.g., Serjeant, 1974; Taylor, 1987). In contrast, the main habitat of planktic foraminifers during summer is the subsurface layer of the WSC between 50 and 200 m water

depth in the Fram Strait (Carstens et al., 1997; Volkmann, 2000). To explain diatom and dinoflagellate cyst records from outer Disko Bugt (West Greenland) inconsistent to North Atlantic climate variability (Moros et al., 2006; Seidenkrantz et al., 2008), Krawczyk et al. (2010) presented an alternative to the seesaw mechanism (e.g., Keigwin and Pickart, 1999). Increased melting of sea ice and the Greenland ice sheet during warmer intervals such as the MCA would result in an increased influx of cold and low-saline water at the surface, which would produce a diatom assemblage indicative of colder conditions (Krawczyk et al., 2010). In contrast, during cooler intervals, such as the LIA, reduced melting of sea ice would reduce dilution of the upper mixed layer and would thus lead to a relative increase of warmer species in the diatom assemblages (Krawczyk et al., 2010). Likewise, this mechanism could apply to dinoflagellates since they also reflect conditions in the uppermost water layers. In the eastern Fram Strait a ca 50-100 m thick surface water layer above the West Spitsbergen Current cools and freshens the underlying AW (Saloranta and Haugan, 2004). As Polyakov et al. (2004) have shown during increased AW inflow there is excess ice and freshwater transport through Fram Strait from the Arctic. Therefore we consider the reconstruction of Bonnet et al. (2010) to mainly to reflect the uppermost water variability possibly influenced by fluctuations of the fresh and cold upper mixed layer. Our planktic foraminifer-based proxies mainly reflect subsurface conditions of the Atlantic Water masses submerging beneath the upper mixed layer. In particular, the early part of the Little Ice Age reveals clear contradictions between both reconstructions. For the interval between 1400 and 1650 AD Bonnet et al. (2010) find warm summer SST while we infer rather cool conditions with the sea ice margin prevailing over the site. Assuming a similar scenario as described by Krawczyk et al. (2010) relatively warm summer SST by Bonnet et al. (2010) would represent reduced melting of sea ice due to a colder period. In contrast, during the second part of the LIA, cold SST (Bonnet et al., 2010) agree with our reconstructed cold climate conditions. Persistently cold conditions may have caused a rather homogeneous thick cold surface water layer, which may be represented by both, planktic foraminifers and dinoflagellates during the later LIA. However, comparison between SSS and SST data from Bonnet et al. (2010) and from this study does not reveal a distinct relationship. Due to the complexity of water masses in the narrow Fram Strait we are thus not able to develop a clear anti-phase relationship of surface and subsurface indicating organisms similar to the one for West Greenland (Krawczyk et al., 2010).

3.6. Conclusions

Our proxy data set suggests variable oceanographic and climatic conditions during the last ca 2,000 years in the eastern Fram Strait, which we attribute to the variable strength of Atlantic Water inflow and the position of the sea ice margin. Stepwise increasing IRD contents unveil a

background trend of increasing iceberg/sea ice abundance confirming a neoglaciation trend known from other studies in the North Atlantic area. Atlantic Water has been permanently present as indicated by the continuous abundance of the subpolar planktic foraminifer species *T. quinqueloba* today indicative of Atlantic Water in the Fram Strait. A fluctuating ice margin was located close to the study site 1 - 700 AD and 1350 - 1730 AD inferred from high and strongly variable planktic foraminifer fluxes. A proximity to the ice margin is also inferred from increased IRD fluxes at 400-700 AD and after 1350 AD which indicate periods of prolonged sea ice melt. During the Medieval Climate Anomaly lower and less variable planktic foraminifer fluxes point to more stable conditions which, however, varied between warmer (1000-1200 AD, after 1300 AD) and cooler (1200-1300 AD) periods. Two phases of the Little Ice Age period have been revealed. The first phase (ca 1350-1750 AD) had high planktic foraminifer fluxes pointing to cold conditions and a fluctuating sea ice margin at the site. After ca 1750 AD decreasing planktic foraminifer fluxes indicate very cold conditions. High IRD contents are attributed to heavy sea ice conditions found also in historical observations and instrumental records. IRD may have also been produced by melting Svalbard glaciers. Subpolar planktic foraminifers in the 150-250 μm fraction and planktic $d^{18}O$ values indicate strengthened Atlantic Water inflow after ca 1860 AD. However, low fluxes and planktic foraminifer assemblages of the 100-250 μm fraction suggest cool surface water conditions until the mid of the 20th century. Changes in all studied proxies indicate warmer temperatures for the past few decades (see Spielhagen et al., 2011) and coincide with positive Atlantic Water temperature anomalies and a retreating sea ice margin for the ca last 100 years (Divine and Dick, 2006; Polyakov et al., 2004, 2005).

Acknowledgements. The German Research Foundation (DFG) provided financial support of K. Werner and R. F. Spielhagen within the Priority Programme 1266 (INTERDYNAMIC, Project HOVAG). K. Zamelczyk was funded by the Norwegian Research Council through the research programs WARMPAST and SciencePub. For technical assistance on stable isotope measurements we are grateful to Lulzim Haxhiaj. We thank Henning A. Bauch and Nicolas Van Nieuwenhove for constructive comments and consultations on this manuscript. We wish to thank the science party and crew onboard RV "Maria S. Merian" during the expedition MSM5/5 for retrieving the sediment core. Finally we appreciate the valueable suggestions and comments by two anonymous reviewers which greatly improved the manuscript.

References

Aagaard, K., Foldvik, A., Hillman, S., 1987. The West Spitsbergen Current: Disposition and Water Mass Transformation. Journal of Geophysical Research 92(C4), 3778-3784.

Andersson, C., Risebrobakken, B., Jansen, E., Dahl, S.O., 2003. Late Holocene surface ocean conditions of the Norwegian Sea (Vøring Plateau). Paleoceanography 18, 1044.

Andrews, J.T., Belt, S.T., Olafsdottir, S., Massé, G., Vare, L.L., 2009. Sea ice and marine climate variability for NW Iceland/Denmark Strait over the last 2000 cal. yr BP. The Holocene 19, 775-784.

Andrews, J.T., Jennings, A.E., Coleman, G.C., Eberl, D.D., 2010. Holocene variations in minderal and grain size composition along the East Greenland glaciated margin (ca 67°-70°N): Local versus long-distance sediment transport. Quaternary Science Reviews 29, 2619-2632.

Bauch, D., Carstens, J., Wefer, G., 1997. Oxygen isotope composition of living *Neogloboquadrina pachyderma* (sin.) in the Arctic Ocean. Earth and Planetary Science Letters 146, 47-58.

Bauch, D., Carstens, J., Wefer, G., Thiede, J., 2000. The imprint of anthropogenic CO_2 in the Arctic Ocean: evidence from planktic $d^{13}C$ data from watercolumn and sediment surfaces. Deep-Sea Research II 47, 1791-1808.

Bauch, H., 1994. Significance of variability in *Turborotalia quinqueloba* (Natland) test size and abundance for paleoceanographic interpretations in the Norwegian-Greenland Sea. Marine Geology 121, 129-141.

Bemis, B.E., Spero, H.J., Bijma, J., Lea, D.W., 1998. Reevaluation of oxygen isotopic composition of planktic foraminifera: Experimental results and revised paleotemperature equations. Paleoceanography 13, 150-160.

Berger, A., Loutre, M.F., 1991. Insolation Values for the Climate of the last 10 Million Years. Quaternary Science Reviews 10, 297-317.

Berstad, I.M., Sejrup, H.P., Klitgaard Kristensen, D., Haflidason, H., 2003. Variability in temperature and geometry of the Norwegian Current over the past 600 yr; stable isotope and grain size evidence from the Norwegian margin. Journal of Quaternary Science 18(7), 591-602.

Bjune, A.E., Seppä, H., Birks, B.J.B., 2009. Quantitative summer-temperature reconstructions for the last 2000 years based on pollen-stratigraphical data from northern Fennoscandia. Journal of Paleolimnology 41, 43-56.

Bonnet, S., de Vernal, A., Hillaire-Marcel, C., Radi, T., Husum, K., 2010. Variability of sea-surface temperature and sea-ice cover in the Fram Strait over the last two millennia. Marine Micropaleontology 74, 59-74.

Broecker, W.S., 2001. Was the Medieval Warm Period Global? Science 291, 1497-1499.

Carignan, J., Hillaire-Marcel, C., de Vernal, A., 2008. Arctic vs. North Atlantic water mass exchanges in Fram Strait from Pb isotopes in sediments. Canadian Journal of Earth Sciences 45, 1253-1263.

Carstens, J., Hebbeln, D., Wefer, G., 1997. Distribution of planktic foraminifera at the ice margin in the Arctic (Fram Strait). Marine Micropaleontology 29, 257-69.

Carstens, J., Wefer, G., 1992. Recent distribution of planktonic foraminifera in the Nansen Basin, Arctic Ocean. Deep-Sea Research 39, S507-S524.

Dahl, O.S., Nesje, A., 1996. A new approach to calculating Holocene winter precipitation by combining glacier equilibrium-line altitudes and pine-tree limits: a case study from Hardangerjokulen, central southern Norway. The Holocene 6, 381-398.

Dahl-Jensen, D., Mosegaard, K., Gundestrup, N., Clow, G.D., Johnsen, S.J., Hansen, A.W., Balling, N., 1998. Past Temperatures Directly from the Greenland Ice Sheet. Science 282, 268-271.

Darling, K.F., Kucera, M., Kroon, D., Wade, C.M., 2006. A resolution for the coiling direction paradox in *Neogloboquadrina pachyderma*. Paleoceanography 21, PA2011.

Divine, D.V., Dick, C., 2006. Historical variability of sea ice edge position in the Nordic Seas. Journal of Geophysical Research 111, C01001.

Duplessy, J.-C., Labeyrie, L., Waelbroeck, C., 2002. Constraints on the ocean oxygen isotopic enrichment between the Last Glacial Maximum and the Holocene: Paleoceanographic implications. Quaternary Science Reviews 21, 315-330.

Eiríksson, J., Bartels-Jónsdóttir, H.B., Cage, A.G., Gudmundsdóttir, E.R., Klitgaard Kristensen, D., Marret, F., Rodrigues, T., Abrantes, F., Austin, W.E.N., Jiang, H., Knudsen, K.-L., Sejrup, H.-P., 2006. Variability of the North Atlantic Current during the last 2000 years based on shelf bottom water and sea surface temperatures along an open ocean/shallow marine transect in western Europe. The Holocene 16(7), 1017-1029.

Førland, E.J., Benestad, R.E., Flatøy, F., Hanssen-Bauer, I., Haugen, J.E., Isaksen, K., Sorteberg, A., Ådlandsvik, B., 2009. Climate development in North Norway and the Svalbard region during 1900-2100. Rapportserie 128, Norsk Polarinstitutt Tromsø, Norway.

Frank, M., 1996. Spurenstoffuntersuchungen zur Zirkulation im Eurasischen Becken des Nordpolarmeeres. PhD thesis Ruprecht-Karls-Universität Heidelberg.

Hass, H.C., 2002. A method to reduce the influence of ice-rafted debris on a grain size record from northern Fram Strait, Arctic Ocean. Polar Research 21, 299-306.

Healy-Williams, N., 1992. Stable isotope differences among morphotypes of *Neogloboquadrina pachyderma* (Ehrenberg): implications for high-latitude palaeoceanographic studies. Terra Nova 4, 693-700.

Hebbeln, D., Wefer, G., 1991. Effects of ice coverage and ice-rafted material on sedimentation in the Fram Strait. Nature 350, 409-411.

Hegseth, E.N., Tverberg, V., 2008. Changed spring bloom timing in a Svalbard (high Arctic) fjord caused by Atlantic Water inflow? SCAR/IASC IPY Open Science Conference July 8-11, 2008, St Petersburg, Russia.

Hop, H., Falk-Petersen, S., Svendsen, H., Kwasniewski, S., Pavlov, V., Pavlova, O., Søreide, J.E., 2006. Physical and biological characteristics of the pelagic system across Fram Strait to Kongsfjorden. Progress in Oceanography 71, 182-231.

Hop, H., Cottier, F., Falk-Petersen, S., Tverberg, V., Kwasniewski, S., Welcker, J., Moe, B., Hegseth, E.N., Gerland, S., Walczowski, W., Dalpadado, P., Klitgaard Kristensen, D., Berge, J., Lydersen, C., Kovacs, K.M., Weslawski, J.M., Gabrielsen, G.W., 2010. Has Kongsfjorden in Svalbard passed a tipping point for persistent change in the marine ecosystem? Arctic Frontiers Conference, Jan 24-29, 2010, Tromsø, Norway.

Hopkins, T.S., 1991. The GIN Sea - A synthesis of its physical oceanography and literature review 1972-1985. Earth-Science Reviews 30, 175-318.

Houghton, J.T.(ed.), Meiro Filho, L.G., Callandar, B.A., Harris, N., Kattenburg, A., Maskell, K., 1996. Climate change 1995: the science of climate change. Cambridge University Press.

Hughes, M.K., Diaz, H.F., 1994. Was there a 'Medieval Warm Period', and if so, where and when? Climatic Change 26, 109-142.

Humlum, O., Elberling, B., Hormes, A., Fjordheim, K., Hansen, O.H., Heinemeier, J., 2005. Late-Holocene glacier growth in Svalbard, documented by subglacial relict vegetation and living soil microbes. The Holocene 15, 396-407.

IPCC, 2007. IPCC Fourth Assessment Report: Climate Change 2007. Contribution of Working Group I to the Fourth Assessment Report of the Intergovernmental Panel on Climate Change, 2007. Solomon, S., Qin, D., Manning, M., Chen, M., Marquis, M., Averyt, K.B., Tignor, M., Miller, H.L. (Eds.), Cambridge University Press. Cambridge, United Kingdom and New York, USA.

Isaksson, E., Kohler, J., Pohjola, V., Moore, J., Igarashi, M., Karlöf, L., Martma, T., Meijer, H., Motoyama, H., Vaikmäe, R., van de Wal, R.S.W., 2005. Two ice-core $d^{18}O$ records from Svalbard illustrating climate and sea ice variability over the last 400 years. The Holocene 15, 501-509.

Jakobsson, M., Macnab, R., Mayer, L., Anderson, R., Edwards, M., Hatzky, J., Schenke, H.W., Johnson, P., 2008. An improved bathymetric portrayal of the Arctic Ocean: Implications for ocean modelling and geological, geophysical and oceanographic analyses. Geophysical Research Letters 35, L07602.

Jennings, A.E., Knudsen, K.L., Hald, M., Vigen Hansen, C., Andrews, J.T., 2002. A mid-Holocene shift in Arctic sea-ice variability on the East Greenland Shelf. The Holocene 12, 49-58.

Jones, P.D., Osborn, T.J., Briffa, K.R., 2001. The Evolution of Climate Over the Last Millennium. Science 292, 662-667.

Kandiano, E.S., Bauch, H.A., 2002. Implications of planktic foraminiferal size fractions for the glacial-interglacial paleoceanography of the polar North Atlantic. Journal of Foraminiferal Research 32, 245-251.

Karcher, M.J., Gerdes, R., Kauker, F., Köberle, C., 2003. Arctic warming: Evolution and spreading of the 1990s warm event in the Nordic seas and the Arctic Ocean. Journal of Geophysical Research 108(C2), 3034.

Kaufman, D.S., Schneider, D.P., McKay, N.P., Ammann, C.M., Bradley, R.S., Briffa, K.R., Miller, G.H., Otto-Bliesner, B.L., Overpeck, J.T., Vinther, B.M., Arctic Lakes 2k Project Members, 2009. Recent Warming Reverses Long-Term Arctic Cooling. Science 325, 1236-1239.

Keigwin, L.D., Pickart, R.S., 1999. Slope Water Current over the Laurentian Fan on Interannual to Millennial Time Scales. Science 286, 520-523.

Klitgaard Kristensen, D., Sejrup, H.P., Haflidason, H., Berstad, I.M., Mikalsen, G., 2004. Eight-hundred-year temperature variability from the Norwegian continental margin and the North Atlantic thermohaline circulation. Paleoceanography 19, 2007.

Koç, N., Jansen, E., 2002. Holocene Climate Evolution of the North Atlantic Ocean and the Nordic Seas - a Synthesis of New Results, in: Wefer, G., Berger, W., Behre, K.-E., Jansen, E. (Eds.), Climate Development and History of the North Atlantic Realm. Springer-Verlag, pp. 165-177.

Kohfeld, K.E., Fairbanks, R.G., Smith, S.L., Walsh, I.D., 1996. *Neogloboquadrina Pachyderma* (sinistral coiling) as Paleoceanographic Tracers in Polar Oceans: Evidence from

Northeast Water Polynya Plankton Tows, Sediment Traps, and Surface Sediments. Paleoceanography 11, 679-699.

Krawczyk, D., Witkowski, A., Moros, M., Lloyd, J., Kuijpers, A., Kierzek, A., 2010. Late-Holocene diatom-inferred reconstruction of temperature variations of the West Greenland Current from Disko Bugt, central West Greenland. The Holocene 20(5), 659-666.

Kucera, M., Weinelt, M., Kiefer, T., Pflaumann, U., Hayes, A., Weinelt, M., Chen, M.-T., Mix, A.C., Barrows, T.T., Cortijo, E., Duprat, J., Juggins, S., Waelbroeck, C., 2005. Reconstruction of sea-surface temperatures from assemblages of planktonic foraminifera: multi-technique approach based on geographically constrained calibration data sets and its application to glacial Atlantic and Pacific Oceans. Quaternary Science Reviews 24, 951-998.

Lamb, H.H., 1965. The early Medieval Warm Epoch and its sequel. Palaeogeography, Palaeoclimatology, Palaeoecology 1, 13-37.

Loeng, H., 1991. Features of the physical oceanographic conditions of the Barents Sea, in: Sakshaug, E., Hopkins, C.C.E., Øritsland, N.A. (Eds.), Proceedings of the Pro Mare Symposium on Polar Marine Ecology, Trondheim, 12-16 May 1990. Polar Research 10, 5-18.

MacLachlan, S.E., Cottier, F.R., Austin, E.N.A., Howe, J.A., 2007. The salinity: $d^{18}O$ water relationship in Kongsfjorden, western Spitsbergen. Polar Research 26, 160-167.

Manabe, S., Stouffer, R.J., 1980. Sensitivity of a Global Climate Model to an Increase of CO_2 Concentration in the Atmosphere. Journal of Geophysical Research 85(C10), 5529-5554.

Manley, T.O., 1995. Branching of Atlantic Water within the Greenland-Spitsbergen Passage: An estimate of recirculation. Journal of Geophysical Research 100(C10), 20627-20634.

Matthews, J.A., Dahl, S.O., Nesje, A., Berrisford, M.S., Andersson, C., 2000. Holocene glacier variations in central Jotunheimen, southern Norway based on distal glaciolacustrine sediment cores. Quaternary Science Reviews 19, 1625-1647.

Meredith, M., Heywood, K., Dennis, P., Goldson, L., White, R., Fahrbach, E., Schauer, U., Østerhus, S., 2001. Freshwater fluxes through the Western Fram Strait. Geophysical Research Letters 28, 1615-1618.

Moberg, A., Sonechkin, D.M., Holmgren, K., Datsenko, N.M., Karlén, W., 2005. Highly variable Northern Hemisphere temperatures reconstructed from low- and high-resolution proxy data. Nature 433, 613-617.

Moros, M., Emeis, K., Risebrobakken, B., Snowball, I., Kuijpers, A., McManus, J., Jansen E., 2004. Sea surface temperatures and ice rafting in the Holocene North Atlantic: climate influences on northern Europe and Greenland. Quaternary Science Reviews 23, 2113-2126.

Moros, M., Jensen, K.G., Kuijpers, A., 2006. Mid-to late-Holocene hydrological and climatic variability in Disko Bugt, central West Greenland. The Holocene 16, 357-367.

Nesje, A., Kvamme, M., Rye, N., Reidar, L., 1991. Holocene glacial and climate history of the Jostedalsbreen region, western Norway: evidence from lake sediments and terrestrial deposits. Quaternary Science Reviews 10, 87-114.

Nesje, A., Dahl, S.O., Andersson, C., Matthews, J., 2000. The lacustrine sedimentary sequence in Sygneskardvatnet, western Norway: a continuous, high-resolution record of the Jostedalsbreen ice cap during the Holocene. Quaternary Science Reviews 19, 1047-1065.

Nesje, A., Dahl, S.O., Thun, T., Nordli, Ø., 2008. The 'Little Ice Age' glacial expansion in western Scandinavia: summer temperature or winter precipitation? Climate Dynamics 30, 789-801.

Nesje, A., 2009. Latest Pleistocene and Holocene alpine glacier fluctuations in Scandinavia. Quaternary Science Reviews 28 (21-22), 2119-2136.

Nørgaard-Pedersen, N., Spielhagen, R.F., Erlenkeuser, H., Grootes, P.M., Heinemeier, J., Knies, J., 2003. Arctic Ocean during the Last Glacial Maximum: Atlantic and polar domains of surface water mass distribution and ice cover. Paleoceanography 18, 1063.

Olsen, A., Ninnemann, U., 2010. Large $d^{13}C$ Gradients in the Preindustrial North Atlantic Revealed. Science 330, 658-659.

O'Neil, J.R., Clayton, R.N., Mayeda, T.K., 1969. Oxygen isotope fractionation in divalent metal carbonates. Journal of Chemical Physics 51, 5547-5558.

Pflaumann, U., Duprat, J., Pujol, C., Labeyrie, L.D., 1996. SIMMAX: A modern analog technique to deduce Atlantic sea surface temperatures from planktonic foraminifera in deep-sea sediments. Paleoceanography 11, 15-35.

Polyakov, I.V., Alekseev, G.V., Timokhov, L.A., Bhatt, U.S., Colony, R.L., Simmons, H.L., Walsh, D., Walsh, J.E., Zahkharov, V.F., 2004. Variability of the Intermediate Atlantic Water of the Arctic Ocean over the last 100 Years. Journal of Climate 17, 4485-4497.

Polyakov, I.V., Beszczynska, A., Carmack, E.C., Dmitrenko, I.A., Fahrbach, E., Frolov, I.E., Gerdes, R., Hansen, E., Holfort, J., Ivanov, V.V., Johnson, M.A., Karcher, M., Kauker, F., Morison, J., Orvik, K.A., Schauer, U., Simmons, H.L., Skagseth, Ø., Sokolov, V.T., Steele, M., Timokhov, L.A., Walsh, D., Walsh, J.E., 2005. One more step toward a warmer Arctic. Geophysical Research Letters 32, L17605.

Quadfasel, D., Gascard, J.-C., Koltermann, K.-P., 1987. Large-Scale Oceanography in Fram Strait During the 1984 Marginal Ice Zone Experiment. Journal of Geophysical Research 92(C7), 6719-6728.

Quadfasel, D., Rudels, B., Kurz, K., 1988. Outflow of dense water from a Svalbard fjord into the Fram Strait. Deep-Sea Research 35, 1143-1150.

Rasmussen, T.L., Thomsen, E., 2009. Stable isotope signals from brines in the Barents Sea: Implications for brine formation during the last glaciation. Geology 37, 903-906.

Reimer, P.J., Baillie, M.G.L., Bard, E., Bayliss, A., Beck, J.W., Blackwell, P.G., Bronk Ramsey, C., Buck, C.E., Burr, G.S., Edwards, R.L., Friedrich, M., Grootes, P.M., Guilderson, T.P., Hajdas, I., Heaton, T.J., Hogg, A.G., Hughen, K.A., Kaiser, K.F., Kromer, B., McCormac, F.G., Manning, S.W., Reimer, R.W., Richards, D.A., Southon, J.R., Talamo, S., Turney, C.S.M., van der Plicht, J., Weyhenmeyer, C.E., 2009. IntCal09 and Marine09 Radiocarbon Age Calibration Curves, 0–50,000 Years cal BP. Radiocarbon 51, 1111-1150.

Robinson, S.G., McCave, I.N., 1994. In Orbital Forcing of Bottom-Current Enhanced Sedimentation on Feni Drift, NE Atlantic, During the Mid-Pleistocene. Paleoceanography 9, 943-972.

Rudels, B., Meyer, R., Fahrbach, E., Ivanov, V., Østerhus, S., Quadfasel, D., Schauer, U., Tverberg, V., Woodgate, R.A., 2000. Water mass distribution in Fram Strait and over the Yermak Plateau in summer 1997. Annales Geophysicae 18, 687-705.

Saloranta, T.M., Haugan, P.M., 2001. Interannual variability in the hydrography of Atlantic water northwest of Svalbard. Journal of Geophysical Research 106(C7), 13931-13943.

Saloranta, T.M., Haugan, P.M., 2004. Northward cooling and freshening of the warm core of the West Spitsbergen Current. Polar Research 23, 79-88.

Sarjeant, W.A.S., 1974. Fossil and living dinoflagellates. Academic Press, London.

Schauer, U., 1995. The release of brine-enriched shelf water from Storfjord into the Norwegian Sea. Journal of Geophysical Research 100(C8), 16015-16028.

Schauer, U., Fahrbach, E., Østerhus, S., Rohardt, G., 2004. Arctic warming through the Fram Strait: Oceanic heat transport from 3 years of measurements. Journal of Geophysical Research 109(C6), C06026.

Schlichtholz, P., Goszczko, I., 2006. Interannual variability of the Atlantic water layer in the West Spitsbergen Current at 76.5°N in summer 1991-2003. Deep-Sea Research I 53, 608-626.

Schlichtholz, P., Houssais, M.-N., 1999. An inverse modelling study in Fram Strait. Part II: water mass distribution and transports. Deep-Sea Research 46, 1137-1168.

Schmidt, G.A., Bigg, G.R., Rohling, E.J., 1999. Global Seawater Oxygen-18 Database. http://data.giss.nasa.gov/o18data/.

Seidenkrantz, M.-S., Roncaglia, L., Fischel, A., Heilmann-Clausen, C., Kuijpers, A., Moros, M., 2008. Variable North Atlantic climate seesaw patterns documented by a late Holocene marine record from Disko Bugt, West Greenland. Marine Micropaleontology 68, 66-83.

Serreze, M.C., Barrett, A., Stroeve, J.C., Kindig, D., Holland, M.M., 2009. The emergence of surface-based Arctic amplification. The Cryosphere 3, 11-19.

Shackleton, N.J., Opdyke, N.D., 1973. Oxygen Isotope and Palaeomagnetic Stratigraphy of Equatorial Pacific Core V28-238: Oxygen Isotope Temperatures and Ice Volumes on a 10^5 Year and 10^6 Year Scale. Quaternary Research 3, 39-55.

Sicre, M.-A., Jacob, J., Ezat, U., Rousse, S., Kissel, C., Yiou, P., Eiríksson, J., Knudsen, K.-L., Jansen, E., Turon, J.-L., 2008. Decadal variability of sea surface temperatures off North Iceland over the last 2000 years. Earth and Planetary Science Letters 268, 137-142.

Simstich, J., Sarthein, M., Erlenkeuser, H., 2003. Paired $d^{18}O$ signals of *Neogloboquadrina pachyderma* (s) and *Turborotalia quinqueloba* show thermal stratification structure in Nordic Seas. Marine Micropaleontology 48, 107-125.

Ślubowska, M.A., Koç, N., Rasmussen, T.L., Klitgaard Kristensen, D., 2005. Changes in the flow of Atlantic water into the Arctic Ocean since the last deglaciation: Evidence from the northern Svalbard continental margin, 80°N. Paleoceanography 20, PA4014.

Ślubowska-Woldengen, M., Rasmussen, T.L., Koç, N., Klitgaard Kristensen, D., Nilsen, F., Solheim, A., 2007. Advection of Atlantic Water to the western and northern Svalbard shelf since 17,500 cal yr BP. Quaternary Science Reviews 26, 463-478.

Spielhagen, R.F., Erlenkeuser, H., 1994. Stable oxygen and carbon isotopes in planktic foraminifers from Arctic Ocean surface sediments: Reflection of the low salinity surface water layer. Marine Geology 119, 227-250.

Spielhagen, R.F., Werner, K., Aagaard-Sørensen, S., Zamelczyk, K., Kandiano, E., Budeus, G., Husum, K., Marchitto, T.M., Hald, M., 2011. Enhanced modern heat transfer to the Arctic by warm Atlantic Water. Science 331, 450-453.

Stuiver, M., Reimer, P.J., 1993. Extended ^{14}C data base and revised CALIB 3.0 ^{14}C age calibration program. Radiocarbon 35(1), 215-230.

Svendsen, J.I., Mangerud, J., 1997. Holocene glacial and climatic variations on Spitsbergen, Svalbard. The Holocene 7, 45-57.

Swift, J.H., Koltermann, K.P., 1988. The Origin of Norwegian Sea Deep Water. Journal of Geophysical Research 93(C4), 3563-3569.

Tarussov, A., 1992. The Arctic from Svalbard to Severnaya Zemlya: climatic reconstructions from ice cores, in: Bradley, R.S., Jones, P.D. (Eds.), Climate since A.D. 1500. Routledge, London, New York, pp. 505-516.

Taylor, F.J.R. (Ed.), 1987. The Biology of Dinoflagellates. Botanical Monographs 21. Blackwell Scientific Publications, Oxford.

Vinje, T., 1999. Barents Sea ice edge variation over the past 400 years. Extended abstract. Workshop on Sea-Ice Charts of the Arctic, Seattle, WA. World Meteorological Organization, WMO/TD No. 949, 4-6.

Vinje, T., 2001. Anomalies and Trends of Sea-Ice Extent and Atmospheric Circulation in the Nordic Seas during the Period 1864–1998. Journal of Climate 14, 255-267.

Volkmann, R., 2000. Planktic foraminifer ecology and stable isotope geochemistry in the Arctic Ocean: implications from water column and sediment surface studies for quantitative reconstructions of oceanic parameters. Berichte zur Polarforschung 361, 1-128.

Volkmann, R., Mensch, M., 2001. Stable isotope composition ($d^{18}O$, $d^{13}C$) of living planktic foraminifers in the outer Laptev Sea and the Fram Strait. Marine Micropaleontology 42, 163-188.

Walton, P., 1952. Techniques for recognition of living foraminifera. Foraminiferal Research 3, 56-60.

Werner, A., 1993. Holocene moraine chronology, Spitsbergen, Svalbard: lichenometric evidence for multiple Neoglacial advances in the Arctic. The Holocene 3, 128-137.

Zamelczyk, K., Husum, K., Rasmussen, T., Hald, M., Werner, K., Spielhagen, R.F., in prep. Climate and surface ocean conditions during the last two millennia in the Fram Strait, Polar North Atlantic: Distribution of planktic foraminifera and shell weight.

CHAPTER 4

ENHANCED MODERN HEAT TRANSFER TO THE ARCTIC BY WARM ATLANTIC WATER

From [Spielhagen, R.F., Werner, K., Aagaard-Sørensen, S., Zamelczyk, K., Kandiano, E., Budeus, G., Husum, K., Marchitto, T.M. and Hald, M. (2011), Enhanced Modern Heat Transfer to the Arctic by Warm Atlantic Water, *Science, 331*, 450-453.]. Reprinted with permission from AAAS.

Original paper available online at http://www.sciencemag.org/content/331/6016/450.full
Data available online at http://doi.pangaea.de/10.1594/PANGAEA.755114

4 ENHANCED MODERN HEAT TRANSFER TO THE ARCTIC BY WARM ATLANTIC WATER

Robert F. Spielhagen,[1,2]* Kirstin Werner,[2] Steffen Aagaard Sørensen,[3] Katarzyna Zamelczyk,[3] Evguenia Kandiano,[2] Gereon Budeus,[4] Katrine Husum,[3] Thomas M. Marchitto,[5] Morten Hald[3]

[1]Academy of Sciences, Humanities, and Literature Mainz, 55131 Mainz, Germany.
[2]Leibniz Institute of Marine Sciences (IFM-GEOMAR), 24148 Kiel, Germany.
[3]Department of Geology, University of Tromsø, 9037 Tromsø, Norway.
[4]Alfred Wegener Institute for Polar and Marine Research, 27515 Bremerhaven, Germany.
[5]Department of Geological Sciences and Institute of Arctic and Alpine Research, University of Colorado, Boulder, CO 80309, USA.

*E-mail: rspielhagen@ifm-geomar.de

The Arctic is responding more rapidly to global warming than most other areas on our planet. Northward-flowing Atlantic Water is the major means of heat advection toward the Arctic and strongly affects the sea ice distribution. Records of its natural variability are critical for the understanding of feedback mechanisms and the future of the Arctic climate system, but continuous historical records reach back only ~150 years. Here, we present a multidecadal-scale record of ocean temperature variations during the past 2000 years, derived from marine sediments off Western Svalbard (79°N). We find that early-21st-century temperatures of Atlantic Water entering the Arctic Ocean are unprecedented over the past 2000 years and are presumably linked to the Arctic amplification of global warming.

Rising air temperatures (*1-3*) and a decline of the sea ice cover (*4, 5*) evidence a rapid warming in the Arctic that has reversed a long-term cooling trend (*6*). Relatively warm Atlantic Water (AW) in the Fram Strait Branch (FSB) of the North Atlantic Current is the major carrier of oceanic heat to the Arctic Ocean (Fig. 4.1). It maintains perennially ice-free conditions in the eastern Fram Strait today and supplies salt to the intermediate and bottom waters of the Arctic Ocean, thereby stabilizing the stratification (*7, 8*). In the eastern Fram Strait, AW with temperatures of 2 to 6°C and salinities of >35.0 is found at 50- to 600-m water depth (Fig. 4.2). Most of the year it is overlain by a mixed layer of lower salinity, seasonally variable temperatures, and ice coverage in extreme winters. These parameters also varied in the past 2000 years, as shown by sea ice observations and sediment core studies (*5, 9*).

Highly variable AW advection to the Arctic in the Late Quaternary has been recorded by proxies like microfossil abundances, flux rates, and species ratios (subpolar versus polar species) in sediment cores. Advection maxima occurred mostly during relatively warm periods (interglacials and interstadials) (*10-12*). The Holocene [past 12 ky ky, thousand years)] was characterized by a thermal maximum at 10 to 9 ky and a cooling thereafter (*13*). Previous studies, however, were unable to clearly resolve variations within a few hundred years or less. Such variations are well known from historical and proxy data of European climate (*14*) and subdivide the last 2 ky into the Roman Warm Period (RWP, until ~600 CE), the Dark Ages Cold Period (DACP, ~600 to ~900 CE), the Medieval Climate Anomaly (MCA, ~900 to ~1500 CE), the Little Ice Age (LIA, ~1500 to ~1900 CE), and the Modern (Industrial) Period. Ages of boundaries between individual periods may vary regionally.

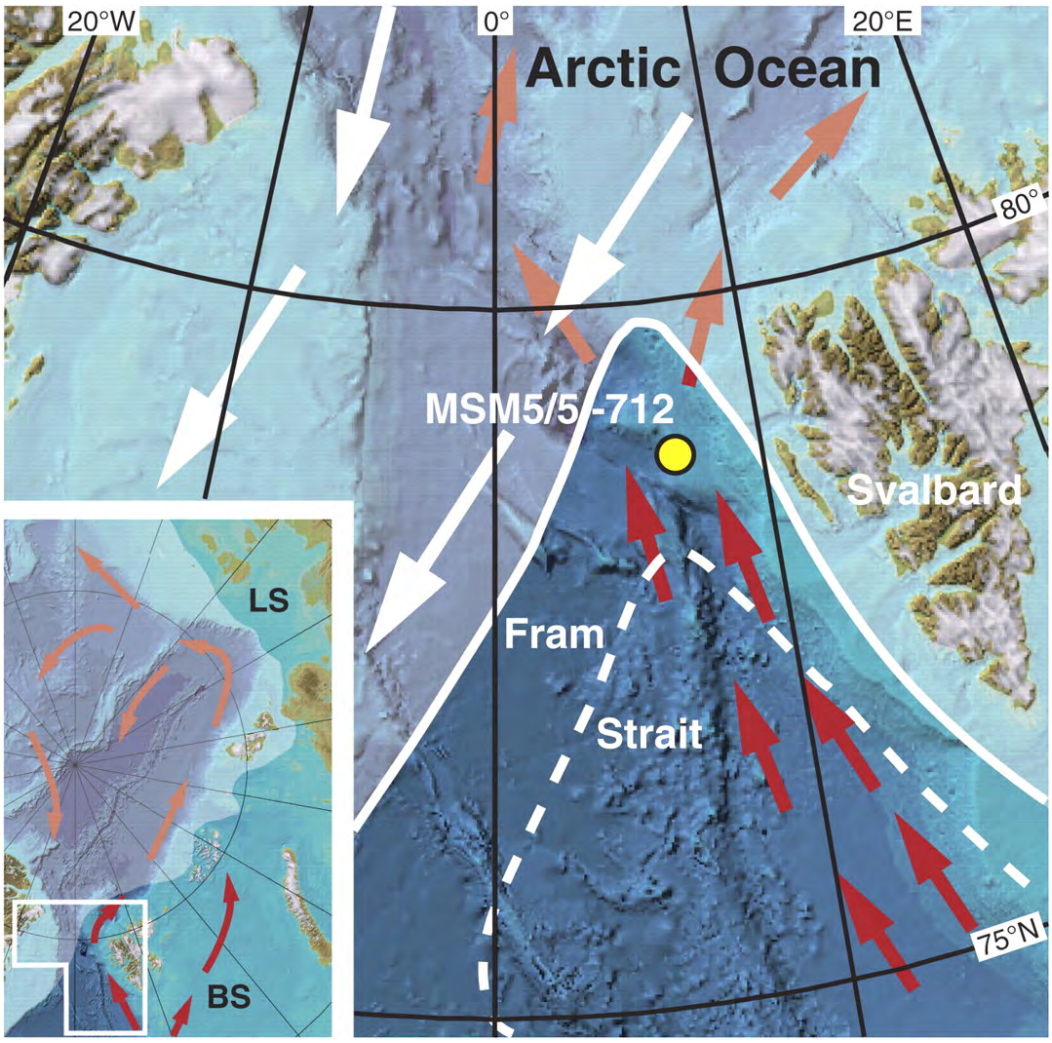

Fig. 4.1: Bathymetric map of the Fram Strait area and the eastern Arctic Ocean (inset; source: http://www.ibcao.org). Average sea ice coverage for April [1989 to 1995; stippled line: 1963 to 1969 (*31*)] and September (inset; 1979 to 2000; source: http://nsidc.org) is indicated by white shading. White arrows indicate ice flow direction in Fram Strait area. Red arrows indicate flow direction of Atlantic Water. Atlantic Water flow is below the halocline waters in the Arctic Ocean proper. Yellow spot marks station MSM5/5-712 at 78°54.94'N, 6°46.04'E, 1491-m water depth. BS, Barents Sea; LS, Laptev Sea.

To reconstruct the temperature variability of AW in the FSB within the past ~2000 years, we investigated planktic foraminifers in a sediment core obtained in August 2007 from the western Svalbard continental margin at site MSM5/5-712 (Fig. 4.1). This site is strategically situated in the path of AW inflow to the Arctic Ocean. Radiocarbon dates in core MSM5/5-712-1 (table S1) revealed sedimentation rates of 18 to 20 cm ky^{-1} for the period 120 BCE to 1475 CE and 27.7 cm ky^{-1} thereafter, resulting in a resolution of 28 and 18 yr per 0.5-cm sample, respectively (Fig. 4.3). The core top had a modern age. Bioturbation by bottom-living organisms is expected to somewhat smooth paleoenvironmental signals, but a quantification of the effect is difficult. Our temperature reconstruction of AW inflow to the Arctic Ocean is based on two independent methods: (i) The SIMMAX modern analog technique (*15*) applied on planktic foraminifer species counts to calculate temperatures at 50-m water depth and (ii) Mg/Ca measurements on the species *Neogloboquadrina pachyderma* (sinistral). Method details are given in the Supporting Online Material (SOM). Habitat and calcification depth of planktic foraminifers in the eastern Fram Strait are below 50-m water depth and reach down to ~300 m, but the distribution maximum is above 150 m (*16*). In this area, plankton blooms usually occur in August (*16*). Thus, our temperature reconstructions reflect mid-summer conditions in the uppermost part of the AW layer, averaged over a few decades.

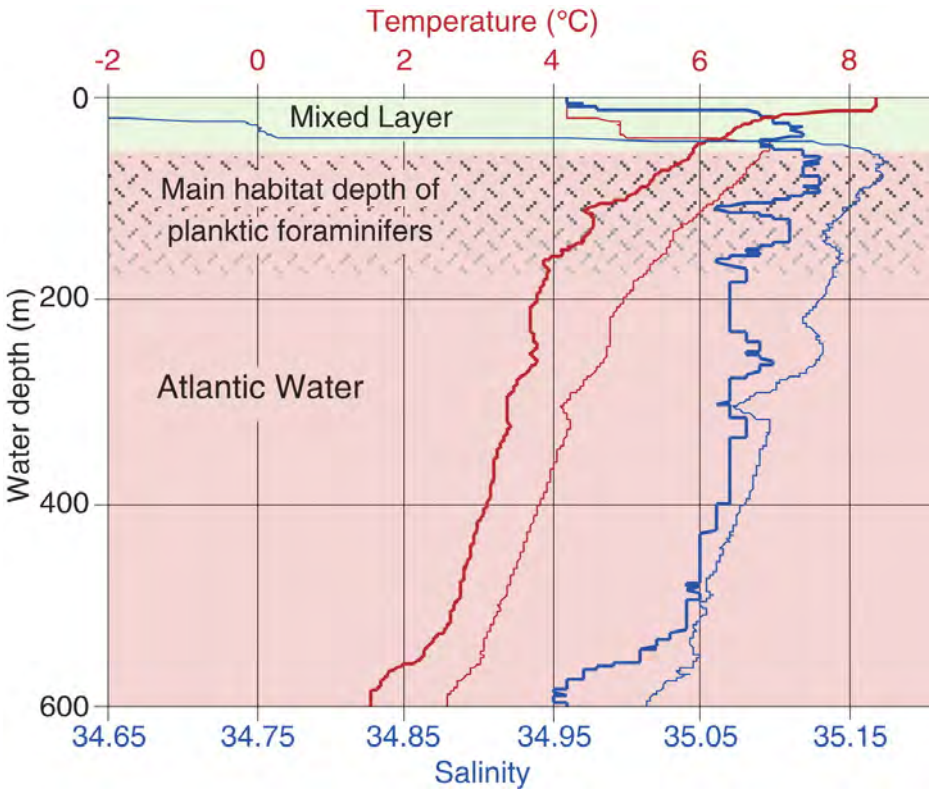

Fig. 4.2: Water mass structure of the upper 600 m at station MSM5/5-712. Seasonal variability of temperature (red lines) and salinity (blue lines) in the Atlantic Water (pink) is revealed by our measurements in summer (4 August 2007; bold lines) and early winter (11 October 2006; thin lines). The main habitat of planktic foraminifers in the eastern Fram Strait (*16, 18*) is marked by a dashed pattern.

Planktic foraminifer associations are useful indicators of water mass distributions and oceanic fronts in the northernmost North Atlantic (*17*). The planktic foraminiferal data from core MSM5/5-712-1 reveal multicentennial changes underlying a high-frequency (multidecadal) variability (Fig. 4.3A; for details of species distributions see fig. S1). High flux rates of both polar and subpolar species characterize the RWP, the MCA-LIA transition, and the Modern Period, whereas low fluxes are recorded for the DACP and the late LIA (Fig. 4.3A). These flux variations likely reflect sea ice cover, since lowest planktic foraminiferal fluxes are today found in the ice-covered areas of the Fram Strait, and highest fluxes at the ice margins (*18*). In sediments from before ~1900 CE, 10 to 40% of all planktic foraminifers belong to subpolar species. In contrast, the youngest sediments reflecting the past ~100 years show a steep increase in subpolar foraminifer fluxes and an unprecedented inversion of the subpolar/polar species ratio, reaching 66% subpolar specimens in the surface sample (Fig. 4.3B). Because the percentage of subpolar specimens is closely related to the water mass distribution, with low values in Arctic waters and high values in AW (*16-18*), highest subpolar foraminifer fluxes and percentages in samples from the Modern Period indicate a strongly increased influence of warm AW advected from the Norwegian Sea.

Results from SIMMAX and Mg/Ca measurements allowed us to quantify the temperature increase associated with the stronger influence of AW off Western Svalbard during the Modern Period. Until ~1850 CE, average summer temperatures varied between 2.8 and 4.4°C (mean ± SE: 3.4°C ± 0.06°C standard error) according to SIMMAX, with low values during the well-known cold periods (early DACP, LIA) and maxima during the early MCA at 800 to 1100 CE (Fig. 4.3C). The record shows strong similarities to terrestrial records of Northern Hemispheric and circum-Arctic temperature variability (*6, 19*) (Fig. 4.3E). AW temperatures since 1890 CE were 4.1 to 6.0°C (mean ± SE: 5.2°C ±0.22°C) and thus ~2°C higher than during the previous 2 ky. The rapid increase to an unprecedented maximum of 6°C calculated for the surface sample apparently started already around 1850 CE. However, the gradual transition may be an artifact caused by bioturbation mixing of foraminifer-poor sediments from the late LIA and foraminifer-rich sediments from the Modern Period. Temperature reconstructions from Mg/Ca measurements give results very similar to those of SIMMAX (Fig. 4.3D). Variability before the Modern Period is high (0.7 to 5.7°C), probably because the Mg/Ca method could not precisely reproduce temperatures below 3°C [(*20*), see discussion in the SOM], but the temperature mean of 3.6°C (±0.3°C, SE) confirms the SIMMAX results. The same agreement applies for the Modern Period: Temperatures since 1890, as calculated from Mg/Ca data, range from 4.4 to 7.1 with a mean value of 5.8°C (±0.5°C, SE). For both methods, the temperature mean of the

Modern Period exceeds all individual values from the preceding 2000 years. These results reveal a rapid warming by ~2°C of uppermost AW in the FSB in the Arctic Gateway during the past ~120 years, consistent with the documented sea ice retreat in the Barents Sea (*5*), terrestrial paleoclimate reference records (*6, 19*) (Fig. 4.3, C to E), and atmospheric measurements (*3*). Notably, modern summer temperatures of uppermost AW in the eastern Fram Strait are >1.5°C higher than multidecadal mean temperature maxima (averaged by bioturbation and sampling) during the MCA.

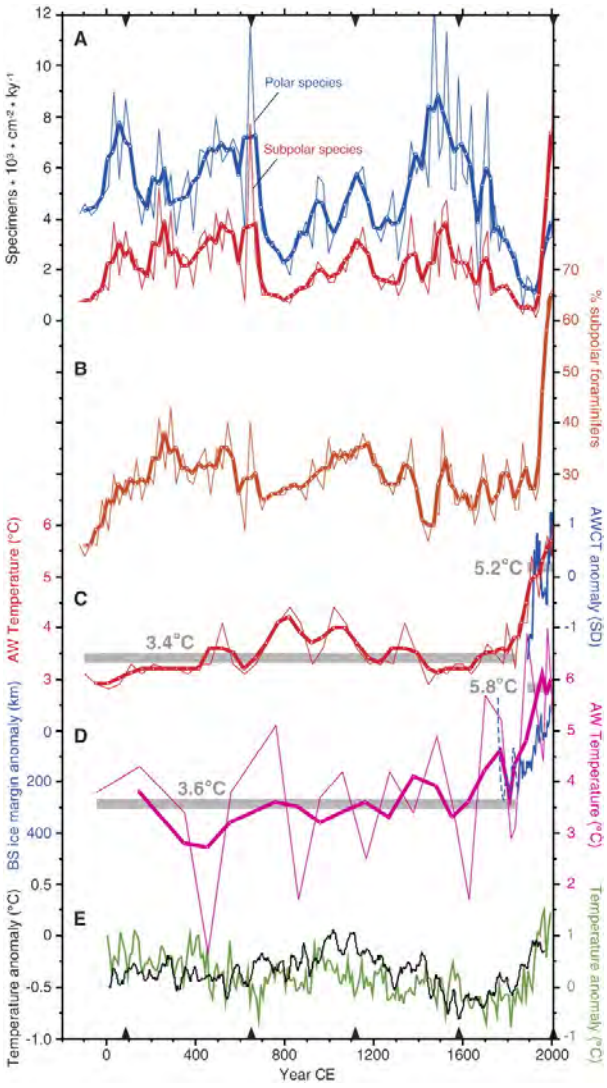

Fig. 4.3: Planktic foraminiferal data and temperature reconstructions of upper Atlantic water in the eastern Fram Strait over the past ~2100 years from sediment core MSM5/5-712-1. Thin lines are raw data, bold lines are three-point running means. Black triangles on the age scale mark calibrated accelerator mass spectrometry ^{14}C ages. (**A**) Fluxes of polar and subpolar planktic foraminifers (100- to 250-µm fraction). (**B**) Percentage of subpolar planktic foraminifers in the 100- zo 250-µm fraction. (**C**) Summer temperatures at 50-m water depth (red) calculated by the SIMMAX Modern Analog Technique. Grey bars mark averages until 1835 CE and 1890 to 2007 CE. Blue line is the normalized Atlantic Water core temperature (AWCT) record (standard deviations) from the Arctic Ocean (1895 to 2002; 6-year averages) obtained from (*21*). (**D**) Summer temperatures (purple) calculated from Mg/Ca ratios in planktic foraminifers *N. pachyderma* (sinistral). Grey bars mark averages until 1835 CE and 1890 to 2007 CE. Blue line is the sea ice margin anomaly (11-year means, less ice is up) in the Barents Sea (BS) obtained from (*5*). Dashed lines mark less reliable data before 1850 CE (**E**) Terrestrial Arctic [green, from (*6*)] and Northern Hemisphere [(black, 25-year means, from (*19*)] temperature anomaly records with reference to the 980 to 1800 CE and 1961 to 1990 CE averages, respectively.

Our reconstructed warming of ~2°C since the LIA matches the reported temperature increase of the Arctic Atlantic Water Layer (AAWL), obtained from observational data of the past ~120 years (*21*) (Fig. 4.3C). At present, there are no subcentennial-scale open ocean proxy data series available to document the temperature evolution of AAWL in the Arctic Ocean proper in the preceding two millennia. Further upstream, in the eastern Norwegian Sea, high-resolution records of summer sea surface temperature (SSST) variability from diatoms (*22*) and stable isotopes of planktic foraminifera (*23*) indicate a warming of ~1.5°C off western Norway since the LIA. However, eastern Norwegian Sea SSSTs in the late 1990s do not clearly deviate from those occurring periodically during the MCA (*22, 23*). Our finding of unequaled warm modern AW temperatures in the eastern Fram Strait with respect to the previous 2000 years (including the warm periods in Roman and Medieval times) may thus express another facet of the Arctic amplification (*1, 24*) of global warming. Recent model results (*25, 26*) reveal the important role of sea ice and atmospheric pressure fields in the Barents Sea as a possible amplifier, which may, at least in part, be responsible for the exceptionally warm AW advection.

Instrumental air and AW temperatures in the Arctic during the 20th century and beyond display quasi-synchronous multidecadal oscillations that make isolation of the industrial warming trend difficult (*3, 21*). Basinwide observations since the 1980s detected multiyear events of AW spreading in the Arctic Ocean which featured both a strong warming and an increased inflow to the Arctic (*7, 27, 28*). Although we cannot quantify from our data the variability of previous AW inflow to the Arctic by volume, our temperature data series and the above observational link suggest that the modern warm AW inflow (averaged over two to three decades) is anomalous and unique in the last 2000 years and not just the latest in a series of natural multidecadal oscillations. Both effects - temperature rise as well as a volume transport increase - introduce a larger heat input into the Arctic Ocean. Although there is no direct contact of the AAWL with the ocean surface in the Arctic, such an increased heat input has far-reaching consequences. The strong AW warming event in the Arctic Ocean in the 1990s caused a shoaling of the AW core and an enhanced heat flux to the surface (*29*), concurrent with decreasing sea ice (*4*). Recent oceanographic data from the Laptev Sea continental margin indicate the impact of warm AW-related water masses on the shallow (<50 m) shelf (*30*), a feature not observed before in a >80-year time series. The data also provide evidence for a significant heat flux to the overlying shelf waters (*30*). Even without any modification of the vertical heat transfer processes, the enhanced temperature contrast between the AW and the surface sea water freezing point (increased from ~5K to 7K as identified here) leads to an increase of the vertical heat flux of ~40%. Any positive feedback mechanism will magnify the effect of this flux increase on the ice cover.

Complementing the strong feedback between ice and atmospheric temperatures (*1*), warming of

the AW layer, unprecedented in the past 2000 years, is most likely another key element in the transition towards a future ice-free Arctic Ocean.

References and Notes

1. J. A. Screen, I. Simmonds, The central role of diminishing sea ice in recent Arctic temperature amplification. *Nature* **464**, 1334-1337, doi:10.1038/nature09051 (2010).
2. R. G. Graversen, T. Mauritsen, M. Tjernström, E. Källén, G. Svensson, Vertical structure of recent Arctic warming. *Nature* **451**, 53-56 (2008).
3. P. Chylek, C. K. Folland, G. Lesins, M. K. Dubeys, M. Muyin Wang, Arctic air temperature change amplification and the Atlantic Multidecadal Oscillation. *Geophys. Res. Lett.* **36**, L14801, doi: 10.1029/2009GL038777 (2009).
4. J. C. Comiso, C. L. Parkinson, R. Gersten, L. Stock, Accelerated decline in the Arctic sea ice cover. *Geophys. Res. Lett.* **35**, L01703, doi:10.1029/2007GL031972 (2008).
5. D. V. Divine, C. Dick, Historical variability of sea ice edge position in the Nordic Seas. *J. Geophys. Res.* **111**, C01001, doi:10.1029/2004JC002851 (2006).
6. D. S. Kaufman *et al.*, Recent warming reverses long-term arctic cooling. *Science* **325**, 1236–1239 (2009).
7. B. Rudels, E. P. Jones, L. G. Anderson, G. Kattner, in *The Polar Ocean and their Role in Shaping the Global Environment*, O. M. Johannessen, R. D. Muench, J. E. Overland, Eds. (Amer. Geophys. Union, Washington DC, 1994), pp. 33–46.
8. U. Schauer, E. Fahrbach, S. Osterhus, G. Rohardt, Arctic warming through the Fram Strait: Oceanic heat transport from 3 years of measurements. *J. Geophys. Res.* **109**, C06026, doi:10.1029/2003JC001823 (2004).
9. S. Bonnet, A. de Vernal, C. Hillaire-Marcel, T. Radi, K. Husum, Variability of sea-surface temperature and sea-ice cover in the Fram Strait over the last two millennia. *Mar. Micropal.* **74**, 59–74, doi:10.1016/j.marmicro.2009.12.001 (2010).
10. D. Hebbeln, T. Dokken, E. S. Andersen, M. Hald, A. Elverhøi, Moisture supply for northern ice-sheet growth during the Last Glacial Maximum. *Nature* **370**, 357 – 360 (1994).
11. T. M. Dokken, M. Hald, Rapid climatic shifts during isotope stages 2–4 in the Polar North Atlantic. *Geology* **24**, 599–602 (1996).
12. R. F. Spielhagen *et al.*, Arctic Ocean deep-sea record of northern Eurasian ice sheet history. *Quat. Sci. Rev.* **23**, 1455–1483 (2004).
13. M. Hald *et al.*, Variations in temperature and extent of Atlantic Water in the northern North Atlantic during the Holocene. *Quat. Sci. Rev.* **26**, 3423–3440 (2007).
14. H. H. Lamb, *Climate: present, past and future* (Methuen & Co., London (1977).
15. U. Pflaumann, J. Duprat, C. Pujol, L. D. Labeyrie, SIMMAX: A modern analog technique to deduce Atlantic sea surface temperatures from planktonic foraminifera in deep-sea sediments. *Paleoceanography* **11**, 15–35 (1996).
16. R. Volkmann, Planktic foraminifers in the outer Laptev Sea and the Fram Strait: Modern distribution and ecology. *J. Foram. Res.* **30**, 157– 176 (2000).
17. T. Johannessen, E. Jansen, A. Flatøy, A. C. Ravelo, in *Carbon Cycling in the Glacial Ocean: Constraints on the Ocean's Role in Global Change*, R. Zahn, T. F. Pedersen, M. A. Kaminski, L. Labeyrie, Eds. (Springer-Verlag, Berlin, 1994), pp. 61–85.

18. J. Carstens, D. Hebbeln, G Wefer, Distribution of planktic foraminifera at the ice margin in the Arctic (Fram Strait). *Mar. Micropal.* **29**, 257-269 (1997).
19. A. Moberg *et al.*, Highly variable Northern Hemisphere temperatures reconstructed from low- and high-resolution proxy data. *Nature* **433**, 613-617.
20. R. Kozdon, A. Eisenhauer, M. Weinelt, M. Y. Meland, D. Nürnberg, Reassessing Mg/Ca temperature calibrations of *Neogloboquadrina pachyderma* (sinistral) using paired $\delta^{44/40}$Ca and Mg/Ca measurements. *Geochem. Geophys. Geosyst.* **10**, Q03005, doi:10.1029/2008GC002169 (2009).
21. I. V. Polyakov *et al.*, Variability of the intermediate Atlantic water of the Arctic Ocean over the last 100 years. *J. Clim.* **17 (23)**, 4485–4497, doi:10.1175/JCLI-3224.1 (2004).
22. N. Koç, E. Jansen, in *Climate Development and History of the North Atlantic Realm*, G. Wefer, W. H. Berger, K.-E. Behre, E. Jansen, Eds. (Springer-Verlag, Berlin 2002), pp. 165-173.
23. D. Klitgaard-Kristensen, H. P. Sejrup, H. Haflidason, I. M. Berstad, G. Mikalsen, Eight-hundred-year temperature variability from the Norwegian continental margin and the North Atlantic thermohaline circulation. *Paleoceanography* **19**, PA2007, doi:10.1029/2003PA000960 (2004).
24. M. Serreze, J. A. Francis, The Arctic Amplification debate. *Clim. Change* **76**, 241-264 (2007)
25. H. Goosse, M. M. Holland, Mechanisms of decadal Arctic climate variability in the Community Climate System Model, Version 2 (CCSM2). *J.Clim.* **18**, 3522-3570 (2005).
26. V. A. Semenov, W. Park, M. Latif, Barents Sea inflow shutdown: A new mechanism for rapid climate changes. *Geophys. Res. Lett.* **36**, L14709, doi 10.1029/2009GL038911 (2009).
27. M. J. Karcher, R. Gerdes, F. Kauker, C. Köberle, Arctic warming: Evolution and spreading of the 1990s warm event in the Nordic seas and the Arctic Ocean. *J. Geophys. Res.* **108 (C2)**, 3034, doi:10.1029/2001JC001265 (2003).
28. I. A. Dmitrenko *et al.*, Toward a warmer Arctic Ocean: Spreading of the early 21st century Atlantic Water warm anomaly along the Eurasian Basin margins, *J. Geophys. Res.*, **113**, C05023, doi:10.1029/2007JC004158 (2008).
29. M. Steele, T. Boyd, Retreat of the cold halocline layer in the Arctic Ocean. *J. Geophys. Res.* **103 (C5)**, 10419-10435 (1998).
30. I. A. Dmitrenko *et al.*, The Arctic Ocean Atlantic water layer impacts the Siberian shelf hydrography. *J. Geophys. Res.* **115**, C08010, doi: 10.1029/2009JC006020 (2010).
31. R. R. Dickson *et al.*, The Arctic Ocean Response to the North Atlantic Oscillation. *J. Clim.* **13 (15)**, 2671-2696 (2000).
32. We thank the captains, crews, and shipboard scientific parties of research vessels *Jan Mayen* and *Maria S. Merian* for assistance during cruises JM06-WP and MSM5/5. R.F.S. and K.W. acknowledge support from the German Research Foundation (Deutsche Forschungsgemeinschaft Priority Core Program 1266 INTERDYNAMIK, project HOVAG); R.F.S. received support from the Academy of Sciences, Humanities, and Literature, Mainz; and S.A.S., K.Z., K.H., and M.H. acknowledge support from the Norwegian Research Council (projects SciencePub and WARMPAST). All data are available at www.pangaea.de (doi:10.1594/PANGAEA.755114).

PAPER III

ATLANTIC WATER ADVECTION VERSUS SEA ICE ADVANCES IN THE EASTERN FRAM STRAIT DURING THE LAST 9 KA – MULTIPROXY EVIDENCE FOR A TWO-PHASE HOLOCENE

Data available online at http://doi.pangaea.de/10.1594/PANGAEA.770168

5 ATLANTIC WATER ADVECTION VERSUS SEA ICE ADVANCES IN THE EASTERN FRAM STRAIT DURING THE LAST 9 KA – MULTIPROXY EVIDENCE FOR A TWO-PHASE HOLOCENE

Kirstin Werner,[1] Robert F. Spielhagen,[1,2] H. Christian Hass,[3] and Torben Struve[1]

[1]Leibniz Institute of Marine Sciences IFM-GEOMAR, Wischhofstraße 1-3, 24148 Kiel, Germany
[2]Academy of Sciences, Humanities, and Literature Mainz, Geschwister-Scholl-Straße 2, 55131 Mainz, Germany
[3]Alfred Wegener Institute for Polar and Marine Research, Wadden Sea Station Sylt, Hafenstraße 43, 25992 List/Sylt, Germany

Abstract

A sediment core from the West Spitsbergen continental margin was studied to reconstruct climate and paleoceanographic variability during the last ca 9 ka in the eastern Fram Strait. Micropaleontological, geochemical, and lithological approaches were applied to derive multidecadal-scale information on the surface and bottom water mass variability and stratification, the intensity of Atlantic Water inflow, fluctuations in oceanic heat flux to the Arctic Ocean, and the position of the sea ice margin. Our multiproxy evidence suggests that the establishment of the modern oceanographic configuration in the eastern Fram Strait occurred stepwise, most probably in response to the postglacial sea level rise and the related onset of modern sea ice production on the shallow Siberian shelves. A first phase comprises the late Early and Mid-Holocene interval (until ca 5 ka) and was generally characterized by relatively unstable conditions. High presence of the subpolar planktic foraminifer species *Turborotalia quinqueloba* implicates strong intensity of Atlantic Water (AW) inflow and/or high temperatures of AW, resulting in a high heat flux to the Arctic basin. Consistent with the decreasing solar insolation slightly decreasing percentages of *T. quinqueloba* after ca 8 ka suggest a modest temperature reduction of the inflowing AW and/or a weakening of its strength. Superimposed on the warm Early and Mid-Holocene conditions were repeated cold events such as the well-known '8.2 ka event'. Other cooling pulses at 6.9, 6.1, and 5.2 cal ka BP were partly of '8.2 ka'-character but may have been spatially more restricted. Our proxy data imply that simultaneous to the complete postglacial flooding of Arctic shallow shelves and the initiation of modern sea ice production a strong advance of polar waters at ca 5.2 cal ka BP initiated modern oceanographic conditions in the eastern Fram Strait. The Late Holocene was marked by the uninterrupted dominance of the cold-water indicating planktic foraminifer species *Neogloboquadrina pachyderma*, a significant

expansion of sea ice/icebergs and strong stratification of the water column. Although planktic foraminiferal assemblages suggest a return of slightly strengthened advection of subsurface Atlantic Water after 3 ka, a relatively stable cold-water layer prevailed at the sea surface and the study site was probably located within the seasonally fluctuating marginal ice zone during the Neoglacial period. According to these results, the Holocene climate and oceanographic development in the eastern Fram Strait was much more variable than previously concluded from marine proxy records and the Greenland ice core records.

5.1. Introduction

The Arctic Ocean reacts very sensitive to global atmospheric changes due to the amplification of climate effects caused by sea ice loss, lowering of the albedo and enhanced heat transport from the ocean to the atmosphere (Manabe and Stouffer, 1980; Serreze et al., 2007). The polar amplification of global climate changes makes the Arctic particularly interesting to study Holocene climate variability and the mechanisms behind it. Kaplan and Wolfe (2006) emphasize the role of ice sheet dynamics not only for glacial periods but also for the Early and Mid-Holocene intervals which have been influenced by the combined effects of the final disintegration of the northern hemisphere ice sheets and the elevated summer insolation. Though with weaker amplitudes compared to glacial climate fluctuations (e.g., Mayewski et al., 2004), Holocene climate anomalies provide appropriate analogues for latest climate excursions such as the ongoing global warming and the Little Ice Age period. The temperature rise within the last 100 to 150 years has been noted already in both terrestrial and marine high-resolution proxy records from the northern hemisphere (Overpeck et al., 1997; Moberg et al., 2005; Kaufman et al., 2009; Mann et al., 2009; Spielhagen et al., 2011).

The eastern Fram Strait is the major deep passage for warm and saline water inflow from the Atlantic to the Arctic and thus plays a crucial role in the heat supply to the Arctic and the closely related sea ice extent (Karcher et al., 2003; Schauer et al., 2004). Greenland ice core records document Holocene climate variability of the northern hemisphere to be exceptionally low compared to fluctuations recorded for preceding glacial and deglacial phases (e.g., Stuiver et al., 1995; Ellison et al., 2006). However, an increasing amount of studies from the Barents Sea/Svalbard area (e.g., Sarnthein et al., 2003; Hald et al., 2004, 2007; Ślubowska et al., 2005; Rasmussen, T.L. et al., 2007; Ślubowska-Woldengen et al., 2007, 2008) and the Nordic Seas (e.g., Koç et al., 1993; Bauch et al., 2001a; Risebrobakken et al., 2003) report significant variations in surface and deep water conditions during the past 10,000 years. Marine studies around Svalbard agree on thermal optimum conditions during the Early Holocene commencing ~10 cal ka BP (e.g., Bauch et al., 2001a; Hald et al., 2004, 2007; Ślubowska et al., 2005; Ebbesen et al., 2007;

Rasmussen, T.L. et al., 2007; Ślubowska-Woldengen et al., 2007, 2008) but show some inconsistencies for the development of the Mid- and Late Holocene. Despite a general agreement on a cooling trend after ~8 cal ka BP (Hald et al., 2004; Ślubowska-Woldengen et al., 2007), some records indicate a relatively warm Mid-Holocene in the Barents Sea/Svalbard area with temperatures higher than for the remainder of the Holocene, albeit still not as high as those of the Early Holocene (e.g., Sarnthein et al., 2003; Hald et al., 2007; Rasmussen, T.L. et al., 2007).

The most pronounced climate excursion of the Holocene period found in Greenland ice core data is the so-called '8.2 ka cooling event' (Stuiver et al., 1995) which was likely triggered by the final outburst drainage from the glacial lakes Agassiz/Ojibway during the final collapse of the Laurentide Ice Sheet (LIS) (Barber et al., 1999). The corresponding immense meltwater release into the North Atlantic (e.g., Stuiver et al., 1995; Rohling and Pälike, 2005) then resulted in a short-lived cool, dry, and possibly windy climate event (Alley et al., 1997). Strong short-term climate fluctuations between ca 8.4 and 8.0 cal ka BP are well pronounced in many records of the North Atlantic (Alley et al., 1997; Risebrobakken et al., 2003; Hall et al., 2004; Moros et al, 2004; Hald et al., 2007; Kleiven et al., 2008). Other studies reveal longer-lasting cool intervals between 8.8 and 8.0 cal ka BP (e.g., Sarnthein et al., 2003; Keigwin et al., 2005; Ellison et al., 2006) attributed to a more sustained LIS meltwater drainage (Keigwin et al., 2005).

An increasing number of studies point to more frequent cooling events during the Holocene (Bond et al., 1997, 2001; Bianchi and McCave, 1999; Chapman and Shackleton, 2000; McDermott et al., 2001; Schulz and Paul, 2002; Risebrobakken et al., 2003; Sarnthein et al., 2003; Wanner et al., 2011) that are not clearly reflected in the Greenland ice core records. Although millennial-scale cyclicity possibly caused by solar output was proposed (e.g., Bond et al., 2001) no consistent evidence for significant Holocene climate cyclicity has been found so far in the northern North Atlantic (e.g., Schulz et al., 2004; Wanner et al., 2011).

In order to derive multi-centennial information on Holocene variability of surface, subsurface, and bottom water mass intensity and stratification, in particular of the Atlantic Water inflow and related fluctuations of the oceanic heat flux to the Arctic Ocean and the position of the sea ice margin in the eastern Fram Strait, the upper ca 210 cm of a sediment core from the Western Svalbard margin were investigated here, covering the past ~8.8 cal ka BP. By means of surface and deepwater proxy indicators such as planktic foraminifer assemblages, planktic and benthic stable isotope signatures as well as lithological parameters, new insights into Holocene variations of surface and deep water conditions are provided, including repeated events of freshwater spreading on the West Spitsbergen continental margin.

5.2. Regional hydrography

The Fram Strait is the only deep connection between the Arctic Ocean and adjacent subpolar oceans. Two major current systems characterize the hydrographical configuration in the Fram Strait (Fig. 5.1). The West Spitsbergen Current (WSC) carries warm (maximum summer temperatures 6°C; Spielhagen et al., 2011) and saline (up to 35.2) Atlantic Water (AW) derived from the North Atlantic Drift to the Arctic Ocean through the eastern Fram Strait. The main heat transport occurs within the warm AW core which is confined to the upper part of the continental slope off Svalbard (Saloranta and Haugan, 2004). Since the WSC is topographically guided along the Barents Sea and Spitsbergen continental slopes (Gammelsrød and Rudels, 1983), it also entrains polar water from the Barents Sea which is anticyclonically transported to the south and west around southern Spitsbergen by the East Spitsbergen Current (ESC) (Hopkins, 1991). North of about 78°N, and close to where our study site is located (Fig. 5.1), the WSC submerges below the colder and low-saline water of Arctic origin and continues as a subsurface current into the Arctic Ocean (e.g., Johannessen, 1986).

The western Fram Strait is perennially covered by sea ice. The East Greenland Current (EGC) transports cold and fresh polar waters ($T<0$°C, $S<34.4$; Schlichtholz and Houssais, 1999; Rabe et al., 2009) and sea ice southward along the Greenland margin out of the Arctic Ocean into the Nordic Seas. The sea ice distribution in the Fram Strait is thus mainly controlled by the outflow of Arctic waters and the intensity of Atlantic Water which today keeps the eastern part of the strait ice-free during most of the year (Vinje, 2001; Fig. 5.1). Where the WSC and the EGC strongly contrasting in physical properties pass each other in opposite directions, meso-scale eddies are generated which carry Atlantic Water westward across the Fram Strait (Johannessen et al., 1987). This part of the AW submerges in the central and western Fram Strait beneath the cold, ice-covered EGC waters and flows southward as the subsurface Return Atlantic Current at intermediate water depth (Gascard et al., 1988; Carstens et al., 1997; Fig. 5.1). In the deeper parts the WSC transports Arctic Intermediate Water (Marnela et al., 2008), Norwegian Sea Deep Water (Schlichtholz and Houssais, 1999) and Greenland Sea Deep Water (Schauer, 1989; Hebbeln, 1991) to the Arctic Ocean, the latter water mass being the result of thermohaline overturning processes in the Nordic Seas (Swift and Koltermann, 1988; Schlichtholz and Houssais, 1999).

Over the last ca 150 years the sea ice extent has varied significantly (Vinje, 2001; Fig. 5.1) and similarly strong sea ice variability can be presumed for the entire Holocene period. Today, the study site is located beneath the Atlantic Water-bearing WSC and thus perfectly suited for tracing Holocene variations of the Atlantic Water inflow.

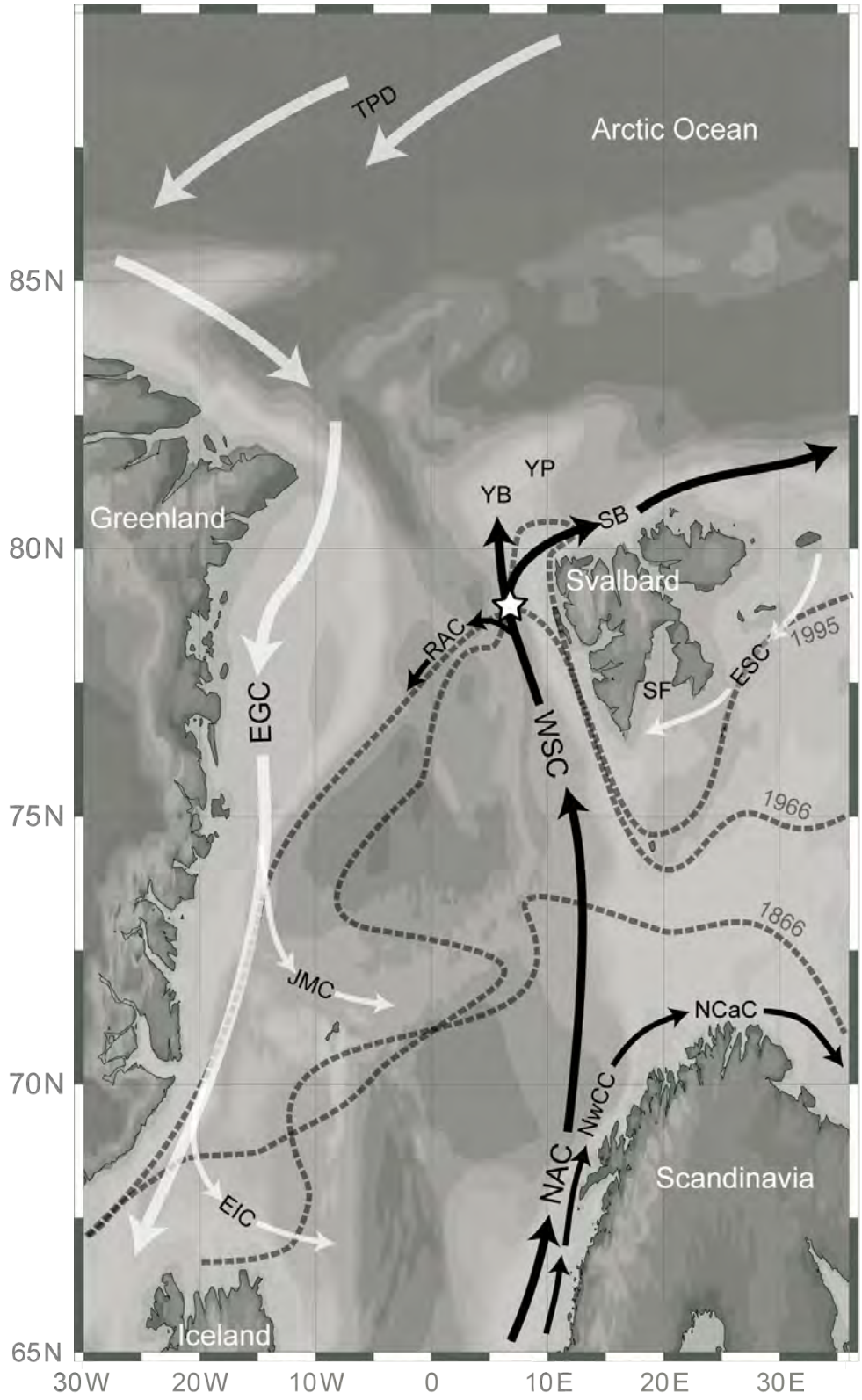

Fig. 5.1: Map of the Nordic Seas and the Fram Strait with main surface/subsurface water currents. Black arrows indicate inflow of warm and saline Atlantic Water to the Arctic Ocean via eastern Fram Strait. White arrows mark cold and low-saline waters of Arctic origin. Also shown are station MSM5/5-712-2 (white star) and selected extreme positions of the sea ice margin (dashed lines with year specification) within the past 150 years after Vinje (2001). AW=Atlantic Water, EGC=East Greenland Current, EIC=East Iceland Current, ESC=East Spitsbergen Current, JMC=Jan Mayen Current, NAC=North Atlantic Current, NCaC=North Cape Current, NwCC= Norwegian Coastal Current, RAC=Return Atlantic Current, SB=Svalbard Branch, SF=Storfjorden, TPD=Transpolar Drift, WSC=West Spitsbergen Current, YB=Yermak Branch, YP=Yermak Plateau.

5.3. Material and methods

The sediment core (kastenlot core) MSM5/5-712-2 was obtained from the western Svalbard continental margin (78°54.94'N, 6°46.04'E, 1490.5 m water depth; Fig. 5.1) during cruise leg MSM5/5 with RV „Maria S. Merian" in summer 2007. The total length of the core was 977 cm. The uppermost 212 cm discussed here consist of olive greyish fine-grained muds apparently representing continuous sedimentation.

Age control is based on ten accelerator mass spectrometry (AMS) radiocarbon dates (see also Giraudeau et al., submitted; Müller et al., submitted). Analyses were conducted at the Leibniz Laboratory of Kiel University, Germany, the University Bordeaux (EPOC), France, and the Poznan Radiocarbon Laboratory, Poland. About 10 mg of calcareous tests of the planktic foraminifer species *Neogloboquadrina pachyderma* were used for measurements. Conversion of radiocarbon dates to calendar years BP (0 BP = 1950 AD) was performed by the calibration software Calib version 6.0 (Stuiver and Reimer, 1993) using the Marine09 calibration data set (Reimer et al., 2009). This calibration implies a standard reservoir correction of 402 years. Linear interpolation was used between calibrated calendar ages. Due to multidecadal time resolution and probable bioturbation which can smooth the paleoenvironmental signal, we rounded all ages to full decades and use centennial notation for the discussion. We refrained from applying a regional average correction ΔR-value since all values provided by the Marine Reservoir Correction Database in CALIB (http://calib.qub.ac.uk/marine/) were obtained from the shallow Svalbard coast area and are therefore not suitable for our site at ca 1500 m water depth. Nevertheless we consider a possible ΔR effect resulting in younger ages when applying our age-depth model.

Sampling was carried out every 1 cm between 10.5 and 211.5 cm core depth. Samples used for analyses of coarse fraction content (weight-% >63μm), ice-rafted debris (IRD), stable isotope measurements, and planktic foraminiferal assemblages were freeze-dried and wet-sieved in deionised water through a 63 μm-sized mesh to remove clay and silt material. Dry bulk density was determined from defined 10 cm^3 samples (10 ml syringes) at a 5 cm interval in the uppermost 50 cm and a 10 to 15 cm interval in the remaining core section. Analyses of coarse fraction content and sortable silt mean grain size, and stable isotope measurements on the planktic foraminifer species *N. pachyderma* and the epibenthic foraminifer species *Cibicidoides wuellerstorfi* were conducted on the entire analyzed section in 1 cm steps. Stable isotope measurements on the planktic foraminifer species *Turborotalia quinqueloba* were carried out every 5 cm and every 1 cm in selected intervals. Planktic foraminiferal assemblages were studied in 1 and 2 cm intervals. IRD contents (lithics 150-250 μm) were determined usually in 5 cm steps and every 1 cm in selected intervals.

For stable oxygen and carbon isotope analysis ca 25 calcareous tests of *N. pachyderma* and *T. quinqueloba* and ca 15 tests of *C. wuellerstorfi* were measured. In order to prevent possible ecological biases of different morphotypes (Healy-Williams, 1992) only "square-shaped" (four-chambered) specimens of *N. pachyderma* were used. The tests were crunched and mingled so that well-mixed aliquots could be used for the measurements. Stable isotope analysis was carried out using a Finnigan MAT 253 mass spectrometer system and a Kiel IV Carbonate Preparation Device at the IFM-GEOMAR Stable Isotope Lab. The carbonate was treated with orthophosphoric acid at 70°C. The analytical accuracy was <0.06‰ for $\delta^{18}O$ and <0.03‰ for $\delta^{13}C$. All measurements were calibrated to Pee Dee Belemnite (PDB) standard (international standard NBS 19). For comparison, oxygen isotope data of *N. pachyderma* were corrected for the ice volume effect following Meland et al. (2008). An ice volume component of 1.05‰ (Duplessy et al., 2002) assuming a sea level 120 m lower than today during the Last Glacial Maximum (Fairbanks et al., 1989) was applied. As suggested by Fairbanks (1989) we used the sea level curve by Lighty et al. (1982) which estimates the glacial ice-volume based on measured glacio-eustatic sea level changes for the last 9 ka.

A representative split of at least 300 planktic foraminiferal tests in the size fraction 100–250 μm was counted and identified to species level to study the planktic foraminiferal assemblages in each sample. The fraction >250 μm was neglected due to an almost complete absence of planktic foraminifers. Planktic foraminifer fluxes were calculated on dry bulk density values and linear sedimentation rates.

Aliquots of the freeze-dried samples were used for the analysis of sortable silt mean grain size ($\overline{SS}$). To remove carbonate and organic matter, samples were treated with acetic acid and hydrogen peroxide, respectively. After adding sodium polyphosphate for better dispersion, the freeze-dried samples were put on a shaker for at least 24 hours. Measurements were performed with a CILAS 1180L laser-diffraction particle analyser. The sortable silt size mean grain size 10-63 μm (Robinson and McCave, 1994) was calculated using the entire granulometric data sets based on vol.%.

To estimate the IRD contents, lithic grains were counted on a representative split (> 100 grains) in the 150-250 μm size fraction. IRD fluxes were calculated on dry bulk density values and linear sedimentation rates.

In order to test the existence of possible periodic or quasiperiodic behaviour (Risebrobakken et al., 2003), all proxy data sets were spectrally analyzed by the Blackman-Tukey method (Blackman and Tukey, 1958) using the AnalySeries 2.0 software (Paillard et al., 1996). In order to remove linear trends, we followed the presetting of the software in resampling at 32- to

100-year intervals. The confidence level was set to 90%. In addition to the interval 8.8 to 0.4 cal ka BP we separately tested the interval 8.8 to 5.0 cal ka BP with the same settings.

5.4. Results

5.4.1. Age control

The stratigraphic record of kastenlot core MSM5/5-712-2 presented here comprises ten AMS radiocarbon datings covering ca 9,000 years (Table 5.1, Fig. 5.2). Linear sedimentation rates range between 45 and 17 cm/ka (Fig. 5.2). Each 1 cm thick sediment slice thus represents between 22 (8.3 to 7.8 cal ka BP) and 68 (before 1.1 cal ka BP) years. Accumulation rates range from 10 to 30 g/cm^2*ka.

Table 5.1: AMS radiocarbon dates and calibrated dates for kastenlot core MSM5/5-712-2. Dating (*) was taken from Aagaard-Sørensen (2011).

Depth, cm	^{14}C age, a	Cal. age, a BP (2σ)	Lab. no
10.0 – 12.0	815 ± 25	454.5 ± 49.5	KIA 45217
20.0 - 22.0	1570 ± 25	1133.5 ± 82.5	KIA 41024
27.0 – 29.0	1985 ± 25	1539.5 ± 96.5	KIA 45218
40.0 – 42.0	2565 ± 25	2232.5 ± 83	KIA 45219
60.0 - 61.0	3365 ± 30	3235.5 ± 97.5	SacA 19113
94.0 - 95.0	4915 ± 30	5214 ± 104	SacA 19114
138.5 - 139.5	6440 ± 30	6926.5 ± 106.5	SacA 19115
168.5 - 169.5	7305 ± 35	7763.5 ± 93.5	KIA 38080
191.5 - 192.5	7815 ± 45	8274 ± 97	KIA 41025
214.0 - 215.0*	8362 ± 45	8924.5 ± 155.5	Poz-30723

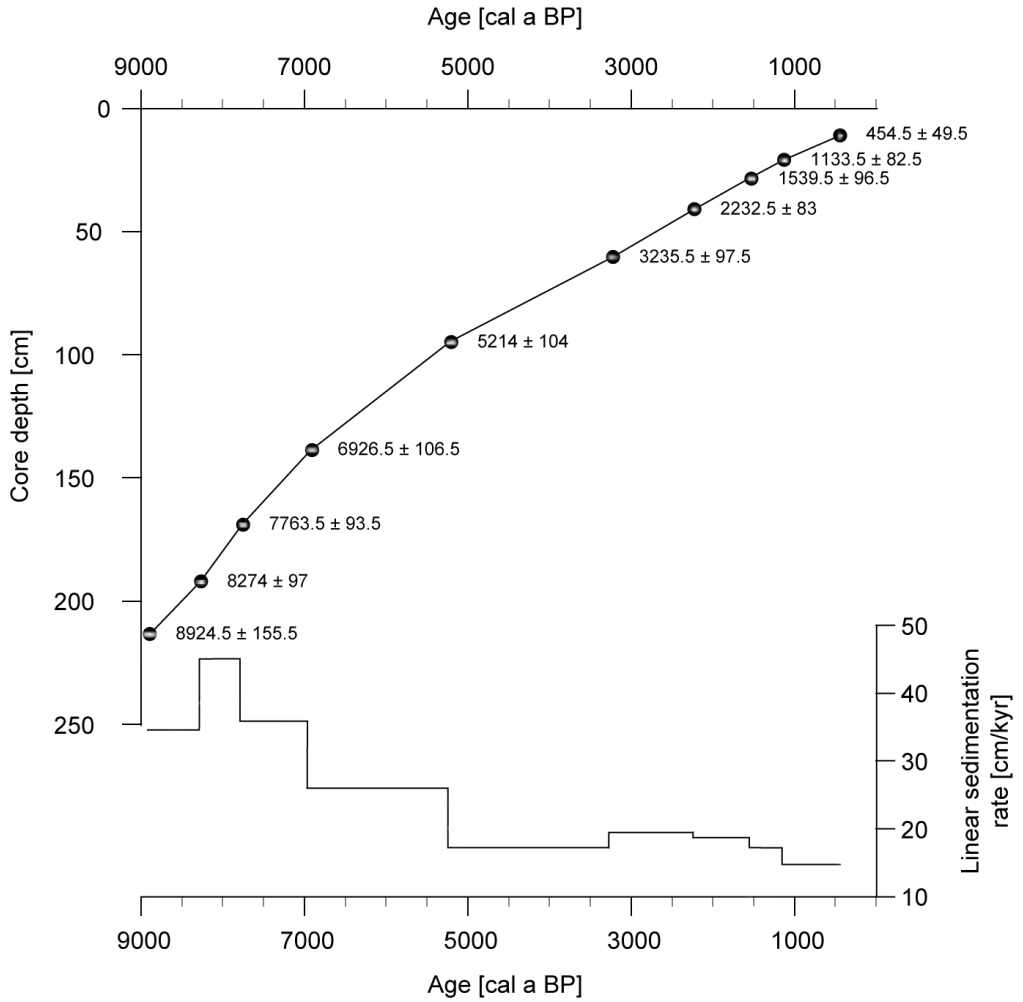

Fig. 5.2: Age-depth model for kastenlot core MSM5/5-712-2. Grey bars within symbols of AMS radiocarbon dates mark 2σ error ranges.

5.4.2. Planktic foraminifer assemblages and fluxes

The planktic foraminifer assemblages consist of two dominant species: *N. pachyderma* is commonly regarded as the only species reflecting polar surface water (Bauch et al., 2001a). The subpolar species *T. quinqueloba* has been found to be indicative for Atlantic Water inflow in the Fram Strait (Volkmann, 2000). Dominance of these two species was described for large areas in the Nordic Seas during the Holocene (Bauch et al., 2001a) and for the modern Fram Strait (Carstens et al., 1997; Volkmann, 2000). Other species found include *Neogloboquadrina incompta*, *Globigerina bulloides*, *Globigerinita uvula*, and *Globigerinita glutinata*. In the notation of the polar species *N. pachyderma* we follow Darling et al. (2006) who showed that sinistral coiling *N. pachyderma* and dextral coiling *N. pachyderma* are two different species. Accordingly, we use the suggested new terms *N. pachyderma* and *N. incompta*, respectively. '*Globigerinita* sp. (juvenile)' denotes specimens of *G. uvula* and *G. glutinata* smaller than 150 µm which cannot always be clearly distinguished. *Globigerinita uvula*, *Globigerinita glutinata*, and *Globigerinita* sp. (juvenile) are shown separately in Fig. 5.3 but are combined in one record as *Globigerinita* sp. in Fig. 5.4a.

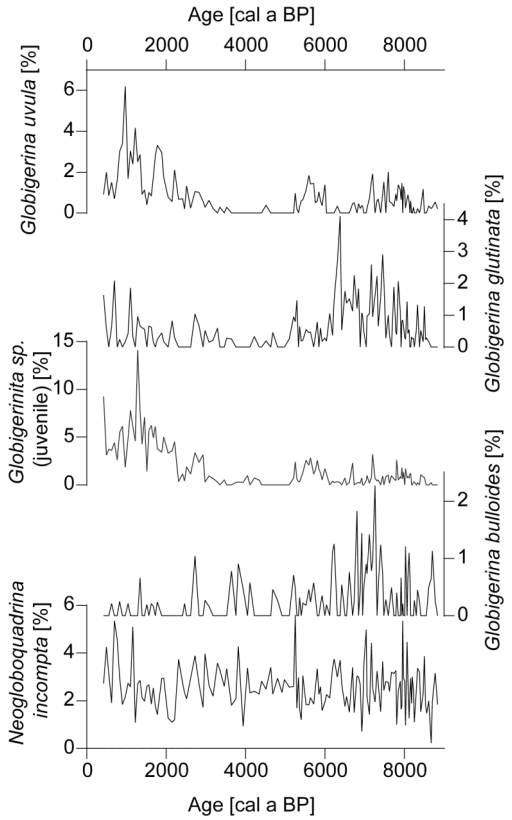

Fig. 5.3: Planktic foraminifer species of minor abundance in core record MSM5/5-712-2. *Globigerinita* sp. (juvenile) denotes specimens of *G. uvula* and *G. glutinata* smaller than 150 μm.

High portions of *N. pachyderma* are seen between 8.2 and 8.0 (up to 68%), between 7.0 and 5.9 cal ka BP (60 to 88%) with peaks at 6.9 and 6.1 cal ka BP, and after 5.2 cal ka BP (>90%; Fig. 5.4a). Nearly inversely related to *N. pachyderma*, *T. quinqueloba* revealed peak portions before 8.2 cal ka BP (up to 75%; Fig. 5.4a). Although still high, *T. quinqueloba* portions continuously decreased (35-71%) between 8.0 and 7.1 cal ka BP. A local maximum of *T. quinqueloba* up to 40% is observed at 6.5 cal ka BP. It again drastically increased (34-64%) between 5.9 and 5.2 cal ka BP but dropped after 5.2 cal ka BP to minimum values <20%. Slight increases of *T. quinqueloba* are noticed around 3 cal ka BP and at 1.9 cal ka BP, thereafter it decreased to <20% (Fig. 5.4a).

Portions of *Globigerinita* sp. were higher between 8.0 and 5 cal ka BP (up to 6%) and increased up to 17% within the past 3 cal ka BP. *N. incompta* percentages fluctuated around 2.5% throughout the studied core section. Apart from some higher relative abundances between 8 and 7 cal ka BP (1-2%), percentages of *G. bulloides* mainly stayed below 1%.

Planktic foraminifer abundances revealed high (up to 1300 ind./g) but strongly fluctuating values before 5 cal ka BP (Fig. 5.4b). Between 5 and 3.5 cal ka BP abundances were low (ca 330 ind./g on average) but increased again thereafter. Before 7.3 cal ka BP planktic foraminifer fluxes had maximum values (up to 32,000 ind./cm^2*ka). Between 5.0 and 3.5 cal ka BP fluxes were low (4200 ind./cm^2*ka on average) but slightly increased again after 3.5 cal ka BP. Isolated peaks are noticed around 5.8 and 5.2 cal ka BP.

5.4.3. Planktic and benthic stable isotopes

If not marked otherwise the following notations for the $\delta^{18}O$ and $\delta^{13}C$ values derived from the respective foraminifer species are used in the text: $\delta^{18}O_{Np}$ and $\delta^{13}C_{Np}$ for *N. pachyderma*, $\delta^{18}O_{Tqu}$ and $\delta^{13}C_{Tqu}$ for *T. quinqueloba*, and $\delta^{18}O_{Cw}$ and $\delta^{13}C_{Cw}$ for *C. wuellerstorfi*. For ice volume-corrected $\delta^{18}O$ values of *N. pachyderma* and *C. wuellerstorfi* we use the notation $\delta^{18}O_{Np(ivc)}$ and $\delta^{18}O_{Cw(ivc)}$, respectively.

Planktic oxygen isotope values measured on *N. pachyderma* vary between 2.89 and 3.59‰ (Fig. 5.4d) throughout the studied core section. Heavier $\delta^{18}O_{Np}$ values (~3.5‰) are noticed around 6.5, 5.5 and around 4 cal ka BP. Light oxygen isotope values are found between 8.5 and 7 and between 6.0 and 5.5 cal ka BP. After ca 3.5 cal ka BP $\delta^{18}O_{Np}$ were higher fluctuating. Ice volume-corrected $\delta^{18}O_{Np(ivc)}$ data are shown in Fig. 5.7g. Noticeable is the overall increasing trend of $\delta^{18}O_{Np(ivc)}$ values. Carbon isotope values of *N. pachyderma* gradually increase until ca 3 cal ka BP to maximum values up to 0.98‰ (Fig. 5.4g) and decrease thereafter (average values of 0.5‰).

A vital effect correction of +1.3‰ and +2.6‰ was applied for stable oxygen and carbon isotope data of *T. quinqueloba*, respectively (Volkmann, 2000). Unlike the drop in $\delta^{13}C_{Np}$ after ca 3 cal ka BP, $\delta^{13}C_{Tqu}$ values (between 0.69 and 2.04‰) steadily increase throughout the record, albeit with strong fluctuations superimposed (Fig. 5.4f). $\delta^{18}O_{Tqu}$ values highly fluctuate between 2.44 and 5.0‰ but show a general increasing trend until ca 1.0 cal ka BP and a strong decrease thereafter (Fig. 5.4e).

Oxygen isotope data of *C. wuellerstorfi* were corrected for their disequilibrium effect by +0.64‰ (Shackleton and Opdyke, 1973; Duplessy et al., 2002). Variations in $\delta^{18}O_{Cw}$ are low and range between 4.2 and 5.1‰ (Fig. 5.5a). $\delta^{18}O_{Cw}$ values continuously decrease until ca 3.7 cal ka BP after which they increased again. The increase after 3.7 cal ka BP is more obvious in the record corrected for the ice volume effect (Fig. 5.7h). Though highly fluctuating between 0.6 and 1.3‰ benthic $\delta^{13}C$ values increase during the entire studied period (Fig. 5.5b). Local maxima are noted between 6.0 and 5.2 cal ka BP while short-term drops of $\delta^{13}C_{Cw}$ are found at 8.2, 6.1, and 5.0 cal ka BP.

Fig. 5.4 (next page): Surface and subsurface water proxy records of MSM5/5-712-2. **a)** Percentages of dominant planktic foraminifer species *N. pachyderma* (blue stippled line) and *T. quinqueloba* (red line) as well as combined record of *G. uvula* and *G. glutinata* as *Globigerinita* sp. (grey line). **b)** Planktic foraminifer abundances (grey line) and fluxes (black line). **c)** IRD fluxes and percentages of sand (size fraction 63-1000 μm). **d-e)** Oxygen isotope records of *N. pachyderma* and *T. quinqueloba*. Thick red lines indicate 3-point moving averages. **f-g)** Carbon isotope records of *T. quinqueloba* and *N. pachyderma*. Thick blue lines indicate 3-point moving averages. Black triangles indicate AMS ^{14}C datings. Blue dashed lines refer to significant drops in *T. quinqueloba* percentages during the Early and Mid-Holocene. Black arrows mark Neoglacial trend clearly represented in almost all surface/subsurface water proxy records. Units I and II indicate subdivision of Early and Mid-Holocene and Late Holocene conditions, respectively.

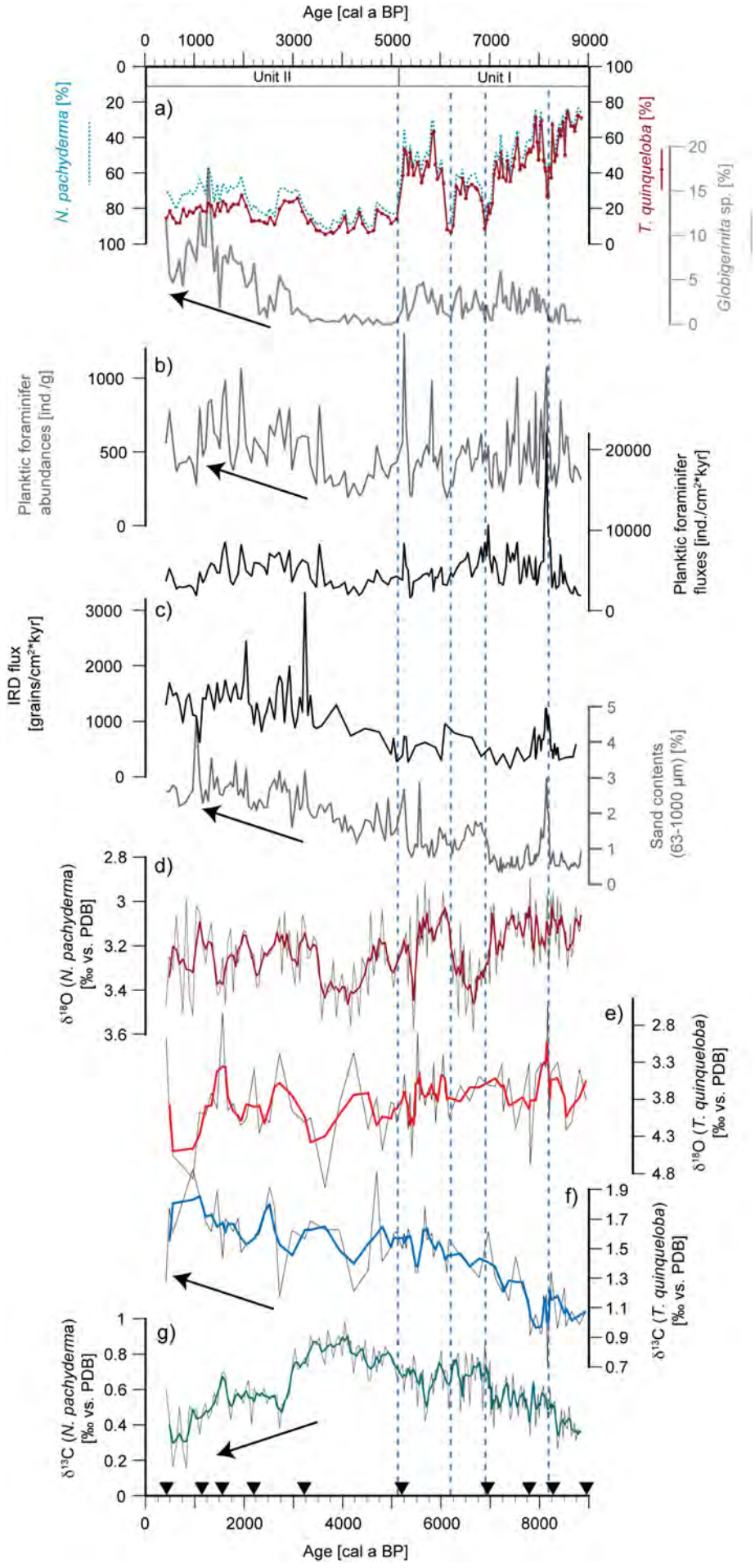
Age [cal a BP]
0 1000 3000 5000 7000 9000
Unit II
Unit I
a)
N. pachyderma [%]
T. quinqueloba [%]
Globigerinita sp. [%]
b)
Planktic foraminifer abundances [ind./g]
Planktic foraminifer fluxes [ind./cm²*kyr]
c)
IRD flux [grains/cm²*kyr]
Sand contents (63-1000 µm) [%]
d)
δ18O (N. pachyderma) [‰ vs. PDB]
e)
δ18O (T. quinqueloba) [‰ vs. PDB]
f)
δ13C (T. quinqueloba) [‰ vs. PDB]
g)
δ13C (N. pachyderma) [‰ vs. PDB]
0 2000 4000 6000 8000
Age [cal a BP]

$\Delta\delta^{18}O$ and $\Delta\delta^{13}C$ were used to estimate the degree of stratification assuming different living habitat layers of planktic foraminifers and accordingly certain water depths. Between ca 8.8 and 5 cal ka BP stratification between the subsurface (*N. pachyderma*) and the bottom water layer (*C. wuellerstorfi*) was relatively high but fluctuated strongly, while a minimum of stratification is concluded from low $\Delta\delta^{18}O$ and $\Delta\delta^{13}C$ of *C. wuellerstorfi* and *N. pachyderma* between ca 5 and 3 cal ka BP (Fig. 5.7d, e). After 3 cal ka BP stratification between bottom and subsurface layers again increased. Stratification of subsurface (*N. pachyderma*) and surface (*T. quinqueloba*) layers was rather low during the late Early and Mid-Holocene interval but increased during the Late Holocene (Fig. 5.7f).

5.4.4. Lithology

A general increase in IRD contents is noted throughout the record (Fig. 5.4c). Fluxes vary between 140 (7.4 cal ka BP) and 3200 (3.2 cal ka BP) grains/cm^2*ka throughout the studied section. Significantly higher IRD fluxes occur between 8.2 and 8.1 cal ka BP and around 6.1 cal ka BP (>1200 and up to 1000 grains/cm^2*ka, respectively).

Coarse fraction content (63-1000 μm) is generally very low (< 2%) in sediments older than ca 7.0 cal ka BP (Fig. 5.4c), with higher portions found only between ~8.2 and 8.0 cal ka BP (up to 3%). After 7 cal ka BP the coarse fraction gradually increases to >4% in the core top sediments.

The sortable silt mean grain size ($\overline{SS}$) strongly varies between 13.8 and 26.7 μm in the studied core section (Fig. 5.5c). $\overline{SS}$ data have been checked for IRD contamination following Hass (2002) and reveal insignificant influence of ice-transported silt. Various impacts of different bottom currents and their entrained sediments complicate the interpretation of $\overline{SS}$ data. We therefore focus on the main trends shown in the 5-point moving average (Fig. 5.5c). Higher $\overline{SS}$ values are observed from 7 to 6 cal ka BP, around 5.0 cal ka BP, and from 3 to 1.8 cal ka BP while lower $\overline{SS}$ values are noted after 8.0, after 7.5, at 5.5, and at 1.5 cal ka BP. Opposite trends of benthic carbon isotopes and $\overline{SS}$ values (Fig. 5.5) are noted in particular for the Early and Mid-Holocene intervals.

Fig. 5.5 (next page): Bottom water proxy records of site 712 for the past ca 9 cal ka BP. **a)** Benthic oxygen isotopes. **b)** Benthic carbon isotopes. **c)** Sortable silt mean grain size. Thick lines mark 3-point moving averages for a) and b) and 5-point moving averages for c). Black arrows display long-term trends in benthic isotope data. Grey dashed lines and grey arrows highlight opposed trends of $\delta^{13}C_{Cw}$ and sortable silt data.

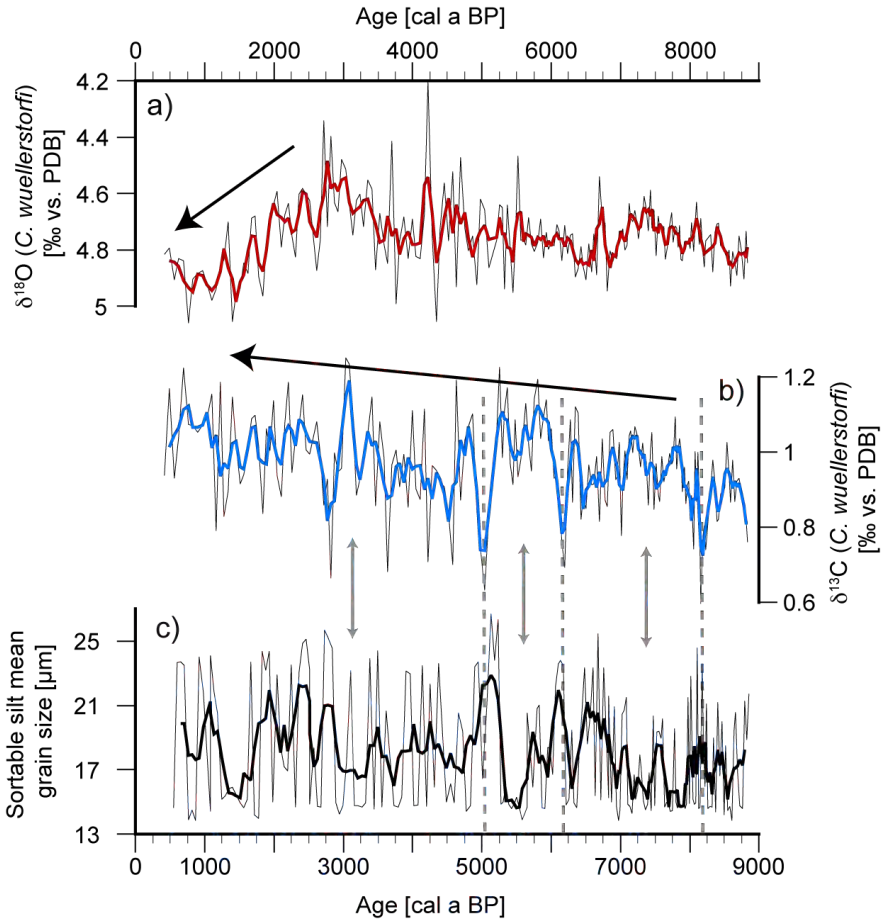

5.4.5. Time series analysis

Surface water related proxy data do not reveal any considerable periodicity. In Fig. 5.6 selected power spectra with evidence of centennial and millennial periodicity are shown for the intervals 8.8-0.4 and 8.8-5.0 cal ka BP. Cyclicity is more pronounced in the interval 8.8-0.4 cal ka BP than in the one spanning from 8.8 to 5.0 cal ka BP which appears reasonable as the latter interval is probably too short to identify distinct cyclicity of >500 years. Planktic oxygen isotope data of *N. pachyderma* and *T. quinqueloba* show periodicities between 250 and 1850 years (Fig. 5.6a, b). Noticeable is also a near-500-year cycle which is likewise pronounced in planktic foraminifer abundances (Fig. 5.6c). Also, bottom water proxies (Fig. 5.6d-f) show pronounced periodicity at about 500 years. Benthic carbon isotope data reveal a pronounced peak at 550 years, in agreement with results by Chapman and Shackleton (2000). The $\overline{SS}$ data reveal stronger periodicities at 800 and 1800 years, which neither resemble findings of a near-1500-year cyclicity (Bond et al., 1997; Bianchi and McCave, 1999) nor evidence 550- or 1000-year periods as suggested by Chapman and Shackleton (2000). Dating uncertainties may account for slight departures, as suggested by Risebrobakken et al. (2003). Thus, the $\overline{SS}$ cycles of 1800, 800, and 475 years may be linked to those of 1500, 1000 and 550 years. However, we like to note that possible dating uncertainties should similarly apply to all investigated parameters.

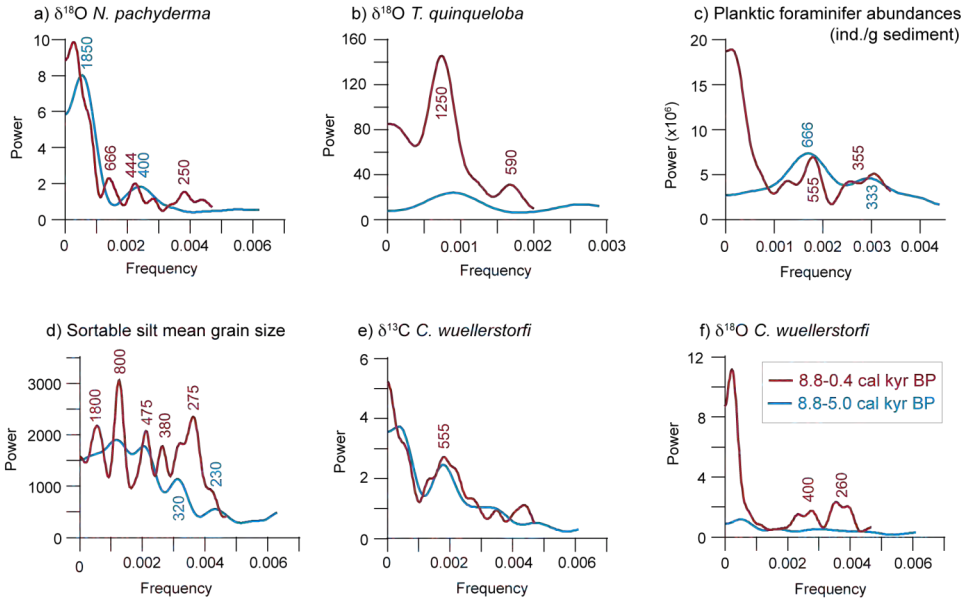

Fig. 5.6: Selected power spectra for surface water **(a-c)** and bottom water **(d-f)** proxy records of MSM5/5-712-2. Different colours indicate the two different intervals: 8.8-0.4 cal ka BP, red; 8.8. to 5.0 cal ka BP, blue. Numbers in graphs indicate obtained periodicities.

5.5. Discussion

5.5.1. Early and Mid-Holocene optimum conditions (8.9 to 5.2 ka)

High portions of *T. quinqueloba* during the Early and Mid-Holocene intervals (Fig. 5.4a; 4.9b) are attributed to intense Atlantic Water inflow and/or warm temperatures of AW to the eastern Fram Strait. The Early Holocene northward expansion of warm Atlantic surface waters into subarctic northern latitudes and increased heat flux to the Arctic Ocean (e.g., Koç et al., 1993; Bauch et al., 2001a; Hald et al., 2007) were probably related to the insolation maximum in the northern hemisphere (Laskar et al., 2004; Fig. 5.7a), and concur with warmest atmospheric temperatures documented in Greenland ice core records (Stuiver et al., 1995; Rasmussen et al., 2006; Vinther et al., 2006; Fig. 5.7a) and terrestrial proxy records (e.g., Svendsen and Mangerud, 1997; Seppä and Birks, 2001; Humlum et al, 2005).

Parallel to the decrease in insolation after 8.0 cal ka BP (Fig. 5.7a) a gradual cooling trend is obvious in our data by slightly decreasing *T. quinqueloba* portions. Carstens et al. (1997) showed that highest particle fluxes are related to maximum bioproductivity at the sea ice margin in the Fram Strait. Accordingly, detected high planktic foraminifer abundances and fluxes may be linked either to ice-free conditions or a sea ice margin seasonally fluctuating over the study site. Greater portions of *G. uvula* after 8 and after 6 cal ka BP (Fig. 5.3) reflect cold and fresh productive surface waters (Rasmussen, T.L., 2007). Relatively light oxygen isotopes measured on calcareous tests of *N. pachyderma* (Fig. 5.4d) are probably associated with warmer temperatures of the inflowing AW but may also be linked to increased admixture of freshwater produced by postglacial melting of ice sheets during the Early and Mid-Holocene intervals. This is in

agreement with strongly decreasing $\delta^{18}O_{Np}$ prior to 9 ka, at the transition between cool deglacial and warm Early Holocene conditions (Aagaard-Sørensen, 2011). In correspondence to lower *T. quinqueloba* portions and reduced SST reconstructed from Mg/Ca ratios at site 712 (Aagaard-Sørensen, 2011), intervals of heavier $\delta^{18}O_{Np}$ between 7.0 and 6.0 cal ka BP and at ca 5.0 cal ka BP were likely linked to a slight cooling of subsurface water masses (Fig. 5.4d).

Evidence for strong AW advection during the Early Holocene has also been indicated west and north of Svalbard by benthic foraminiferal assemblages (Ślubowska-Woldengen et al., 2008). From planktic foraminiferal investigations in the Barents Sea area, Sarnthein et al. (2003) concluded relatively warm conditions that lasted until ca 7 cal ka BP. This is consistent with findings by Duplessy et al. (2001) in the northern Barents Sea, by Rasmussen, T.L. et al. (2007) on the SW Svalbard margin, and by Bauch et al. (2001a) on the eastern flank of the Jan Mayen Ridge in the Nordic Seas. All studies reveal Holocene thermal optimum conditions until ca 7 cal ka BP and a pervasive cooling thereafter. In the Nordic Seas, continuous surface cooling set in at ca 6 cal ka BP (Bauch et al., 2001a).

Though not approaching the high temperatures of the Early Holocene, our data reveal another Mid-Holocene warm interval between 6.1 and 5.2 cal ka BP, in agreement with findings from the Western Barents Sea and in the Lofoten Basin (Sarnthein et al.; 2003; Fig. 5.7c; Bauch and Weinelt, 1997). In accordance with Hald et al. (2007) the strong warming signal in our record may be related to the amplification of Early Holocene warm conditions in the Fram Strait caused by an insulating meltwater coverage and limited heat loss to the atmosphere (Haugan, 1999).

Benthic oxygen isotope values derived from *C. wuellerstorfi* (Fig. 5.5) are relatively constant until ca 5 cal ka BP, probably indicating stable deepwater temperatures and/or salinities. Stable carbon isotope values of *N. pachyderma*, *T. quinqueloba*, and *C. wuellerstorfi* show similar increasing trends, though the rise of benthic $\delta^{13}C_{Cw}$ values is less pronounced (Figs. 5.4, 5.5). An increasing trend of $\delta^{13}C_{Cw}$ since ca 8.0 cal ka BP has also been noted on the eastern flank of the Jan Mayen Ridge in the Nordic Seas (Bauch et al., 2001a). In general, analogies in planktic and benthic carbon isotope trends may be indicative of a similar source of water masses. Based on parallel peaks in planktic and benthic oxygen isotope records from site 712 within the past two millennia, Werner et al. (2011) concluded on a close linkage between AW and bottom water masses in the area. High carbon isotope values are generally attributed to well-ventilated water masses (e.g., Spielhagen and Erlenkeuser, 1994). Gradually better ventilation of the entire water mass is thus inferred for the entire water column during the Early and Mid-Holocene. The trend to increasing planktic carbon isotope values may indicate a gradual migration of planktic foraminifers to a shallower habitat depth. Indeed, it has been shown that depth preferences of the foraminifer species *N. pachyderma* and *T. quinqueloba* in the Fram Strait depend on the surface water conditions

(Carstens et al., 1997; Kozdon et al., 2009). Under sea ice coverage, planktic foraminifers calcify in deeper water depth (150-200 m) whereas at ice-free conditions their habitat depth is located at ca 50-100 m (Carstens et al., 1997). Due to better ventilation of surface water masses compared to the subsurface layer we assume that planktic-derived $\delta^{13}C$ values may reflect conditions in the respective habitat depth and reveal higher values in surface than in subsurface water masses. A relatively thick freshwater-rich layer that may have prevented planktic foraminifers from ascending towards the surface could then have resulted in the low planktic $\delta^{13}C$ values derived from subsurface-living foraminifers during the Early Holocene compared to higher planktic $\delta^{13}C$ values during the Mid-Holocene (Figs. 5.4f, g, 5.5). Possibly, such a low-salinity layer may have prevailed over the site in response to the still ongoing deglacial melting during the Early Holocene. Haugan (1999) proposed that heavy ice conditions west of Spitsbergen can generate a stable surface freshwater layer during spring which acts as an insulation layer for subsurface Atlantic-derived heat and can prevent unhindered heat flux to the atmosphere. Accordingly, an upper mixed layer of significantly lower salinity may have prevented substantial heat loss to the atmosphere from the Atlantic Water-bearing WSC during the Early Holocene. Limited heat loss may then explain the transport of very high portions of *T. quinqueloba* indicative of strong AW inflow (Volkmann, 2000) found during the Early Holocene. Apparently, this surface layer of cold and fresh waters only gradually disappeared during the Mid-Holocene period when maximum $\delta^{13}C_{Np}$ values indicate weakest stratification between 5 and 3 cal ka BP (Fig. 5.7d-f) and planktic foraminifera may have migrated to the uppermost surface water layer.

Alternatively, stepwise increasing planktic carbon isotope values during the Early and Mid-Holocene which also have been found in the subpolar North Atlantic region (e.g., Bauch et al., 2001a; Sarnthein et al., 2003; Fig. 5.9) and in the Barents and Kara Seas (Lubinski et al., 2001), have been explained by the deglacial/Holocene sea level rise (Lubinski et al., 2001). Continuous flooding of the glacially exposed shelf areas in the Kara and Laptev Seas may have resulted in an increasing transport of well-ventilated shelf waters to the Arctic Ocean until sea-level stabilized at ca 6 ^{14}C ka (Bauch et al., 1999; Stein et al., 2004).

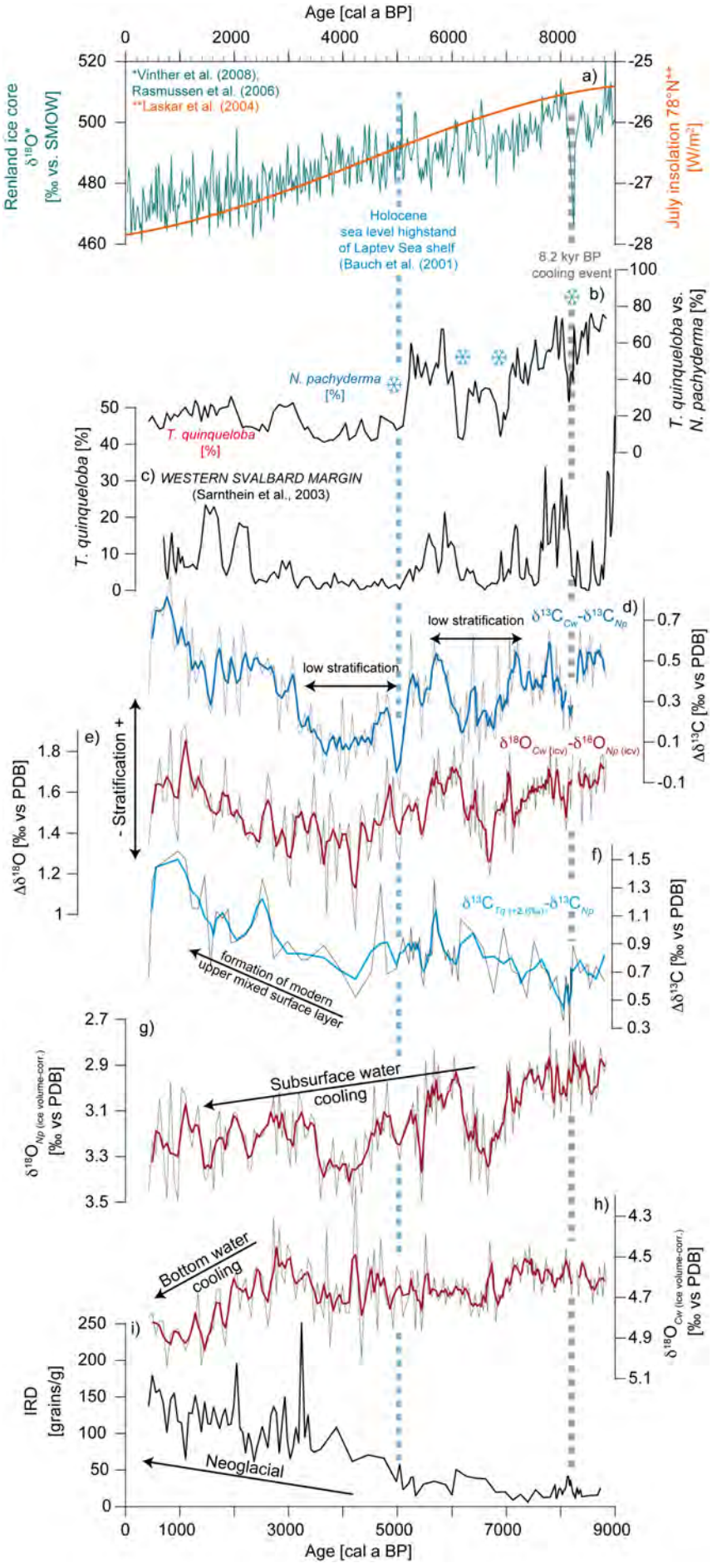
Age [cal a BP]
Renland ice core δ18O* [‰ vs. SMOW]
*Vinther et al. (2008), Rasmussen et al. (2006)
**Laskar et al. (2004)
July insolation 78°N** [W/m²]
Holocene sea level highstand of Laptev Sea shelf (Bauch et al. (2001)
8.2 kyr BP cooling event
N. pachyderma [%]
T. quinqueloba [%]
T. quinqueloba vs. N. pachyderma [%]
c) WESTERN SVALBARD MARGIN (Sarnthein et al., 2003)
low stratification
δ13CCw-δ13CNp
δ18OCw (icv)-δ18ONp (icv)
- Stratification +
Δδ18O [‰ vs PDB]
Δδ13C [‰ vs PDB]
δ13CTq (+2.6‰)-δ13CNp
formation of modern upper mixed surface layer
δ18ONp (ice volume-corr.) [‰ vs PDB]
Subsurface water cooling
Bottom water cooling
δ18OCw (ice volume-corr.) [‰ vs PDB]
IRD [grains/g]
Neoglacial

Fig. 5.7 (previous page): Surface, subsurface, and deepwater proxy data of sediment core 712. **a)** Greenland ice core data (green line; Vinther et al., 2008; Rasmussen et al., 2006) and solar irradiance (orange line; Laskar et al., 2004). **b)** Percentages of *T. quinqueloba* versus *N. pachyderma*. Short-lived cool events indicated by sudden drops of *T. quinqueloba* are marked by ice crystals. **c)** Relative abundances of the subpolar planktic foraminifer species *T. quinqueloba* from the Western Barents Sea (Sarnthein et al., 2003). **d)** Differences between carbon isotope values of *C. wuellerstorfi* and *N. pachyderma*. **e)** Differences between oxygen isotope values of *C. wuellerstorfi* and *N. pachyderma* (both are corrected for ice volume, ivc). **f)** Differences between carbon isotope values of *T. quinqueloba* (corrected for vital effect) and *N. pachyderma*. **g)** Ice-volume corrected oxygen isotope record of *N. pachyderma*. **h)** Ice-volume corrected oxygen isotope record of *C. wuellerstorfi*. **i)** Contents of ice-rafted debris.

5.5.2. Repeated 8.2 ka-like coldwater events

Superimposed on the relatively warm conditions and the strong AW advection to the site during the late Early and Mid-Holocene were repeated significant short-lived coolings indicated by drastic increases of the cold water-adapted planktic foraminifer species *N. pachyderma* at 8.2, 6.9, 6.1, and 5.2 cal ka BP (Figs. 5.4a, 5.7b). The peak of *N. pachyderma* percentages at 8.2 cal ka BP is related to the cool '8.2 ka event' which was most likely caused by a large freshwater release into the North Atlantic region (e.g., Stuiver et al., 1995; Rohling and Pälike, 2005) initiated by the final collapse of the Laurentide ice sheet and its associated outburst drainages from the glacial lakes Agassiz/Ojibway (Barber et al., 1999). The '8.2 ka cooling event' has been detected in many records from the northern North Atlantic and subpolar north (e.g., Risebrobakken et al., 2003; Sarnthein et al., 2003; Hald et al., 2007; Kleiven et al., 2008).

In our record, the '8.2 ka event' is well pronounced and spans a 400 year-interval, with most distinctive conditions at ca 8.2 cal ka BP (Fig. 5.8). Most significant is the shift in planktic foraminifer assemblages. The polar planktic species *N. pachyderma* became dominant (>68%) and relative abundances of *T. quinqueloba* decreased strongly from ~8.4 to 8.2 cal ka BP (from >60 to 26%). High planktic foraminifer fluxes and a concurrent short-lived rise in IRD and sand contents accompanied the strong increase in *N. pachyderma* and indicate increased sea ice/iceberg abundance during the '8.2 ka event', probably related to an advance of the sea ice margin over the study site. Stable isotope records of *N. pachyderma* do not reflect the 8.2 cal ka BP cooling but the $\delta^{18}O$ record of *T. quinqueloba* exhibits both a maximum and minimum in $\delta^{18}O$ around 8.2 cal ka BP (Fig. 5.4d, e), potentially related to sudden shifts in the calcification depth of this foraminifer species within highly unstable surface water conditions. After 8.1 cal ka BP *T. quinqueloba* portions increased and again reached high values of >60% at about 8.0 cal ka BP.

According to our record, also the deepwater was affected during the '8.2 cal ka BP event', as indicated by a short strong decrease in benthic $\delta^{13}C_{Cw}$ reflecting reduced deepwater ventilation. Low $\overline{SS}$ values precede minimum carbon isotope values and point to a short phase of sluggish bottom currents prior to the event. During the '8.2 ka event' as such, relatively high $\overline{SS}$ values accompany the minimum of benthic carbon isotopes. Low bottom water velocities prior to and high velocities of less-ventilated water masses during the 8.2 ka event as such may point to a

bottom water source area outside the eastern Fram Strait, likely in the Greenland Sea where Norwegian Sea Deep Water is produced (Rudels and Quadfasel, 1991). Short-lived decreases in benthic carbon isotope values around 8 cal ka BP in the Nordic Seas have been assigned to decreased bottom water ventilation possibly due to an entrainment of relatively fresh water into the thermohaline system (Bauch et al., 2001a). Low benthic carbon isotope values have also been found on the South Iceland Rise (Thornalley et al., 2010) for a similar, but much stronger cooling event, the Younger Dryas (YD), which has often been compared to the 8.2 ka event (e.g., Alley et al, 1997; Hass, 2002). Thornalley et al. (2010) suggest that an associated decrease in ventilation during the YD event occurred in response to a reduction in the strength of the meridional overturning circulation (MOC), possibly triggered by a freshwater discharge event. Freshwater-induced reductions of the thermohaline convection further south may thus have had a delayed effect arriving as rather sluggish bottom water inflow at our study site in the eastern Fram Strait, indicated by low $\overline{SS}$. Only when the thermohaline convection had re-strengthened again in the Nordic Seas and bottom water velocities had increased consequently, these water masses with low carbon isotope ratios that had formed in the Nordic Seas during the preceding low-overturning period reached Fram Strait. However, this hypothesis is in contrast to a study of sediments on the Yermak Plateau further north of our investigated site where low sortable silt suggest low bottom current speed during the 8.2 cal ka event as such (Hass, 2002).

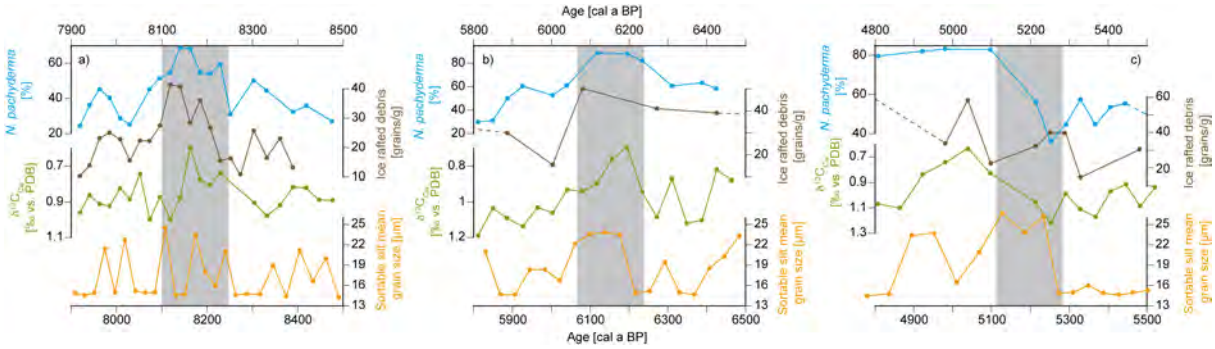

Fig. 5.8: Close-up views of the three major freshwater events in the eastern Fram Strait referred to in the text. **a)** the '8.2 ka cooling event', **b)** the cold event at ca 6.2 cal ka BP, **c)** the onset of Neoglacial conditions in the eastern Fram Strait at ca 5.2 cal ka BP. Note the reversed scale of benthic carbon isotope data.

Conditions similar to those during the '8.2 ka event' apparently occurred repeatedly between 9 and 5 cal ka BP in the eastern Fram Strait. They are most pronounced around ca 5.2 cal ka when increases in *N. pachyderma* portions, high planktic foraminifer fluxes and abundances, and IRD increases indicate the arrival of polar waters and the seasonally fluctuating sea ice margin over the study site (Fig. 5.8c). A minimum of benthic $\delta^{13}C_{Cw}$ values points to reduced bottom water ventilation as found for the 8.2 ka event. Again, sluggish bottom water currents

indicated by low $\overline{SS}$ values preceded the cooling while velocity increased drastically during the event as such. This may point to a similar process as discussed above for the '8.2 ka event'.

Other drastic short-lived coolings occurred at 6.9 and 6.1 cal ka BP and were most significant in terms of *N. pachyderma* percentages rising up to >88%. Similar to the cold events at 8.2 and 5.2 cal ka BP, the cooling in surface water masses at 6.1 cal ka BP was also preceded by reduced bottom water velocities indicated by low $\overline{SS}$ values (Fig. 5.8b). Subsequently, a decline of bottom water ventilation shown by minimum benthic $\delta^{13}C_{Cw}$ values parallel a re-strengthening of bottom water inflow concluded from increased $\overline{SS}$ values. The similarity of this pattern to cold events with freshened surface waters at 8.2 and 5.2 cal ka BP may allow to conclude on the '6.1 cal ka BP cooling' as another event of wider extent. Indeed, in a statistical analysis of worldwide distributed proxy time series, Wanner et al. (2011) found indications for far-reaching cold relapses at ca 8.2, 6.5 to 5.9 and 4.8 to 4.5 ka BP which interrupted periods of relatively stable and warmer climate during the Holocene. This is also consistent with cold events/phases of reduced thermohaline overturn concluded by low $\overline{SS}$ values at ~8.2, 6.6, and 4.0 cal ka BP on the Yermak Plateau (Hass, 2002).

Similar to our detected cooling events another relatively abrupt cooling has been noted by Aagaard-Sørensen (2011) around 9 cal ka BP at site 712. This event is characterised by increases of *N. pachyderma* and ice-rafted material and is likely related to the 9.3 ka event reported elsewhere (e.g., Bond et al., 1997 (event 6); Came et al., 2007; Rasmussen, S.O. et al., 2007). A sudden cooling event around 9.4 ka BP has also been found in mollusk shell studies on Svalbard (Yuan et al., 2011).

From repeated ice-rafting events south of Iceland, Bond et al. (1997) concluded on near-1,500-year Holocene cyclicity in the North Atlantic influenced by solar-induced atmospheric variations (Bond et al., 2001). Bond events 6, 5, and 4 (Bond et al., 1997) may correspond to the cooling events detected at site 712 in the eastern Fram Strait at 9.3, 8.2 and 6.1 cal ka BP, other IRD events were not found in our record. Corresponding to the results of Bond et al. (1997), Bianchi and McCave (1999) revealed a 1,500-year periodicity in the deepwater flow in the North Atlantic based on their $\overline{SS}$ record, with a more active thermohaline circulation during times when the climate of northern Europe was warmer. Although the general pattern of our $\overline{SS}$ data is similar to the data set of Bianchi and McCave (1999), time series analysis carried out on our $\overline{SS}$ data do not provide clear evidence for a pronounced 1500-year cyclicity (Fig. 5.6). Located on the Western Svalbard margin, our core site may have been additionally affected by glaciomarine sedimentation processes of the adjacent Svalbard fjords which often overlay weaker thermohaline overturn signatures in the area. However, benthic carbon isotope data indicate a 550-year cycle in agreement with Holocene ice core data from Greenland (Stuiver et al., 1995)

and North Atlantic sediment core data (Chapman and Shackleton, 2000) and may suggest that deepwater variations in the Fram Strait were linked to changes in the thermohaline convection. Consistently, Werner et al. (2011) found increased $\overline{SS}$ values at site 712 during the Medieval Climate Anomaly and the Modern Warming in contrast to low $\overline{SS}$ values during the Little Ice Age period. This furthermore points to a linkage between thermohaline overturn processes in the Nordic Seas and deepwater variability in the eastern Fram Strait.

Our surface water proxies do not reveal any sign of periodicity which can be attributed to the appearance of cold events with freshened surface waters. Came et al. (2007) also noticed abrupt events in the subpolar North Atlantic that tend to occur within a broad millennial band but do not show any periodicity. However, except for the 9.3 and 8.2 ka BP events, the timing of events recorded by Came et al. (2007) differs significantly from that at site 712. It was recently shown by Wanner et al. (2011) that the several cold relapses which interrupted periods of relatively stable and warmer climate during the Holocene did not follow a strictly regular or cyclic appearance. Wanner et al. (2011) suggested that the complex pattern of these short-term coolings was caused by a combination of decreasing solar insolation, possibly a slow-down of the thermohaline circulation, regional effects and possibly feedbacks. In the case of the eastern Fram Strait, beside the decreasing insolation we consider repeated advances and retreats of the sea ice margin to be most important for the strong surface water fluctuations during the Early and Mid-Holocene. Advances of the Arctic Front (Johannessen et al., 1994), i.e., the boundary between Atlantic and Arctic water masses, serve as the best explanation for the strong shifts in surface ocean conditions. The fact that the sea ice advances often occurred in combination with a slow-down of the thermohaline convection appears reasonable since small amounts of excess freshwater added to the surface in the regions of deepwater formation are sufficient to prevent convection (Aagaard and Carmack, 1989).

Though not periodic, distinct similarities exist between our cooling events and cold relapses detected by means of statistical analysis of proxy time series by Wanner et al. (2011) at 8.2 ka BP, between 6.5 and 5.9 ka BP (here at 6.1 cal ka BP), and between 4.8 and 4.5 (here: 5.2 cal ka BP). The cold event at ca 5.2 cal ka BP revealed by our study seems to be somewhat offset from the (younger) interval found by Wanner et al. (2011) but may be part of the 'cool poles, dry tropics period' between 6 and 5 cal ka BP (Mayewski et al., 2004).

Correlating our cold events with freshened surface waters to glacier advances on Spitsbergen proves difficult due to the lack of sufficient high-resolution records from Spitsbergen. However, evidence from possible glacier growth already since ca 7 cal ka BP and a general increase on glacier-related iceberg rafting between 9 and 4 cal ka BP have been found in Isfjorden, West Spitsbergen (Forwick and Vorren, 2007, 2009).

5.5.3. Late Holocene cooling (5.2 to 0.4 ka)

Neoglacial cooling in the second half of the Holocene has been revealed by proxy reconstructions not only from the North Atlantic, subpolar (e.g., Seppä and Birks, 2001; Jennings et al., 2002; Moros et al., 2004; Seidenkrantz et al., 2008; Andrews et al., 2009, 2010) and polar (Werner, 1993; Fisher et al., 1994; Vinther et al., 2006) northern hemisphere regions but also in a global context (Wanner et al., 2008 and references therein). Wanner et al. (2008) attributed the Neoglacial cooling in the northern hemisphere to the decreasing solar radiation, the southward shift of the Intertropical Convergence Zone and a summer cooling trend over the northern continental landmasses and the North Atlantic Ocean.

Our record shows a rather abrupt initiation of the Neoglacial cooling in the eastern Fram Strait at ca 5.2 cal ka BP. The drastic decrease of *T. quinqueloba* percentages from more than 50% to less than 15% within ca 150 years after 5.2 cal ka BP indicates strongly weakened Atlantic Water inflow and/or a sudden drop of AW temperatures (Fig. 5.7b). Correspondingly, the polar planktic foraminifer species *N. pachyderma* became dominant, indicating low temperatures at the sea surface/subsurface. Decreases in *T. quinqueloba* percentages were also detected after 5 cal ka BP in the Nordic Seas (Bauch and Weinelt, 1997). The cooling at 5.2 cal ka BP differs from short-lived cooling events at 8.2, 6.9, and 6.1 ka BP as it initiated persistent cool conditions lasting throughout the remainder of the studied core section, as indicated by the dominance of *N. pachyderma* and continuously increasing IRD contents. Mg/Ca-based SST estimations from station 712 (Aagaard-Sørensen, 2011) also reveal a cooling at about 5.2 cal ka BP. Low planktic foraminifer fluxes, low biomarker accumulation rates (Müller et al., submitted) and minimum portions of *T. quinqueloba* until ca 3.2 cal ka BP (Fig. 5.4a) point to restricted bioproductivity and intense sea ice coverage between ca 5 and 3 cal ka BP. Lighter $\delta^{18}O_{Np}$ from 5.0 to 5.2 cal ka BP and higher values between 4.6 and 3.6 cal ka BP likely reflect fresher and colder surface water conditions, respectively (Fig. 5.4d). The fact that the fluctuations in $\delta^{18}O_{Tqu}$ (Fig. 5.4e) are much stronger than those of $\delta^{18}O_{Np}$ is probably related to rapid shifts in the living habitat depths of *T. quinqueloba* caused by a variable thickness of the surface layer.

Significantly increasing IRD contents and portions of the sand fraction as well as rising planktic foraminifer abundances after ca 3 cal ka BP suggest that site 712 was probably in the area of the seasonally fluctuating ice margin during the Late Holocene. Increased IRD contents in Late Holocene sediments were recorded at many sites in the northern North Atlantic (e.g., Jennings et al., 2002; Sarnthein et al., 2003; Moros et al., 2006; Rasmussen, T.L. et al., 2007; Ślubowska-Woldengen et al., 2008) and off southeast Greenland (Williams, 1993; Andrews et al., 1997; Jennings et al., 2002, 2011). Biomarker studies of core 712 indicate sea ice marginal conditions since ca 3 cal ka BP (Müller et al., submitted) and thus corroborate our results. An

increased contribution of cold and productive surface waters is also concluded from increasing portions of *G. uvula* after 3.2 cal ka BP in our record (Fig. 5.3), in accordance with findings on the SW Svalbard margin (Rasmussen, T.L. et al., 2007). A return of polar conditions during the Late Holocene period and cooling and freshening of western and northern Svalbard shelf bottom waters and reduced influence of AW compared to the Early Holocene have also been found by investigation of benthic foraminiferal census data (Ślubowska-Woldengen et al., 2008).

There is evidence for glacier re-advances in western Norway (Nesje and Kvamme, 1991) and North America (Denton and Karlén, 1973) at about 5.3 cal ka BP strongly supporting our findings. Also Svendsen and Mangerud (1997) related the first well-pronounced formation of a glacier after warm Holocene conditions in West Spitsbergen between 5 and 4 cal ka BP to the Neoglacial cooling.

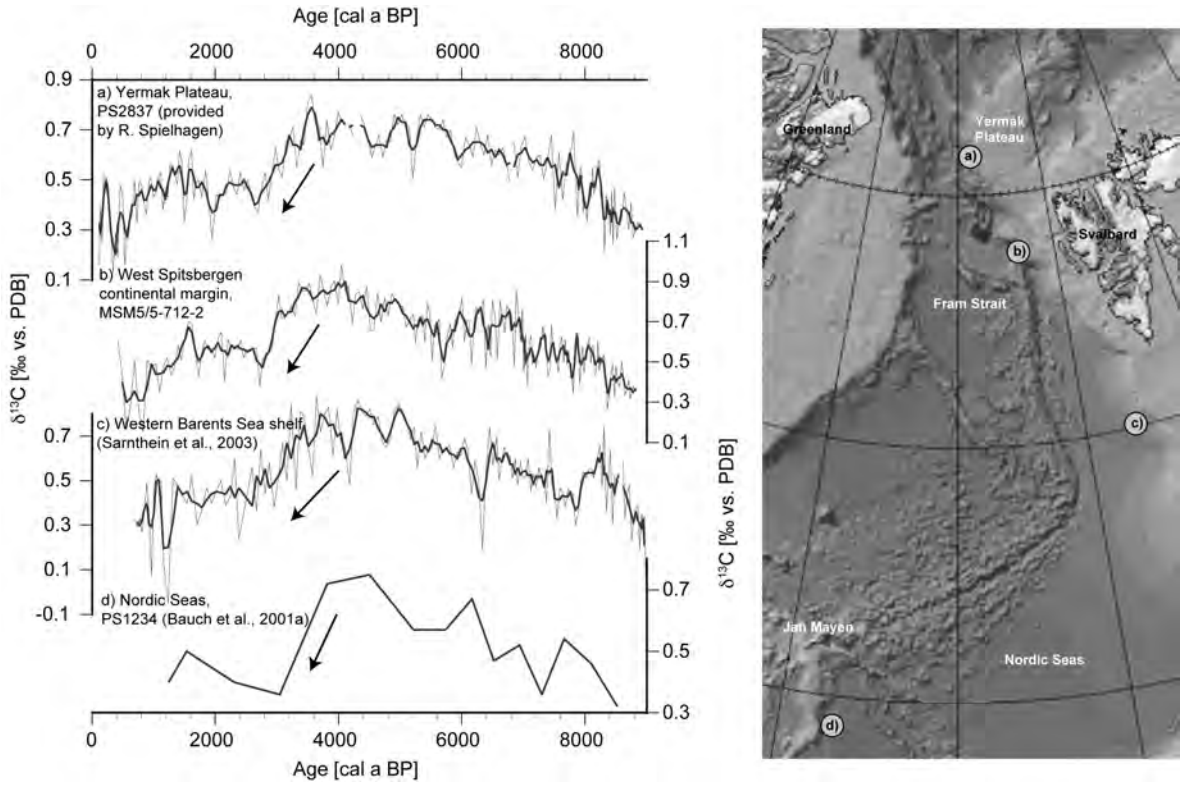

Fig. 5.9: Carbon isotope records derived from calcareous tests of *N. pachyderma* and their location in the subpolar North Atlantic and the Fram Strait (map by Jakobsson et al., 2008).

Carbon isotope values measured on *N. pachyderma* are gradually decreasing after ca 3.5 cal ka BP (Figs. 5.4g, 5.7). Carbon isotope values of *T. quinqueloba* (Fig. 5.4f) and *C. wuellerstorfi* (Fig. 5.5) do not follow this trend but steadily increase until ca 0.4 cal ka BP, suggesting a better ventilation of both surface and bottom water masses. A thickening of the meltwater/sea ice-bearing surface layer may have caused a probably density-driven (Kozdon et al., 2009) downward migration of *N. pachyderma* and might be the reason for measured lower $\delta^{13}C_{Np}$ values during the past ca 3 cal ka BP, indicating weaker ventilation of surface/subsurface water masses inhabited

by *N. pachyderma*. In contrast, *T. quinqueloba* being a symbiont-bearing (near-)surface dweller bound to seasonally open conditions (Simstich et al., 2003; Kucera et al., 2005) may have stayed in the well-ventilated uppermost surface water masses, as may be concluded from continuously increasing $\delta^{13}C_{Tqu}$ values (Fig. 5.4f). Decreases in $\delta^{13}C_{Np}$ since 4 or 3 cal ka BP have also been noted in records from the northern North Atlantic (e.g., Bauch and Weinelt, 1997; Bauch et al., 2001a; Sarnthein et al., 2003, Fig. 5.9). This allows to conclude that the drop in $\delta^{13}C_{Np}$ may indicate either a wider distribution of an upper low saline meltwater layer in the Nordic Seas and the Fram Strait possibly related to reduced evaporation due to cooler atmospheric temperatures and/or increased moisture supply, or a supraregional reorganization of the oceanic carbon cycle.

The trend towards lower $\delta^{13}C_{Np}$ values runs parallel to an increase of benthic oxygen isotopes of about 0.4 ‰ (Fig. 5.5) which may either be related to a cooling of ca 1.4°C or increasing salinity of about 0.8 in the bottom water. Higher salinity of bottom waters may be caused by stronger AW inflow but might also be generated through injection of high-salinity waters produced by brine rejection during winter sea ice formation in southern and western Svalbard fjords (Quadfasel et al., 1988; Schauer et al., 1995; Rudels et al., 2005; Rasmussen and Thomsen, 2009). Since a lack of local weathering input from Svalbard to site 712 during the Late Holocene is inferred from the investigation of radiogenic isotope variability (Chapter 6) we exclude a dominant contribution of brines to bottom water masses at the site during that time. In contrast, a slight strengthening of warm and saline AW inflow as indicated by increasing *T. quinqueloba* portions might have affected bottom water masses hereby causing a salinity change. However, a salinity change of 0.8 in bottom waters appears rather unrealistic. Moreover, $\delta^{18}O_{Cw}$ values have been continuously low when maximum intensity of AW inflow occurred during the Early and Mid-Holocene interval, while prior to 10 cal ka BP higher $\delta^{18}O_{Cw}$ values (unpublished data) probably indicate lower temperatures of bottom waters in a generally colder environment during the final deglacial phase. Likewise, we consider the increased $\delta^{18}O_{Cw}$ of the Late Holocene to indicate a temperature shift parallel to the surface water cooling after 5 cal ka BP.

We propose two major components to be responsible for the Neoglacial cooling in the eastern Fram Strait, (1) the Arctic Ocean-related increased export of sea ice and freshwater from the north and (2) the shifts in water masses arriving from the south.

Bauch et al. (2001b) showed that postglacial flooding of the Laptev Sea shelves was only finalized ca 5 cal ka BP when the modern sea level was reached. By means of ostracodes, the onset of modern-like conditions with perennial sea ice in the Arctic Ocean was determined at ca 6 to 5 cal ka BP and found to be consistent with high-latitude Neoglacial cooling and glacier advances (Cronin et al., 2010). Thus, at ca 5 cal ka BP Arctic sea ice production, which predominantly takes place on the shallow Arctic shelf areas, reached its modern dimension.

Apparently, the dramatic shift in our planktic foraminiferal data at ca 5.2 cal ka BP and the associated sea ice advance over the study site coincides with the timing of establishment of the modern sea level and sea ice production. From driftwood analyses and modelling experiments it was suggested that during the Mid-Holocene enhanced riverine discharge of freshwater caused an eastward shift of the TPD and strengthened sea ice export through Fram Strait (Dyke et al., 1997; Prange and Lohmann, 2003). The associated southeastward expansion of the ice cover in the Fram Strait, the bottleneck of sea ice export from the Arctic Ocean, eventually resulted in the strong shift to cooler conditions at our study site after 5.2 cal ka BP. In contrast, Arctic sea ice production during the Early Holocene may have been somewhat limited by higher atmospheric temperatures caused by high insolation (possibly amplified in the Arctic basin due to lowered albedo effects), the reduced area for sea ice production on the shallow Arctic shelves because of the lower sea-level, and a stronger influx of warmer Atlantic Water masses.

A low-resolution record from the western Fram Strait has shown that relative abundances of *T. quinqueloba* in the 63-125µm fraction dropped from 9% to <1% at about 8 cal ka BP, followed by a strong dominance of *N. pachyderma* indicating cool conditions (Bauch et al., 2001a). Higher resolution core records are still lacking for this area, but a gradual advance of the EGC-derived sea ice and coldwater transport from the northwest towards a southeastern direction may explain the opposite findings between eastern and western Fram Strait for the Holocene. While the western Fram Strait was already perennially sea ice-covered after 8 cal ka BP, the coldwater front only reached the eastern Fram Strait after 5.2 cal ka BP when conditions similar to the pre-industrial period were established. Owing to the melting induced by warm Atlantic Water inflow, seasonally ice-free conditions likely prevailed since 5 cal ka BP with short-term exceptions such as during the colder phase between ca 5 and 3 cal ka BP and the Little Ice Age (Werner et al., 2011).

Decreasing $\delta^{13}C_{Np}$ values were found for the entire subpolar North Atlantic section after 3 cal ka BP (Bauch and Weinelt, 1997; Bauch et al., 2001a; Sarnthein et al., 2003; this study; Fig. 5.9), in contrast to high $\delta^{13}C$ values of *T. quinqueloba*, indicating good ventilation of the uppermost surface layer. Decreasing solar insolation is the most likely candidate for the reconstructed cooling of the surface and bottom waters. An increased Arctic sea ice export and a linked southeastward expansion of the low-saline surface waters exported from the Arctic explain a density driven downward movement of *N. pachyderma* and the associated uptake of lower $^{13}C/^{12}C$ ratios from lesser ventilated subsurface water masses. While the cooling is well-pronounced in the bottom water $\delta^{18}O_{Cw}$, it is not pronounced in surface/subsurface water $\delta^{18}O$ derived from planktic foraminifers, probably due to the compensating effect of temperature and salinity on $\delta^{18}O$ in Arctic and sub-Arctic waters (Spielhagen and Erlenkeuser, 1994) and the migration

activity of planktic foraminifers within the water column causing a "dampening" effect which is also seen in Mg/Ca-based SST estimates (Aagaard-Sørensen, 2011).

Bauch et al. (2001a) point out the link between decreasing $\delta^{13}C_{Np}$ and the development of the modern steep east-to-west temperature gradient and an onset of the "modern-type-circulation" in the Nordic Seas. The modern east-west temperature gradient apparently evolved only after the modern 'Arctic ice factory" was established and a strong export of Arctic sea ice and cold-water masses to the GIN Seas could be initiated. The export of Arctic cold-water masses probably also had implications on the initiation of the present-day thermohaline convection and the establishment of the modern climate (Broecker, 1991). Modern-type surface water stratification in the eastern Fram Strait, characterized by a cold and fresh thin upper surface layer separated from the subsurface inflow of warm and saline Atlantic-derived water (Aagaard et al., 1987; Saloranta and Haugan, 2004; Schauer et al., 2004) could thus probably only develop in the course of the widespread Late Holocene freshening in the northern North Atlantic (Bauch and Weinelt, 1997).

A slight warming trend is concluded from increased portions of *T. quinqueloba* (24-28%) between 3.1 and 2.8 and at ca 1.9 cal ka BP (Fig. 5.4a). However, during the Late Holocene *T. quinqueloba* never achieved the high portions of the Early and Mid-Holocene. Mg/Ca-based SST estimations (Aagaard-Sørensen, 2011) support our conclusions from planktic foraminifer assemblages and show low SST until 3.2 cal ka BP as well as maximum temperatures of 5°C at ca 1.1 cal ka BP. Sarnthein et al. (2003) found a similar pattern on the western Barents Sea shelf and attributed an increase of *T. quinqueloba* percentages after 3 cal ka BP to a slight increase of the thermohaline circulation during the Late Holocene. Evidence for increased AW inflow after 3 cal ka has also been found in the Franz Victoria Trough (Lubinski et al., 2001) and in the Nordic Seas (Hald and Aspeli, 1997; Risebrobakken et al., 2003; Thornalley et al., 2009).

The warming in subsurface waters apparently contrasts the simultaneously occurring increased sea ice cover on the Yermak Plateau and over site 712 reconstructed by means of the sea ice proxy IP_{25} (Müller et al., 2009; submitted) and increased IRD contents (this study). Dynamic changes in the relative contributions of water masses of the North Atlantic subpolar (SPG) and subtropical (STG) gyres have been attributed to the variable strength of the North Atlantic Current for the present (Hátún et al., 2005) and for the past (Thornalley et al., 2009; Born et al., 2011) and may also provide an explanation for the apparent contradiction between cold surface and warm subsurface waters at site 712 during the Late Holocene. Thornalley et al. (2009) found a negative relationship between Holocene salinity variations south of Iceland and in the Labrador Sea (Solignac et al., 2004). Phases of strong inflow of warm and saline Atlantic Waters coincide with a SPG weakened by freshening. Freshwater inputs to the Labrador Sea

prevent deep convection and reduce the SPG circulation resulting in enhanced northward flow of North Atlantic Drift waters which have entrained warmer and saline STG waters (Hátún et al., 2005). Thornalley et al. (2009) found evidence for such linkage throughout the main part of the Holocene in the northeast North Atlantic. Decreasing $\delta^{13}C_{Np}$ values (Bauch et al., 2001a; Sarnthein et al., 2003; this study) and evidence of enhanced sea ice abundances during the past ca 3 cal ka BP (Müller et al., submitted) suggest a considerable freshening of the surface layer not only in the eastern Fram Strait but also in the Nordic Seas. In this context, the freshening of surface waters in the eastern Fram Strait and assumed increased freshwater supply to the Nordic Seas be related to a weakened SPG caused by increased export of Arctic sea ice and a possible freshening of Labrador Sea waters during the past ca 3 cal ka BP. The concurrent strengthening of AW inflow is associated with the North Atlantic Drift waters increasingly entraining warmer and saline STG and enhanced northward transport of higher saline AW. However, in contrast to the freshening of surface waters in the eastern Fram Strait indicated by our data, the weakening of the SPG could not clearly be related to Labrador Sea freshening during the Late Holocene (Thornalley et al., 2009).

5.6. Conclusions

Multiproxy data from the West Spitsbergen continental margin covering the past ca 9 cal ka BP suggest that the transition from late Early Holocene thermal optimum conditions to the modern (pre-industrial) situation occurred stepwise, most likely in response to the complete postglacial flooding of the shallow Siberian shelves and the onset of modern sea ice production. The Early and Mid-Holocene periods were highly unstable due to short-lived salinity changes attributed to Arctic Ocean-derived sea ice and freshwater advances over the study site. Planktic foraminifer assemblage data infer a strong Atlantic Water inflow and/or increased surface water temperatures which occurred in response to the maximum insolation during the Early Holocene. A slight weakening of AW inflow is noted after 8 cal ka BP, but continuously high percentages of subpolar planktic foraminifer species indicate generally warm conditions lasting until ca 5.2 cal ka BP. Repeated short-lived strong coldwater advances interrupted the warm conditions in the eastern Fram Strait at 8.2, 6.9, 6.1, and 5.2 cal ka BP. The temporal structure of the cooling events at 6.1 and 5.2 cal ka BP was similar to that of the well-known cooling pulse around ca 8.2 ka and allows to conclude on a likewise weakening of the thermohaline convection during these events. Consistent with findings of Wanner et al. (2011), no clear periodicity could be detected between the various cooling events in the eastern Fram Strait.

Pre-industrial conditions only established after the cooling event at 5.2 cal ka BP which was most likely related to an advance of the cold waters and Arctic sea ice and to the Neoglacial onset

in the eastern Fram Strait. More stable but significantly cooler conditions prevailed during the entire Late Holocene period, parallel to the decreased insolation. Strong discharge of Arctic sea ice and polar water transported southeastward by the ice-covered East Greenland Current caused heavy winter sea ice conditions and relatively short ice-free summer seasons in the eastern Fram Strait, most likely in combination with a weaker/subsiding subsurface Atlantic Water inflow and/or inflow of cool Atlantic Water. A slight re-strengthening of AW inflow after 3 cal ka BP is seen from planktic foraminifer assemblages, in accordance with other proxy data from the same core site (Aagaard-Sørensen, 2011) and the Barents Sea/Svalbard area (Sarnthein et al., 2003). Simultaneously, decreasing planktic carbon isotope values may infer a freshening of the uppermost surface water layer and reduced ventilation of the subsurface water layer associated with the descend of planktic foraminifers in the water column. Decreasing planktic carbon isotope values are also known from other records in the northern North Atlantic during the past ca 3 cal ka BP and suggest a wider distribution of an upper low saline meltwater layer in the Nordic Seas and the Fram Strait, possibly in relation with reduced evaporation due to cooler atmospheric temperatures during the Late Holocene.

Outlook

The presented manuscript will be submitted to an acknowledged internationally scientific journal. Few extra works will be included prior to submission involving a sea surface temperature reconstruction on the basis of the SIMMAX modern analogue technique (Pflaumann et al., 1996).

Acknowledgements. The German Research Foundation (DFG) provided financial support of K. Werner and R. F. Spielhagen within the Priority Programme 1266 (INTERDYNAMIC, Project HOVAG). We are grateful to Jacques Giraudeau and the Environnements et Paléoenvironnements OCéaniques (University Bordeaux, EPOC) for providing three AMS datings. Thanks to Jan Oesterwalbesloh for his kind support in the laboratory, to Lulzim Haxhiaj for technical assistance on stable isotope measurements, and to Henning Bauch and Dorothea Bauch for valuable discussions. Finally, we thank the science party and crew onboard RV "Maria S. Merian" during the expedition MSM5/5 for retrieving the sediment core.

References

Aagaard, K., Foldvik, A. and Hillman, S.R. (1987) The West Spitsbergen Current: Disposition and Water Mass Transformation. *Journal of Geophysical Research* 92, 3778-3784.

Aagaard, K. and Carmack, E.C. (1989) The Role of Sea ice and Other Fresh Water in the Arctic Circulation. *Journal of Geophysical Research* 94/C10, 14485-14498.

Aagaard-Sørensen, S. (2011) Late Glacial - Holocene climatic variability and sedimentary environments on northern continental shelves. Ph.D. thesis, Univ. of Tromsø, Norway.

Alley, R.B., Mayewski, P.A., Sowers, T., Stuiver, M., Taylor, K.C. and Clark, P.U. (1997) Holocene climatic instability: A prominent, widespread event 8200 years ago. *Geology* 25/6, 483-486.

Andrews, J.T., Smith, L.M., Preston, R., Cooper, T. and Jennings, A.E. (1997) Spatial and temporal patterns of iceberg rafting (IRD) along the East Greenland margin, ca. 68°N, over the last 14 cal. ka. *Journal of Quaternary Science* 12, 1-13.

Andrews, J.T., Belt, S.T., Olafsdottir, S., Massé, G. and Vare, L.L. (2009) Sea ice and marine climate variability for NW Iceland/Denmark Strait over the last 2000 cal. yr BP. *The Holocene* 19, 775-784.

Andrews, J.T., Jennings, A.E., Coleman, G.C. and Eberl, D.D. (2010) Holocene variations in mineral and grain size composition along the East Greenland glaciated margin (ca 67°-70°N): local versus long-distance sediment transport. *Quaternary Science Reviews* 29, 2619-2632.

Barber, D.C., Dyke, A., Hillaire-Marcel, C., Jennings, A.E., Andrews, J.T., Kerwin, M.W., Bilodeau, G., McNeely, R., Southon, J., Morehead, M.D. and Gagnoni, J.-M. (1999) Forcing of the cold event of 8,200 years ago by catastrophic drainage of Laurentide lakes. *Nature* 400*,* 344-348.

Bauch, H.A., Kassens, H., Erlenkeuser, H., Grootes, P.M. and Thiede, J. (1999) Depositional environment of the Laptev Sea (Arctic Siberia) during the Holocene. *Boreas* 28, 194-204.

Bauch, H.A., Erlenkeuser, H., Spielhagen, R.F., Struck, U., Matthiessen, J., Thiede, J. and Heinemeier, J. (2001a) A multiproxy reconstruction of the evolution of deep and surface waters in the subarctic Nordic seas over the last 30,000 yr. *Quaternary Science Reviews* 20*,* 659-678.

Bauch, H.A., Mueller-Lupp, T., Taldenkova, E., Spielhagen, R.F., Kassens, H., Grootes, P.M., Thiede, J., Heinemeier, J. and Petryashov, V.V. (2001b) Chronology of the Holocene trangression at the North Siberian margin. *Global and Planetary Change* 31*,* 125-139.

Bauch, H.A. and Weinelt, M.S. (1997) Surface Water Changes in the Norwegian Sea during last Deglacial and Holocene Times. *Quaternary Science Reviews* 16*,* 1115-1124.

Bianchi, G.G. and McCave, I.N. (1999) Holocene periodicity in North Atlantic climate and deep-ocean flow south of Iceland. *Nature* 397*,* 515-517.

Blackman, R.B. and Tukey, J.W. (1958) The measurement of Power Spectra From the Point of View of Communicating Engineering. Dover publications, Mineola, N.Y, 190 pp.

Bond, G., Showers, W., Cheseby, M., Lotti, R., Almasi, P., deMenocal, P., Priore, P., Cullen, H., Hajdas, I. and Bonani, G. (1997) A Pervasive Millennial-Scale Cycle in North Atlantic Holocene and Glacial Climates. *Science* 278*,* 1257-1266.

Bond, G., Kromer, B., Beer, J., Muscheler, R., Evans, M.N., Showers, W., Hoffmann, S., Lotti-Bond, R., Hajdas, I. and Bonani, G. (2001) Persistent Solar Influence on North Atlantic Climate During the Holocene. *Science* 294*,* 2130-2136.

Born, A., Nisancioglu, K.H., and Risebrobakken, B. (2011) Late Eemian warming in the Nordic Seas as seen in proxy data and climate models. *Paleoceanography* 26, PA2207.

Broecker, W.S. (1991) The Great Ocean Conveyor. *Oceanography* 4, 79-89.

Came, R.E., Oppo, D.W. and McManus, J.F. (2007) Amplitude and timing of temperature and salinity variability in the subpolar North Atlantic over the past 10 k.y. *Geology* 35, 315-318.

Carstens, J., Hebbeln, D. and Wefer, G. (1997). Distribution of planktic foraminifera at the ice margin in the Arctic (Fram Strait). *Marine Micropaleontology* 29, 257-269.

Chapman, M.R. and Shackleton, N.J. (2000) Evidence of 550-year and 1000-year cyclicities in North Atlantic circulation patterns during the Holocene. *The Holocene* 10, 287-291.

Cronin, T.M., Gemery, L., Briggs Jr., W.M., Jakobsson, M., Polyak, L. and Brouwers, E.M. (2010) Quaternary Sea-ice history in the Arctic Ocean based on a new Ostracode sea-ice proxy. *Quaternary Science Reviews* 10, 3415-3429.

Darling, K., Kucera, M. Kroon, D. and Wade, C.M. (2006) A resolution for the coiling direction paradox in *Neogloboquadrina pachyderma*. *Paleoceanography* 21, PA2011.

Denton, G.H and Karlén, W. (1973) Holocene Climatic Variations – Their Pattern and Possible Cause. *Quaternary Research* 2, 155-205.

Duplessy, J.-C, Ivanova, E., Murdmaa, I., Paterne, M. and Labeyrie, L. (2001) Holocene paleoceanography of the northern Barents Sea and variations of the northward heat transport by the Atlantic Ocean. *Boreas* 30, 2-16.

Duplessy, J.-C., Labeyrie, L. and Waelbroeck, C. (2002) Constraints on the ocean oxygen isotope enrichment between the Last Glacial Maximum and the Holocene: paleoceanographic implications. *Quaternary Science Reviews* 21, 315-330.

Dyke, A.S., England, J., Reimnitz, E. and Jette, J. (1997) Changes in driftwood delivery to the Canadian Arctic Archipelago: the hypothesis of postglacial oscillations of the Transpolar Drift. *Arctic* 50, 1-16.

Ebbesen, H., Hald, M. and Eplet, T.H. (2007) Lateglacial and early Holocene climatic oscillations on the Svalbard margin, European Arctic. *Quaternary Science Reviews* 26, 1999-2011.

Ellison, C.R.W., Chapman, M.R. and Hall, I.R. (2006) Surface and Deep Ocean Interaction During the Cold Climate Event 8200 Years Ago. *Science* 312, 1929-1932.

Fairbanks, R.G. (1989) A 17,000-year glacio-eustatic sea level record: influence of glacial melting rates on the Younger Dryas event and deep-ocean circulation. *Nature* 342, 637-642.

Fisher, D.A., Koerner, R.M. and Reeh, N. (1994) Holocene climatic records from Agassiz Ice Cap, Ellesmere Island NWT, Canada. *The Holocene* 5, 19-24.

Forwick, M. and Vorren, T.O. (2007) Holocene mass-transport activity and climate in outer Isfjorden, Spitsbergen: marine and subsurface evidence. *The Holocene* 17, 707-716.

Forwick, M. and Vorren, T.O. (2009) Late Weichselian and Holocene sedimentary environments and ice rafting in Isfjorden, Spitsbergen. *Palaeogeography, Palaeoclimatology, Palaeoecology* 280, 258-274.

Gammelsrød, T. and Rudels, B. (1983) Hydrographic and current measurements in the Fram Strait, August 1981. *Polar Research* 1, 115-126.

Gascard, J.-C., Kergomard, C., Jeannin, P.-F. and Fily, M. (1988) Diagnostic Study of the Fram Strait Marginal Ice Zone During Summer from 1983 and 1984 Marginal Ice Zone Experiment Lagrangian Observations. *Journal of Geophysical Research* 93/C4, 3613-3641.

Giraudeau, J., Garcia, J., Dylmer, C.V., Husum, K., Werner, K., Spielhagen, R.F., Müller, J., Moros, M. and Risebrobakken, B. (submitted to *Marine Micropaleontology*) The contribution

of coccolithophores to the sedimentation of biogenic carbonates in the northern North Atlantic: A paleo (Holocene) perspective.

Hald, M., Ebbesen, H., Forwick, M., Godtliebsen, F., Khomenko, L., Korsun, S., Ringstad Olsen, L. and Vorren, T.O. (2004) Holocene paleoceanography and glacial history of the West Spitsbergen area, Euro-Arctic margin. *Quaternary Science Reviews* 23, 2075-2088.

Hald, M., Andersson, C., Ebbesen, H., Jansen, E., Klitgaard-Kristensen, D., Risebrobakken, B., Salomonsen, G.R., Sarnthein, M., Sejrup, H.P. and Telford, R.J. (2007) Variations in temperature and extent of Atlantic Water in the northern North Atlantic during the Holocene. *Quaternary Science Reviews* 26, 3423-3440.

Hald, M. and Aspeli, R. (1997) Rapid climate shifts of the northern Norwegian Sea during the deglaciation and the Holocene. *Boreas* 26, 16-28.

Hall, I.R., Bianchi, G.G. and Evans, J.R. (2004) Centennial to millennial scale Holocene climate-deep water linkage in the North Atlantic. *Quaternary Science Reviews* 23, 1529-1536.

Hass, H.C. (2002) A method to reduce the influence of ice-rafted debris on a grain site record from northern Fram Strait. *Polar Research* 21(2), 299-306.

Hátún, H., Sandø, A.B., Drange, H., Hansen, B. and Valdimarsson, H. (2005) Influence of the Atlantic Subpolar Gyre on the Thermohaline Circulation. *Science* 309, 1841-1844.

Haugan, P.M. (1999) Structure and heat content of the West Spitsbergen Current. *Polar Research* 18(2), 183-188.

Healy-Williams, N. (1992) Stable isotope difference among morphotypes of *Neogloboquadrina pachyderma* (Ehrenberg): implications for high-latitude palaeoceanographic studies. *Terra Nova* 4, 693-700.

Hebbeln, D. (1991) Spätquartäre Stratigraphie und Paläozeanographie in der Fram-Straße. *Berichte aus dem Fachbereich Geowissenschaften der Universität Bremen* 22, 1-174.

Hopkins, T.S. (1991) The GIN Sea – a synthesis of its physical oceanography and literature review 1972-1985. *Earth Science Reviews* 30, 175-318.

Humlum, O., Elberling, B., Hormes, A., Fjordheim, K., Hansen, O.H. and Heinemeier, J. (2005) Late-Holocene glacier growth in Svalbard, documented by subglacial relict vegetation and living soil microbes. *The Holocene* 15/3, 396-407.

Jennings, A.E., Knudsen, K.L., Hald, M., Vigen Hansen, C. and Andrews, J.T. (2002) A mid-Holocene shift in Arctic sea-ice variability on the East Greenland Shelf. *The Holocene* 12/1, 49-58.

Jennings, A.E., Andrews, J. and Wilson, L. (2011) Holocene environmental evolution of the SE Greenland Shelf North and South of the Denmark Strait: Irminger and East Greenland current interactions. *Quaternary Science Reviews* 30, 980-998.

Johannessen, O.M. (1987) Introduction: Summer Marginal Ice Zone Experiments During 1983 and 1984 in Fram Strait and the Greenland Sea. *Journal of Geophysical Research* 92/C7, 6716-6718.

Johannessen, T., Jansen, E., Flatøy, A. and Ravelo, A. (1994) The relationship between surface water masses, oceanographic fronts and paleoclimatic proxies in surface sediments of the Greenland, Iceland, Norwegian Seas. In: Zahn, R. et al. (Eds.), Carbon Cycling in the Glacial Ocean: Constraints of the Ocean's Role in Global Change, pp. 61-85, Springer, Berlin.

Kandiano, E.S. and Bauch, H.A. (2002) Implications of foraminiferal size fractions for the glacial-interglacial paleoceanography of the polar North Atlantic. *Journal of Foraminiferal Research* 32, 245-251.

Kaplan, M.R. and Wolfe, A.P. (2006) Spatial and temporal variability of Holocene temperatures in the North Atlantic region. *Quaternary Research* 65, 223-231.

Karcher, M.J., Gerdes, R., Kauker, F. and Köberle, C. (2003) Arctic warming: Evolution and spreading of the 1990s warm event in the Nordic seas and the Arctic Ocean. *Journal of Geophysical Research* 108/C2, 3034.

Kaufman, D.S., Schneider, D.P., McKay, N.P., Ammann, C.M., Bradley, R.S., Briffa, K.R., Miller, G.H., Otto-Bliesner, B.L., Overpeck, J.T., Vinther, B.M. and Arctic Lakes 2k Project Members (2009) Recent Warming Reverses Long-Term Arctic Cooling. *Science* 325*,* 1236-1239.

Keigwin, L.D., Sachs, J.P., Rosenthal, Y. and Boyle, E.A. (2005) The 8200 year B.P. event in the slope water system, western Subpolar North Atlantic. *Paleoceanography* 20, PA2003.

Kleiven, H.F., Kissel, C., Laj, C., Ninnemann, U.S., Richter, T.O. and Cortijo, E. (2008) Reduced North Atlantic Deep Water Coeval with the Glacial Lake Agassiz Freshwater Outburst. *Science* 319*,* 60-64.

Koç, N., Jansen, E. and Haflidason, H. (1993) Paleoceanographic reconstructions of surface ocean conditions in the Greenland, Iceland and Norwegian Seas through the last 14 ka based on diatoms. *Quaternary Science Reviews* 12*,* 115-140.

Koç, N. and Jansen, E. (2002) Holocene climate evolution of the North Atlantic Ocean and the Nordic Seas – a synthesis of new results. In Wefer, G. et al. (Eds.), Climate Development and History of the North Atlantic Realm, pp. 165-177, Springer-Verlag, Heidelberg/Berlin.

Kozdon, R., Eisenhauer, A., Weinelt, M., Meland, M.Y and Nürnberg, D. (2009) Reassessing Mg/Ca temperature calibrations of *Neogloboquadrina pachyderma* (sinistral) using paired $\delta^{44/40}$ and Mg/Ca measurements. *Geochemistry, Geophysics, Geosystems* 10/3, Q03005.

Kucera, M., Weinelt, M., Kiefer, T., Pflauman, U., Hayes, A., Weinelt, M., Chen, M.-T., Mix, A.C., Barrows, T.T., Cortijo, E., Duprat, J., Juggins, S. and Waelbroeck, C. (2005) Reconstruction of sea-surface temperatures from assemblages of planktonic foraminifera: multi-technique approach based on geographically constrained calibration data sets and its application to glacial Atlantic and Pacific Oceans. *Quaternary Science Reviews* 24, 951-998.

Laskar, J., Robutel, P., Joutel, F., Gastineau, M., Correia, A.C.M. and Levrard, B. (2004) A long-term numerical solution for the insolation quantities of the Earth. *Astronomy & Astrophysics* 428, 261-285.

Lighty, R.G., Macintyre, I.G. and Stuckenrath, R. (1982) *Acropora Palmata* Reef Framework: A Reliable Indicator of Sea Level in the Western Atlantic for the Past 10,000 Years. *Coral Reefs* 1, 125-130.

Lubinski, D.J., Polyak, L. and Forman, S.L. (2001) Freshwater and Atlantic water inflows to the deep northern Barents and Kara seas since ca 13 ^{14}C ka: foraminifera and stable isotopes. *Quaternary Science Reviews* 20, 1851-1879.

Manabe, S. and Stouffer, R.J. (1980) Sensitivity of a Global Climate Model to an Increase of CO_2 Concentration in the Atmosphere. *Journal of Geophysical Research* 85/C10, 5529-5554.

Mann, M.E., Zhank, Z., Rutherford, S., Bradley, R.S., Hughes, M.K., Shindell, D., Ammann, C., Faluvegi, G. and Ni, F. (2009) Global Signatures and Dynamical Origins of the Little Ice Age and Medieval Climate Anomaly. *Science* 326, 1256-1259.

Marnela, M., Rudels, B., Olsson, K.A., Andersson, L.G., Jeansson, E., Torres, D.J., Messias, M.-J., Swift, J.H. and Watson, A.J. (2008) Transports of Nordic Seas water masses and excess SF_6 through Fram Strait to the Arctic Ocean. *Progress in Oceanography* 78, 1-11.

Mayewski, P.A., Rohling, E.E., Stager, C., Karlén, W., Maasch, K.A., Meeker, L.D., Meyerson, E.A., Gasse, F., van Krefeld, S., Holmgren, K., Lee-Thorp, J., Rosqvist, G., Rack, F., Staubwasser, M., Schneider, R. and Steig, E.J. (2004) Holocene climate variability. *Quaternary Research* 62, 243-255.

Meland, M.Y., Dokken, T.M., Jansen, E. and Hevrøy, K. (2008) Water mass properties and exchange between the Nordic seas and the northern North Atlantic during the period 23-6 ka: Benthic oxygen isotope evidence. *Paleoceanography* 23, PA1210.

McDermott, F., Frisia, S., Huang, Y., Longinelli, A., Spiro, B., Heaton, T.H.E., Hawkesworth, C.J., Borsato, A., Keppens, E., Fairchild, I.J., van der Borg, K., Verheyden, S. and Selmo, E. (1999) Holocene climate variability in Europe: Evidence from d18O, textural and extension rate variations in three speleothems. *Quaternary Science Reviews* 18 (8-9), 1021-1038.

Moberg, A., Sonechkin, D.M., Holmgren, K., Datsenko, N.M and Karlén, W. (2005) Highly variable Northern Hemisphere temperatures reconstructed from low- and high-resolution proxy data. *Nature* 433*,* 613-617.

Moros, M., Emeis, K., Risebrobakken, B., Snowball, I., Kuijpers, A., McManus, J. and Jansen, E. (2004) Sea surface temperatures and ice rafting in the Holocene North Atlantic; climate influences on northern Europe and Greenland. *Quaternary Science Reviews* 23, 2113-2126.

Moros, M., Andrews, J.T., Eberl, D.D. and Jansen, E. (2006) Holocene history of drift ice in the northern North Atlantic: Evidence for different spatial and temporal modes. *Paleoceanography* 21, PA2017.

Müller, J., Massé, G., Stein, R. and Belt, S.T. (2009) Variability of sea-ice conditions in the Fram Strait over the past 30,000 years. *Nature Geoscience* 2, 772-776.

Müller, J., Werner, K., Stein, R., Fahl, K., Moros, M. and Jansen, E. (submitted to *Quaternary Science Reviews*) Holocene cooling culminates in Neoglacial sea ice oscillations in Fram Strait.

Nesje, A. and Kvamme, M. (1991) Holocene glacier and climate variations in western Norway: Evidene for early Holocene glacier demise and multiple Neoglacial events. *Geology* 19, 610-612.

Overpeck, J., Hughen, K., Hardy, D., Bradley, R., Case, R., Douglas, M., Finney, B., Gajewski, K., Jacoby, G., Jennings, A., Lamoureux, S., Lasca, A., MacDonald, G., Moore, J., Retelle, M., Smith, S., Wolfe, A. and Zielinski, G. (1997) Arctic Environmental Change of the Last Four Centuries. *Science* 278, 1251-1256.

Paillard, D., Labeyrie, L. and Yiou, P. (1996) Macintosh program performs time-series analysis. *Eos Trans. AGU, TI.* 379.

Pflaumann, U., Duprar, J., Pujol, C. and Labeyrie, L.D. (1996) SIMMAX: A modern analog technique to deduce Atlantic sea surface temperatures from planktonic foraminifera in seep-sea sediments. *Paleoceanography* 1, 15-35.

Prange, M. and Lohmann, G. (2003) Effects of mid-Holocene river runoff on the Arctic ocean/sea-ice system: a numerical study. *The Holocene* 13*,* 335-342.

Quadfasel, D., Rudels, B. and Kurz, K. (1988) Outflow of dense water from a Svalbard fjord into the Fram Strait. *Deep Sea Research* 35, 1153-1150.

Rabe, B., Schauer, U., Mackensen, A., Karcher, M., Hansen, E. and Beszczynska-Möller, A. (2009) Freshwater components and transports in the Fram Strait – recent observations and changes since the late 1990s. *Ocean Science* 5*,* 219-233.

Rasmussen, S.O., Andersen, K.K., Svensson, A.M., Steffensen, J.P., Vinther, B.M., Clausen, H.B., Siggaard-Andersen, M.-L., Johnsen, S.J., Larsen, L.B., Dahl-Jensen, D., Bigler, M., Röthlisberger, R., Fischer, H., Goto-Azuma, K., Hansson, M.E. and Ruth, U. (2006) A new Greenland ice core chronology for the last glacial termination. *Journal of Geophysical Research* 111*,* D06102.

Rasmussen, S.O., Vinther, B.M., Clausen, H.B. and Andersen, K.K. (2007) Early Holocene climate oscillations recorded in three Greenland ice cores. *Quaternary Science Reviews* 26*,* 1907-1914.

Rasmussen, T.L., Thomsen, E., Ślubowska, M.A., Jessen, S., Solheim, A. and Koç, N. (2007) Paleoceanographic evolution of the SW Svalbard margin (76°N) since 20,000 ^{14}C yr BP. *Quaternary Research* 67*,* 100-114.

Rasmussen, T.L. and Thomsen, E. (2009) Stable isotope signals from brines in the Barents Sea: Implications for brine formation during the last glaciation. *Geology* 37, 903-906.

Reimer, P.J., Baillie, M.G.L., Bard, E., Bayliss, A., Beck, J.W., Blackwell, P.G., Bronk Ramsey, C., Buck, C.E., Burr, G.S., Edwards, R.L., Friedrich, M., Grootes, P.M., Guilderson, T.P., Hajdas, I., Heaton, T.J., Hogg, A.G., Hughen, K.A., Kaiser, K.F., Kromer, B., McCormac, F.G., Manning, S.W., Reimer, R.W., Richards, D.A., Southon, J.R., Talamo, S., Turney, C.S.M., van der Plicht, J. and Weyhenmeyer, C.E. (2009) INTCAL09 and MARINE09 Radiocarbon Age Calibration Curves, 0-50,000 years Cal BP. *Radiocarbon* 51, 1111-1150.

Risebrobakken, B., Jansen, E., Andersson, C., Mjelde, E. and Hevrøy, K. (2003) A high-resolution study of Holocene paleoclimatic and paleoceanographic changes in the Nordic Seas. *Paleoceanography* 18/1, 1017.

Robinson, S.G. and McCave, I.N. (1994) Orbital forcing of bottom-current enhanced sedimentation of Feni Drift, NE Atlantic, during the mid-Pleistocene. *Paleoceanography* 9/6, 943-972.

Rohling, E.J. and Pälike, H. (2005) Centennial-scale climate cooling with a sudden cold event around 8,200 years ago. *Nature* 434*,* 975-979.

Rudels, B., Björk, G., Nilsson, J., Winsor, P., Lake, I. and Nohr, C. (2005) The interaction between waters from the Arctic Ocean and the Nordic Seas north of Fram Strait and along the East Greenland Current: results from the Arctic Ocean-02 Oden expedition. *Journal of Marine Systems* 55, 1-30.

Rudels, B. and Quadfasel, D. (1991) Convection and deep water formation in the Arctic Ocean-Greenland Sea System. *Journal of Marine Systems* 2, 435-450.

Saloranta, T.M. and Haugan, P.M. (2004) Northward cooling and freshening of the warm core of the West Spitsbergen Current. *Polar Research* 23(1), 447-461.

Sarnthein, M., van Kreveld, S., Erlenkeuser, H., Grootes, P.M., Kucera, M., Pflaumann, U. and Schulz, M. (2003) Centennial-to-millennial-scale periodicities of Holocene climate and sediment injections off the western Barents shelf, 75°N. *Boreas* 32, 447-461.

Schauer, U. (1989) Hydrographie der Fram Straße. In: Meinke, J. (Ed.), Fram Straße – Hydrobiologische und geowissenschaftliche Schlüsselregion zwischen Nordpolarmeer und Europäischem Nordmeer. – Ergebnisse eines Workshops am 4.4.1989 in Hamburg, Institut für Meereskunde, Hamburg.

Schauer, U. (1995) The release of brine-enriched shelf water from Storfjord into the Norwegian Sea. *Journal of Geophysical Research* 100, 16,015-16,028.

Schauer, U., Fahrbach, E., Osterhus, S. and Rohardt, G. (2004) Arctic warming through Fram Strait: Oceanic heat transport from 3 years of measurement. *Journal of Geophysical Research* 109*,* C06026.

Schlichtholz, P. and Houssais, M.-N. (1999) An inverse modelling study in Fram Strait. Part II: water mass distribution and transports. *Deep-Sea Research* 46*,* 1137-1168.

Schlichtholz, P. and Goszczko, I. (2006) Interannual variability of the Atlantic water layer in the West Spitsbergen Current at 76.5°N in summer 1991-2003. *Deep-Sea Research I* 53*,* 608-626.

Schulz, M., Paul, A. and Timmermann, A. (2004) Glacial-interglacial contrast in climate variability at centennial-to-millennial timescales: observations and conceptual model. *Quaternary Science Reviews* 23*,* 2219-2230.

Schulz, M. and Paul, A. (2002) Holocene Climate Variability on Centennial-to-Millennial Time Scales: 1. Climate Records from the North Atlantic Realm. In: Wefer, G. et al. (Eds.), Climate Development and History of the North Atlantic Realm, pp. 41-54, Springer-Verlag, Berlin/Heidelberg.

bSeidenkrantz, M.-S., Roncaglia, L., Fischel A., Heilmann-Clausen, C., Kuijpers, A. and Moros, M. (2008) Variable North Atlantic climate seesaw patterns documented by a late Holocene marine record from Disko Bugt, West Greenland. *Marine Micropaleontology* 68, 66-83.

Seppä, H. and Birks, H.J.B. (2001) July mean temperature and annual precipitation trends during the Holocene in the Fennoscandian tree-line area: pollen-based climate reconstructions. *The Holocene* 11*,* 527-539.

Serreze, M.C., Holland, M.M. and Stroeve, J. (2007) Perspectives on the Arctic's Shrinking Sea-Ice Cover. *Science* 315*,* 1533-1536.

Shackleton, N.J. and Opdyke, N.D. (1973) Oxygen Isotope and Palaeomagnetic Stratigraphy of Equatorial Pacific Core V28-238: Oxygen Isotope Temperatures and Ice Volumes on a 10^5 Year and 10^6 Year Scale. *Quaternary Research* 3, 39-55.

Simstich, J., Sarnthein, M. and Erlenkeuser, H. (2003) Paired $\delta^{18}O$ signals of *Neogloboquadrina pachyderma* (s) and *Turborotalia quinqueloba* show thermal stratification structure in Nordic Seas. *Marine Micropaleontology* 48, 107-125.

Ślubowska, M.A., Koç, N., Rasmussen T.L. and Klitgaard-Kristensen, D. (2005) Changes in the flow of Atlantic water into the Arctic Ocean since the last deglaciation: Evidence from the northern Svalbard continental margin, 80°N. *Paleoceanography* 20, PA4014.

Ślubowska-Woldengen, M.A., Rasmussen T.L., Koç, N., Klitgaard-Kristensen, D., Nilsen, F. and Solheim, A. (2007) Advection of Atlantic Water to the western and northern Svalbard shelf since 17,500 cal yr BP. *Quaternary Science Reviews* 26, 463-478.

Ślubowska-Woldengen, M.A., Koç, N., Rasmussen T.L., Klitgaard-Kristensen, D., Hald, M. and Jennings, A.E. (2008) Time-slice reconstructions of ocean circulation changes on the continental shelf in the Nordic and Barents Sea during the last 16,000 cal yr B.P. *Quaternary Science Reviews* 27, 1476-1492.

Solignac, S., de Vernal, A., and Hillaire-Marcel, C. (2004) Holocene sea-surface conditions in the North Atlantic – contrasted trends and regimes in the western and eastern sectors (Labrador Sea vs. Iceland Basin). *Quaternary Science Reviews* 23, 319-334.

Spielhagen, R.F., Werner, K., Aagaard-Sørensen, S., Zamelczyk, K., Kandiano, E., Budeus, G., Husum, K., Marchitto, T.M. and Hald, M. (2011) Enhanced Modern Heat Transfer to the Arctic by Warm Atlantic Water. *Science* 331, 450-453.

Spielhagen, R.F. and Erlenkeuser, H. (1994) Stable oxygen and carbon isotopes in planktic foraminifers from the Arctic Ocean surface sediments: reflection of the low salinity surface water layer. *Marine Geology* 119, 227-250.

Stein, R., Dittmers, K., Fahl, K., Kraus, M., Matthiessen, J., Niessen, F., Pirrung, M., Polyakova, Ye., Schoster, F., Steinke, T. and Fütterer, D.K. (2004) Arctic (paleo) river discharge and environmental change: evidence from the Holocene Kara Sea sedimentary record. *Quaternary Science Reviews* 23, 1485-1511.

Stuiver, M., Grootes, P.M. and Baraziunas, T.F. (1995) The GISP2 $\delta^{18}O$ Climate Record of the Past 16,500 Years and the Role of the Sun, Ocean, and Volcanoes. *Quaternary Research* 44, 341-354.

Stuiver, M. and Reimer, P.J. (1993) Extended ^{14}C Data Base and Revised Calib 3.0 ^{14}C Calibration Program. *Radiocarbon* 35, 215-230.

Svendsen, J.I. and Mangerud, J. (1997) Holocene glacial and climatic variations on Spitsbergen, Svalbard. *The Holocene* 7/1, 45-57.

Swift, J.H. and Koltermann, K.P. (1988) The Origin of Norwegian Sea Deep Water. *Journal of Geophysical Research* 93/C4, 3563-3569.

Thornalley, D.J.R., Elderfield, H. and McCave, I.N. (2009) Holocene oscillations in temperature and salinity of the surface subpolar North Atlantic. *Nature* 457, 711-714.

Thornalley, D.J.R., Elderfield, H. and McCave, I.N. (2010) Intermediate and deep water paleoceanography of the northern North Atlantic over the past 21,000 years. *Paleoceanography* 25, PA1211.

Vinje, T. (2001) Anomalies and Trends of Sea-Ice Extent and Atmospheric Circulation in the Nordic Seas during the Period 1864-1998. *Journal of Climate* 14, 255-267.

Vinther, B.M., Clausen, H.B., Johnsen, S.J., Rasmussen, S.O., Andersen, K.K., Buchardt, S.L., Dahl-Jensen, D., Seierstad, I.K., Siggaard-Andersen, M.-L., Steffensen, J.P., Svensson, A., Olsen, J. and Heinemeier, J. (2006) A synchronized dating of three Greenland ice cores throughout the Holocene. *Journal of Geophysical Research* 111, D13102.

Volkmann, R. (2000) Planktic foraminifer ecology and stable isotope geochemistry in the Arctic Ocean: implications from water column and sediment surface studies for quantitative reconstructions of oceanic parameters. *Berichte zur Polarforschung* 361, 1-128.

Wanner, H., Beer, J., Bütikofer, J., Crowley, T.J., Cubasch, U., Flückiger, J., Goosse, H., Grosjean, M., Joos, F., Kaplan, J.O., Küttel, M., Müller, S.A., Prentice, I.C., Solomina, O., Stocker, T.F., Tarasov, P., Wagner, M. and Widmann, M. (2008) Mid- to Late Holocene climate change: an overview. *Quaternary Science Reviews* 27, 1791-1828.

Wanner, H., Solomina, O., Grosjean, M., Ritz, S.P. and Jetel, M. (2011) Structure and origin of Holocene cold events. *Quaternary Science Reviews* 30, 3109-3123.

Werner, A. (1993) Holocene moraine chronology, Spitsbergen, Svalbard: lichenometric evidence for multiple Neoglacial advances in the Arctic. *The Holocene* 3, 128-137.

Werner, K., Spielhagen, R.F., Bauch, D., Hass, H.C., Kandiano, E. and Zamelczyk, K. (2011) Atlantic Water advection to the eastern Fram Strait – Multiproxy evidence for late Holocene variability. *Palaeogeography, Paleaoclimatology, Palaeoecology* 308, 264-276.

Williams, K.M. (1993) Ice sheet and ocean interactions, margin of east Greenland ice sheet (14 ka to present): diatom evidence. *Paleoceanography* 8, 69-83.

Yuan, L., Sun, L., Wei, G., Long, N., Xie, Z. and Wang, Y. (2011) 9,400 yr B.P.: the mortality of mollusk shell (Mya truncata) at high Arctic is associated with a sudden cooling event. *Environmental Earth Science* 63, 1385-1393.

PAPER IV

IMPLICATIONS FOR SURFACE AND DEEP WATER VARIABILITY IN THE EASTERN FRAM STRAIT OVER THE PAST 8,500 YEARS DERIVED FROM NEODYMIUM AND LEAD ISOTOPE COMPOSITIONS

6 IMPLICATIONS FOR SURFACE AND DEEP WATER VARIABILITY IN THE EASTERN FRAM STRAIT OVER THE PAST 8,500 YEARS DERIVED FROM NEODYMIUM AND LEAD ISOTOPE COMPOSITIONS

Kirstin Werner[1], Claudia Teschner[1], Robert F. Spielhagen[1,2], and Martin Frank[1]

[1]Leibniz Institute of Marine Sciences IFM-GEOMAR, Wischhofstraße 1-3, 24148 Kiel, Germany
[2]Academy of Sciences, Humanities, and Literature Mainz, Geschwister-Scholl-Straße 2, 55131 Mainz, Germany

Abstract

A sediment core from the West Spitsbergen continental margin (79°54'N, 6°46'E) has been investigated for seawater-derived neodymium and lead isotope compositions stored in ferromanganese oxyhydroxide coatings of the sediment particles to reconstruct Holocene changes in the sources of bottom waters passing the site. The radiogenic isotope data are used in combination with a multitude of proxy indicators for the climatic and oceanographic development of the eastern Fram Strait during the past 8,500 years (chapters 3 and 5). Core top samples from the area have been analysed for their radiogenic isotope compositions to calibrate the downcore data and reveal relatively high (radiogenic) neodymium isotope compositions between -9.7 and -9.1. These values correspond well to the downcore isotope signatures within the uppermost ca 40 cm of the sediment core (ε_{Nd} -9.1 to -8.8) and concur with cool conditions and high sea ice abundances after ca 2.8 cal ka BP (Late Holocene) as indicated by other proxies. In contrast, warmer conditions of the Early and Mid-Holocene were accompanied by lower, less radiogenic neodymium isotope ratios similar to present-day seawater in the Nordic Seas (ε_{Nd} -10.6 to -10.1). A significantly higher admixture of deepwater from the Nordic Seas to the core site is thus inferred for the earlier periods of the Holocene. For the marked shift to more radiogenic neodymium isotope compositions after 2.8 cal ka BP which occurs coeval with the well-known Neoglacial trend in the northern North Atlantic region three hypotheses are discussed. Increased boundary exchange of seawater with basaltic formations at the margins of the Nordic Seas may have caused the more radiogenic signature of deeper waters in the eastern Fram Strait during the Late Holocene. Alternatively, increased inflow of Canadian Basin Deep Water which carries a Pacific component and can be traced crossing the Arctic Ocean basins and entering the Fram Strait today (Björk et al., 2010) may have contributed to the more radiogenic neodymium isotope ratios. Moreover, increases in fine-grained ice-rafted material (IRF) since about 3 cal ka BP concur with the shift to higher ε_{Nd} values. In the Fram Strait, high amounts of IRF entrained by

Arctic sea ice are released into the seawater upon melting. During the Late Holocene fast sedimentation of ice-rafted material may have led to rapid burial of IRF and hereby to the fast storage of its ε_{Nd} values obtained elsewhere in the Arctic Ocean. Possible source areas for highly radiogenic IRF are the shallow Arctic shelves, in particular the Kara Sea shelf which today has seawater ε_{Nd} values of -6 to -5 (Porcelli et al., 2009). Lead isotope ratios reveal a dominant contribution of anthropogenic lead in core top samples as well as in the uppermost sediment layers indicating bioturbation mixing. Higher $^{206}Pb/^{204}Pb$ values (>19.0) during the warm Early and Mid-Holocene periods may be related to enhanced chemical weathering on Svalbard and increased glacial and riverine input of young granitic (more radiogenic) material to the West Spitsbergen margin.

6.1. Introduction

The Fram Strait as the only deep water connection of the world's oceans to the Arctic plays a substantial role for the heat influx to the Arctic Ocean (Rudels et al., 2000; Karcher et al., 2003; Schauer et al., 2004) and controls freshening of the Nordic Seas through the Arctic sea ice export (Mauritzen and Häkkinen, 1997). Water mass transit through Fram Strait in both southward and northward directions thus contributes significantly to thermohaline convection processes. Warm and saline Atlantic Water (AW) either returning in the Fram Strait or crossing the Arctic basin, provides a substantial part of cooled, high-saline AW masses (Arctic Intermediate Water, AIW) to join the East Greenland Current (EGC) in the western Fram Strait hereby contributing to the deepwater renewal processes in the Nordic Seas (Mauritzen, 1996, Rudels et al., 1999; Anderson et al., 1999). The variability of the thermohaline convection in the Nordic Seas and thus of the present-day climate system (Broecker, 1991) is also controlled by the Arctic sea ice extent (Mauritzen and Häkkinen, 1997; Lohmann and Gerdes, 1998; Holland et al., 2001). Arctic sea ice coverage not only controls atmospheric and ocean surface temperatures through its albedo and insulating effects but also supplies freshwater to the regions of deepwater formation when exported via Fram Strait.

Studies of the past behaviour of the twofold current system in the Fram Strait provide insight on the variations of the interaction between the Arctic Ocean and the Nordic Seas. Compared to glacial periods, climate variations during the Holocene period (since ca 11.7 cal ka BP) have been of much smaller scale and are thus often used as analogues for present-day and potential future climate scenarios. The Holocene in the eastern Fram Strait was in particular characterised by variations of Atlantic Water inflow and sea ice extent. Strong inflow of warm and saline AW associated with maximum insolation (e.g., Berger and Loutre, 1991) resulted in relatively high sea surface temperatures west of Svalbard during the Early and Mid-Holocene

(chapter 5). A major cooling after ca 5 cal ka BP was associated with a southeast advance of cold polar waters and the summer sea ice margin and a concurrent weakening of the AW inflow. Stable oxygen and carbon isotopes derived from benthic foraminifera confirm a substantial cooling of bottom water masses since ca 3 cal ka BP. However, deepwater flow and its past variability in the eastern Fram Strait and the Arctic Ocean are still a matter of debate (Jones, 2001). The contributions of different water masses to the deeper parts of the WSC are as yet not completely understood. Studies carried out since the 1980s by e.g., Aagaard et al. (1985, 1987, 1991), Swift and Koltermann (1988), Rudels (1986), Rudels and Quadfasel (1991), Jones et al. (1995), and Schlichtholz and Houssais (1999) have revealed a major contribution of Norwegian Sea Deep Water (NSDW) to the deeper water masses in the eastern Fram Strait. NSDW is considered to form by mixing of waters from the polar oceans in the Greenland Sea (Rudels and Quadfasel, 1991).

In order to reconstruct changes in Holocene bottom and surface water mixing, as well as to detect the influence of weathering inputs from nearby landmasses, potentially suggesting local impacts such as brine water influx, we investigated the neodymium and lead isotopic signals of seawater on the Western Svalbard continental margin for the past ca 8.5 ka. Our aim was to test if the analysis of seawater-derived radiogenic isotope compositions extracted from ferromanganese oxyhydroxide coatings of bottom sediments can help to elucidate Holocene variations of exchanges between the Nordic Seas and the Arctic Ocean through Fram Strait or which other processes may have impacted bottom sediments of eastern Fram Strait, an area which is today located in the area of the fluctuating summer sea ice margin and is thus largely influenced by discharge of sea ice sediments to the seawater. The radiogenic isotope data are combined with high-resolution multiproxy data reflecting Holocene surface/subsurface and bottom water conditions on the West Spitsbergen continental margin (see also chapters 3 to 5). Proxies used for the reconstruction include planktic foraminiferal assemblages, planktic and benthic stable isotope records, as well as lithological parameters. In order to obtain a calibration of the Nd and Pb isotope compositions extracted from the sediments to the modern bottom water mass signatures in the area, a set of core top samples from different water depths in the eastern Fram Strait has also been investigated for present-day Nd and Pb isotope signatures.

6.2. Hydrographical settings

Atlantic Water (AW) advection through eastern Fram Strait is the main heat source of the Arctic Ocean (Schauer et al., 2004). In subsurface water depths, relatively warm and saline AW (summer temperatures ≤ 6°C, S ≤ 35.2; Spielhagen et al., 2011) is advected via eastern Fram Strait into the Arctic Ocean by the West Spitsbergen Current (WSC) which is the northward

propagation of the Norwegian Atlantic Current. Close to study area presented here (Fig. 6.1), AW submerges beneath a cold and fresh upper mixed layer of Arctic origin and continues as a subsurface current into the Arctic Ocean (Johannessen, 1986). On its way north, the AW core encounters and melts Arctic sea ice and produces a less saline upper mixed layer at the surface (Rudels et al., 2005). As a consequence, a large part of the eastern Fram Strait remains ice-free even in winter (e.g., Vinje, 2001). The AW inflow is topographically constrained to the eastern Fram Strait and can reach a thickness of up to 700 m at the Western Svalbard margin (Schlichtholz and Goszszko, 2006).

Fig. 6.1 (next page): a) Map of the Arctic Ocean (Jakobsson et al., 2008) with intermediate and deepwater currents of the Nordic Seas and the Arctic Ocean (JMFZ=Jan Mayen Fracture Zone, MJR=Morris Jesup Rise). Yellow arrows in the Arctic Ocean basins show schematic circulation of the Upper Polar Deep Water down to depths of about 1700 m (Jones et al., 2001). Yellow arrows in the Nordic Seas and the Fram Strait indicate large-scale intermediate and deep circulation modified from Lacan and Jeandel (2004b). Also shown are the most important surface water currents in the Fram Strait. White arrows reflect cold and fresh waters of Arctic origin. Red dashed arrows indicate warm and saline Atlantic Water inflow through Fram Strait and the Barents Sea. The white star marks the investigated core site MSM5/5-712. Grey squares (with white frame) refer to present-day seawater ε_{Nd} values listed in Table 6.2. Grey squares (without frame) are present-day seawater ε_{Nd} values in river mouth areas after Porcelli et al. (2009) and Zimmermann et al. (2009). Bering Strait inflow is taken from Piepgras and Jacobsen (1988), Dahlqvist et al. (2007), and Amakawa et al. (2009). White oval marks average ε_{Nd} value of sediment leachates in the Kara Sea (Filippova, 2011), white triangle indicates average ε_{Nd} value of sea ice sediment (detritus) after Tütken et al. (2002). Grey hexagons show ε_{Nd} value of rock material for Greenland (Lacan and Jeandel, 2004a), for the western Norwegian Caledonian margin (Lacan and Jeandel, 2004b and references therein), for West Siberia (Polar Ural: Edwards and Wasserburg, 1985; Putorana Basalts: Sharma et al., 1992). **b)** Compilation of ε_{Nd} values of rock material on Svalbard from the literature: 1: Tütken et al. (2002) and references therein; 2: Andersson et al. (2008) and references therein; 3: Johansson and Gee (1999); 4: Peucat et al. (1989); 5: Johansson et al. (2002). Also included are potential $^{206}Pb/^{204}Pb$ isotope values taken from Winter et al. (1997) for Caledonian Orogenic Belts of Greenland, Scotland, Ireland and Norway (white hexagon).

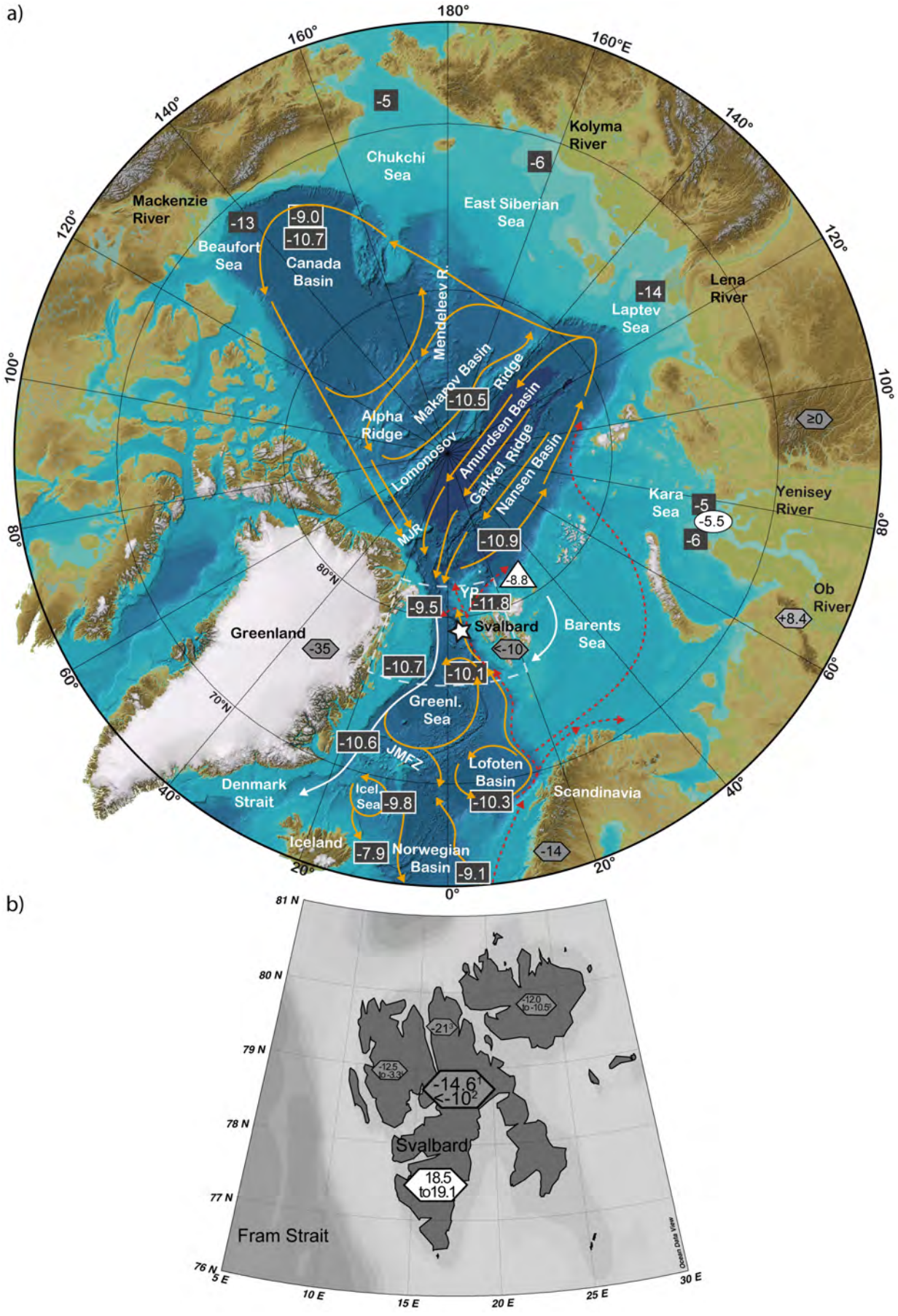
a)
180°
160°
160°E
140°
140°
120°
120°
100°
100°
80°
80°
60°
60°
40°
40°
20°
20°
0°
-5
Chukchi Sea
-6
Kolyma River
East Siberian Sea
Mackenzie River
-13
Beaufort Sea
-9.0
-10.7
Canada Basin
Mendeleev R.
-14
Laptev Sea
Lena River
Makarov Basin
Ridge
-10.5
Alpha Ridge
Amundsen Basin
Lomonosov
Gakkel Ridge
Nansen Basin
≥0
Kara Sea
-5
-5.5
-6
Yenisey River
MJR
-10.9
80°N
-8.8
YP
-11.8
-9.5
Svalbard
Barents Sea
Ob River
+8.4
Greenland
-35
-10
-10.7
-10.1
70°N
Greenl. Sea
-10.6
JMFZ
Lofoten Basin
Denmark Strait
Icel. Sea
-9.8
-10.3
Scandinavia
Iceland
-7.9
Norwegian Basin
-9.1
-14
b)
81 N
80 N
79 N
78 N
77 N
76 N
5 E
10 E
15 E
20 E
25 E
30 E
-12.0 to -10.5
-21
-12.5 to -3.3
-14.6 to -10
Svalbard
18.5 to 19.1
Fram Strait
Ocean Data View

In intermediate and bottom depths, the WSC transports Arctic Intermediate Water (AIW) and Norwegian Sea Deep Water (NSDW), respectively. Little is known about the northward transport of AIW created in the Nordic Seas (Marnela et al., 2008). NSDW which dominates the deepwater inflow through eastern Fram Strait (e.g., Aagaard et al., 1985; Swift and Koltermann, 1988, Jones et al., 1995; Fig. 6.2) has temperatures between -1.1 and 0°C and a salinity range of 34.90 to 34.92 (Schlichtholz and Houssais, 1999). Schlichtholz and Houssais (1999) suggested that newly produced NSDW forms by mixing of some old NSDW arriving from the Nordic Seas with Arctic Ocean Deep Waters from different sources, such as upper Polar Deep Water (uPDW), Eurasian Basin Deep Water (EBDW) and Canadian Basin Deep Water (CBDW) (Fig. 6.2). For a detailed description of the individual water masses we refer to the studies of Schlichtholz and Houssais (1999) and Rudels et al. (2000, 2002, 2005). Since deepwater inflow from the Nordic Seas has been detected in the western Fram Strait at ca 78°50'N (Rudels et al., 2005) and at the northern slope of Yermak Plateau (Jones et al., 1995) where it most likely merges with Eurasian Basin Deep Water (Rudels et al., 2005), it apparently passes the presented study site at 78°55'N on its way into the Arctic Ocean.

In the western part of the Fram Strait cold and fresh polar surface waters and sea ice are transported southward with the East Greenland Current (EGC, Fig. 6.1). Waters of the EGC are formed by mixing of southward flowing less dense Polar Water ($T < 0°C$, $S < 34.5$; e.g., Falck et al., 2005) with deeper waters from the Arctic Ocean (Budéus and Ronski, 2009). While a considerable fraction of surface waters of the EGC has been identified to be of Pacific origin (Jones et al., 2003), cooled Atlantic Water either returning in the Fram Strait as the Recirculation Atlantic Current (RAC; Rudels et al., 2005) or after crossing the Arctic basin (Arctic Atlantic Water, AAW) is entrained into the southward directed EGC in western Fram Strait (Fig. 6.1) at intermediate depth (e.g., Marnela et al., 2008; Fig. 6.2).

6.3. Radiogenic isotopes

Studies of radiogenic isotope compositions of dissolved Nd and Pb have achieved increasing attention in paleoceanographic and paleoclimate reconstructions over the past ca 15 years (van de Flierdt and Frank, 2010). Of particular advantage is the independency of radiogenic isotopes from stable isotope fractionation induced by biological activity or physical processes (e.g., van de Flierdt et al., 2006; Gutjahr et al., 2007). Dissolved radiogenic isotope signatures in seawater originate from weathering processes of the continental crust and are delivered in dissolved or detrital form by riverine and eolian inputs to the ocean where they subsequently exchange with seawater (e.g., Frank, 2002; Lacan and Jeandel, 2005). Margin/seawater

interactions (boundary exchange) must be considered as a further source for isotope signatures of seawater, in particular in the Nordic Seas where basaltic formations can largely influence water masses (e.g., Lacan and Jeandel, 2004b, 2005). The neodymium isotope signature of seawater changes through time with an average oceanic residence time of 400 to 2,000 years (Tachikawa et a., 1999; Frank, 2002; Arsouze et al., 2009), which is similar to the global mixing time of oceans (about 1500 years; Broecker, 1982). High particle reactivity of lead accounts for a shorter residence time of about 50 years for radiogenic lead isotopes (^{206}Pb, ^{207}Pb, ^{208}Pb) in the ocean (e.g., Frank, 2002, and references therein; Haley et al., 2008) and makes it thus a useful tracer for local changes of weathering input to the ocean and short distance water mass mixing (Stumpf et al., 2009). Therefore, today all natural Pb isotope compositions in seawater have been overprinted by anthropogenic-induced lead (e.g., Schaule and Patterson, 1981). In surface waters, the residence time of lead is much shorter (<5 years) (Hamelin et al., 1990). Thus, in the Arctic Ocean where a considerable portion of sediment material is released by sea ice, anthropogenic lead contamination is strongly mirrored in underlying sediments (Gobeil et al., 2001).

Variations of the $^{143}Nd/^{144}Nd$ ratio are expressed in $\varepsilon_{Nd} = [(^{143}Nd/^{144}Nd_{Sample})/(^{143}Nd/^{144}Nd)_{CHUR}-1)] \times 10{,}000$ (CHUR: chondritic uniform reservoir is the present-day average earth value of 0.512638; Jacobsen and Wasserburg, 1980). Remote from continental inputs, water masses hold different neodymium isotopic signatures dependent from their source areas and can serve as quasi-conservative tracer of water mass mixing and ocean circulation (Piepgras and Wasserburg, 1980; Frank, 2002). Under oxic conditions, radiogenic isotopic compositions of bottom waters are incorporated by authigenic ferromanganese oxyhydroxide coatings of bottom sediments in pore waters and can be directly extracted from bulk sediments (Rutberg, et al., 2000; Bayon et al., 2002; Gutjahr et al., 2007; Stumpf et al., 2011).

This approach has been previously applied to sediments in the Arctic Ocean and in the North Atlantic for both the pre-Quaternary and Quaternary (Winter et al., 1997; Haley et al., 2007; Crocket et al., 2011). Studies of the neodymium isotope composition carried out on Arctic Ocean sediments of both the leachable fraction and the bulk residues, the latter used in order to investigate the provenance regions of the sediment material, revealed a significant contribution of sea ice-rafted material from the shallow Siberian shelves to central Arctic and the Fram Strait bottom sediments (Eisenhauer et al., 1999; Tütken et al., 2002; Haley et al., 2007, 2008). Sediment leachates of core top samples on the Kara Sea shelf revealed radiogenic Nd isotope compositions around -5.5 (Filippova, 2011; Fig. 6.1) which were probably caused by riverine input and subsequent exchange with radiogenic weathering products derived from the Putorana basalts ($\varepsilon_{Nd} \geq 0$; Sharma et al., 1992) in the Siberian hinterland (e.g., Haley et al., 2008; Filippova, 2011).

6.4. Present-day seawater ε_{Nd} signatures in Arctic and sub-Arctic waters

Atlantic Water entering eastern Fram Strait from the south at intermediate water depth is less radiogenic (ε_{Nd} ~ -11 in 600 m; Fig. 6.2), compared to the deeper flowing NSDW (Lacan and Jeandel, 2004b). The latter has acquired a more radiogenic ε_{Nd} signature between -10.1 (1500 m water depth) and -10.5 (3400 m water depth) through margin/seawater interactions as the waters flow along the west and south of the highly radiogenic Norwegian Basin basaltic margins (i.e., the islands of Jan Mayen, Iceland, and Faroe; Lacan and Jeandel, 2004b). In the Nansen and Makarov basins, these Nordic Seas-derived waters have been detected with similar ε_{Nd} signatures of -10.9 and -10.5, respectively (Porcelli et al., 2009; Table 6.1) in agreement with the Atlantic Water pathway in the intermediate layer of the Arctic Ocean (Rudels et al., 1994). Measurements in the northwestern Fram Strait (Andersson et al., 2008; Fig. 6.2), however, significantly contrast the NSDW seawater ε_{Nd} signature. Here, more radiogenic ε_{Nd} values characterize the cold and fresh Arctic outflow waters of both the surface and deeper waters down to 1300 m water depth (Table 6.1, Figs. 6.1 and 6.2). Relatively radiogenic Pacific waters enter through Bering Strait (ε_{Nd}~-5; Piepgras and Jacobsen, 1988) and account for radiogenic seawater ε_{Nd} values of -9 found in deeper waters (2500 m) of the Canada Basin (Porcelli et al., 2009; Fig. 6.1). Since Pacific waters could be traced crossing the Arctic Ocean and entering the Fram Strait from the north (e.g., Jones et al., 2003; Björk et al., 2010), radiogenic seawater signatures found in the western Fram Strait may have their origin through mixing with Canadian Basin Deep Waters which hold a higher radiogenic Pacific component (Andersson et al., 2008; Porcelli et al., 2009).

Riverine input from the Arctic shallow shelves, and in particular from the Siberian margins, is another significant component of Arctic deep waters. Yearly discharges of the rivers Lena, Ob and Yenisey account for half of the complete river runoff into the Arctic Ocean (Aagaard and Carmack, 1989, and references therein). Through water-shelf interactions during winter, such as sea ice formation and associated sinking of dense brine waters to the bottom (Bauch et al., 1995), river waters can strongly alter the seawater ε_{Nd} signatures on the shelves (Porcelli et al., 2009). While the eastern Laptev Sea shelf waters are relatively unradiogenic (ε_{Nd}~-14), more radiogenic riverine input of the rivers Yenisey and Ob (ε_{Nd}~-5 and -6, respectively) strongly contributes to the radiogenic neodymium isotope compositions of the Kara Sea shelf waters (Porcelli et al., 2009; Zimmermann et al., 2009).

Table 6.1: Selected seawater ε_{Nd} signatures from the Nordic Seas and the Arctic Ocean (see also Fig. 6.1).

Station number	Water depth, m	Latitude (N)	Longitude	ε_{Nd} (2σ)
Nansen Basin #4 (Andersson et al., 2008)	2500	84°16.87'	33°39.81' E	-10.9 ± 0.4
Fram Strait #5 (Andersson et al., 2008)	1324	81°20.28'	7°20.73' W	-9.5 ± 0.7
North Svalbard #2 (Andersson et al., 2008)	100	80°25.85'	15°31.05' E	-11.8 ± 0.4
# 20 (Lacan and Jeandel, 2004b)	2491	69°21'	6°85' W	-9.8 ± 0.2
# 21 (Lacan and Jeandel, 2004b)	1431	66°55'	10°11' W	-7.9 ± 0.2
# 25 (Lacan and Jeandel, 2004b)	1385	64°65'	4°18' E	-9.1 ± 0.2
# 26 (Lacan and Jeandel. 2004b)	1700	69°03'	7°95' E	-10.3 ± 0.2
# 29 (Lacan and Jeandel. 2004b)	1513	77°67'	7°69' E	-10.1 ± 0.3
# SGN 32 (Lacan and Jeandel, 2004a)	1840	77°02'	3°45' W	-10.7 ± 0.2
# SGN 46 (Lacan and Jeandel, 2004a)	900	72°52'	16°11' W	-10.6 ± 0.2
# Makarov (Porcelli et al., 2009)	1000	87°54.97'	154°22.50' E	-10.5 ±0.4
#4 (Porcelli et al., 2009)	2500	73°49.50'	152°00.73' W	-9.0 ± 0.4
#3 (Porcelli et al., 2009)	1000	75°12.51'	149°56.96' W	-10.7 ±0.4

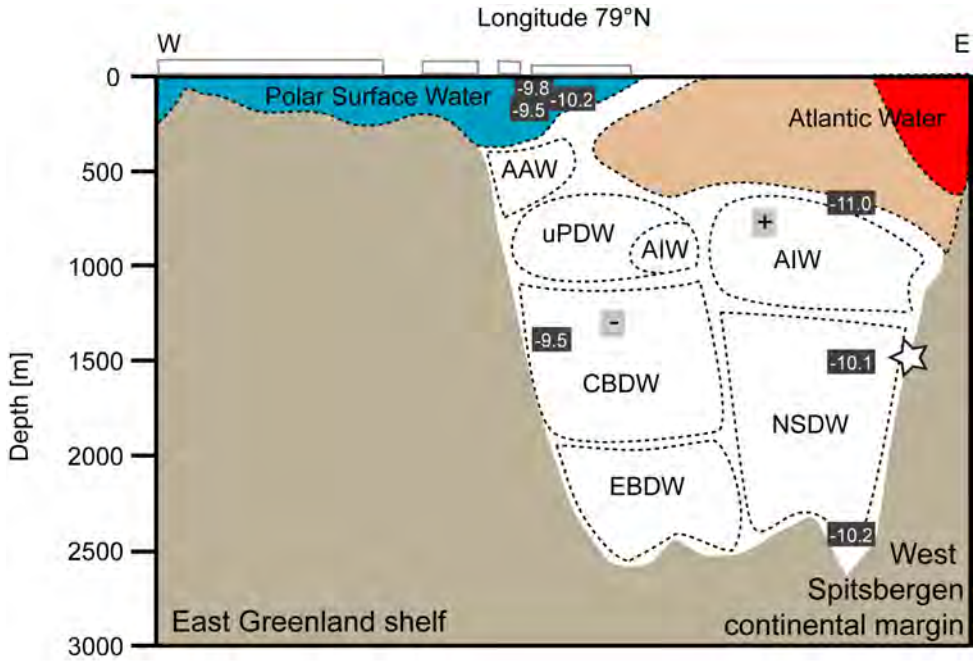

Fig. 6.2 (previous page): Schematic cross section of Fram Strait at 79°N. Approximate positioning of water masses was compiled from Schauer (1989), Hebbeln (1991), Rudels et al. (2000, 2002), Schauer et al. (2004), and Marnela et al. (2008). The sizes of the fields indicating the individual water masses do not reflect actual volume or velocity estimates. Present-day seawater neodymium isotope compositions are marked in grey squares. Numbers are taken from station Fram Strait #5 (western Fram Strait; Andersson et al., 2008) and Station 29 (eastern Fram Strait; Lacan and Jeandel, 2004b). For exact station position see Table 6.2. AAW = Arctic Atlantic Water, AIW = Arctic Intermediate Water, CBDW = Canadian Basin Deep Water, EBDW = Eurasian Basin Deep Water, NSDW = Norwegian Sea Deep Water. Major flow directions are indicated by '+' (northward) and '-' (southward). White star marks approximate position of sediment core 712 on the West Spitsbergen continental margin.

6.5. Material and methods

Samples for downcore investigation of Nd and Pb isotope compositions were obtained from two sediment cores (kastenlot and box core) recovered from station MSM5/5-712 at the western Svalbard continental margin (78°54.94'N, 6°46.04'E, 1490.5 m water depth, Fig. 6.1) during cruise leg MSM5/5 of the RV „Maria S. Merian" in summer 2007. Detailed stratigraphy and proxy datasets of box core MSM5/5-712-1 covering the past ca 2,000 years have been reported in Spielhagen et al. (2011) and Werner et al. (2011). Sediment colour measurements were carried out at discrete 1 cm steps, using a handheld Minolta CM-2002 Spectrophotometer. Chronology and multiproxy records of the uppermost 210 cm of kastenlot core MSM5/5-712-2 are presented in chapter 5. In addition, we investigated a set of core top samples from different water depths in the eastern Fram Strait for present-day Nd and Pb isotope signatures (Table 6.2).

Since all core top samples and the two cores were recovered during cruise MSM5/5 we will omit 'MSM5/5' in the station notation and refer to the station numbers only in the following. The presented downcore data are a combination of records from both box core 712-1 and kastenlot core 712-2. We thus will refer to the entire downcore record as 712 if not marked elsewise. The core top sample retrieved from box core 712-1 is identified as 712-1.

Sample preparation

Extraction of seawater Nd and Pb isotope signals from ferromanganese coatings of bulk sediments was carried out following a slightly modified version of the methods suggested by Gutjahr et al. (2007) and Stumpf et al. (2010). Samples were processed in acid-cleaned polypropylene 50 ml centrifuge tubes. About 2 g of freeze-dried and coarsely ground bulk sediment material were rinsed twice with 20 ml of deionised water (Milli-Q system, MQ water). To remove carbonate, the samples were treated with a 44%-acetic acid/1M-Na acetate buffer. In those cases where the carbonate was not completely dissolved, the samples were put on a shaker overnight in a solution of 10 ml MQ water and 10 ml acetic acid to remove the remaining carbonate and were thoroughly rinsed with MQ water thereafter. For the leaching process to dissolve the ferromanganese oxyhydroxide coatings, about 20 ml of the leaching solution (0.05 M-hydroxylamine hydrochloride/44%-acetic acid solution buffered to pH 3.6 with NaOH) was

added to the samples and left to react in an ultrasonic bath for about 1 h followed by a shaker for 1 h. After centrifugation, the supernatant containing the dissolved seawater fraction of the coatings was pipetted off into Teflon vials for further chemical treatment.

Separation and purification of Pb, Nd, and Sr

We followed standard procedures for ion chromatographic separation and purification of the elements (for Nd: Cohen et al., 1988; Barrat et al., 1996; Le Fèvre and Pin, 2005; for Pb: Galer and O'Nions; 1989; Lugmair and Galer, 1992; and for Sr: Horwitz et al., 1992; Bayon et al., 2002). Separation of Pb was carried out on cation exchange columns (50 µl AG1-X8 resin, mesh size 100-200 µm). Alkaline elements were separated from rare earth elements (REEs) on cation exchange columns (0.8 ml AG50W-X12 resin, mesh size 200-400 µm). Separation of Nd from other REEs was conducted on columns with 2 ml Ln Spec resin (mesh size 50-100 µm). Purification of Sr was achieved on columns with 50 µl Sr Spec resin (mesh size 50-100 µm).

Isotope measurements

Nd, Pb and Sr isotope analyses were conducted on a Nu Plasma MC-ICPMS at IFM-GEOMAR, Kiel. All Nd isotope ratios ($^{143}Nd/^{144}Nd$) presented were corrected for mass bias following an exponential law using ($^{146}Nd/^{144}Nd = 0.7219$) and normalized to the accepted value of the JNdi-1 standard of 0.512115 (Tanaka et al., 2000). Repeated measurements of the JNdi-1 standard gave a reproducibility of 0.28 ε_{Nd} units (2σ).

A standard bracketing method following Albarède et al. (2004) was applied to determine lead isotope ratios. All presented Pb isotope values were normalized to the accepted values for the NBS981 standard (Abouchami et al., 1999). The 2σ reproducibility for NBS981 was 0.0075 for $^{206}Pb/^{204}Pb$, 0.0101 for $^{207}Pb/^{204}Pb$, 0.0326 for $^{208}Pb/^{204}Pb$, 0.0009 for $^{208}Pb/^{206}Pb$ and 0.0002 for $^{207}Pb/^{206}Pb$.

The $^{87}Sr/^{86}Sr$ signature was measured to support the seawater origin of the extracted Nd and Pb isotope signals from the ferromanganese coatings (Rutberg et al, 2000; Piotrowski et al., 2005; Gutjahr et al., 2007). $^{87}Sr/^{86}Sr$ ratios were corrected for isobaric interference (^{86}Kr, ^{87}Rb) and mass bias (using $^{86}Sr/^{88}Sr = 0.1194$; Steiger and Jäger, 1977). All Sr isotope data were normalized to the accepted value of standard NBS987 ($^{87}Sr/^{86}Sr = 0.710245$). The 2σ external reproducibility during measurements was $\pm$ 0.00002.

6.6. Results

6.6.1. Neodymium isotopes

Core top samples from the western continental Svalbard margin show radiogenic ε_{Nd} values ranging from -9.1 to -9.7 except for station 715-3 which displays a less radiogenic value of -10.2 (Table 6.2; Fig. 6.3a). To our knowledge there are no modern seawater ε_{Nd} data available from the deep eastern Fram Strait to compare with. However, surface (8 and 100 m depth) and deeper (1324 m) waters of the northwestern Fram Strait revealed radiogenic ε_{Nd} values between -9.8 and -9.5 (Andersson et al., 2008; Figs. 6.1 and 6.2). Since the AMS radiocarbon dating of the core top sample at station 712-1 (1490 m water depth) based on shells of planktic foraminifera (Spielhagen et al., 2011) revealed a modern age containing bomb radiocarbon we are confident that the surface ε_{Nd} value of -9.1 represents the present-day value for station 712-1. Likewise, we infer similar present-day ε_{Nd} values for the West Spitsbergen continental margin as corroborated by core top measurements in this study.

The unradiogenic ε_{Nd} value (-10.2) from station 715-3 is consistent with present-day seawater ε_{Nd} values of North Atlantic Drift waters obtained in the eastern Fram Strait (-10.1) by Lacan and Jeandel (2004b; their station #29) and further south in the Nordic Seas, as well as in the western Fram Strait area under the influence of the East Greenland Current (Lacan and Jeandel, 2004a; Fig. 6.1; Table 6.1). Due to the fact that all other core top stations located close to site 715-3 reveal values of -9.1 to -9.7, we suggest that station 715-3, which was not ^{14}C-dated, probably has an age older than 2,000 years leading to an ε_{Nd} signature similar to those found in the downcore record of 712 for the interval between 8.5 and 2.8 cal ka BP (-10.6 to -10.0; see below). In support of this, unpublished magnetic susceptibility data (F. Niessen) suggest that a sediment core obtained from the same site as core top sample 715-3 does not include Late Holocene sediments.

During the past ca 8,500 years, neodymium isotope signatures vary between -10.6 and -8.8 (Table 6.3, Fig. 6.3b). Prior to 2.8 cal ka BP ε_{Nd} values (-10.6 to -10.0) are in very good agreement with water column data from the present-day Nordic Seas (ε_{Nd} values of -10.3 to -10.7; Piepgras and Wasserburg, 1987; Lacan and Jeandel, 2004b). A trend to more radiogenic values from -10.6 to -10.0 is obvious between 8.5 and 2.8 cal ka BP. Two excursions at 5.2 and 3.3 cal ka BP mark more radiogenic values of -9.7 and -9.5, respectively. After 2 cal ka BP ε_{Nd} values increased to significantly more radiogenic values between -9.1 and -8.8. One excursion of a lesser radiogenic ε_{Nd} value (-10.2) is found in the sample at 2.75 cm core depth (ca 50 cal year BP/~1900 AD).

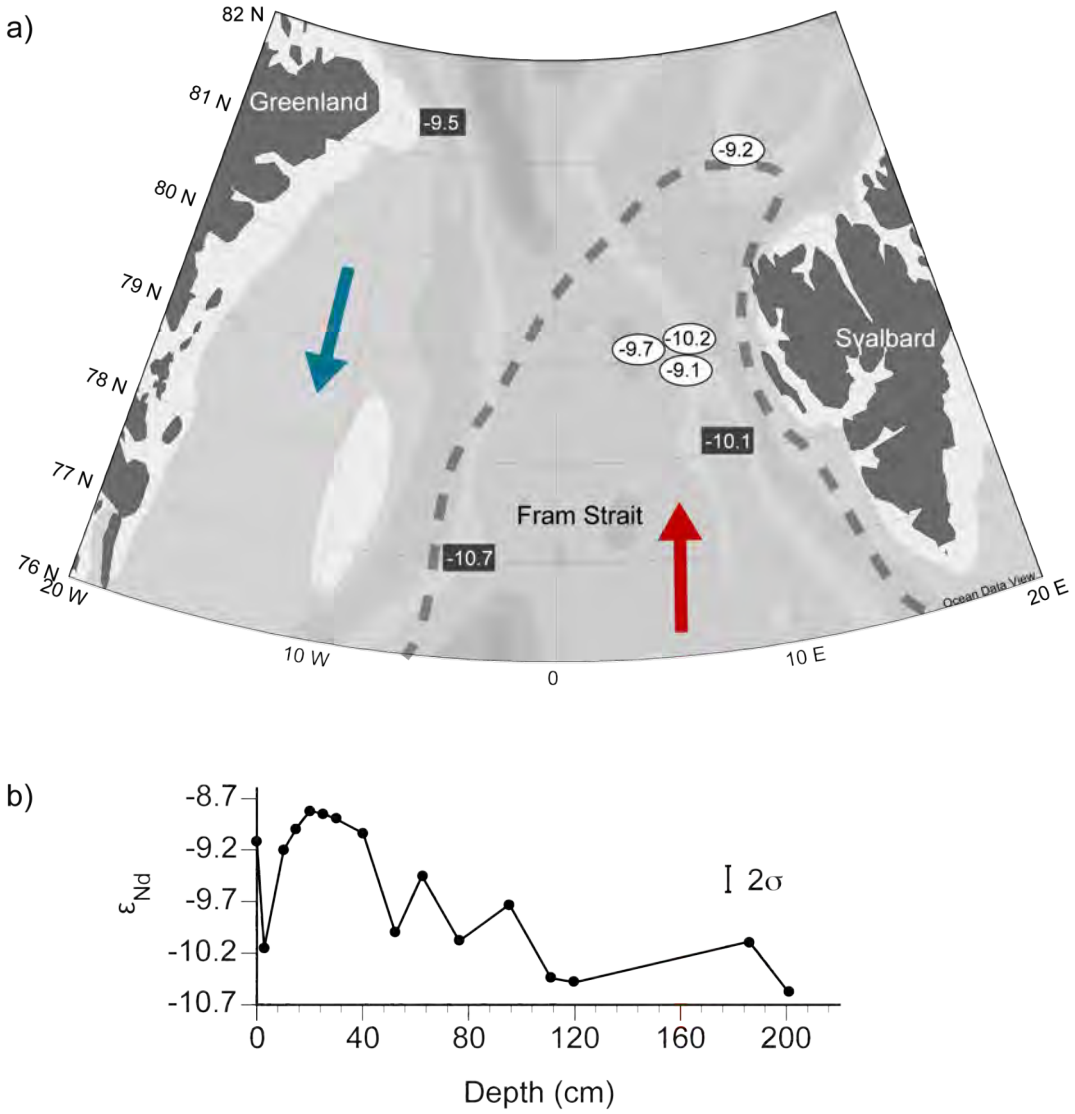

Fig. 6.3: a) Neodymium isotope composition of ferromanganese coatings from core top samples in the eastern Fram Strait (white ovals, see Table 6.2). For comparison, selected seawater ε_{Nd} values from the Fram Strait are shown (grey rectangles, see Table 6.1). The arrows mark the prevailing surface/subsurface current system of warm and saline Atlantic Water inflow (red) and cold and fresh Arctic outflow waters (blue). Also shown is the approximate summer sea ice margin (grey dashed line). **b)** Neodymium isotope record of sediment leachates in core 712 versus depth.

Measured core top ε_{Nd} values from the area match those obtained from downcore samples of station 712 during the past ca 2 cal ka BP. The core top samples had been stained with Rose Bengal onboard for foraminiferal investigations prior to isotope analysis. However, the consistence between core top and downcore data of core 712 (not stained with Rose Bengal), as well as near-seawater Sr isotope signatures of core top samples and the overprint by anthropogenic-derived lead (see section 1.6.2) support a reliable reflection of modern bottom water Nd isotope values in the core top samples.

Table 6.2: Measured radiogenic isotope values of core top samples from the eastern Fram Strait.

Site	Water depth, m	Latitude (N)	Longitude (E)	ε_{Nd} (2σ) ± 0.28	$^{206}Pb/^{204}Pb$ (2σ) ± 0.0075	$^{207}Pb/^{204}Pb$ (2σ) ± 0.0101	$^{208}Pb/^{204}Pb$ (2σ) ± 0.0326	conc. Pb	$^{86}Sr/^{87}Sr$ (2σ) ± 0.00002
712-1	1490.5	78°54.94'	6°46.04'	-9.11	18.441	15.610	38.333	753.5	in progress
715-3	1480.5	79°11.98'	6°15.24'	-10.22	18.472	15.615	38.357	1828.98	0.71020
716-2	1253.9	79°14.11'	7°13.26	insufficient Nd	18.400	15.608	38.304	1786.95	0.71144
718-1	1334.9	79°42.92'	5°56.52'	insufficient Nd	18.481	15.609	38.353	1020.63	0.71174
723-1	1350.7	79°9.66'	5°20.27'	-9.69	18.457	15.616	38.341	3093.57	in progress
725-2	1960	80°57.00'	11°19.37'	-9.23	18.573	15.618	38.493	2075.09	in progress

Table 6.3: Measured radiogenic isotope data of downcore samples from station 712. For the age of the core top sample we apply the year of core retrieval 2007.

Core site MSM5/5	Depth, cm	Cal. age, yr BP/ Age, yr AD*	ε_{Nd} (2σ) ± 0.28	$^{206}Pb/^{204}Pb$ (2σ) ± 0.0075	$^{207}Pb/^{204}Pb$ (2σ) ± 0.0101,	$^{208}Pb/^{204}Pb$ (2σ) ± 0.0326	conc. Pb	$^{86}Sr/^{87}Sr$ (2σ) ±0.00002
712-1 (box core)	core top	bomb radiocarbon >1960 AD (-57/2007*)	-9.11	18.441	15.610	38.333	753.5	in progress
	0.25	-48/1998*	insufficient Nd	18.461	15.619	38.350	1425.53	0.71024
	2.75	40/1910*	-10.15	18.444	15.617	38.335	2484.8	in progress
	5.25	128/1822*	insufficient Nd	18.573	15.628	38.513	334.3	in progress
	10.25	305/1645*	-9.20	18.787	15.637	38.726	265.31	in progress
	15.25	492/1458*	-8.98	18.899	15.630	38.793	176.43	0.71023
	20.25	769/1181*	-8.82	18.952	15.641	38.867	137.16	in progress
	25.25	1027/923*	-8.85	19.009	15.642	38.901	150.72	in progress
	30.25	1278/672*	-8.90	19.013	15.640	38.908	171.67	in progress
	35.75	1559/391*	insufficient Nd	19.039	15.649	38.950	66.39	0.71011
	40.25	1789/161*	-9.04	19.064	15.664	39.001	139.31	in progress
712-2 kastenlot core)	52.5	2810	-10.01	19.149	15.663	39.041	170.26	in progress
	62.5	3352	-9.45	19.100	15.654	38.994	171.74	in progress
	76.5	4167	-10.08	19.127	15.654	39.00 4	175.19	in progress
	95.5	5252	-9.73[3]	19.150[2]	15.657	39.013	175.92	0.71006
	111	5849	-10.44	19.165	15.662	39.024	278.15	in progress
	120	6195	-10.48	19.165	15.663	39.024	274.98	in progress
	186	8141	-10.09	19.212	15.670	39.071	191.83	0.70996
	201	8534	-10.58	19.135	15.652	38.975	210.65	in progress

6.6.2. Lead isotopes

Measured core top sediments from the eastern Fram Strait report less radiogenic $^{206}Pb/^{204}Pb$ values around 18.4 (Table 6.2, Fig. 6.4a). The $^{206}Pb/^{204}Pb$ composition of the eastern Fram Strait stations are in line with the range of anthropogenic $^{206}Pb/^{204}Pb$ values reported for recent Western European sources (Véron and Church, 1997) and for the Greenland Sea and Eurasian basin (17.75 to 18.38; Gobeil et al., 2001). The core top sample from station 725-2 north of Svalbard reveals slightly more radiogenic values near 18.6 which might indicate a stronger dilution of anthropogenic lead with natural Pb within the bioturbated mixed-layer (Hamelin et al., 1990) and an associated older age of the core top sample at site 725-2.

All three lead isotope data sets of the core record reveal a decreasing trend since ca 8.5 cal ka BP (Fig. 6.4b). Prior to 1.0 cal ka BP, $^{206}Pb/^{204}Pb$ data exceed the pre-anthropogenic value suggested by Gobeil et al. (2001) (Fig. 6.4b) and must therefore derive from a different source. The shift to less radiogenic values (from 15.664 to 15.649) around ca 1.6 cal ka BP is rather abrupt in the $^{207}Pb/^{204}Pb$ record compared to the more gradual decrease in the $^{206}Pb/^{204}Pb$ and $^{208}Pb/^{204}Pb$ data.

A stronger shift to less radiogenic lead isotope data is found at ca 1.0 cal ka BP and probably marks the mixing with anthropogenic-derived, less radiogenic lead within the uppermost sediment layer affected by bioturbation. From ca 1.1 cal ka BP, $^{206}Pb/^{204}Pb$ isotope values continuously decreased towards significantly less radiogenic values around 18.4. These values are in line with the measured core top data in the Fram Strait as well as core top data obtained from sediment leachates in the Arctic Ocean (Gobeil et al., 2001), both reflecting the input of anthropogenic lead. Given that the anthropogenic input started about 150 years ago, on a core depth of 6 cm, the decrease in $^{206}Pb/^{204}Pb$ and other Pb isotope ratios (Fig. 6.4b) clearly reflects a bioturbation mixing signal within at least the uppermost ca 15 cm. We note that our results agree with measurements of $^{206}Pb/^{204}Pb$ isotope composition from a sediment core from the same site (JM06-WP-04-MC, 78°54'N, 6°46'E) where a gradient between less radiogenic anthropogenic (18.483) and higher radiogenic $^{206}Pb/^{204}Pb$ (18.930) was indicated within the uppermost ca 20 cm (Carignan et al., 2008).

The contamination of the sediment leachates in both core top and downcore samples with relatively young, anthropogenic lead can furthermore be used to confirm the successful extraction of a true seawater Pb signal from ferromanganese coatings (Haley et al., 2008).

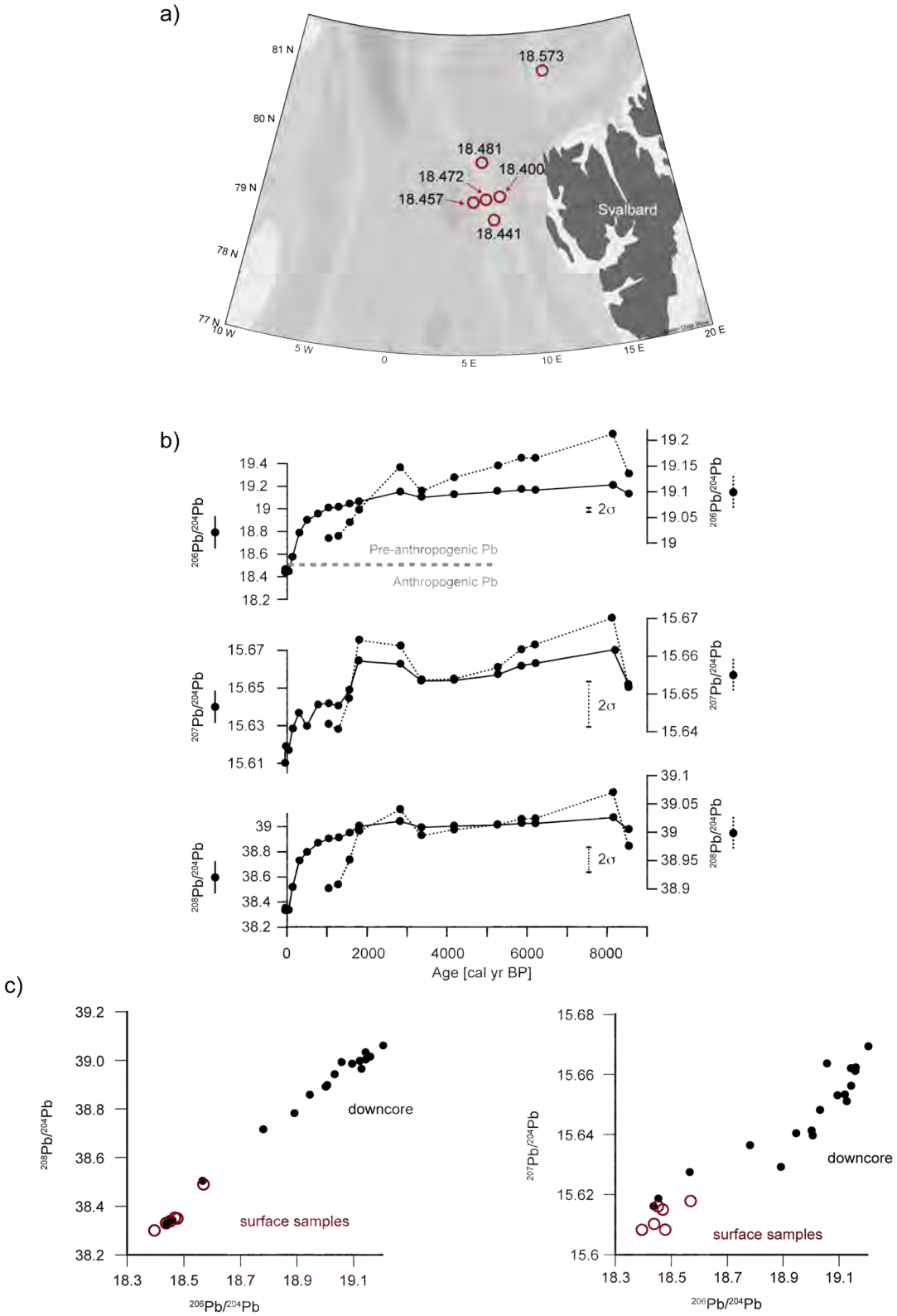

Fig. 6.4: Lead isotope signatures in the eastern Fram Strait. **a)** $^{206}Pb/^{204}Pb$ isotope values of core top samples on the West Spitsbergen continental margin. **b)** Downcore variations of $^{206}Pb/^{204}Pb$, $^{207}Pb/^{204}Pb$, and $^{208}Pb/^{204}Pb$ from site 712. Black solid (stippled) lines show variations with (without) bioturbation mixing. 2σ is shown for the data record without bioturbation effects. Grey stippled line marks assumed pre-anthropogenic/anthropogenic $^{206}Pb/^{204}Pb$ isotope ranges in Fram Strait sediments. **c)** $^{208}Pb/^{204}Pb$ vs. $^{206}Pb/^{204}Pb$ and $^{207}Pb/^{204}Pb$ vs. $^{206}Pb/^{204}Pb$ ratios for core top (red, open circles) and downcore (black circles) samples.

6.7. Nd and Pb isotope data within a multiproxy context

Figures 6.5 and 6.6 show the variations of ε_{Nd} and $^{206}Pb/^{204}Pb$ values for the past ca 8.5 cal ka BP together with the most indicative proxies for surface/subsurface and bottom water conditions during the Holocene. The climatic and oceanographic development on the Western Svalbard margin during the past ca 8.5 cal ka BP is discussed in detail in chapter 5. Our proxy record reconstruction comprises the later part of the warm Early Holocene, the Mid- and the Late Holocene. The Early and Mid-Holocene both had strong Atlantic Water inflow as revealed by high portions (up to >70%) of the subpolar planktic foraminiferal species *Turborotalia quinqueloba* (Fig. 6.5b) which is indicative for Atlantic Water inflow in the eastern Fram Strait (Volkmann, 2000). After 5 cal ka BP a sudden drop in the *T. quinqueloba* percentages to <20% marks a significant weakening of the AW inflow. During the Late Holocene, high portions of the polar planktic foraminiferal species *Neogloboquadrina pachyderma* (sinistral coiling) indicate cool surface water conditions which were accompanied by gradually increasing ice-rafted debris (IRD) contents (Fig. 6.5d) pointing to increased sea ice/iceberg abundances over the site. The summer sea ice margin was thus probably located approximately above the core site. During the past ca 3 cal ka BP, a decrease in planktic $\delta^{13}C$ values (Fig. 6.5e) indicates less-ventilated subsurface waters which was probably associated with a freshening of surface waters and a correspondent migration of planktic foraminifers towards subsurface water depth (chapter 5). The freshening of surface waters was accompanied by slight increases in the portions of *T. quinqueloba* which suggests a modest strengthening of subsurface AW advection during the Late Holocene.

The benthic oxygen isotope record displays a trend to lighter $\delta^{18}O$ values until 3 cal ka BP (Fig. 6.6). Benthic oxygen isotopes are considered to mainly report variations in deep ocean temperature and global ice volume (Shackleton and Opdyke, 1973; Shackleton, 1977; Fontanier et al., 2006). They are less affected by local changes in freshwater fluxes compared to planktic $\delta^{18}O$ (Bauch et al., 2001). However, in the Svalbard region the benthic $\delta^{18}O$ composition may have been affected by high-salinity waters produced by brine rejection during winter in Storfjorden (Quadfasel et al., 1988; Schauer, 1995; Rasmussen and Thomsen, 2009) and/or at the West Spitsbergen continental shelves (Rudels et al., 2005).

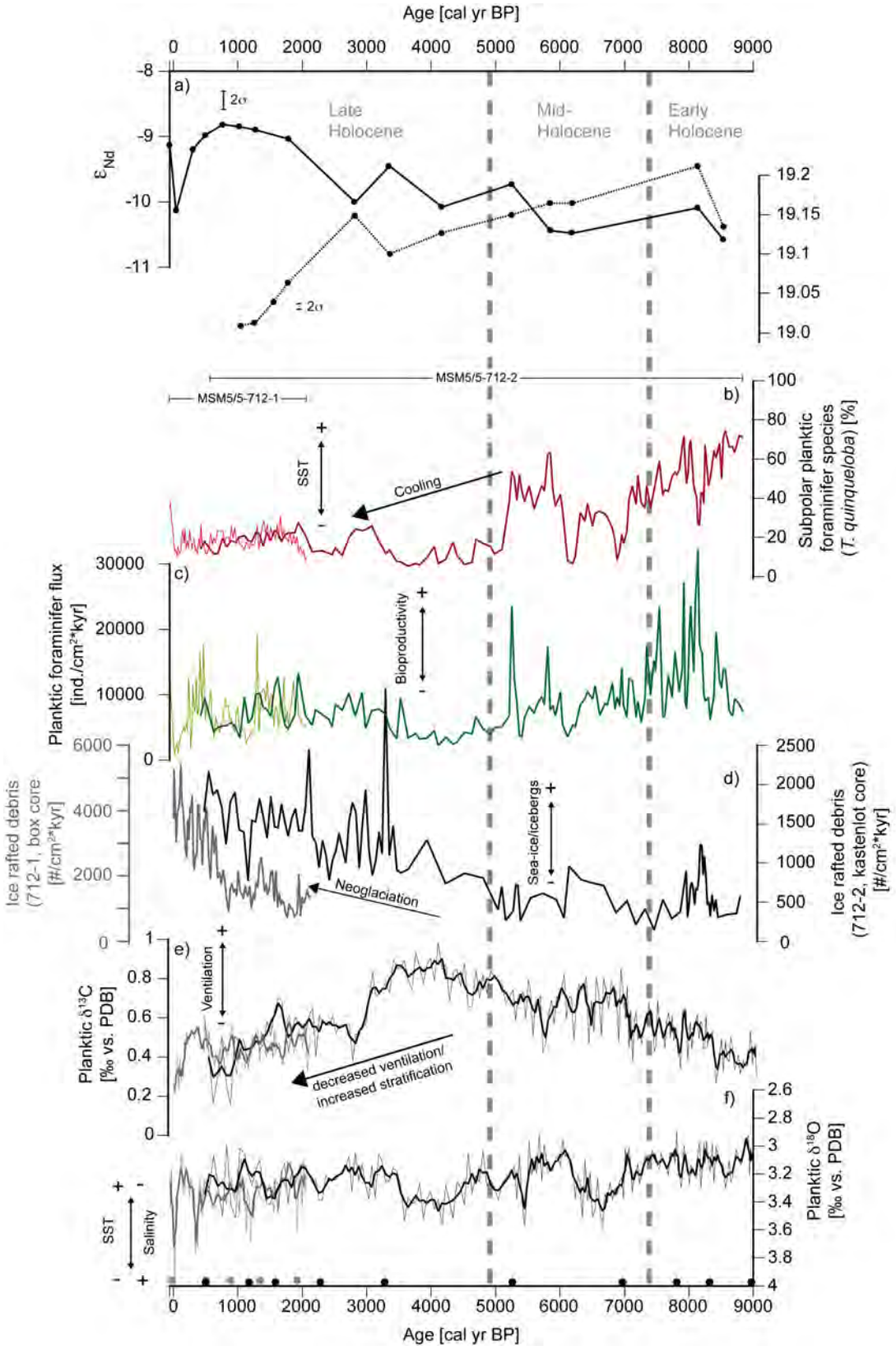

Fig. 6.5: Downcore **a)** Nd and Pb isotope variations from station MSM5/5-712. **b)** Percentages of the subpolar planktic foraminifer species *T. quinqueloba* indicative for Atlantic Water inflow. **c)** Planktic foraminifer fluxes indicative for bioproductivity. **d)** Ice-rafted debris. **e, f)** Planktic stable isotope data measured on calcareous tests of *N. pachyderma* (sin.). Dots mark AMS ^{14}C dating, black for kastenlot core (712-2) and grey for box core (712-1). Stippled grey bars show subdivision of the Holocene. Thick lines in e) and f) indicate 3-point running mean.

After ca 3 cal ka BP benthic $\delta^{18}O$ values increased simultaneously with the increasing ε_{Nd} values. Since the neodymium isotope composition of shelf sediments and the bedrock of northern Svalbard is known to be less radiogenic ($\varepsilon_{Nd} \sim -14$; Tütken et al., 2002; Andersson et al., 2008 and references therein, Fig. 6.1b), brine waters originating from the southern or western part of Svalbard would, however, lower the ε_{Nd} signal. Instead, measured ε_{Nd} values of the past ca 2 cal ka BP reveal a trend to more radiogenic values. We therefore infer the clearly pronounced increase in benthic oxygen isotope values to be indicative for cooling of bottom water masses during the Late Holocene rather than variations in bottom water salinity due to contributions of brine waters formed in Svalbard fjords which would probably have transported low radiogenic weathering material to the site. A cooling of bottom water masses is furthermore in line with the increased abundances of sea ice/ice bergs during the Late Holocene indicated by higher IRD contents (chapter 5) and increased abundances of the sea ice proxy IP25 carried out on sediments from site 712 (Müller et al., submitted). In summary, the shift to radiogenic ε_{Nd} values since the past 3 ka corresponds to cooler bottom and surface waters, increased sea ice abundances as well as to a modest strengthening of AW advection at subsurface water depth.

The assumed bioturbation likely has influenced both the lead and neodymium isotope data. Apart from the contaminant Pb isotope values within the uppermost sediment layer affected by bioturbation, the lead isotope data cannot clearly be related to the multitude of proxy data shown in figures 6.5 and 6.6. Winter et al. (1997) and references therein have reported present-day average $^{206}Pb/^{204}Pb$ isotope composition for the Caledonian Orogenic Belts of Greenland Scotland, Ireland, and Norway, and of which Svalbard also is a product (Harland and Gayer, 1972), ranging between 18.5 and 19.1 (Fig. 6.1b). Thus, during the Early and Mid-Holocene the inflowing North Atlantic Drift Waters may be imprinted by radiogenic $^{206}Pb/^{204}Pb$ values predominantly associated with input weathering material from the Western Svalbard continental margin. However, radiogenic $^{206}Pb/^{204}Pb$ values up to 19.2 even exceed the range of 18.5 and 19.1 suggested by Winter et al. (1997). It has been shown that Pb released by acid leaching of fresh granitoids is more radiogenic than acid-leached Pb from older material (Erel et al., 1994). Accordingly, Harlavan et al. (1998) suggested a linkage of freshly weathered soil material on glacial moraines (both acid leachates and completely dissolved soil material) and higher radiogenic lead isotope compositions whereas older soil material revealed lower radiogenic lead isotope values. During the warmer and probably wetter climate of the Early and Mid-Holocene periods on Svalbard (e.g., Svendsen and Mangerud, 1997) chemical weathering processes were likely increased and provided higher abundances of fresh, higher radiogenic soil material. Part of this weathering material was probably released into the Svalbard fjords by glacial

and riverine transport and may therefore also account for the relatively radiogenic $^{206}Pb/^{204}Pb$ during the Early Holocene phase.

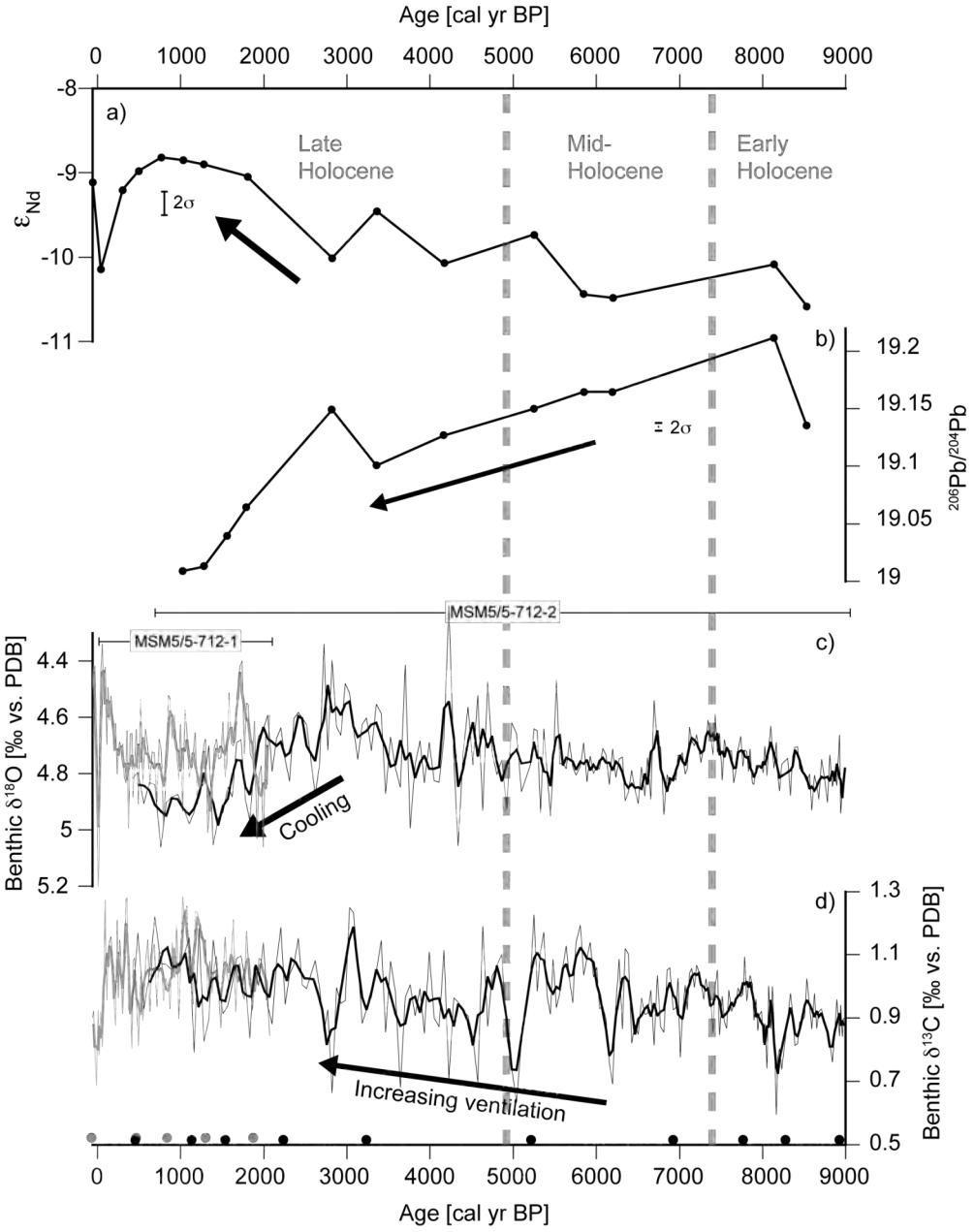

Fig. 6.6: a) Downcore Nd and **b)** $^{206}Pb/^{204}Pb$ isotope variations from station MSM5/5-712 along with benthic **c)** oxygen and **d)** carbon isotope records retrieved from Kastenlot core MSM5/5-712-2 (black) and from box core MSM5/5-712-1 (grey). Thick lines in (c) and (d) indicate 3-point running mean. Benthic stable isotope data were measured on calcareous tests of the epibenthic foraminifer species *Cibicidoides wuellerstorfi*. Grey bars indicate approximate subdivisions of the Holocene period. Black (MSM-712-2) and grey (MSM5/5-71-1) dots represent AMS radiocarbon datings (chapters 3 and 5).

6.8. Discussion

6.8.1. Pathways of anthropogenic lead to the eastern Fram Strait

Since atmospheric fluxes of Pb to the Arctic are low (Hong et al., 1994; Akeredolu et al., 1994) efficient delivery of contaminant Pb to polar basins is assumed to rather occur by ocean transport (Gobeil et al., 2001). Gobeil et al. (2001) considered two possible pathways of contaminant lead to be transported to the Arctic Basins and the Fram Strait. Atlantic Water inflow to the Arctic Ocean via Fram Strait and the Barents Sea may have transported anthropogenic lead produced by radionuclides from European nuclear fuel reprocessing plants discharged to the sea (Gobeil et al., 2001, and references therein). In contrast, export of anthropogenic Pb produced by eastern European or Russian sources from the Laptev Sea toward the Greenland Sea may have been transported via the Transpolar Drift (TPD) stream either as particulate Pb on sea ice or dissolved in water, i.e., in the contaminated sea ice as such (Gobeil et al., 2001). Both pathways may also account for the unradiogenic lead isotope composition of the presented core top stations in the eastern Fram Strait which are directly located under the AW inflow which may have imprinted the underlying sediments with the anthropogenic lead signature. It appears also possible that anthropogenic lead was transported to the eastern Fram Strait across the Arctic by sea ice since presented stations are located in the marginal ice zone (Hebbeln and Wefer, 1991) where large amounts of ice-rafted material transported across the Arctic by the TPD are released into the ocean (Pfirman et al., 1997). The possible impact of ice-rafted material to the radiogenic isotope compositions in the eastern Fram Strait is further discussed in section 6.8.2.3.

6.8.2. Deepwater inflow to the eastern Fram Strait since ca 8.5 ka

The interval between 8.5 and 2.8 cal ka BP reveals less radiogenic ε_{Nd} values (-10.6 to -10.0), similar to the seawater ε_{Nd} signatures of present-day deep waters in the Nordic Seas (ε_{Nd}~-10.5 to -10.8; Piepgras and Wasserburg, 1987; Lacan and Jeandel, 2004b). Accordingly, during the Early to Mid-Holocene, deepwater originating from the Norwegian Sea probably dominated the deeper waters on the West Spitsbergen continental margin.

The reasons for the more radiogenic ε_{Nd} values (-8.8 to -9.1) after ca 2.8 cal ka BP appear more complex with respect to a Late Holocene change of both surface and bottom water conditions. In the following, we provide three hypotheses for possible causes of the considerable shift in neodymium isotope values in the Late Holocene.

6.8.2.1. Hypothesis 1: Boundary exchange with basaltic formations in the Nordic Seas

Lacan and Jeandel (2005) showed that boundary exchange processes (Fig. 6.7b) along the continental margins of both granitic and basaltic lithology could explain the neodymium isotope composition, in particular of water masses in the Nordic Seas (Fig. 6.7a). Today, boundary exchange with the highly radiogenic (ε_{Nd} values of ~+7; Lacan and Jeandel, 2004b) basaltic formations of the islands of Iceland, Jan Mayen, and Faroe at the margins of both the Denmark Strait and the Norwegian Basin is a major process that impacts the Nd isotope signature of Denmark Strait Overflow Waters (DSOW; ε_{Nd} -8.4±1.4; Lacan and Jeandel, 2004a), the Iceland-Scotland Overflow Waters (ISOW; ε_{Nd} -11 and -9; Lacan and Jeandel, 2004b), and the waters in the Faroe Shetland channel (ε_{Nd} up to -7.7; Piepgras and Wasserburg, 1987 and ε_{Nd} -8.2±0.6; Lacan and Jeandel, 2004b; Fig. 6.7a). Since a part of the DSOW is too dense to cross the 620 m deep sill (Rudels et al., 2005) it continues eastward north of Iceland, in deeper waters of the East Iceland Current, and eventually flows south through the deeper (840 m) Faroe Shetland channel (Rudels et al., 2005). Lacan and Jeandel (2004b) noted a significant and progressive increase of the neodymium isotope composition along the pathway of the NSDW from the Greenland Sea and into the Norwegian Basin (Rudels et al., 1986). Part of the newly formed Greenland Sea Deep Water (containing outflow waters from western Fram Strait, in particular EBDW and CBDW, as well as older NSDW; Schlichtholz and Houssais, 1999) that is not overflowing the sills is assumed to flow eastward into the Norwegian Sea as newly formed NSDW which then returns into the Arctic Ocean (Rudels et al., 1986). This NSDW most probably joins the deeper layers of the WSC flowing below the Atlantic core layer in the eastern Fram Strait (Fig. 6.7a). On its way towards the Arctic Ocean, NSDW that had acquired a radiogenic neodymium isotope signature through boundary exchange processes, may thus pass the study site in the eastern Fram Strait where its seawater-derived precipitates leave a higher radiogenic signature in ferromanganese coatings of the bottom sediments.

We consider this scenario to also possibly have caused the shift to more radiogenic Nd isotope values found after ca 2.8 cal ka BP. Enhanced boundary exchange of NSDW with younger basaltic formations from the Nordic Seas margins may have caused an enhanced uptake of highly radiogenic ε_{Nd} signatures during the Late Holocene. A shift to more radiogenic ε_{Nd} values between 2 and 3 cal ka BP in bottom waters of Fram Strait coincides with increasing benthic oxygen isotope values which imply cooler bottom water conditions for the Late Holocene compared to Early and Mid-Holocene conditions (Fig. 6.4). Since the modern-type east-west temperature gradients in the Nordic Seas only established during the later Holocene (Bauch et al., 2001), a strengthening of the meridional overturning circulation during the Neoglacial phase might have resulted in an increased transport of deeper water masses from the

Nordic Seas to the eastern Fram Strait. A plausible link between a cooling of bottom water and increased boundary exchange between 2 and 3 cal ka BP remains, however, elusive and cannot be solved by the present data sets. We therefore consider this hypothesis to be the one least likely.

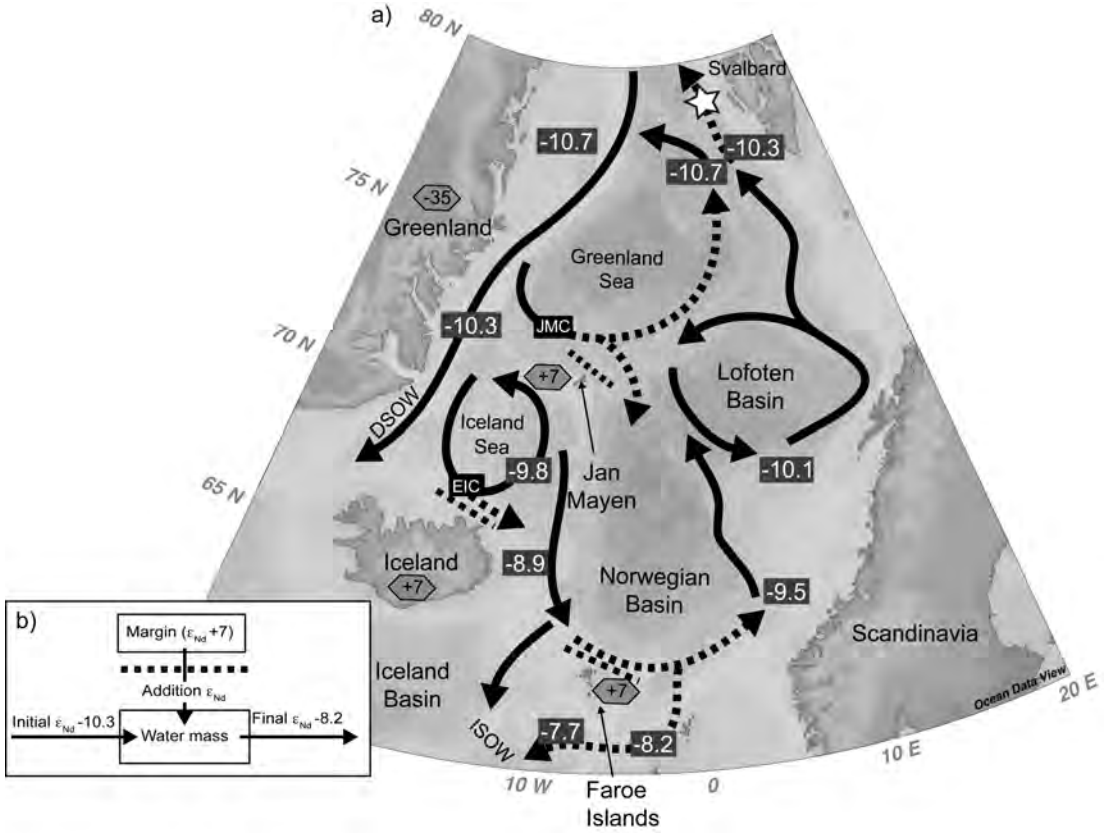

Fig. 6.7: a) Present-day current pattern and seawater ε_{Nd} signatures (numbers in squares) in the Nordic Seas (after Lacan and Jeandel, 2004b, and references therein) versus ε_{Nd} signature of basaltic formations of Iceland, Jan Mayen and Faroe (numbers in hexagons; Lacan and Jeandel, 2004a, b). Stippled lines mark possible margin/ocean contact areas. Stippled arrows indicate potential transport pathways of ε_{Nd}-modified NSDW to the study site (white star). **b)** Simplified box model for boundary exchange (only from margin to ocean) after Lacan and Jeandel (2005). Also indicated are the surface currents East Iceland Current (EIC) and Jan Mayen Current (JMC).

6.8.2.2. Hypothesis 2: Contribution of Canadian Basin Deep Water

Present-day Canadian Basin Deep Water (CBDW) reveal radiogenic neodymium isotope compositions of -7 to -9 at all water depths in the Canadian Basin (Porcelli et al., 2009), which have been ascribed to the inflow of Pacific Water with high radiogenic ε_{Nd} signatures through Bering Strait (-5; Piepgras and Jacobsen, 1988; Dahlqvist et al., 2007; Amakawa et al., 2009). Today, Pacific Water inflow through Bering Strait has been estimated at ~0.83 Sv (Roach et al., 1995). Riverine or Pacific water input as well as boundary exchange with sediments along the shelf of the Canadian archipelago may in addition contribute to the radiogenic ε_{Nd} values in CBDW (Andersson et al., 2008; Porcelli et al., 2009).

Fig. 6.8: Schematic illustration of proposed inflow of Canadian Basin Deep Water (blue arrow) at 2000 m water depth into Fram Strait after Björk et al. (2010). Small solid blue arrow marks possible recirculation of CBDW in the Fram Strait and back into the Eurasian Basin along the Gakkel Ridge (Björk et al., 2010). Also shown are present-day seawater ε_{Nd} signatures (grey squares) in the Fram Strait (Lacan and Jeandel, 2004b; Andersson et al., 2008), in the Canada Basin and in the Bering Strait (Dahlqvist et al., 2007; Porcelli et al., 2009) as well as average ε_{Nd} values in sediment leachates of core top samples (white ovals) in the eastern Fram Strait (this study). Small stippled blue arrow with question mark suggest a possible additional pathway of CBDW north of Fram Strait where a seawater-derived radiogenic ε_{Nd} value of -9.2 was measured in ferromanganese coatings of core top sample 725-2 (Table 6.2).

In the western Fram Strait, the major outflow area of Arctic Ocean sea ice and freshwater, Andersson et al. (2008) found highly radiogenic ε_{Nd} values (-9.8) in the entire water column (Figs. 6.2, 6.8). This may either have been caused by direct transport of highly radiogenic Nd-bearing Pacific Ocean waters, or by boundary exchange with sediments along the shelf of the Canadian archipelago (Andersson et al., 2008). Canadian Basin Deep Water (CBDW) has been traced in surface waters of western Fram Strait as far south as Denmark Strait (Jones et al., 2003) and in deep waters of 2000 m depth across the Arctic Ocean and in the Fram Strait (Björk et al., 2010). The authors supposed that on its way across the Arctic basins CBDW continues along the ridge towards Greenland and further along its northernmost continental slope (Fig. 6.8). A significant part of the CBDW is assumed to blend into the deeper Arctic outflow waters in western Fram Strait. Furthermore, Björk et al. (2010) proposed a possible north-eastward turn of CBDW north of 80°N on the western slope of Yermak Plateau hereby following the topography

of northern Fram Strait. The CBDW is then assumed to continue northward into the Arctic Ocean where it may flow along the Gakkel Ridge. This assumed return position of the CBDW north of 80°N has not been verified yet by measurements. Part of the CBDW-bearing deep Arctic outflow waters may thus either spread in the entire northern part of Fram Strait or return further south in the Fram Strait towards the Arctic Ocean and may thus also arrive at our study site at ca 78.5°N, hereby leaving its radiogenic imprint on the underlying sediments in ca 1500 m water depth (Fig. 6.8). Figure 6.8 also shows a potential pathway of the CBDW to pass site 725-2 north of Fram Strait at 89.50°N, 11.2°E where sediment leachates (2000 m water depth) revealed radiogenic ε_{Nd} values (-9.23). Less radiogenic neodymium isotope compositions found in seawater samples north of Svalbard (Andersson et al., 2008) would not contradict the radiogenic imprint of CBDW to deeper waters since those water samples from 100 and 450 m water depth (see also Fig. 6.1) are under the present-day influence of Atlantic Water with ε_{Nd} signatures of ~ -10.5 (Andersson et al., 2008).

A contribution of CBDW would serve as an explanation for the relatively radiogenic Nd isotope signatures of the core top samples (between -8.8 to -9.1) compared to the less radiogenic values of about -10.5 influenced by North Atlantic Drift waters found further south in the Nordic Seas and Fram Strait (e.g., Lacan and Jeandel, 2004b; Andersson et al., 2008, and references therein). It may also apply for past variations of ε_{Nd} values revealed by the downcore record presented here. While during the Early and Mid-Holocene intervals strong inflow of AW and NSDW accounted for relatively less radiogenic ε_{Nd} values (~ -10), enhanced inflow of CBDW during the past ca 3 cal ka BP may be the reason for the shift to radiogenic ε_{Nd} values. A reason for increased contribution of CBDW to Arctic bottom water outflow through Fram Strait after 2.8 cal ka BP remains, however, unclear but may be linked to the onset of the modern circulation pattern (chapter 5).

6.8.2.3. Hypothesis 3: Radiogenic isotope signatures in sea ice sediments

Seasonal sea ice formed on the shallow Siberian and North American shelves (Darby and Bischof, 2004) pick up lithic grains which are carried to the Fram Strait by the two major sea ice drift processes, the Transpolar Drift (TPD) and the Beaufort Gyre (BG), until released at the sea ice margin upon melting (Pfirman et al., 1989). In particular, a large part of sea ice formed on the Kara and Laptev Sea shelves is transported by the Siberian branch of the TPD stream across the Eurasian Basin and exits the Arctic Ocean through Fram Strait, hereby joining the East Greenland Current (Pfirman et al., 1989, 1997; Fig. 6.9). Fram Strait thus acts as an ablation area for Arctic sea ice (e.g., Kwok and Rothrock, 1999; Darby and Bischof, 2004; Cámara-Mor et al., 2010) where the warm Atlantic Water causes melting and release of sea ice sediments year round

in the marginal ice zone of Fram Strait (e.g., Hebbeln and Wefer, 1991; Dethleff and Kuhlman, 2010).

Our study area is located in the zone of the widely fluctuating summer sea ice margin in the eastern Fram Strait (see also chapters 3 and 5) where warm Atlantic Water encounters cold surface waters and Arctic sea ice. Highest particle fluxes occur in the direct vicinity of the sea ice margin (Hebbeln and Wefer, 1991) and ice-rafted material sinks down to accumulate and mix with current-transported bottom sediments. Entrainment of sediments by sea ice mainly occurs along the shallow continental margins and is largely restricted to silt and clay-sized material, rarely containing grains larger than 0.1 mm (Nürnberg et al., 1994; Lisitzin, 2002; Darby, 2003). This is consistent with findings by Dethleff and Kuhlmann (2010) who showed that Arctic sea ice that is entering Fram Strait particularly delivers fine-grained ice-rafted material. Accordingly, the sortable silt mean grain size fraction of sediments from the Yermak Plateau contains a certain amount of fine-grained ice-rafted material (Hass, 2002). In our record the coarse sediment fraction (250-1000 μm) accounts only for at maximum 1.7 weight% of the bulk sediment (Fig. 6.9b) whereas the major part of sea ice sediments is considered to be fine-grained. In the following, we will therefore use the term ‚ice-rafted fines (IRF)' for this fraction of fine-grained sediments, which has been transported to the eastern Fram Strait by sea ice.

High sedimentation rates of 20 to 30 cm/1000 years found in our record within the past ca 3,000 years are most likely linked to increased release of sea ice sediments associated with increased sea ice abundance in the Fram Strait during the Late Holocene Neoglacial trend (chapters 3 and 5), in response to post-glacial sea level rise and initiation of modern-scale sea ice production (Dyke et al., 1997; Bauch et al., 1999; Prange and Lohmann, 2003). Bacon et al. (1976) have determined the turnover time for particles in the mixed layer of the Atlantic Ocean to be ca 0.1 year. During sinking, the ice-rafted fine material may have been exposed to the local seawater for only a relatively short time which may not have been sufficient to acquire the particular neodymium isotope composition of the surrounding bottom water layer. To our knowledge, there have been no quantitative estimates on the duration of precipitation of ferromanganese coatings on marine sediments yet.

Fig. 6.9 (next page): a) Sea ice drift from Kara Sea towards eastern Fram Strait (black arrow) after Pfirman et al. (1997). Included are ε_{Nd} values from the Kara Sea (seawater: Porcelli et al., 2009; sediment leachates: Filippova, 2011) and its source areas in Western Siberia (Edwards and Wasserburg, 1985; Sharma et al., 1992). Also shown are ε_{Nd} values from sea ice sediments (detrital fraction) in the Barents Sea (Tütken et al., 2002) and the Fram Strait (seawater: Andersson et al., 2008; sediment leachates: this study). Grey squares = seawater, white ovals = sediment leachates, white triangles = sea ice sediments; light grey hexagon = source rock material. **b)** Percentages of the sand fraction 250-1000 μm during the past ca 9,000 years from core 712. **c)** The main sea ice drift streams of the Arctic Ocean. Grey stippled line marks section shown in a).

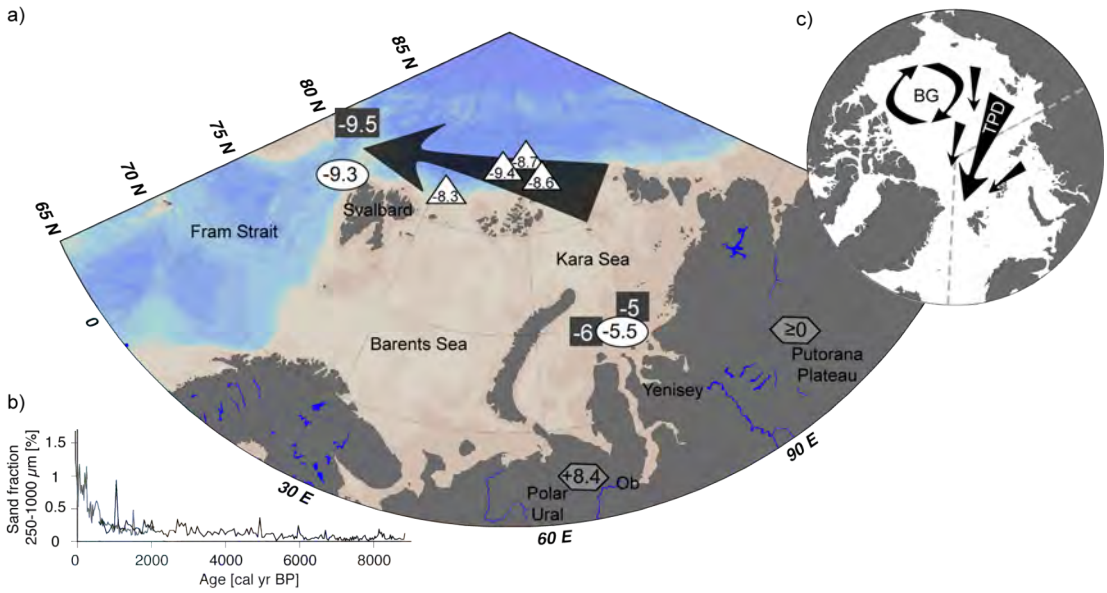

Although part of the ice-rafted material is assumed to arrive from Svalbard glaciers (Werner et al., 2011) the majority of the IRF was probably picked up by sea ice on the Siberian shelves and subsequently transported by the Transpolar Drift. We therefore consider that the IRF grains acquired their absorbed seawater ε_{Nd} signature elsewhere in the Arctic shelf seas. While low seawater Nd isotope composition in the Mackenzie river mouth (-13; Porcelli et al., 2009) rules out the Beaufort Gyre as a major source for ice-rafted material, significantly more radiogenic ε_{Nd} compositions have been found on the Siberian shelves. In particular, riverine input of the Yenisey and Ob Rivers contribute to high radiogenic neodymium isotope composition in the Kara Sea seawater (ε_{Nd} ~ -5.2 and -6.1, respectively; Porcelli et al., 2009) and surface sediment leachates (ε_{Nd} ~ -5.5; Fillipova, 2011; Fig. 6.9). The riverine discharge of Yenisey and Ob into the Kara Sea is almost twice as large as the discharge of the Lena River into the Laptev Sea (RIMS data) and thus transports large amounts of particulate matter onto the shelves. By means of granulometric and mineralogical analyses, Dethleff and Kuhlmann (2010) showed that sea ice sediments released in the eastern part of Fram Strait in particular had been incorporated by sea ice on the Kara Sea and western Laptev Sea. Possible sources of radiogenic sediment material, which had possibly imprinted waters of the Ob and Yenisey Rivers that subsequently discharged into the Kara Sea, were discussed by Filippova (2011) and include the Siberian Putorana basalts (e.g., Schoster et al., 2000; Stein et al., 2004) with radiogenic ε_{Nd} values ≥ 0 (Sharma et al., 1992) and the Polar Ural Mountains (ε_{Nd} ~+8.4; Edwards and Wasserburg, 1985). River waters probably acquired their radiogenic ε_{Nd} values through boundary exchange with adjacent rock material while flowing through and/or with suspended matter originating from a radiogenic source area which was transported by the Ob and Yenisey Rivers onto the Kara Sea shelf (Stein et al., 2004; see also Filippova, 2011). The suspended matter may have been entrained by sea ice and transported towards Fram Strait by the TPD. This is corroborated by the reported sea ice

pathway from the Kara Sea to the eastern Fram Strait by Pfirman et al. (1997) and coincides with radiogenic neodymium isotope composition of -9.4 to -8.3 in the detrital fraction of sea ice sediments en route in the Barents Sea (Tütken et al., 2002; Fig. 6.9). River waters and suspended matter are probably impacted by the same radiogenic source within the catchment areas of Ob and Yenisey Rivers. Local contamination by a 'seawater signal' in authigenic oxyhydroxides has also been found in other studies such as by Bayon et al. (2004) who reported on preformed ferromanganese oxyhydroxide coatings associated with Congo River material in the Angola Basin. Andersson et al. (2008) noted that neodymium which derived from river water input can also be transported offshore and at a later stage influence the isotopic composition of the deeper waters in the Arctic. However, for the shallow Siberian shelves we rather assume a sea ice-related transport of radiogenic ε_{Nd} values to the Arctic Ocean and the Fram Strait. Sea ice transport may also provide an alternative transport mechanism for the high neodymium ratios found near the North Pole during glacial periods after 2 Myr (Haley et al., 2007).

The third hypothesis matches well with the revealed proxy reconstruction discussed in chapter 5 and above and is thus our favoured explanation. A significant contribution of ice-rafted material to Arctic Ocean and Fram Strait sediments has been proposed previously by e.g., Eisenhauer et al. (1999). Increased contribution of sea ice sediments derived from the Siberian shelves and transported by the Transpolar Drift to the eastern Fram Strait since the Late Holocene would not only serve as an explanation for a shift of ε_{Nd} during the Late Holocene but may also explain the low anthropogenic-derived $^{206}Pb/^{204}Pb$ compositions in core top and downcore sediments affected by bioturbation mixing. The unradiogenic anthropogenic lead signature thus may have been produced by eastern European or Russian sources and transported via the Transpolar Drift (TPD) to the Fram Strait as suggested by Gobeil et al. (2001).

Prior to the significant shift at 2.8 cal ka BP, two outliers of higher radiogenic ε_{Nd} values at 5.2 and 3.3 cal ka BP (-9.7 and -9.5, respectively) may correspond to earlier short-term advances of the sea ice margin to the site and associated release of sea ice transported material during generally cooler conditions since ca 5 cal ka BP in the eastern Fram Strait (chapter 5).

The less radiogenic ε_{Nd} signature (-10.15) in the sample from 2.75 cm (Figs. 6.5, 6.10) clearly differs from radiogenic values (-9.1 to -8.8) in the uppermost ca 40 cm of the studied core section. Although the overall bioturbation mixing depth covers at least the uppermost ca 15 cm of the sediment core as was shown by anthropogenic lead impact (see above), the less radiogenic ε_{Nd} signature at 2.75 cm did apparently not affect adjacent samples at 0 and 10.25 cm. Thus, we assume that bioturbation mixing may not have been effective enough to completely homogenize the bioturbated sediment layer. Although the colour scan data (Fig. 6.10b-d) indicate a more

reddish sediment layer, anoxic conditions and an associated ascent of pore water and dissolution of ferromanganese oxyhydroxides are unlikely to have occurred since it would have similarly affected adjacent sediment samples. However, future studies of adjacent sediment samples are needed to confirm the less radiogenic ε_{Nd} value at 2.75 cm core depth.

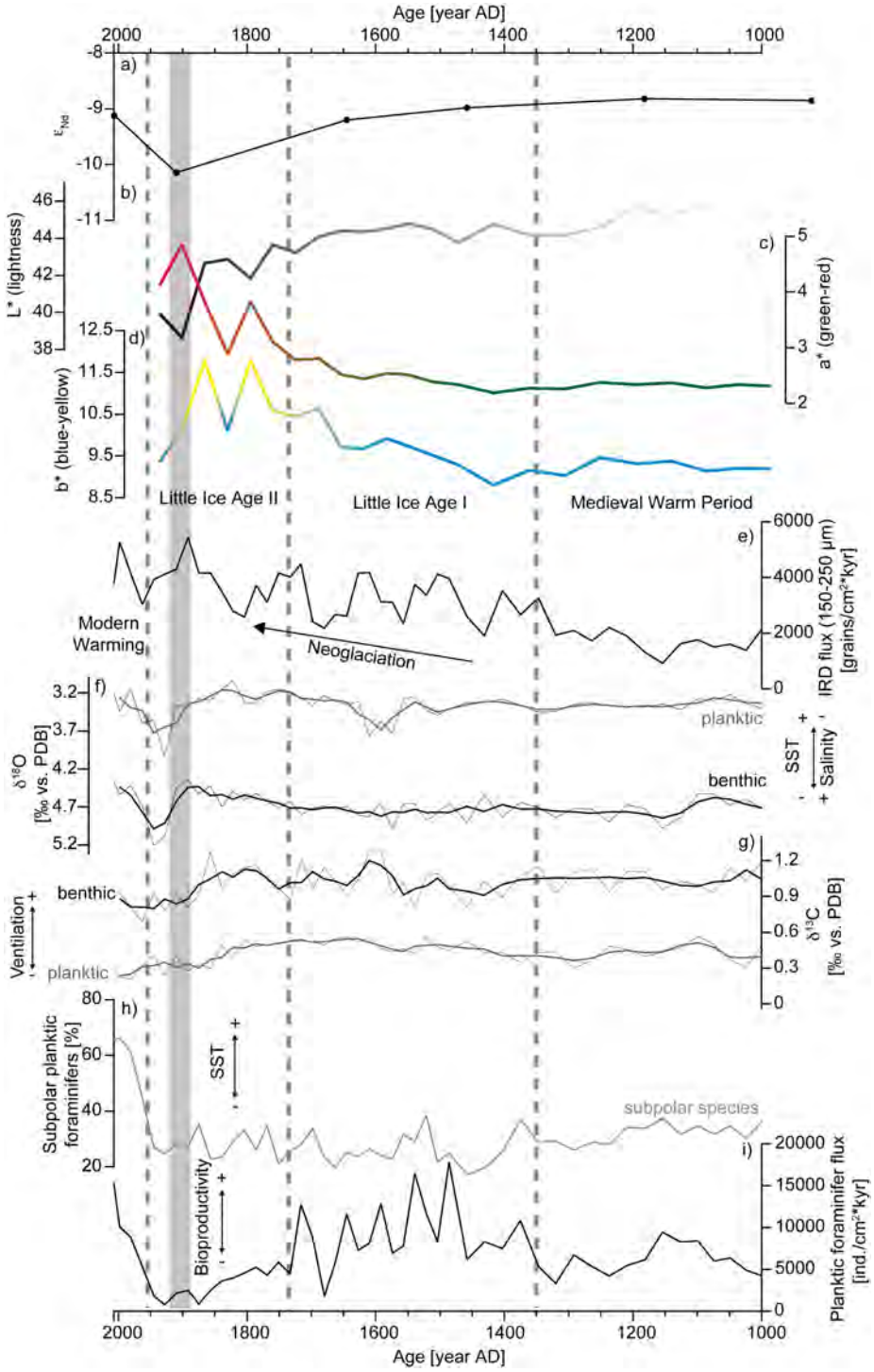

Fig. 6.10: Multiproxy record from station MSM5/5-712-1 (box core) for the last ca 1000 years. **a)** Downcore Nd isotope variations. **b-d)** Colour scan data. The spherical L*a*b* colour space was used with lightness L*, red-green chromaticity a* and blue-yellow chromaticity b*. **e)** IRD fluxes **f)** Oxygen and **g)** carbon isotope records from calcareous foraminifer tests of *N. pachyderma* (sin.) (planktic) and *C. wuellerstorfi* (benthic). **h)** Percentages of subpolar planktic foraminifers. **i)** Planktic foraminifer flux as an indicator for paleoproductivity. The grey solid bar marks the outlying sample at 2.75 cm. Grey dashed lines indicate climate intervals discussed in Spielhagen et al. (2011) and Werner et al. (2011). Note the age scale is given in years AD.

Assuming this value is correct would further support the third hypothesis. The measured ε_{Nd} signal of -10.15 in the sample from 2.75 cm displays a signature found in the Nordic Seas (Lacan and Jeandel, 2004b; Andersson et al., 2008 and references therein). According to the age model (Spielhagen et al., 2011) the core depth of 2.75 cm would correspond to an age of ~1910 AD. Werner et al. (2011) have shown that very cold conditions affected surface water layers in the eastern Fram Strait well into the 20th century which were likely associated with late conditions of the Little Ice Age (LIA). Bock et al. (2005) found a major decrease of ε_{Nd} (-17) during the Little Ice Age period in the Baltic Sea, which the authors attribute to a combined effect of a negative North Atlantic Oscillation mode and decreased soil erosion caused by the reduced agricultural activity. However, the relatively unradiogenic ε_{Nd} signal of -10.15 found at site 712 may have been rather caused by inflowing AIW or NSDW. During the LIA, the sea ice margin advanced to a position south of our study site. As a consequence, the IRD particle load transported by the Arctic sea ice had been released further south. Instead of a major IRD input to bottom sediments as during most of the Late Holocene when the sea ice margin fluctuated over the study site, bottom sediments rather acquired the less radiogenic seawater ε_{Nd} by the inflowing bottom waters derived from North Atlantic Drift waters under permanent sea ice coverage during ca 1910 AD.

6.9. Conclusions

Core top samples obtained from the West Spitsbergen continental margin have been investigated for radiogenic neodymium and lead isotope compositions of authigenic early diagenetic ferromanganese oxyhydroxide coatings to calibrate the data to present-day bottom water distributions. On the basis of this calibration a Nd and Pb isotope record of bottom waters at site 712 in the eastern Fram Strait covering the past ca 8.5 cal ka BP has been established, which is compared with information from a multiproxy data set obtained from the same core (chapter 5).

Low $^{206}Pb/^{204}Pb$ values (~18.4) document an overprint of anthropogenic lead seen also in other studies from the North Atlantic and the Arctic Ocean (e.g., Gobeil et al., 2001). The downcore lead isotope data show a consistent trend to less radiogenic lead isotope compositions from ca 8.5 to 1.0 cal ka BP. Radiogenic seawater $^{206}Pb/^{204}Pb$ values of the Early and Mid-Holocene may be related to a predominant imprint of Caledonian Orogenic Belts of Greenland Scotland, and Ireland through weathering. In addition, increased chemical weathering may have accounted for more radiogenic $^{206}Pb/^{204}Pb$ ratios during the Early Holocene. Less radiogenic anthropogenic-derived $^{206}Pb/^{204}Pb$ ratios were found in the uppermost ca 15 cm of the sediment core indicating the zone of bioturbation mixing.

The neodymium isotope compositions of the surface samples consistently display a relatively radiogenic signature (~-9). Today, the Fram Strait area is primarily influenced by the inflow of North Atlantic Drift Waters and Norwegian Sea Deep Water (Schlichtholz and Houssais, 1999) mainly produced in the Nordic Seas. Neodymium isotope values from the Nordic Seas reveal a less radiogenic neodymium isotope composition (-10.5 to -10.1; Lacan and Jeandel, 2004b; Andersson et al., 2008 and references therein). A corresponding neodymium isotope composition found in the downcore record prior to 2.8 cal ka BP (-10.6 to -10.1) is thus clearly related to the dominant advection of deep waters from the Nordic Seas. After ca 2.8 cal ka BP ε_{Nd} values significantly increased to values between -9.1 and -8.8, comparable to ε_{Nd} signatures of the core top samples. Proxy data from the core site (chapter 3 and 5) indicate that the shift to higher ε_{Nd} values after ca 2.8 cal ka BP was accompanied by a cooling of surface and bottom waters as well as increased sea ice abundances.

Three hypotheses have been discussed to explain such drastic change in ε_{Nd} values. Increased boundary exchange of seawater with the basaltic formations of Jan Mayen, Iceland and Faroe, possibly related to the onset of modern AMOC since ca 3 cal ka BP, may have caused the more radiogenic imprint of the deeper waters in the eastern Fram Strait. Alternatively, increased inflow of radiogenic Canadian Basin Deep Water to the Fram Strait may have caused the radiogenic ε_{Nd} values since the Late Holocene. A third and favoured explanation considers the Fram Strait as a major ablation area for ice-rafted material entrained by Arctic sea ice delivered by the Transpolar Drift. An increase in ice-rafted fine material since ca 3 cal ka BP concurs with the shift to higher ε_{Nd} values. Increased discharge of IRF material may have led to a rapid burial and storage of the sediment material which had acquired its radiogenic ε_{Nd} values elsewhere on the Arctic shallow shelves. A potential source area for the radiogenic ε_{Nd} values in ice-rafted material is the Kara Sea shelf where seawater-derived neodymium isotope compositions of both seawater and oxyhydroxide coatings of sediment leachates reveal radiogenic values between -6 and -5 (Porcelli et al., 2009; Filippova, 2011).

Outlook

The dataset presented here will be complemented by radiogenic isotope (Nd, Pb, Sr) analyses of the detrital fraction in sediment cores from station MSM5/5-712. In addition, we will study the radiogenic isotope composition in sediment leachates and detritus of a sediment core with high-resolution Holocene coverage which is located northeast of site 712 and is thus more under the influence of the East Greenland Current. In addition, sea water samples from a transect on 79°N (bottom and surface water) obtained during cruise leg ARK-XXVI/1 onboard RV Polarstern in summer 2011 will be analysed to further validate the provided hypotheses. The given manuscript

will then be complemented with the additional data and submitted to an international peer-reviewed scientific journal.

Acknowledgements. The German Research Foundation (DFG) provided financial support of K. Werner within the Priority Programme 1266 (INTERDYNAMIC, project HOVAG). We thank Roland Stumpf, Dorothea Bauch, and Torben Struve for valuable comments and discussions. We are grateful to the science party and crew onboard RV "Maria S. Merian" during the expedition MSM5/5 for retrieving the sediment core.

References

Aagaard, K., Swift, J.H. and Carmack, E.C. (1985) Thermohaline Circulation in the Arctic Mediterranean Seas. *Journal of Geophysical Research* 90, 4833-4846.

Aagaard, K., Foldwik, A. and Hillman, S.R. (1987) The West Spitsbergen Current: Disposition and Water Mass Transformation. *Journal of Geophysical Research* 92, 3778-3784.

Aagaard, K., Fahrbach, E., Meincke, J. and Swift, J.H. (1991) Saline Outflow From the Arctic Ocean: Its Contribution to the Deep Waters of the Greenland, Norwegian, and Iceland Seas. *Journal of Geophysical Research* 96, 20,433-20,441.

Aagaard, K. and Carmack, E.C. (1989) The Role of Sea Ice and Other Fresh Water in the Arctic Circulation. *Journal of Geophysical Research* 94, 14,485-14,498.

Abouchami, W., Galer, S.J.G. and Koschinsky, A. (1999) Pb and Nd isotopes in NE Atlantic Fe-Mn crust: proxies for trace metal paleosources and paleocean circulation. *Geochimica et Cosmochimica Acta* 63, 1489-1505.

Albarède, F., Telouk, P., Blichert-Toft, J., Boyet, M., Agranier, A. and Nelson, B. (2004) Precise and accurate isotopic measurements using multiple-collector ICPMS. *Geochimica et Cosmochimica Acta* 68, 2725-2744.

Alleman, L.Y., Véron, A.J., Church, T.M., Flegal, A.R. and Hamelin, B. (1999) Invasion of the abyssal North Atlantic by modern anthropogenic lead. *Geophysical Research Letters* 26, 1477-1480.

Akeredolu, F.A., Barrie, L.A., Olson, M.P., Oikawa, K.K., Pacyna, J.M. and Keeler, G.J. (1994) The Flux of Anthropogenic Trace Metals into the Arctic from the Mid-latitudes in 1979/80. *Atmospheric Environment* 28, 1557-1572.

Amakawa, H., Sasaki, K. and Ebihara, M. (2009) Nd isotopic composition in the central North Pacific. *Geochimica et Cosmochimica Acta* 73, 4705-4719.

Anderson, L.G., Jones, E.P. and Rudels, B. (1999) Ventilation of the Arctic Ocean estimated by a plume entrainment model constrained by CFCs. *Journal of Geophysical Research* 104, 13423-13429.

Andersson, P.S., Porcelli, D., Frank, M., Björk, G., Dahlqvist, R. and Gustafsson, Ö. (2008) Neodymium isotopes in seawater from the Barents Sea and Fram Strait Arctic-Atlantic gateways. *Geochimica et Cosmichimica Acta* 72, 2854-2867.

Arsouze, T., Dutay, J.-C., Lacan, F. and Jeandel, C. (2009) Reconstructing the Nd oceanic cycle using a coupled dynamical-biogeochemical model. *Biogeosciences* 6, 5549-5588.

Bacon, M.P., Spencer, D.W. and Brewer, P.G. (1976) $^{210}PB/^{226}Ra$ and $^{210}Po/^{210}Pb$ disequilibria in seawater and suspended particulate matter. *Earth and Planetary Science Letters* 32, 277-296.

Barrat, J.A., Keller, F. and Amossé, J. (1996) Determination of rare earth elements in sixteen silicate reference samples by ICP-MS after Tm addition and ion exchange separation. *Geostandard Newsletter* 20, 133-139.

Bauch, D., Schlosser, P. and Fairbanks, R.G. (1995) Freshwater balance and the sources of deep and bottom waters in the Arctic Ocean inferred from the distribution of $H_2{}^{18}O$. *Progress in Oceanography* 35, 53-80.

Bauch, H.A., Kassens, H., Erlenkeuser, H., Grootes, P.M. and Thiede, J. (1999) Depositional environment of the Laptev Sea (Arctic Siberia) during the Holocene, *Boreas* 28, 194-204.

Bauch, H.A., Erlenkeuser, H., Spielhagen, R.F., Struck, U., Matthiessen, J., Thiede, J. and Heinemeier, J. (2001) A multiproxy reconstruction of the evolution of deep and surface waters in the subarctic Nordic seas over the last 30,000 yr. *Quaternary Science Reviews* 20, 659-678.

Bayon, G., German, C.R., Boella, R.M., Milton, J.A., Taylor, R.N. and Nesbitt, R.W. (2002) An improved method for extracting marine sediment fractions and its application to Sr and Nd isotopic analysis. *Chemical Geology* 187, 179-199.

Bayon, G., German, C.R., Burton, K.W., Nesbitt, R.W. and Rogers, N. (2004) Sedimentary Fe-Mn oxyhydroxides as paleoceanographic archives and the role of Aeolian flux in regulation oceanic dissolved REE. *Earth and Planetary Science Letters* 224, 477-492.

Berger, A. and Loutre, M.F. (1991) Insolation values for the Climate of the last 10 Million Years. *Quaternary Science Reviews* 10, 297-317.

Björk, G., Anderson, L.G., Jakobsson, M., Antony, D., Eriksson, B., Eriksson, P.B., Hell, B., Hjalmarsson, S., Janzen, T., Jutterström, S., Linders, J., Löwemark, L., Marcussen, C., Olsson, K.A., Rudels, B., Sellén, E. and Sølvsten, M. (2010) Flow of Canadian basin deep water in the Western Eurasian Basin of the Arctic Ocean. *Deep-Sea Research I* 57, 577-586.

Bock, B., Liebetrau, V., Eisenhauer, A., Frei, R. and Leipe, T. (2005) Nd isotope signature of Holocene Baltic Mn/Fe precipitates as monitor of climate change during the Little Ice Age. *Geochimica et Cosmichimica Acta* 69, 2253-2263.

Broecker, W.S. (1982) Ocean chemistry during glacial time. *Geochimica et Cosmichimica Acta* 46, 1689-1705.

Broecker, W.S. (1991) The Great Ocean Conveyor. *Oceanography* 4, 79-89.

Budéus, G. and Ronski, S. (2009) An Integral View of the Hydrographic Development in the Greenland Sea Over a Decade. *The Open Oceanography Journal* 3, 8-39.

Cámara-Mor, P., Masqué, P., Garcia-Orellana, J., Cochran, J.K., Mas, J.L., Chamizo, E. and Hanfland, C. (2010) Arctic Ocean sea ice drift origin derived from artificial radionuclides. *Science of the Total Environment* 408, 2249-3358.

Carignan, J., Hillaire-Marcel, C. and de Vernal, A. (2008) Arctic vs. North Atlantic water mass exchanges in Fram Strait from Pb isotopes in sediments. *Canadian Journal of Earth Sciences* 45, 1253-1263.

Cohen, A.S., O'Nions, R.K., Siegenthaler, R. and Griffin, W.L. (1988) Chronology of the pressure-temperature history recorded by a granulite terrain. *Contributions to Mineralogy and Petrology* 98, 303-311.

Crocket, K.C., Vance, D., Gutjahr, M., Foster, G.L. and Richards, D.A. (2011) Persistent Nordic deep-water overflow to the glacial North Atlantic. *Geology* 39, 515-518.

Dahlqvist, R., Andersson, P.S. and Porcelli, D. (2007) Nd isotopes in Bering Strait and Chukchi Water. *Geochimica et Cosmichimica Acta* 71, A196.

Darby, D.A. (2003) Sources of sediment found in the sea ice from the western Arctic Ocean – New insights into processes of entrainment and drift patterns. *Journal of Geophysical Research* 108(C8), 3257.

Darby, D.A. and Bischof, J.F. (2004) A Holocene record of changing Arctic Ocean ice drift analogous to the effects of the Arctic Oscillation. *Paleoceanography* 19, PA1027.

Dethleff, D. and Kuhlmann, G. (2010) Fram Strait sea-ice sediment provinces based on silt and clay compositions identify Siberian Kara and Laptev seas as main source regions. *Polar Research* 29, 265-282.

Dyke, A.S., England, J., Reimnitz, E. and Jette, J. (1997) Changes in driftwood delivery to the Canadian Arctic Archipelago: the hypothesis of postglacial oscillations of the Transpolar Drift, *Arctic* 50*,* 1-16.

Edwards, R.L. and Wasserburg, G.J. (1985) The age and emplacement of obducted oceanic crust in the Urals from Sm-Nd and Rb-Sr systematics. *Earth and Planetary Science Letters* 72, 389-404.

Eisenhauer, A., Meyer, H., Rachold, V., Tütken, T., Wiegand, B., Hansen, B.T., Spielhagen. R.F., Lindeman, F. and Kassens, H. (1999) Grain size separation and sediment mixing in Arctic Ocean sediments: evidence from the strontium isotope systematic. *Chemical Geology* 158, 173-188.

Erel, Y., Harlavan, Y. and Blum, J.D. (1994) Lead isotope systematics of granitoid weathering. *Geochimica et Cosmichimica Acta* 58, 5299-5306.

Falck, E., Kattner, G. and Budéus, G. (2005) Disappearance of Pacific Water in the northwestern Fram Strait. *Geophysical Research Letters* 32, L14619

Filippova, A. (2011) Tracing Holocene weathering input into the Kara Sea with radiogenic isotopes (Sr and Nd). Master Thesis, St. Petersburg, Russia

Fontanier, C., Mackensen, A., Jorissen, F.J., Anschutz, P., Licari, L. and Griveaud, C. (2006) Stable oxygen and carbon isotopes of live benthic foraminifera from the Bay of Biscay: Microhabitat and seasonal variability. *Marine Micropaleontology* 58, 159-183.

Frank, M. (2002) Radiogenic Isotopes: Tracers of Past Ocean Circulation and Erosional Input. *Reviews of Geophysics* 40, 1-38.

Galer, S.J.G. and O'Nions, R.K. (1989) Chemical and isotopic studies of ultramafic inclusions from the San Carlos volcanic field, Arizona: a bearing on their petrogenesis. *Journal of Petrology* 30, 1033-1064.

Gobeil, C., Macdonald, R.W., Smith, J.N. and Beaudin, L. (2001) Atlantic Water Flow Pathways Revealed by Lead Contamination in Arctic Basin Sediments. *Science* 293, 1301-1304.

Gutjahr, M., Frank, M., Stirling, C.H., Klemm, V., van de Flierdt, T. and Halliday, A.N. (2007) Reliable extraction of a deepwater trace metal isotope signal from Fe-Mn oxyhydroxide coatings of marine sediments. *Chemical Geology* 242, 351-370.

Haley, B., Frank, M., Spielhagen, R.F. and Eisenhauer, A. (2007) Influence of brine formation on Arctic Ocean circulation over the past 15 million years. *Nature Geoscience* 1, 68-72.

Haley, B., Frank, M., Spielhagen, R.F. and Fietzke, J. (2008) Radiogenic isotope record of Arctic Ocean circulation and weathering inputs of the past 15 million years. *Paleoceanography* 23, PA1S13.

Hamelin, B., Grousset, F. and Sholkovitz, E.R. (1990) Pb isotopes in surficial pelagic sediments from the North Atlantic. *Geochimica et Cosmochimica Acta* 54, 37-47.

Harland, W.B. and Gayer, R.A. (1972) The Arctic Caledonides and earlier Oceans. *Geological Magazine* 109, 289-314.

Harlavan, Y., Erel, Y. and Blum, J.D. (1998) Systematic changes in lead isotopic composition with soil age in glacial granitic terrains. *Geochimica et Cosmochimica Acta* 62, 33-46.

Hass, H.C. (2002) A method to reduce the influence of ice-rated debris on a grain size record from northern Fram Strait, Arctic Ocean. *Polar Research* 21, 299-306.

Hebbeln, D. (1991) Spätquartäre Stratigraphie und Paläozeanographie in der Fram-Straße. *Berichte aus dem Fachbereich Geowissenschaften der Universität Bremen* 22, 1-174.

Hebbeln, D. and Wefer G. (1991) Effects of ice coverage and ice-rafted material on sedimentation in the Fram Strait. *Nature* 350, 409-411.

Holland, M.M, Bitz C.M., Eby, M. and Weaver, A.J. (2001) The Role of Ice-Ocean Interactions in the Variability of the North Atlantic Thermohaline Circulation. *Journal of Climate* 14, 656-675.

Hong, S., Candelone J.-P., Patterson, C.C. and Boutron, C.F. (1994) Greenland Ice Evidence of Hemispheric Lead Pollution Two Millennia Ago by Greek and Roman Civilizations. *Science* 265, 1841-1843.

Horwitz, E.P., Chiarizia, R. and Dietz, M.L. (1992) A novel strontium-selective extraction chromatographic resin. *Solvent Extraction and Ion Exchange* 10, 313-336.

Jacobsen, S.B. and Wasserburg, G.J. (1980) Sm-Nd isotopic evolution of chondrites. *Earth and Planetary Science Letters* 50, 139-155.

Jakobsson, M., Macnab, R., Mayer, L., Anderson, R., Edwards, M., Hatzky, J., Schenke, H.W. and Johnson, P. (2008) An improved bathymetric portrayal of the Arctic Ocean: implications for ocean modelling and geological, geophysical and oceanographic analyses. *Geophysical Research Letters* 35, L07602.

Johannessen, O.M. (1986) Brief overview of the physical oceanography. In: Hurdle, B.G. (Ed.), The Nordic Seas. Springer, New York, pp. 103-127.

Johansson, Å., Larionov, A.N., Tebenkov, A.M., Ohta, Y. and Gee, D.G. (2002) Caledonian granites of western and central Nordaustlandet, northeast Svalbard. *GFF* 124, 135-148.

Johansson, Å. and Gee, D.G. (1999) The late Palaeproterozoic Eskolabreen granitoids of southern Ny Friesland, Svalbard Caledonides – geochemistry, age, and origin. *GFF* 121, 113-126.

Jones, E.P., Rudels, B. and Anderson, L.G. (1995) Deep waters of the Arctic Ocean: origins and circulation. *Deep Sea Research I* 42, 737-760.

Jones, E.P. (2001) Circulation in the Arctic Ocean. *Polar Research* 20, 139-146.

Jones, E.P., Swift, J.H., Anderson, L.G., Lipizer, M., Civitarese, G., Falkner, K.K., Kattner, G. and McLaughlin, F. (2003) Tracing Pacific water in the North Atlantic Ocean. *Journal of Geophysical Research* 108, 3116.

Karcher, M.J., Gerdes, R., Kauker, F. and Köberle, C. (2003) Arctic warming: Evolution and spreading of the 1990s warm event in the Nordic seas and the Arctic Ocean. *Journal of Geophysical Research* 108, 3034.

Kwok, R. and Rothrock, D.A. (1999) Variability of Fram Strait ice flux and North Atlantic Oscillation. *Journal of Geophysical Research* 104, 5177-5189.

Lacan, F. and Jeandel, C. (2004a) Denmark Strait water circulation traced by heterogeneity in neodymium isotopic compositions. *Deep-Sea Research I* 51, 71-82.

Lacan, F. and Jeandel, C. (2004b) Neodymium isotopic composition and rare earth element concentrations in the deep and intermediate Nordic Seas: Constraints on the Iceland Scotland Overflow Water signature. *Geochemistry, Geophysics, Geosystems* 5, Q11006

Lacan, F. and Jeandel, C. (2005) Neodymium isotopes as a new tool for quantifying exchange fluxes at the continent-ocean interface. *Earth and Planetary Science Letters* 232, 245-257

Le Fèvre, B. and Pin, C. (2005) A straightforward separation scheme for concomitant Lu-Hf and Sm-Nd isotope ratio and isotope dilution analysis. *Analytica Chimica Acta* 543, 209-221.

Lisitzin, A.P. (2002) Sea-Ice and Iceberg Sedimentation in the Ocean – Recent and Past. Springer-Verlag, Berlin, 563 pp.

Lohmann, G. and Gerdes, R. (1998) Sea Ice Effects on the Sensitivity of the Thermohaline Circulation. *Journal of Climate* 11, 2789-2803.

Lugmair, G.W. and Galer, S.J.G. (1992) Age and isotopic relationships among the angrites Lewis Cliff 86010 and Angra dos Reis. *Geochimica et Cosmochimica Acta* 56, 1673-1694.

Marnela, M., Rudels, B., Olsson, K.A., Anderson, L.G., Jeansson, E., Torres, D.J., Messias, M.-J., Swift, J.H. and Watson, A.J. (2008) Transports of Nordic Seas water masses and excess SF_6 through Fram Strait to the Arctic Ocean. *Progress in Oceanography* 78, 1-11.

Mauritzen, C. (1996) Production of dense overflow waters feeding the North Atlantic across the Greenland-Scotland Ridge. Part 1: Evidence for a revised circulation scheme. *Deep-Sea Research* 43, 769-806.

Mauritzen, C. and Häkkinen, S. (1997) Influence of sea ice on the thermohaline circulation in the Arctic-North Atlantic Ocean. *Geophysical Research Letters* 24, 3257-3260.

Müller, J., Werner, K., Stein, R., Fahl, K., Moros, M. and Jansen, E. (submitted to *Quaternary Science Reviews*) Holocene cooling culminates in Neoglacial sea ice oscillations in Fram Strait.

Nürnberg, D., Wollenburg, I., Dethleff, D., Eicken, H., Kassens, H., Letzig, T., Reimnitz, E. and Thiede, J. (1994) Sediments in Arctic sea ice: Implications for entrainment, transport and release. *Marine Geology* 119, 185-214.

Peucat, J.J., Ohta, Y., Gee, D.G. and Bernard-Griffith, J. (1989) U-Pb, Sr and Nd evidence for Grenivillan and latest Proterozoic tectonothermal activity in the Spitsbergen Caldonides, Arctic Ocean. *Lithos* 22, 275-285.

Pfirman, S., Gascard, J.-C., Wollenburg, I., Mudie, P. and Abelmann, A. (1989) Particle-laden Eurasian Arctic sea ice: observations from July and August 1987. *Polar Research* 7, 59-66.

Pfirman, S., Colony, R., Nürnberg, D., Eicken, H. and Rigor, I. (1997) Reconstructing the origin and trajectory of drifting Arctic sea ice. *Journal of Geophysical Research* 102, 12,575-12,586.

Piepgras, D.J. and Jacobsen, S.B. (1988) The isotopic composition of neodymium in the North Pacific. *Geochimica et Cosmochimica Acta* 52, 1373-1381.

Piepgras, D.J. and Wasserburg, G.J. (1980) Neodymium isotopic variations in seawater. *Earth and Planetary Science Letters* 50, 128-138.

Piepgras, D.J. and Wasserburg, G.J. (1987) Rare earth element transport in the western North Atlantic inferred from Nd isotopic observations. *Geochimica et Cosmochimica Acta* 51, 1257-1271.

Piotrowski, A.M., Goldstein, S.L., Hemming, S.R. and Fairbanks, R.G. (2005) Temporal relationships of carbon cycle and ocean circulation at glacial boundaries. *Science* 307, 1933-1938.

Porcelli, D., Andersson, P.S., Baskaran, M., Frank, M., Björk, G. and Semiletov, I. (2009) The distribution of neodymium isotopes in Arctic Ocean basins. *Geochimica et Cosmochimica Acta* 73, 2645-2659.

Prange, M. and Lohmann, G. (2003) Effects of mid-Holocene river runoff on the Arctic ocean/sea-ice system: a numerical study, *The Holocene* 13*,* 335-342.

Quadfasel, D., Rudels, B. and Kurz, K. (1988) Outflow of dense water from a Svalbard fjord into the Fram Strait. *Deep Sea Research* 35, 1153-1150.

Rasmussen, T.L. and Thomsen, E. (2009) Stable isotope signals from brines in the Barents Sea: Implications for brine formation during the last glaciation. *Geology* 37, 903-906.

ArcticRIMS database/R-ArcticNet (v4.0) (2011) A Regional, Hydrometeorological Data Network for the pan-Arctic Region (http://rims.unh.edu/)

Roach, A.T., Aagaard, K., Pease, C.H., Salo, S.A., Weingartner, T., Pavlov, V. and Kulakov, M. (1995) Direct measurements of transport and water properties through the Bering Strait. *Journal of Geophysical Research* 100, 18,443-18,457.

Rudels, B. (1986) The θ-S relations in the northern seas: Implications for the deep circulation. *Polar Research* 4, 133-159.

Rudels, B., Jones, E.P., Anderson, L.G. and Kattner, G. (1994) On the intermediate depth waters of the Arctic Ocean. In: Johannessen, O.M., Muench, R.D., Overland, J.E. (Eds.), The role of the Polar Oceans in Shaping the Global Climate. American Geophysical Union, Washington D.C., pp. 33-46.

Rudels, B., Friedrich, H.J. and Quadfasel, D. (1999) The arctic circumpolar boundary current. *Deep-Sea Research II* 46, 1023-1062

Rudels, B., Meyer, R., Fahrbach, E., Ivanov, V.V., Østerhus, S. and Quadfasel, D. (2000) Water mass distribution in Fram Strait and over the Yermak Plateau in summer 1997. *Annales Geophysicae* 18, 687-705.

Rudels, B., Fahrbach, E., Meincke, J., Budéus, G. and Eriksson, P. (2002) The East Greenland Current and its contribution to the Denmark Strait overflow. *ICES Journal of Marine Systems* 59, 1133-1154.

Rudels, B., Björk, G., Nilsson, J., Winsor, P., Lake, I. and Nohr, C. (2005) The interaction between waters from the Arctic Ocean and the Nordic Seas north of Fram Strait and along the East Greenland Current: results from the Arctic Ocean-02 Oden expedition. *Journal of Marine Systems* 55, 1-30.

Rudels, B. and Quadfasel, D. (1991) Convection and deep water formation in the Arctic Ocean-Greenland Sea System. *Journal of Marine Systems* 2, 435-450.

Rutberg, R.L., Hemming, S.R. and Goldstein, S.L. (2000) Reduced North Atlantic Deep Water flux to the glacial Southern Ocean inferred from neodymium isotope ratios. *Nature* 405, 935-938.

Schauer, U. (1989) Hydrographie der Fram Straße. In: Meinke, J. (Ed.), Fram Straße – Hydrobiologische und geowissenschaftliche Schlüsselregion zwischen Nordpolarmeer und Europäischem Nordmeer. – Ergebnisse eines Workshops am 4.4.1989 in Hamburg, Institut für Meereskunde, Hamburg.

Schauer, U. (1995) The release of brine-enriched shelf water from Storfjord into the Norwegian Sea. *Journal of Geophysical Research* 100, 16,015-16,028.

Schauer, U., Fahrbach, E., Østerhus, S. and Rohardt, G. (2004) Arctic warming through the Fram Strait: oceanic heat transport from 3 years of measurements. *Journal of Geophysical Research* 109, C06026.

Schaule, B.K. and Patterson, C.C. (1981) Lead concentrations in the northeast Pacific: evidence for global anthropogenic perturbations. *Earth and Planetary Science Letters* 54, 97-116.

Schlichtholz, P. and Goszczko, I. (2006) Interannual variability of the Atlantic water layer in the West Spitsbergen Current at 76.5°N in summer 1991 -2003. *Deep-Sea Research I* 53, 608-626.

Schlichtholz, P. and Houssais, M.-N. (1999) An inverse modeling study in Fram Strait. Part II: water mass distribution and transports. *Deep-Sea Research II* 46, 1137-1168.

Schoster, F., Behrends, M., Müller, C., Stein, R. and Wahsner, M. (2000) Modern river discharge and pathways of supplied material in the Eurasian Arctic Ocean: evidence from mineral assemblages and major and minor element distribution. *International Journal of Earth Sciences* 89, 486-495.

Shackleton, N.J. (1977) Carbon-13 in *Uvigerina*: tropical rainforest history and the Eqautorial Pacific carbonate dissolution cycles. In: Anderson, N.R., Malahoff, A. (Eds.), The Fate of Fossil Fuel CO_2 in the Oceans. Plenum. New York, pp. 401-427.

Shackleton, N.J. and Opdyke, N.D. (1973) Oxygen isotope and paleomagnetic stratigraphy of equatorial Pacific core V28-238: oxygen isotope temperature and ice volumes on a 10^5 and 10^6 year scale. *Quaternary Research* 3, 39-55.

Sharma, M., Basu, A.R. and Nesterenko, G.V. (1992) Temporal Sr-, Nd- and Pb-isotopic variations in the Siberian flood basalts: Implications for the plume-source characteristics. *Earth and Planetary Science Letters* 113, 365-381.

Spielhagen, R.F., Werner, K., Aagaard Sørensen, S., Zamelczyk, K., Kandiano, E., Budéus, G., Husum, K., Marchitto, T.M. and Hald, M. (2011) Enhanced Modern Heat Transfer to the Arctic by Warm Atlantic Water. *Science* 331, 450-453.

Steiger, R.H. and Jäger, E. (1977) Subcommission on geochronology: convention on the use of decay constants in geo- and cosmochronology. *Earth and Planetary Science Letters* 36, 359-362.

Stein, R., Dittmers, K., Fahl, K., Kraus, M., Matthiessen, J., Niessen, F., Pirrung, M., Polyakova, Ye., Schoster, F., Steinke, T. and Fütterer, D.K. (2004) Arctic (paleo) river discharge and environmental chage: evidence from the Holocene Kara Sea sedimentary record. *Quaternary Science Reviews* 23, 1485-1511.

Stumpf, R., Frank, M., Schönfeld, J. and Haley, B.A. (2010) Late Quaternary variability of Mediterranean Outflow Water from radiogenic Nd and Pb isotopes. *Quaternary Science Reviews* 29, 2462-2472.

Svendsen, J.I. and Mangerud, J. (1997) Holocene glacial and climatic variations on Spitsbergen, Svalbard. *The Holocene* 7, 45-57.

Swift, J.H. and Koltermann, K.P. (1988) The Origin of Norwegian Sea Deep Water. *Journal of Geophysical Research* 93, 3563-3569.

Tachikawa, K., Jeandel, C., Roy-Barman, M. (1999) A new approach to the Nd residence time in the ocean: the role of atmospheric inputs. *Earth and Planetary Science Letters* 170, 433-446.

Tanaka, T., Togashi, S., Kamioka, H., Amakawa, H., Kagami, H., Hamamoto, T., Yuhara, M., Orihashi, Y., Yoneda, S., Shimizu, H., Kunimaru, T., Takahashi, K., Yanagi, T., Nakano, T., Fujimaki, H., Shinjo, R., Asahara, Y., Tamimizu, M. and Dragusanu, C. (2000) JNdi-1: a neodymium isotopic reference in consistency with LaJolla neodymium. *Chemical Geology* 168, 279-281.

Tütken, T., Eisenhauer, A., Wiegand, B. and Hansen, B.T. (2002) Glacial-interglacial cycles in Sr and Nd isotopic composition of Arctic marine sediments triggered by the Svalbard/Barents Sea ice sheet. *Marine Geology* 182, 351-372.

Van de Flierdt, T., Robinson, L.F., Adkins, J.F. and Hemming, S.R. (2006) Temporal stability of the neodymium isotope signature of the Holocene to glacial North Atlantic. *Paleoceanography* 21, PA4102.

Van de Flierdt, T. and Frank, M. (2010) Neodymium isotopes in paleoceanography. *Quaternary Science Reviews* 29, 2439-2441.

Véron, A.J. and Church, T.M. (1997) Use of stable lead isotopes and trace metals to characterize air mass sources into the eastern North Atlantic. *Journal of Geophysical Research* 102, 28,049-28,058.

Vinje, T. (2001) Anomalies and Trends of Sea ice Extent and Atmospheric Circulation in the Nordic Seas during the Period 1864-1998. *Journal of Climate* 14, 255-267.

Volkmann, R. (2000) Planktic foraminifer ecology and stable isotope geochemistry in the Arctic Ocean: implications from water column and sediment surface studies for quantitative reconstructions of oceanic parameters. *Berichte zur Polarforschung* 361, 1-128.

Werner, K., Spielhagen, R.F., Bauch, D., Hass, H.C., Kandiano, E. and Zamelczyk, K. (2011) Atlantic Water advection to the eastern Fram Strait – Multiproxy evidence for late Holocene variability. *Palaeogeography, Palaeoclimatology, Palaeoecology* 308, 264-276.

Winter, B.L., Johnson, C.M. and Clark, D.L. (1997) Strontium, neodymium, and lead isotope variations of authigenic and silicate sediment components from the Late Cenozoic Arctic Ocean: Implications for sediment provenance and the source of trace metals in seawater. *Geochimica et Cosmochimica Acta* 61, 4181-4200.

Zimmermann, B., Porcelli, D., Frank, M., Andersson, P.S., Baskaran, M., Lee, D.-C. and Halliday. A.N. (2009) Hafnium isotopes in Arctic Ocean water. *Geochimica et Cosmochimica Acta* 73, 3218-3233.

APPENDICES

A: SUPPORTING ONLINE MATERIAL (CHAPTER 4)

B: COLOUR SCAN DATA (CHAPTER 6)

Appendix A: Supporting Online Material (Chapter 4)

METHODS

Sediment sampling, preparation, and CTD measurements

The 46 cm long sediment core MSM5/5-712-1 was obtained by a giant box corer (50x50x60 cm) from RV *Maria S. Merian* on August 4, 2007. A surface sample was taken with a spoon by skimming off the uppermost ~0.5 cm and preserved in ethanol with Rose Bengal to stain alive microorganisms. A plastic archive box was pressed horizontally into the core, thereby avoiding vertical compression. Slices of 0.5 cm thickness (~25 cm^3) were taken manually from this box, freezed-dried, washed in deionized water through a 63 μm mesh and split into several size fractions. Dry bulk density was determined every 5 cm from defined 10 cm^3 samples. Temperature and conductivity measurements at the position of site MSM5/5-712 were performed with calibrated Seabird 911 Plus CTDs from RV *Jan Mayen* (October 12, 2006; site JM06-WP-02) and RV *Maria S. Merian* (August 4, 2007: site MSM5/5-713-1). Uncertainties are <0.005°C and <0.005 practical salinity units.

Radiocarbon dating

Five accelerator mass spectrometry ^{14}C datings (Table S1) were performed at the Leibniz Laboratory of Kiel University on ~2000 specimens of the planktic foraminifer *Neogloboquadrina pachyderma* (sin.) per sample. Dated material from the surface sample contained additional planktic foraminiferal species. The surface sample contained many Rose Bengal stained foraminifers and yielded ^{14}C from nuclear bomb tests (103.47 pMC). We therefore assigned a Zero age (year of core sampling) to the sediment-water interface. ^{14}C results of the other samples were calibrated to calendar years by the CALIB 6.0 programme (*S1*) with the Marine09 data set (*S2*) and a standard reservoir correction of 402 years. A stratigraphic model of calendar year ages was established by linear interpolation between the calibrated AMS ^{14}C ages.

SIMMAX palaeotemperature reconstruction

Planktic foraminiferal counts were performed on representative splits (~500 specimens per sample) of the 100-250 μm fraction on all samples to register also small subpolar species which have an abundance maximum in the 100-150 μm fraction (*S3*) (Fig. S1). The 150-250 size fraction was counted every 1 cm for the interval before 1835 AD and every 0.5 cm thereafter (uppermost 5 cm) to calculate summer palaeotemperatures (July-September) at 50 m water depth using the SIMMAX technique (*S4*) and the 2003 core-top reference data set (*S5*). SIMMAX normally uses the >150 μm fraction but we checked the >250 μm fraction and found that it contains only

negligible numbers of planktic foraminifers. The method proved to reach a better accuracy that other classical modern analog and transfer function techniques, especially in high latitudes (*S4, S5)*. The reconstructed SSTs are calculated as mean SSTs of the ten best analogs weighted by the similarity indices which estimate the degree of analogy of foraminiferal assemblages between the core samples and modern core top samples from the data base in Ref. *S5*. Our similarity indices are >0.99 for all analyzed samples except 0.25 and
0.5 cm (0.97). All these values fall within the "very good" similarity range (*S4*). Below 3°C SIMMAX tends to overestimate temperatures (*S5*). Thus, the reconstructed temperature increase from the Little Ice Age to the Modern (Industrial) Period probably represents a minimum value.

Mg/Ca palaeotemperature reconstruction

For Mg/Ca analysis ~50 tests of *N. pachyderma* (sin.) per sample were picked from the 100-150 μm fraction. The size interval was kept narrow in order to avoid a possible size-dependent bias (*S6*). In preparation of Mg/Ca measurements, foraminifers were gently crushed between glass slides. Subsequently each sample underwent the trace metal cleaning procedures described elsewhere (*S7, S8*). Samples were analyzed for Mg/Ca by magnetic sector single-collector ICP-MS on a Thermo-Finnigan Element2, using methods adapted from Rosenthal et al. (*S9*) with a long-term 1σ precision of Mg/Ca for of 0.5% (*S10*). Four samples were rejected due to low post-cleaning mass recovery (< 5μg $CaCO_3$) (*S10*), leaving a total of 26 reliable Mg/Ca data (including two replicates). Elemental ratios of Fe/Ca and Al/Ca (detrital material) and Mn/Ca (secondary diagenetic coatings) were analyzed coincidental with Mg/Ca. No values of Mn/Ca exceeded 24 μmol mol^{-1} which is well below the threshold for likely trace metal contamination (*S11*). One sample (0.25 cm) had Fe/Ca and Al/Ca values exceeding 100 μmol mol^{-1}. However, this single sample was not omitted as its Mn/Ca ratio did not show signs of contamination and its Mg/Ca value was similar to surrounding samples. To convert the measured Mg/Ca ratios into temperatures we used the *N. pachyderma* equation of Elderfield and Ganssen (*S12*): Mg/Ca (mmol mol^{-1}) = 0.5 exp 0.10 T. This equation is indistinguishable from the Norwegian Sea *N. pachyderma* (sin.) calibration of Nürnberg (*S13*) and the cultured *N. pachyderma* (dex.) calibration of von Langen et al. (*S14*). Application of an alternative equation Of Kozdon et al. (*S15*) results in consistently lower temperatures throughout the core which are also lower than the SIMMAX results.

Tests from the upper 10 cm of the core showed some signs of dissolution and were fragile. Generally, partly dissolved tests should be avoided as they may give too low Mg/Ca ratios and the reconstructed temperatures may be underestimated (*S16*). With respect to core MSM5/5-712-1, however, we regard the close similarity between temperatures reconstructed from independent

SIMMAX and Mg/Ca results as evidence of a minor effect of dissolution. Were dissolution of importance, it would affect also the planktic foraminifer associations used for SIMMAX. Fragile subpolar species would be more easily dissolved than the only polar, robust species *N. pachyderma* (sin.), eventually leading to lower calculated SIMMAX temperatures especially for the youngest time interval. Thus, carbonate dissolution within the uppermost part of the core would result in an underestimatation (by both methods) of the Atlantic Water temperature difference between the Modern (Industrial) Period and, e.g., the Medieval Climate Anomaly.

Replicate Mg/Ca analysis on separate picks at 0 cm and 28 cm core depth revealed differences of 0.01 mmol mol^{-1} and 0.12 mmol mol^{-1}, respectively. Although this is insufficient to provide a robust estimate of reproducibility, a pooled standard deviation of order 0.05-0.1 mmol mol^{-1} is typical for foraminifera (e.g., Refs. *S17, S18*). The standard deviation for each interval before and after 1850 was 0.1 mmol mol^{-1}, which translates to relatively large temperature ranges at the cold end of the Elderfield and Ganssen (*S12*) exponential calibration: +1.3/-1.5°C pre-industrial and +1.1/-1.2°C post-industrial. Since this is close to our estimated reproducibility, we cannot interpret the temperature variability *within* each interval, which we suggest is dominated by random error. However the *mean* within each interval is well constrained, with standard errors (stdev/sqrt(n)) of ±0.3°C pre-industrial and ±0.5°C post-industrial.

REFERENCES

S1. M. Stuiver, P. J. Reimer, Extended ^{14}C database and revised CALIB radiocarbon calibration program. *Radiocarbon* **35**, 215-230 (1993).

S2. P. J. Reimer *et al.* IntCal09 and Marine09 radiocarbon age calibration curves, 0–50,000 years cal BP. *Radiocarbon* **51 (4)**, 1111–50 (2009).

S3. E. S. Kandiano, H. A. Bauch, Implications of planktic foraminiferal size fractions for the glacial-interglacial paleoceanography of the polar North Atlantic. *J. Foram. Res.* **32**, 245-251 (2002).

S4. U. Pflaumann, J. Duprat, C. Pujol, L. D. Labeyrie, SIMMAX: A modern analog technique to deduce Atlantic sea surface temperatures from planktonic foraminifera in deep-sea sediments. *Paleoceanography* **11**, 15-35 (1996).

S5. U. Pflaumann *et al.* Glacial North Atlantic: Sea-surface conditions reconstructed by GLAMAP 2000. *Paleoceanography* **18 (3)**, 1065, doi:10.1029/2002PA000774 (2003).

S6. H. Elderfield, M. Vautravers, M. Cooper, The relationship between shell size and Mg/Ca, Sr/Ca, $\delta^{18}O$, and $\delta^{13}C$ of species of planktonic foraminifera. *Geochem. Geophys. Geosyst.* **3 (8)**, 1052, doi:10.1029/2001GC000194 (2002).

S7. E. A. Boyle, L. D. Keigwin, Comparison of Atlantic and Pacific paleochemical records for the last 215,000 years: changes in deep ocean circulation and chemical inventories. *Earth Planet. Sci. Lett.* **76**, 135-150 (1985/86).

S8. E. A. Boyle, Y. Rosenthal, in *The South Atlantic: Present and Past Circulation* (eds Wefer, G., Berger, W. H. & Siedler, G.) 423-443 (Springer, Berlin 1996).

S9. Y. Rosenthal, M. P. Field, R. M. Sherrell, Precise determination of element/calcium ratios in calcareous samples using sector field inductively coupled plasma mass spectrometry. *Analytical Chemistry* **71**, 3248–3253 (1999).

S10. T. M. Marchitto, Precise multielemental ratios in small foraminiferal samples determined by sector field ICP-MS. *Geochem. Geophys. Geosyst.* **7**, Q05P13, doi:10.1029/2005GC001018 (2006).

S11. S. Barker, M. Greaves, H. Elderfield, A study of cleaning procedures used for foraminiferal Mg/Ca paleothermometry. *Geochem. Geophys. Geosyst.* **4 (9)**, 8407, doi: 10.1029/2003GC000559 (2003).

S12. H. Elderfield, G. Ganssen, Past temperature and d^{18}O of surface ocean waters inferred from foraminiferal Mg/Ca ratios. *Nature* **405**, 442-445, doi:10.1038/35013033 (2000).

S13. D. Nürnberg, Magnesium in tests of Neogloboquadrina pachyderma sinistral from high northern and southern latitudes. *J. Foram. Res.* **25 (4)**, 350-368.

S14. P. J. von Langen, D. K. Pak, H.J. Spero, D. W. Lea, Effects of temperature on Mg/Ca in neogloboquadrinid shells determined by live culturing. *Geochem. Geophys. Geosyst.* **6**, Q10P03, doi:10.1029/2005GC000989.

S15. R. Kozdon, A. Eisenhauer, M. Weinelt, M. Y. Meland, D. Nürnberg, Reassessing Mg/Ca temperature calibrations of *Neogloboquadrina pachyderma* (sinistral) using paired $\delta^{44/40}$Ca and Mg/Ca measurements. *Geochem. Geophys. Geosyst.* **10**, Q03005,
doi:10.1029/2008GC002169 (2009).

S16. S. Barker, I. Cacho, H. Benway, K. Tachikawa, Planktonic foraminiferal Mg/Ca as a proxy for past oceanic temperatures: A methodological overview and data compilation for the Last Glacial Maximum. *Quat. Sci. Rev.* **24 (7-9)**, 821-834 (2005),

S17. D. W. Lea, D. K. Pak, H. J. Spero, Climate impact of Late Quaternary equatorial Pacific sea surface temperature variation. *Science.* **289**, 1719-1724 (2000),

S18. T. M. Marchitto, S. P. Bryan, W. B. Curry, D. C. McCorkle, Mg/Ca temperature calibration for the benthic foraminifer *Cibicidoides pachyderma*, *Paleoceanography*, **22(1)**, PA1203, doi:10.1029/2006PA001287, 2007.

Table S1. Results of radiocarbon datings

Depth (cm)	Interval (cm)	Laboratory Code	^{14}C age[a] (yr B.P.)	Standard deviation (^{14}C yr)	Calendar age (CALIB 6.0) using Marine09 data set and 402 yr reservoir correction		
					Mean (yr B.P.)	Standard deviation (yr)	Year A.D.
0.25	0.0-0.5	KIA39656	Bomb age[b]				2007[c]
14.75	14.5-15.0	KIA39262	820	25	476	23	1486
21.50	21.0-22.0	KIA39041	1290	30	838	45	1112
30.75	30.5-31.0	KIA39263	1760	25	1303	25	647
42.00	41.5-42.5	KIA38079	2270	25	1878	39	72

[a] Results are ^{13}C-corrected. [b] Sample contained 103.47 pMC. [c] Assumed age for 0 cm core depth, based on considerations described in Methods.

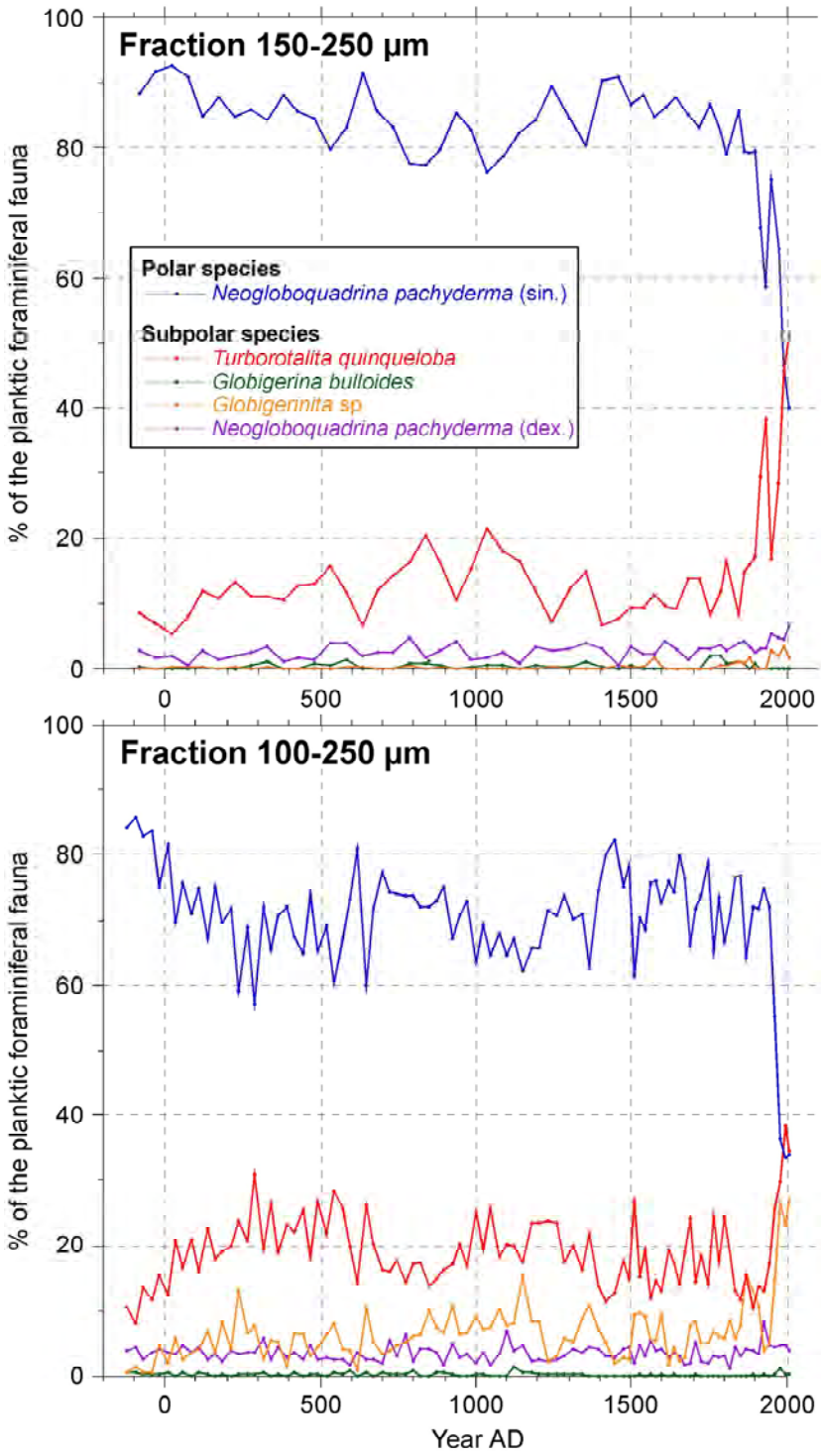

Fig. S1. Results of planktic foraminifer counts for the 150-250 µm (top) and 100-250 µm (bottom) fractions of sediment core MSM5/5-712-1. Data are given as relative abundance. Sample spacing is 0.5 cm (1 cm for samples older than AD 1844 in the 150-250 µm fraction). *Globigerinita* sp. accounts for *G. uvula* and *G. glutinata* which cannot always be distinguished when smaller than 150 µm. As a rule, the relative abundance of subpolar species appears higher when small specimens (size 100-150 µm) are included in the counting procedure. In particular, *Globigerinita* sp. are almost neglected when small specimens are not counted.

Appendix B: Colour scan data (Chapter 6)

Depth [m]	Age [AD]	L*	a*	b*
0.02	1936	39.94	4.12	9.35
0.03	1901	38.64	4.85	10.14
0.04	1866	42.66	3.83	11.77
0.05	1830	42.87	2.89	10.1
0.06	1795	41.83	3.83	11.78
0.07	1760	43.64	3.1	10.58
0.08	1724	43.22	2.78	10.44
0.09	1689	44.07	2.81	10.64
0.1	1654	44.39	2.52	9.71
0.11	1618	44.34	2.44	9.68
0.12	1583	44.52	2.54	9.92
0.13	1548	44.78	2.51	9.73
0.14	1512	44.49	2.39	9.52
0.15	1472	43.75	2.34	9.29
0.16	1417	44.74	2.19	8.8
0.17	1361	44.16	2.27	9.16
0.18	1306	44.17	2.26	9.03
0.19	1251	44.58	2.38	9.46
0.2	1195	45.64	2.34	9.31
0.21	1140	45.21	2.37	9.37
0.22	1087	45.86	2.28	9.14
0.23	1037	45.45	2.34	9.2
0.24	986	45.51	2.31	9.19
0.25	936	45.76	2.27	8.9
0.26	886	45.85	2.38	9.18
0.27	836	45.71	2.46	9.31
0.28	785	45.8	2.42	9.15
0.29	735	45.21	2.39	9.2
0.3	685	45.01	2.4	9.35
0.31	634	42.83	2.45	9.67
0.32	583	43.5	2.34	9.26
0.33	532	43.74	2.29	9.02
0.34	481	43.49	2.32	9.37
0.35	430	43.38	2.39	9.42
0.36	379	44.52	2.25	9.13
0.37	328	45.05	2.26	8.94
0.38	276	46.11	2.33	9.19
0.39	225	45.33	2.29	8.92
0.4	174	45.49	2.3	9.1
0.41	123	45.37	2.3	9.19
0.42	72	45.54	2.29	9.28
0.43	21	44.73	2.22	9.08
0.44	-30	44.2	2.35	9.42